



HAL
open science

Modular Multilevel Converter Control for HVDC Operation: Optimal Shaping of the Circulating Current Signal for Internal Energy Regulation

Gilbert Bergna Diaz

► **To cite this version:**

Gilbert Bergna Diaz. Modular Multilevel Converter Control for HVDC Operation: Optimal Shaping of the Circulating Current Signal for Internal Energy Regulation. Other. CentraleSupélec; Norwegian University of Science and Technology (Trondheim, Norvège), 2015. English. NNT : 2015CSUP0017 . tel-01349299

HAL Id: tel-01349299

<https://theses.hal.science/tel-01349299>

Submitted on 27 Jul 2016

HAL is a multi-disciplinary open access archive for the deposit and dissemination of scientific research documents, whether they are published or not. The documents may come from teaching and research institutions in France or abroad, or from public or private research centers.

L'archive ouverte pluridisciplinaire **HAL**, est destinée au dépôt et à la diffusion de documents scientifiques de niveau recherche, publiés ou non, émanant des établissements d'enseignement et de recherche français ou étrangers, des laboratoires publics ou privés.



N d'ordre:2015-17-TH

CentraleSupélec & NTNU

École Doctorale STITS

Sciences et Technologies de l'Information des Télécommunications et des Systèmes

THÈSE DE DOCTORAT

en co-tutelle internationale

DOMAINE : SCIENCES POUR L'INGÉNIEUR
Spécialité : Énergie

Soutenue le 03 Juillet 2015

par :

Gilbert BERGNA DIAZ

Modular Multilevel Converter Control for HVDC Operation

Optimal Shaping of the Circulating Current Signal for Internal Energy Regulation

Directeur de thèse : Pr. Jean-Claude VANNIER - CENTRALESUPÉLEC
Directeur de thèse : Pr. Marta MOLINAS - NTNU
Co-encadrant : Pr. Amir ARZANDÉ - CENTRALESUPÉLEC

Composition du jury :

Président du jury: Pr. Olav FOSSO - NTNU
Rapporteurs: Pr. Maria PIETRZAK-DAVID - INP - ENSEEIHT
Pr. Maryam SAEEDIFARD - GEORGIA TECH
Examineurs : Pr. Xavier GUILLAUD - École Centrale de Lille
Pr. Eric LABOURÉ - Université Paris Sud
Pr. Daniel SADARNAC - CENTRALESUPÉLEC
Membres invités : Erik BERNE - EDF R&D
Philippe ÉGROT - EDF R&D

Acknowledgments

THIS thesis is the result of my time as a PhD candidate engineer at EDF R&D in Moret-sur-Loing, in the south of Paris. This work would not have been possible without the vision of my supervisors at EDF, Erik Berne and Philippe Egrot, who initially created the project on Modular Multilevel Converters to which this thesis is devoted. Equally important, was the inspiration I received from Dr. Maialen Boyra who encouraged me to pursue my master project in this research domain and a PhD thereafter, which led to me to meet Erik and Philippe. Working at EDF gave me a valuable learning experience in industry and applied research, providing continual contact with real world problems. It was a great pleasure to work directly with Erik, who allowed me enough space to explore my creativity while keeping me grounded and focused on the important objectives of the project.

Part of my time was spent at the Energy department of Supélec in Gif-sur-Yvette, where I met head of the department, Jean-Claude Vannier, and Pr. Amir Arzandé. I am very grateful to Jean-Claude for his constant support and belief in me since the very first days that I arrived in France. Jean-Claude became my main supervisor at Supélec and led me to work with Amir, whose technical prowess, intellect and enthusiasm were indispensable for the construction of the prototype (not to mention his unceasing capacity to look after everyone around him!). I am also grateful to the technician of the department, Damien Huchet, for providing a helping hand whenever needed. I also thank Pr. Romeo Ortega for his willingness to get involved in our project.

I was very fortunate during my PhD to collaborate with Pr. Marta Molinas from NTNU in Trondheim. Little did I know that when I first made contact with Marta that this would be the start of a new chapter in my life that would transform my PhD into a double degree between Supélec and NTNU. In Marta I found both a mentor and a friend, whose continual support, guidance and encouragement enabled me to realize my academic goals and grow as a researcher. Marta has been a constant source of inspiration and taught me to fight for what I believe in. The breakthrough in my thesis came when she introduced me to Pr. Alejandro Garcés, who at the time was finishing his PhD at NTNU, and Dr. Jon Are Suul, researcher at SINTEF energy, to both of whom I owe much gratitude. Our work together resulted in several publications described in this thesis as well as a lasting friendship.

Besides scientific challenges, these past years have also been filled with many memorable occasions with the people closest to me. At Supélec, I made many good friends both within and outside the department, who helped me to persevere when times were difficult. In particular, I would like to thank Donovan, Louise, Nikola, Marija, German, Dany, Alex, Miguel, Carmen, Ivan and the rest of the crew. I am equally grateful to Juan-Manuel and Bego from EDF for our entertaining conversations during the long commute between EDF and Paris. At NTNU, I shared many good times with Santiago, René, Raymundo Atsede and Elisabetta, who helped ease my transition from Paris to Trondheim. I also have Ole, Andrzej, Jef and Giuseppe from

SINTEF to thank for making me feel at home in my new town. I would also like to thank my good friends Luis, Rafa, Claire, Yansong, Javi, Lucia, and Raphaele.

Above all, I would like to thank Emma for help with the writing and proofreading of this Thesis, but most of all, for putting up with me when the stress got the better of me, for giving me the strength to carry on and for never failing to turn a bad day into a good one.

Finally, none of this would have ever been possible without the support of my family, who despite the distance, have always been there for me when I most needed it.

Abstract

ELECTRICITY will most probably be the dominant form of energy in the upcoming future. Triggered by the decline of fossil fuels along with their elevated and volatile prices, the threat that they represent to national energy security, and growing environmental concerns as consequence of their negative effect on climate change, Europe has decided to undertake an ambitious and multidisciplinary project called the *SuperGrid*. Such an initiative will serve as a transcontinental highway for renewable energy, [1], allowing for geographical smoothing effects to help minimize the disadvantages inherent to the intermittent renewable sources. In more simple words, this so-called *SuperGrid* will interconnect the offshore wind and wave power from the North sea, with the photovoltaic (PV) and concentrated solar power (CHP) from the south, as well as geothermal and biomass generation, and indeed, large hydro-power dams (located in Norway and Switzerland among other countries) that will serve as Europe's energy storage. The main challenge is of course the continental-size distances of the interconnections, which were not possible using the traditional AC technology. Nowadays, such ambitious projects have become feasible as high voltage direct current (HVDC) technology enters the scene, thanks to semi-conductor breakthroughs and advances in power electronics; more precisely, voltage source converters (VSC)-based high voltage direct current (HVDC) links.

It seems to be getting clear that the Modular Multilevel Converter (MMC) proposed by Professor Marquart in 2003 [2] has emerged as the the most suitable power converter for such application, since it has several advantages with respect to its predecessors, such as its high modularity, scalability and lower losses.

When this research project was undertaken in 2011, there was not yet a clear control strategy defined that could be used to operate the MMC in an optimal and stable manner since the topology was still very new. Moreover, this strategy needed to take into account the final HVDC application and withstand grid fault scenarios. Thus, the present Thesis was carried out with the aim of overcoming such crucial issues, by proposing a control philosophy in the MMC natural phase coordinates that was obtained from the application of mathematical optimization using Lagrange multipliers to the energy-based model of the MMC for balanced and unbalanced grid conditions. Furthermore, global asymptotic stability issues involving the MMC were addressed, and a simple and local approach for ensuring the global stability of the complex MMC-multi-terminal HVDC system was implemented.

Contents

Acknowledgments	iii
Abstract	v
Nomenclature and Abbreviations	xxi
Résumé de la thèse en Langue Française	xxv
1 Introduction	1
1.1 Objectives	2
1.1.1 General objective	2
1.1.2 Specific objectives	2
1.2 Main contributions	3
1.3 Scope	4
1.4 List of publications	4
1.5 Layout of the Thesis	7
2 The Modular Multilevel Converter	9
2.1 Introduction	9
2.2 HVDC technology	10
2.2.1 Beginings	10
2.2.2 The revolution: VSC technology	11
2.3 Basic structure and functionality of the MMC	12
2.3.1 Sub-module analysis	14
2.3.2 Balancing algorithm	16
2.3.3 Grid connected MMCs	18
2.4 Equations representing the operation of the MMC	20

2.4.1	Step by step derivation of the MMC main equations	20
2.4.2	Two mathematical models in matrix representation for the MMC	25
2.4.3	Considerations for controlling the capacitive energy	28
2.5	Circuit modeling approaches for the modular multilevel converter	28
2.5.1	Detailed or high-fidelity model of the MMC	29
2.5.2	Reduced circuit modelling based on ON/OFF resistors	29
2.5.3	Controlled voltage sources-based models	31
2.5.4	Analytical models	34
2.5.5	Averaged MMC models	35
2.6	MMC models comparison and validation	35
2.6.1	Comparison under balanced and unbalanced AC grid conditions	36
2.6.2	Models validation under DC short-circuits	38
2.6.3	Concluding remarks on the MMC modelling techniques	41
2.7	On the need of a circulating current control	41
2.8	Insertion index “continuous” modulation methods classification	42
2.9	State of the art of circulating current control schemes	44
2.9.1	Direct Modulation	45
2.9.2	Open loop control based on estimation of stored energy	45
2.9.3	Circulating current suppression controller	48
2.9.4	Arm energy closed-loop control scheme in the “abc” frame	49
2.9.5	Double decoupled synchronous reference frame (DDSRF) control for 3-phase MMC	50
2.10	Motivation for a new circulating current control scheme for the MMC	54
3	Optimization of the Circulating Current Signal for Phase Independent Energy Shaping and Regulation	59
3.1	Introduction	59
3.2	Introduction to the instantaneous abc theory	61
3.2.1	Active and nonactive current calculation by means of a minimization method	61
3.2.2	Generalized compensation theory for active filters based on mathematical optimization	62
3.3	MMC circulating current calculation for phase independent control	64

3.3.1	MMC constant circulating current	64
3.3.2	MMC constant energy sum	66
3.3.3	Generalized equation	67
3.4	Implementation by means of stationary multi-resonant controllers	68
3.5	Simulation results	69
3.5.1	Steady state performance	70
3.5.2	Operating under unequal arm energy references	70
3.5.3	Comparison with the existing controllers	71
3.5.4	MMC-HVDC simulation	72
3.6	Conclusion	74
4	Circulating Current Signal Estimation based on Adaptive Filters: Faster Dynamics and Reduced THD	77
4.1	Introduction	77
4.2	On harmonic sensitivity and slow dynamics of the circulating current reference signal generation based on Lagrange multipliers	78
4.2.1	Harmonic sensitivity	79
4.2.2	Risk of slow dynamics	79
4.3	The second order generalized integrator configured as a quadrature signal generator	80
4.4	Circulating current reference calculation based on single-phase voltage, power and energy estimation for MMCs	82
4.4.1	Estimation of single-phase fundamental frequency voltage and power . . .	83
4.4.2	Estimation of the single-phase RMS voltage	83
4.4.3	Estimation of the single-phase average power	83
4.4.4	Estimation of the single-phase average values for the MMC energy sum and difference	84
4.5	Simulation results	84
4.6	Proof of concept via lab experimental prototype	86
4.6.1	Experimental setup	86
4.6.2	Experimental Results	87
4.7	Conclusion	93
5	Circulating Current Signal for Constant Power under Unbalanced Grid Conditions: The MMC Energy Buffer	95

CONTENTS

5.1	Introduction	95
5.2	Investigating MMC conceptual possibilities under unbalanced operation using a simplified energetic macroscopic representation	97
5.3	Circulating current reference adapted for unbalanced operation	99
5.4	Grid current control strategies	101
5.5	Power references assignment	102
5.6	Results	103
5.6.1	Former control equation for independent control per phase	104
5.6.2	Performance of the novel circulating current reference formulation adapted for unbalanced operation under different grid current control strategies	105
5.6.3	Influence of the power reference assignment in transient state under unbalances	108
5.7	Conclusion	109
6	Stability of the MMC: Passivity-based Stabilization	111
6.1	Introduction	111
6.2	Global tracking passivity-based PI controller for modular multilevel converters	113
6.2.1	Tracking problem for the MMC	113
6.2.2	Passivity of the bi-linear incremental model	115
6.2.3	A PI tracking controller	116
6.2.4	MMC controller summary	117
6.3	Generating the reference signals using a closed loop virtual energy estimator	118
6.3.1	Phase independent energy regulation	119
6.3.2	Generation of references for constant DC power under unbalanced grid conditions	122
6.4	Results	123
6.4.1	Phase independent control	123
6.4.2	Constant DC power control	123
6.5	Conclusions	125
7	Conclusions and Future Research	127
7.1	Conclusions	127
7.1.1	On the proposed control philosophy and linear control scheme	127

7.1.2	On stability issues and non-linear control proposal	129
7.2	Future research	131
7.2.1	Minimizing the energy difference during unbalances	131
7.2.2	Perspectives on weak grid operation of MMCs	131
7.2.3	Improving the MMC state estimation	131
7.2.4	Adaptive PI stabilization of the MMC	131
7.2.5	Control by interconnection applied to the MMC	132
 Appendices		 133
 A Global Tracking Passivity-based PI Controller		 135
A.1	Introduction	135
A.2	Global tracking problem	136
A.3	Passivity of the bilinear incremental model	136
A.4	A PI global tracking controller	137
A.5	Conclusions	138
 B Lyapunov’s Global Asymptotic Stability Proof		 139
B.1	Introduction	139
B.2	Revisiting the MMC equations	140
B.2.1	State equations	140
B.2.2	Control equations	140
B.3	Single-phase MMC stability proof	141
B.3.1	Deviation variables equation system	142
B.3.2	Global asymptotic stability	142
B.4	Three-phase voltage source MMC stability proof	144
B.4.1	Deviation equations	144
B.4.2	Global asymptotic stability	147
B.5	Conclusion	149

CONTENTS

List of Figures

2.1	2-level VSC topology	11
2.2	2-level VSC typical waveform	11
2.3	Principle of operation of the multilevel converter	12
2.4	MMC typical waveform	12
2.5	Topology of a general phase of the modular multilevel converter	13
2.6	Two most common basic structures of a SM: a) half-bridge structure, b) full-bridge structure	13
2.7	Current flowing in the SM semiconductor devices in normal operation: a) active SM and positive current, b) active SM and negative current, c) bypassed SM and positive current, d) bypassed SM and negative current	14
2.8	SM equivalent representation for blocked operation	15
2.9	Ideal Switches SM Equivalent Representation for Normal Operation	15
2.10	6-level MMC individual capacitor waveforms using an ideal balancing algorithm	17
2.11	6-level MMC individual capacitor waveforms using a more efficient balancing algorithm	17
2.12	31-level MMC upper arm individual capacitor waveforms sorting at 100Hz	18
2.13	31-level upper and lower MMC multi-valve voltage outputs	18
2.14	Topology of a grid-connected single-phase modular multilevel converter	19
2.15	Topology of a grid-connected three-phase modular multilevel converter	19
2.16	Reduced circuit model based on ON/OFF resistors: a) SM equivalent representation, b) equivalent multi-valve	30
2.17	Multi-valve Thévenin's equivalent based on ON/OFF resistors	31
2.18	Controlled voltage sources-based MMC model representation	32
2.19	Models comparison and validation under balanced and unbalanced grid conditions	37
2.20	Zoom-in on balanced conditions for models validation	37
2.21	Model validation: upper and lower multi-valve outputs	37

LIST OF FIGURES

2.22	Zoom-in on unbalanced event for models validation	38
2.23	MMC models validation under a permanent DC fault with no blocking state	38
2.24	MMC models validation under a permanent DC fault	39
2.25	Modified version of the MMC controlled voltage sources-based multi-valve model suitable for representing the blocking/de-blocking action of the SMs	40
2.26	MMC models validation under a non-permanent DC fault	40
2.27	Open Loop Control Scheme	46
2.28	Circulating current suppression control scheme	48
2.29	Arm energy closed-loop control scheme	49
2.30	Decoupled double synchronous reference frame (DDSRF) control for 3-phase MMC	51
3.1	MMC phase control scheme	67
3.2	Multi-resonant shunt control structure for the circulating current	69
3.3	Steady state MMC variables: a) MMC arm capacitor sum and b) circulating current under the constant circulating current scenario $\alpha = 0$. c) MMC arm capacitor sum and d) circulating current under the constant energy sum scenario $\alpha = 1$	70
3.4	MMC capacitive energy variables: a) MMC capacitive energy sum and b) difference under the constant circulating current scenario $\alpha = 0$. c) MMC capacitive energy sum and d) difference under the constant energy sum scenario $\alpha = 1$	70
3.5	Dynamic performance of the MMC state variables: MMC capacitor voltages with a) $\alpha = 0$ and c) $\alpha = 1$. Circulating currents with b) $\alpha = 0$ and d) $\alpha = 1$	71
3.6	Dynamic performance of the MMC capacitive energy variables: energy sum with a) $\alpha = 0$ and c) $\alpha = 1$. Energy difference with b) $\alpha = 0$ and d) $\alpha = 1$	71
3.7	CCSC vs. proposed control strategy; Part I: (a-b) 3-phase MMC capacitive energy, (c-d) phase-independent average capacitive energy	72
3.8	CCSC vs. proposed control strategy: (a-b) circulating currents, (c-d) average value of the phase energy difference between upper and lower arms	72
3.9	Capacitive energy sum by arm $w_{\Sigma k}$ under different step reference change per phase: closed loop control (CLC) [3] vs. control proposal	72
3.10	Circulating currents using a) close loop control and the control proposal with b) $\alpha = 0$ and c) $\alpha = 1$	73
3.11	Schematic representation of an MMC-based HVDC system	73
3.12	MMC-HVDC station I - energy references step changes. a) Energy sum, b) energy difference, c) MMC capacitor voltages, d) circulating currents and e) DC Link Voltage.	73
3.13	MMC-HVDC station II- energy references step changes.a) Energy sum, b) energy difference, c) MMC capacitor voltages, d) circulating currents and e) active power.	74

3.14	MMC-HVDC station I - Power references step changes. a) Energy sum, b) energy difference, c) MMC capacitor voltages, d) circulating currents and e) DC Link Voltage.	74
3.15	MMC-HVDC station II - Power references step changes. a) Energy sum, b) energy difference, c) MMC capacitor voltages, d) circulating currents, e) active and reactive power.	74
4.1	Explicitly frequency-adaptive SOGI-QSG	81
4.2	Frequency Response of SOGI-QSG	81
4.3	Generation of circulating current minimized reference using Power, Voltage and Energy Estimations based-on 4 SOGI-QSG	82
4.4	Internal emf (e_{vk}) for a 5-level MMC	84
4.5	Circulating currents reference (i_{ck}^*): a) Without adaptive filters and b) with adaptive filters	85
4.6	Resulting circulating currents (i_{ck}): a) Without adaptive filters and b) with adaptive filters	85
4.7	Instantaneous MMC single-phase power (p_{vk}): a) Without adaptive filters and b) with adaptive filters.	85
4.8	Average MMC single-phase power ($\overline{p_{vk}}$) calculated using a) Low Pass Filters (LPF) and b) SOGI-based adaptive filters.	86
4.9	MMC Internal voltage RMS calculated using a) Low Pass Filters (LPF) and b) SOGI-based adaptive filters	86
4.10	Capacitive Energy Sum between MMC arms $w_{\Sigma k}$ resulting from the proposed control strategy using a) low-pass filters and b) using SOGI-based adaptive filters	86
4.11	Capacitive Energy Difference between MMC resulting from the proposed control strategy using a) Low Pass Filters and b) Adaptive filters	87
4.12	MMC Upper and Lower Capacitor Voltages Sum per phase (u_{ck}^{Σ}) resulting from the proposed control strategy using a) Low Pass Filters and b) Adaptive filters	87
4.13	MMC circulating currents (i_{ck}) resulting from the proposed control strategy using a) Low Pass Filters and b) Adaptive filters	87
4.14	a) MMC arm capacitor voltage sum under unbalanced reference change and b) circulating currents, both resulting from the proposed control strategy using SOGI-adaptive filters. Behavior under different reference step changes per phase.	88
4.15	Overview of the laboratory setup for verification of the proposed control strategy	88
4.16	SM Equivalent Representation for Blocked Operation	89
4.17	Current flowing in the SM Semiconductor devices in normal operation: a) Bypassed SM and Positive Current, b) Active SM and Positive Current	90

LIST OF FIGURES

4.18 Pre-charging the SM capacitors of the single phase MMC lab prototype before normal operation: a) Sequential charging of SM capacitors, b) circulating and load currents 90

4.19 Turning on the proposed control strategy at t=40.9: a) MMC 2N SM Capacitors, b) Circulating and Load currents 90

4.20 Load change: 10Ω to 60Ω, and back again: a) MMC SM capacitor voltages, b) MMC Circulating and load currents 91

4.21 Energy sum reference step change: a) MMC SM capacitor voltages and b) circulating and load currents under a energy sum reference increase; c) MMC SM capacitor voltages and d) circulating and load currents under a energy sum reference decrease. 91

4.22 Energy difference reference step change: a) MMC SM capacitor voltages and b) circulating and load currents under a energy difference reference increase; c) MMC SM capacitor voltages and d) circulating and load currents under a energy difference reference decrease. 91

4.23 Effect of changing the balancing frequency in the SM capacitor voltages under the proposed control strategy 92

4.24 Effect of changing the balancing frequency on the MMC circulating and load currents under the proposed control strategy 92

4.25 Effect of changing the balancing frequency on the MMC output voltage under the proposed control strategy 92

5.1 Reduced model of the MMC to emphasize its energy buffering capacity, view from a macroscopic perspective. 97

5.2 Schematic diagram of the proposed control 103

5.3 Thévenin’s grid equivalent voltage 104

5.4 MMC variables during under unbalanced grid operation using the former circulating current reference formula. a) Grid currents, b) grid active power, c) MMC capacitive phase energy, d) power at the MMC DC terminals 104

5.5 MMC variables during under unbalanced grid operation using the former circulating current reference formula. a) MMC capacitor voltages, b) circulating currents, c) energy difference between arms d) reactive power. 105

5.6 MMC variables during unbalanced grid operation. Part I: a) Grid Currents, b) Grid Active Power, c) MMC capacitive phase energy, d) power at the MMC DC terminals 105

5.7 MMC variables during unbalanced grid operation. Part II: a) MMC capacitor voltages, b) circulating currents, c) energy difference between arms d) reactive power 105

5.8	Power at the DC terminals of the MMC facing an unbalanced grid operation between $t = 200ms$ and $t = 600ms$, under the following control schemes: a) CCSC, b) control proposal with main power reference assignment by P_{ac}^{ref} c) control proposal with main power reference assignment by P_{dc}^{ref}	108
5.9	Establishing the main power reference at the AC grid PCC via P_{ac}^{ref} - MMC variables during an unbalanced grid operation between $t = 200ms$ and $t = 600ms$. a) grid currents, b) grid active power, c) MMC capacitive phase energy, d) power at the MMC DC terminals; e) MMC capacitor voltages, f) circulating currents, g) energy difference between arms h) reactive power.	109
5.10	Establishing the main power reference at the DC terminals via P_{dc}^{ref} - MMC variables during an unbalanced grid operation between $t = 200ms$ and $t = 600ms$. a) grid currents, b) grid active power, c) MMC capacitive phase energy, d) power at the MMC DC terminals; e) MMC capacitor voltages, f) circulating currents, g) energy difference between arms h) reactive power. e) MMC capacitor voltages, f) circulating currents, g) energy difference between arms and h) reactive power. . .	109
6.1	MMC control scheme: global tracking passivity-based PI with proposed virtual energy state and control variables estimator	118
6.2	Proposed state and control variable estimator -based on virtual MMC energy model	120
6.3	MMC $2N$ Individual Capacitor Voltages, b) MMC output voltage	123
6.4	Phase-independent control of a single phased MMC: a) Circulating Current, b) Grid current and c) MMC Sum of capacitor voltages by arm.	123
6.5	Phase-independent control of a single phased MMC: a) Passive output and b) Insertion Indexes.	123
6.6	Voltage at the point of common coupling	124
6.7	Power and energy trends establishing the primary power reference at the AC grid PCC, via the grid currents: a) Power at the dc terminals (in red) and at the PCC of the AC grid (in blue) and b) MMC 3-phase aggregate capacitive energy	124
6.8	Power and energy trends establishing the primary power reference at the DC terminals of the MMC, via the circulating currents: a) Power at the dc terminals (in red) and at the PCC (in blue) and b) MMC 3-phase aggregate capacitive energy . .	125
6.9	MMC state variables references and measures (x_* & x): a) circulating currents, b) grid currents and c) capacitor voltages sum per arm - phase "a" d) passive outputs and e) insertion indexes	125
6.10	MMC state variables references and measures (x_* & x): a) circulating currents, b) grid currents and c) capacitor voltages sum per arm - phase "a" d) passive outputs and e) insertion indexes	125
B.1	Single phase MMC with I_{vk} and V_{dc} considered as perturbations	141
B.2	Three-phase MMC acting as a voltage source	144

LIST OF FIGURES

List of Tables

2.1	Simulation parameters for MMC models comparison and validation	36
2.2	Waveform color legend for the 8 different MMC models	36
2.3	Qualitative comparison between state of the art high level control schemes and justification of new proposal	57
3.1	MMC Parameters	70
3.2	HVDC Parameters	75
4.1	Low number of levels MMC Parameters	84
4.2	Experimental setup parameters	88
4.3	PI parameters	89
5.1	MMC parameters	104
6.1	MMC Parameters	124

Nomenclature and Abbreviations

Symbols

In general, uppercase symbols express constant values regardless of whether they are references established by the control action or simply the result of an averaging technique. Lowercase symbols express instantaneous time-varying variables.

i_c	Circulating Current [A]
u_c	Driving Voltage of the Circulating Current [V]
i_v	Grid Current [A]
e_v	Driving Voltage of the Grid Currents [V]
i_u	Upper Arm Current [A]
i_l	Lower Arm Current [A]
$u_{c(i)}$	Individual Capacitor Voltage [V]
u_c^Σ	Sum of the capacitor voltages within an <i>arm</i> .
$v_{c(i)}$	Voltage output of an individual sub-module [V]
v_c	Voltage output of a multi-valve [V]
v_{dc}	Voltage between the DC terminals of the MMC [V]
v_{pcc}	Voltage at the point of common coupling [V]
v_{mmc}	Output AC voltage of the MMC [V]
$n_{(i)}$	Insertion Index of the Individual Sub-Module i
n	Insertion Index of the Multi-Valve
n_u	Upper Arm Insertion Index
n_l	Lower Arm Insertion Index
g	Gate Signal of the IGBT
m	Modulation Index
w_u	Upper arm capacitive energy [J]

NOMENCLATURE AND ABBREVIATIONS

w_l	Lower arm capacitive energy [J]
w_Σ	Sum of the capacitive energies between the upper and lower arms [J]
w_Δ	Difference between the capacitive energies of the upper and lower arm [J]
p	Instantaneous power [W]
P, p	Active power [W]
Q, q	Reactive power [VAr]
S	Apparent power [VA]
P_{ac}	Active power at the AC point of common coupling
P_{dc}	Power at the DC terminals of the MMC
D	Diode
C	Sub-Module Capacitance [F]
L	Arm Inductance [H]
R	Arm Resistance [Ω]
L_f	Filter (Grid-side) Inductance [H]
R_f	Filter (Grid-side) Resistance [R]
L'	Equivalent grid inductance [H]
R'	Equivalent grid resistance [R]
N	Number of Sub-Modules in a MMC arm
t	Time [s]
f	Frequency [Hz]
T	Period-time of periodic signal [s]
ΔT	Simulation time step [s]
ω	Angular frequency [rad/s]
γ	Phase angle [rad]

Subscripts

u	Upper Arm
l	Lower Arm
v	Grid variable
k	Generic phase "k"
$p.u.$	Variable is in per unit
Σ	Sum between the upper and lower arm
Δ	Difference between the upper and lower arm
abc	Three-phase quantities in the natural reference frame
$\alpha\beta$	Quantities in the stationary $\alpha\beta$ reference frame
dq	Quantities in the rotating synchronous dq reference frame
\star	Equilibrium trajectory in steady state

Superscripts

ref, \star	Reference Value
$+$	Positive Sequence Quantity
$-$	Negative Sequence Quantity
o	Zero Sequence Quantity
3φ	Aggregate three phase quantity
$\overline{(\cdot)}$	Denotes Average Values of Physical Variables
rms	Rout Mean Squared Value
$\hat{(\cdot)}$	Estimated Variable using Adaptive Filters
$\tilde{(\cdot)}$	Incremental Representation: $\tilde{(\cdot)} = (\cdot) - (\cdot)_{\star}$
$\dot{(\cdot)}$	Derivative
\top	Transpose
λ	Lagrange multiplier
\mathcal{L}	Lagrange function
V	Storage Function
x	State Variable Vector of the MMC
u	Control Variable Vector of the MMC
y	Passive output of the MMC

Abbreviations

MMC	Modular Multilevel Converter
PCC	Point of Common Coupling
SM	Sub-Module
HB	Half Bridge
FB	Full Bridge
VSC	Voltage Source Converter
HVDC	High Voltage - Direct Current
SOGI	Second Order Generalized Integrator
QSG	Quadrature Signal Generator
THD	Total Harmonic Distortion
PLL	Phase Lock Loop
LPF	Low Pass Filter
OLC	Open Loop Control
CLC	Closed Loop Control
DDSRF	Double Decoupled Synchronous Reference Frame
DM	Direct Modulation
CCSC	Circulating Current Suppression Controller
PWM	Pulse Width Modulation
SVM	Space Vector Modulation

Résumé de la thèse en Langue Française

Dans le cadre du programme de croissance Européen 2020, la commission européenne a mis en place officiellement un chemin à long terme pour une économie à faible émission de carbone, en aspirant une réduction d'au moins 80% des émissions de gaz à effet de serre, d'ici 2050. Répondre à ces exigences ambitieuses, impliquera un changement majeur de paradigme, et notamment en ce qui concerne les infrastructures du réseau électrique. La forme du futur réseau électrique sera inévitablement caractérisée par sa capacité d'intégrer différentes sources d'énergies renouvelables à grande échelle : à partir de sources d'énergies offshore comme les parcs éoliens, ainsi que des sources terrestres, comme par exemple l'énergie solaire photovoltaïque (PV) et concentrée (CSP), l'énergie géothermique, etc. De plus, des projets d'interconnexion des réseaux électriques européens avec ceux des pays voisins (Afrique du Nord, Moyen-Orient, Russie, etc.) sont à l'étude afin de faciliter l'accès aux sources d'énergie renouvelable et en accroître le foisonnement sur le réseau électrique. Enfin, la pénétration des sources d'énergie distribuées jouera un rôle crucial dans la mutation du réseau électrique à moyen et long terme.

Indépendamment du développement de systèmes de production d'électricité décentralisés, facilité par l'émergence de smart grids, il est fort probable que des infrastructures de transport d'électricité à haute tension auront un rôle crucial à

jouer, dans l'optique de transmettre de l'énergie renouvelable à grande échelle et sur des longues distances, jusqu' aux centres de consommation importants, comme la plupart des grandes villes européennes. Il demeure difficile d'envisager une approche ne combinant pas de manière optimale ces deux paradigmes (centralisée / décentralisée).

En ce qui concerne le réseau de transport, le réseau paneuropéen ou SuperGrid, il n'existe plus de barrières technologiques à une telle réalisation puisque les liaisons haute tension à courant continu (HVDC) basés sur la technologie des convertisseurs à sources de tension ont ouvert la voie à la gestion d'un tel réseau.

Actuellement, les principaux projets sur les réseaux de transport identifiés par les acteurs du domaine électrique haute tension et soutenus par les instruments législatifs et financiers de l'Union Européenne peuvent être regroupés en quatre groupes (voir [4]):

- Le réseau offshore de la mer du Nord
- Le réseau de l'Europe de sud-ouest et de la zone-méditerranéenne
- Le réseau d'Europe centrale et du sud-est,
- Le plan d'interconnexion des marchés énergétiques Baltiques.

Les percées dans la technologie des semi-conducteurs et les avancées avec les nouvelles topologies d'électronique de puissance et leurs contrôle-commandes, ont contribué à l'impulsion donnée au processus en cours de réaliser un tel SuperGrid.

Une percée technologique majeure a eu lieu en 2003, avec le convertisseur modu-

laire multi-niveaux (MMC ou M2C), présenté par le professeur Marquardt, et qui est actuellement la topologie d'électronique de puissance la plus adaptée pour les stations HVDC. En effet, le MMC offre de nombreux avantages par rapport à ses prédécesseurs, tels que la diminution des pertes de commutation et du stress sur les modules de puissance, la structure modulaire facilite son fonctionnement et son exploitation, son adaptabilité technique au réseau HVDC, et ses faibles exigences de filtrage, pour en nommer quelques-uns.

Cependant, cette structure de conversion introduit également un certain nombre de défis relativement complexes tels que les courants "additionnels" qui circulent au sein du convertisseur, entraînant des pertes supplémentaires et un fonctionnement potentiellement instable. En outre, le MMC a comme exigence spécifique l'équilibrage de l'énergie capacitive stockée dans ses différents bras, en même temps que le transfert de la puissance entre les réseaux alternatif et continu auxquels il est connecté. Ce projet de thèse vise à concevoir des stratégies de commande "de haut niveau" pour contrôler le MMC adaptées pour les applications à courant continu-haute tension (HVDC), dans des conditions de réseau AC équilibrés et déséquilibrés. La stratégie de commande optimale identifiée est déterminée via une approche pour la conception du type "de haut en bas", inhérente aux stratégies d'optimisation, où la performance souhaitée du convertisseur MMC donne la stratégie de commande qui lui sera appliquée. Plus précisément, la méthodologie d'optimisation des multiplicateurs de Lagrange est utilisée pour calculer le signal minimal de référence du courant de circulation du MMC dans son repère naturel, capable simultanément de :

- réguler avec succès les énergies stockées dans les bras du convertisseur

- réduire les pertes et les variations de tension des condensateurs
- découpler efficacement les oscillations de puissance qui auraient lieu sur le réseau AC en cas de déséquilibres et les empêcher de se propager côté DC.

Les travaux de recherche de cette thèse ont été développés en tenant compte de deux paradigmes principaux: la nécessité d'une nouvelle philosophie de commande pour le MMC entièrement dans son repère naturel (coordonnées abc) et une méthode pour assurer la stabilité asymptotique globale visant à des applications multi-terminales. Les deux posent de nouveaux défis importants pour la commande et la sécurité du fonctionnement d'un éventuel SuperGrid. En effet, résoudre complètement tous ces défis au sein d'une seule thèse de doctorat est illusoire. Par conséquent, l'accent a été mis sur quatre tâches principales:

1. calcul de la référence optimale pour le courant circulant du MMC en utilisant la méthode des multiplicateurs de Lagrange, en coordonnées de phases "abc";
2. commande linéaire du courant circulant en boucle fermée dynamiquement performante;
3. utilisation du convertisseur MMC comme pare-feu pour les oscillations en puissance;
4. stabilisation du convertisseur MMC via l'emploi de commandes passives;

L'étude et l'analyse théorique ont été complétées par des simulations avec Matlab / Simulink, EMTP et OPAL-RT, et validées sur un prototype expérimental de convertisseur MMC.

La thèse est organisée de la manière suivante. Après une courte introduction, le chapitre 2 présente la topologie du MMC et les équations dynamiques permettant de décrire mathématiquement son fonctionnement. La stratégie de modulation du convertisseur est analysée, et un système de classification est proposé concernant la modulation. De plus, huit modèles de simulation du convertisseur, avec différents degrés de simplification, sont détaillés, étudiés, comparés et validés par rapport à un modèle de référence. Le chapitre se termine par une discussion sur les stratégies de commande issues de la littérature identifiées lorsque ce projet a été entrepris. Un examen de l'existant vis-à-vis des objectifs fixés initialement a justifié la nécessité d'une nouvelle stratégie de commande pour le courant circulant.

Dans le chapitre 3, un nouveau système de commande pour permettre la régulation indépendante par phase de l'énergie stockée au sein du MMC dans son repère naturel et basé sur l'optimisation mathématique est présenté.

Dans le chapitre 4, la réponse dynamique de la stratégie de commande proposée est améliorée alors que la sensibilité harmonique est réduite en utilisant des filtres adaptatifs basés sur les intégrateurs généralisés de second ordre pour estimer les variables de tension, puissance et énergie monophasées. De plus, la stratégie de commande proposée est validée expérimentalement sur un démonstrateur de MMC.

Le chapitre 5 étend les résultats précédents pour y inclure le cas déséquilibré, résultant en une stratégie alternative de commande en mesure d'assurer une puissance constante aux bornes DC du MMC indépendamment du réseau AC. Cette nouvelle stratégie est

également obtenue en utilisant la méthode d'optimisation mathématique basée sur les multiplicateurs de Lagrange.

Enfin, le chapitre 6 explore les possibilités de garantie de la stabilité d'un MMC avec l'utilisation d'un régulateur PI basé sur la méthode non-linéaire de la passivité et d'un estimateur en boucle fermée utilisant un modèle virtuel de l'énergie du MMC. Cette stratégie résulte de la nécessité d'une approche locale pour assurer la stabilité d'un système plus complexe, tel qu'un SuperGrid.

Un résumé de la thèse avec des observations finales et un aperçu des sujets de recherche futurs sur la base des résultats présentés est donné dans le chapitre 7.

Un résumé de chacun des chapitres est présenté ci-dessous.

La technologie des convertisseurs sources de tensions (VSC) et l'apparition du convertisseur modulaire multi-niveau (MMC)

Le transistor bipolaire à grille isolée (IGBT) a été utilisé comme composant élémentaire pour la construction des valves de convertisseur HVDC à la fin des années 1990. Contrairement aux thyristors, l'IGBT est capable d'interrompre le courant chaque fois qu'il est nécessaire de le faire, indépendamment de la tension alternative du réseau. Cette apparente petite différence a permis le développement d'un nouveau champ d'application pour la technologie HVDC [12]. L'utilisation d'IGBTs a exigé un changement conséquent dans la façon dont les stations HVDC ont été conçues et contrôlées

pour aboutir à la réalisation de stations VSC (Voltage Source Converter). Comme les convertisseurs sont "auto-commutables" un réseau AC fort n'est pas nécessairement requis, offrant la possibilité d'interconnecter des réseaux totalement passifs. En outre, le VSC peut bénéficier des fréquences de commutation plus élevées (1-2 kHz) pour réduire l'encombrement par rapport aux convertisseurs commutés en ligne (LCC), avec des filtres de tailles réduites pour atténuer les harmoniques haute fréquence [14]. Enfin, la topologie VSC permet de contrôler indépendamment la puissance active et réactive [12] en ajoutant un important degré de flexibilité dans le système électrique.

Les convertisseurs de source de tension ont traversé une série distincte de transformations. Les premières générations de VSC étaient fondées sur des topologies deux niveaux en utilisant des techniques de "Modulation par Largeur d'Impulsion" (MLI ou PWM) avec des fréquences de commutation élevées (kHz), ce qui entraîne d'importantes pertes de conversion avec les modules de puissance employés (3%) [13]. Ce type de VSC à deux niveaux, a été commercialisé par ABB sous le nom "HVDC Light 1ère Génération" à partir de 1997. La deuxième génération de VSC de ABB a dérivé de la topologie *Neutral Point Clamped* (NPC) à trois niveaux, réduisant les pertes totales de 3% à 1,8% [14]. Leur 3ème génération de VSC qui est apparu en 2006 a diminué les pertes d'un facteur plus important (1,4%) malgré un retour à la topologie deux niveaux en bénéficiant d'une MLI optimisée.

L'évolution la plus récente dans les topologies VSC est le convertisseur modulaire multi-niveaux (MMC) proposé par le Prof. Marquardt [2]. Il a été introduit commercialement par Siemens en 2010 sous le nom de "HVDC Plus" dans le projet "Trans

Bay Cable” aux Etats-Unis, fonctionnant à 400 MW et ± 200 kV. On estime que la structure MMC permet de réduire encore les pertes (entre 0,9% et 1%) et n’a presque pas de besoins de filtrage. Les produits commerciaux “HVDC MaxSine” d’Alstom et “HVDC Light 4ème génération” d’ABB ont introduit des concepts similaires basés sur le MMC en 2014 et 2015, respectivement [13]. L’approche multiniveau modulaire n’offre théoriquement aucune limite sur le nombre de modules [12]. Chacun des sous-modules individuels est commandé pour générer un petit échelon de tension, agissant en tant que source de tension discrète. En contrôlant de façon incrémentielle chaque étape, une tension presque sinusoïdale est générée à la sortie alternative des “multi-valves,” ce qui réduit significativement la nécessité du filtrage.

Motivation pour une nouvelle stratégie de régulation du courant de circulation du MMC

Au début de cette thèse en 2011, seule une poignée de stratégie de commande pour la topologie MMC a pu être trouvée dans la littérature. Dans la section 2.9 de ce manuscrit, les stratégies de commande qui ont influencé le plus les résultats de cette thèse sont examinées. Ces stratégies de commande sont comparées avec la proposition de ce manuscrit, dans les paragraphes ci-dessous.

La stratégie de modulation directe [3] n’a pas pour objectif de contrôler le courant circulant. Par conséquent, cette stratégie n’est pas considérée comme un candidat approprié pour commander le MMC en raison du risque de fonctionnement instable et des possibles résonances. Cependant, celle-ci fournit un outil puissant et très simple pour

l'analyse de l'interaction des différents harmoniques qui se produisent dans le MMC, pour le dimensionnement et pour la sélection de manière adéquate des paramètres du convertisseur, comme cela a été démontré avec succès par Ilves et al dans [28], et [40].

La stratégie de commande en boucle ouverte [3, 7] continue à être l'une des stratégies les plus attrayantes pour commander le MMC. Son avantage principal est sa simplicité de mise en œuvre: les indices d'insertion sont uniquement calculés sur la base de l'estimation du point d'équilibre, et implémentés "en boucle ouverte," excluant la nécessité de toute boucle de rétroaction. D'ailleurs, il a été démontré à l'aide des critères de stabilité de Lyapunov dans [31] que le MMC avec cette stratégie en boucle ouverte est globalement asymptotiquement stable. Cependant, ceci est un phénomène assez commun de très nombreux systèmes étant globalement asymptotiquement stable en boucle ouverte. La fermeture de la boucle présente un fort intérêt pour assurer la robustesse à l'égard des perturbations, des erreurs dans le processus d'estimation du point d'équilibre, et des incertitudes paramétriques. L'ensemble de ces points sont pertinents dans le cadre de l'étude du MMC, ce qui suggère qu'une boucle de rétroaction pour les courants et tensions pourrait s'avérer utile.

De plus, une limitation des systèmes en boucle ouverte est le temps de réponse imposé par les constantes de temps propres au système. En fermant la boucle, la performance dynamique peut être modifiée avec l'action de commande en boucle fermée. La stratégie en boucle fermée proposée dans [3] a pu résulter en un comportement instable si seules des boucles de rétroaction pour les tensions de condensateurs ont été employées, sans régulation du courant circulant, justifiant alors l'emploi d'une boucle ouverte.

Le *Circulating current suppression controller (CCSC)* [17], contrairement à la commande en boucle fermée de [3], présente une boucle de rétroaction pour réguler le courant interne mais sans régulation de la tension des bras des condensateurs. La boucle de rétroaction assure la robustesse et une bonne performance dynamique pour le courant, mais le système de commande complet comportant la régulation des variables de tension n'est pas proposé. De plus, l'implémentation du contrôleur dans le repère tournant "DQO" présente l'inconvénient de ne pas fournir un contrôle direct et explicite du courant circulant indépendamment par phase.

Le contrôle *DDSRF* du MMC proposé dans le cadre de cette thèse [J0], est une tentative de prolonger le CCSC en incluant une boucle de régulation pour l'énergie des condensateurs des bras du MMC, tout en gardant une boucle de régulation pour le courant circulant afin d'assurer de bonnes performances dynamiques et la robustesse du contrôle de l'ensemble des variables du convertisseur. Le principal inconvénient de cette technique de commande est sa complexité: la méthode est également dans le repère tournant en coordonnées "DQO," nécessitant plusieurs transformations du cadre de référence à cause des différentes fréquences présentes dans le MMC, naturellement couplées.

Un deuxième inconvénient significatif de l'utilisation des coordonnées "DQO" est la difficulté de commander les valeurs moyennes de l'énergie capacitive stockée dans les différent bras du MMC, indépendamment par phase. Seules les valeurs homopolaires peuvent être régulées. En d'autres mots, c'est l'addition des valeurs des variables des trois phases qui peut être contrôlée directement et non la valeur moyenne dans chaque phase. Ce n'est pas un problème dans les convertisseurs classiques VSC à deux-niveaux

car les courants dans chaque phase n'ont pas de composantes continus. Au contraire, l'énergie stockée dans un convertisseur MMC et ses courants internes présentent une composante continue importante dans chaque phase. De ce fait, réguler les variables du MMC indépendamment s'avère avantageux.

Pour conclure, une nouvelle stratégie de commande du MMC a été jugée nécessaire. Un tel système de commande doit être basé sur quatre boucles d'asservissement, à savoir une pour chacune des variables d'état du MMC afin de garantir la robustesse. Cette stratégie doit être développée dans le repère naturel stationnaire en utilisant les coordonnées "abc" pour réduire la complexité de mise en œuvre et permettre la régulation des variables du convertisseur de façon indépendante par phase. En outre, cette stratégie doit avoir une bonne performance dynamique.

Optimisation du signal de référence du courant circulant pour le contrôle de l'énergie indépendamment par phase

Le comportement dynamique du convertisseur modulaire multi-niveaux (MMC) a été étudié [3, 7, 8], et des tentatives ont été faites afin de le modéliser efficacement [9, 10, 11, 27]. Bien que la topologie du MMC puisse paraître assez simple, la tâche de réguler l'énergie capacitive de ses bras, tout en effectuant un transfert de puissance stable est relativement complexe. Cette question a éveillé l'intérêt de nombreux chercheurs et a conduit à un certain nombre de publications telles que celles examinées dans le chapitre 2 [3, 29, 17, 39], ainsi que d'autres efforts importants tels que [7, 3, 41, 42, 43,

29, 44, 45, 17, 39, 46], y compris des propositions de commandes prédictives [47, 48, 49, 50, 51, 52] et des stratégies de commande pour les défauts asymétriques [33, 32]. La plupart des stratégies de commande proposées jusqu'à présent ont profité du fait que le convertisseur MMC fonctionne avec deux courants pratiquement indépendants (i.e. le courant de charge ou côté réseau, et le courant circulant aussi appelé différentiel). Le courant côté réseau est généralement utilisé soit pour contrôler la puissance active soit pour réguler la tension du bus continu. En outre, il peut fournir un support de tension AC en injectant de manière adéquate la puissance réactive nécessaire, tel qu'un convertisseur source de tension de deux ou trois niveaux.

Par contre, le courant différentiel, qui pourrait être défini comme un courant qui circule naturellement "à l'intérieur" du MMC sans interagir directement avec le réseau AC, a été utilisé dans plusieurs propositions de commande pour équilibrer et distribuer l'énergie totale du MMC entre chaque bras [3]. Ce courant a également été régulé de manière à éliminer son ondulation naturelle à deux fois la fréquence du réseau [17]. Des publications précédentes tels que [53] et [J0] ont proposé une solution dans laquelle une composante harmonique du courant différentiel, avec une fréquence de deux fois la fréquence fondamentale du réseau, est rajoutée afin de réduire les oscillations de tension. Compte tenu du nombre élevé de condensateurs dans le MMC pour les applications HVDC et du fait que les condensateurs DC sont sensibles aux variations de tension, la taille du convertisseur peut être notablement réduite avec une telle solution. Pour cela, l'énergie capacitive stockée dans chaque phase doit être maintenue constante, tandis que la différence d'énergie moyenne entre les multi-valves supérieures et inférieures est maintenue à zéro. Certaines des régulations permettant d'atteindre

cet objectif ([J0]) sont obtenues dans un ou plusieurs systèmes de référence synchrones, exigeant l'utilisation de transformations mathématiques en combinaison avec la théorie de la puissance instantanée de [54].

Cette méthodologie complique la réalisation de cette tâche, car il existe un couplage fort entre les variables d'énergie dans le repère tournant "dqo", et le découplage n'est pas toujours simple. Pour surmonter cet obstacle, les théories de puissance en repère naturel, dites en abc, sont préférés. Plusieurs auteurs ont recherché des théories de puissance instantanée appropriées dans le repère naturel pour calculer la référence du courant, y compris [55, 56, 57, 58]. Néanmoins, la plupart de ces théories n'aboutissent pas nécessairement au point de fonctionnement optimal. Par conséquent une approche généralisée fondée sur l'optimisation mathématique en utilisant la méthode des multiplicateurs de Lagrange dans un cadre ABC est préférée. Cette stratégie, proposé dans [54] et généralisée dans [59], renforce la théorie classique de puissance en ABC [60] pour la compensation de puissance réactive et le filtrage actif. En raison de la généralité et la polyvalence de cette méthode basée sur les multiplicateurs de Lagrange, il est possible d'appliquer cette technique d'optimisation aux MMC, menant à une approche générale de commande de puissance dans le repère naturel stationnaire (ABC) dédiée. Un premier essai a été publié dans [C6]. Néanmoins, il s'agit là de résultats obtenus à un stade encore très précoce. Par la suite, des améliorations significatives et claires ont été faites et les principales conclusions ont été publiées dans [J1] et [C10], via une reformulation de l'ensemble du problème d'optimisation mathématique pour obtenir un système de commande plus simple et plus efficace. Cette stratégie de commande pour le MMC basée sur l'optimisation mathématique est une des contributions principales

de cette thèse.

Estimation du courant différentiel basée sur des filtres adaptatifs: pour une dynamique rapide et un THD réduit

Générer les signaux de référence du courant différentiel en utilisant l'optimisation mathématique dans le repère naturel, et sa mise en œuvre en utilisant les contrôleurs de courant multi-résonants offre plusieurs avantages: régulation indépendante des valeurs moyennes de l'énergie du MMC stockée dans chaque bras d'une manière directe et explicite et capacité de contrôler le courant de circulation et les formes d'onde des somme d'énergies capacitives. En plus de la régulation indépendante par phase, le courant de référence résultant donne un aperçu utile sur le comportement du MMC, pour améliorer la compréhension du convertisseur ou pour estimer les points d'équilibre du MMC, pour être par exemple utilisés dans la conception de commandes non-linéaires. Finalement, la stratégie de commande proposée est robuste car elle repose sur quatre boucles de rétroaction par phase (c'est-à-dire, deux pour les énergies capacitives et deux pour les courants). Ceci implique que, dans certaines conditions, la commande n'est pas sensible aux paramètres du MMC, ni à des erreurs dans l'estimation du point d'équilibre, ou à des perturbations indésirables.

Bien que cette approche ait montré son utilité et sa polyvalence, deux inconvénients restaient à éliminer afin de l'améliorer:

1. L'utilisation de la valeur moyenne des variables sinusoïdales (via des filtres passe-bas LPF) pour la génération du courant différentiel de référence entraîne une dy-

namique relativement lente.

2. l'interaction des harmoniques avec le régulateur lorsqu'il est employé sur un MMC constitué d'un faible nombre de niveaux.

La deuxième contribution de cette thèse a été de résoudre ces problèmes avec l'utilisation de filtres adaptatifs basés sur des intégrateurs généralisés de second ordre (SOGI), configurés comme des générateurs de signal en quadrature (QSG), pour estimer les variables d'entrée nécessaires pour le calcul des références du courant différentiel, tel qu'a été publié dans [C12]. Avec cette stratégie, les variables d'entrée ont une performance dynamique supérieure par rapport à l'utilisation de filtres passe-bas alors que le THD des signaux de référence est simultanément réduit. En plus d'améliorer la dynamique de la commande et de faciliter le réglage des contrôleurs du système, l'utilisation des filtres adaptatifs offre une capacité intrinsèque pour un fonctionnement avec des variations de fréquence, particulièrement utile pour implémenter une telle commande aux MMC opérant dans des réseaux faibles ainsi que pour des entraînements motorisés en haute ou moyenne tension.

Dans cette thèse, les filtres adaptatifs basés sur les SOGIs ont été utilisés avec succès pour l'amélioration de la performance de la stratégie de commande proposée dans le chapitre 3, où l'optimisation mathématique à partir des multiplicateurs de Lagrange a permis de déterminer les signaux de référence du courant différentiel dans les coordonnées naturelles "abc" pour commander le MMC. Plus précisément, quatre filtres adaptatifs basé sur les SOGI ont été utilisés pour estimer la composante de fréquence fondamentale et l'amplitude des valeurs instantanées et efficace de la tension interne du MMC, les valeurs instantanées et moyennées de la puissance de sortie, et les valeurs

moyennes de la somme et de la différence de l'énergie capacitive des bras du MMC, utilisées comme variables d'entrée pour l'équation de génération de référence du courant différentiel. L'amélioration de la performance dynamique du régulateur, la réduction de la sensibilité à la distorsion harmonique des signaux de commande et la simplicité de mise au point des paramètres de régulation ont été permis par l'emploi des filtres adaptatifs.

Ceci a été validé à partir de résultats de simulation ainsi qu'avec un démonstrateur expérimental monophasé de 11 niveaux. Ainsi, la commande présentée semble adaptée pour contrôler la dynamique interne des MMC, aussi bien pour des applications dans le transport d'électricité ainsi que pour des applications de commande de machines, quel que soit le niveau de tension et le nombre de sous-modules.

Calcul de la référence du courant différentiel pour maintenir la puissance constante en régime déséquilibré

Pour les systèmes HVDC utilisant la technologie de convertisseur de sources de tension (VSC), et surtout pour les futurs systèmes multi-terminaux, il sera d'une grande importance d'éviter que les oscillations de puissance provoquées par des conditions déséquilibrées sur le réseau AC ne se propagent dans le système DC. Pour les convertisseurs VSC conventionnels à 2 ou 3 niveaux, ceci est un défi qui ne peut être atteint qu'en contrôlant les courants de réseau du convertisseur de sorte que le flux de puissance triphasée instantanée côté AC soit constant, comme décrit dans [77, 78, 79, 80, 81, 82, 38]. La topologie du MMC, avec son stockage d'énergie

capacitif distribué, présente un degré de liberté supplémentaire dans la commande du convertisseur qui peut être profitable lors de conditions de réseau déséquilibré. Ainsi, le MMC peut être commandé pour agir comme un pare-feu vis-à-vis des oscillations de puissance lors d'événements asymétriques, en empêchant les oscillations de puissance côté AC de se propager dans le système à courant continu. En outre, la capacité distribuée du MMC peut être contrôlée pour répondre à la tâche ci-dessus en contrôlant le courant différentiel. Cela implique que les courants de réseau du MMC peuvent être contrôlés pour d'autres fins comme par exemple maintenus équilibrés [C7].

Dans [33, 34, 35, 36, 83] et [C7], des stratégies de commande utilisant le courant différentiel ont été proposées pour résoudre ce problème. Néanmoins, elles reposent sur l'utilisation des transformations de Clarke ou Park, augmentant considérablement la complexité de la régulation indépendante des énergies des bras du MMC.

Le problème d'optimisation qui a été formulé dans cette thèse a donné lieu à la formule de référence de génération du signal du courant différentiel. Une telle procédure d'optimisation a toutefois considéré les phases du MMC totalement indépendantes. Cette formulation ne permet pas d'optimiser le fonctionnement d'un convertisseur triphasé dans des conditions de réseau AC déséquilibré.

Pour atteindre une approche adéquate pour contrôler le MMC et éviter les oscillations de puissance DC dans des conditions de réseau asymétriques, la formule de référence du courant différentiel est généralisée en incluant dans la formulation du problème d'optimisation une contrainte assurant une puissance constante aux bornes

DC du convertisseur. Il sera montré que cette procédure aboutie à une formule analytique unique pour le calcul des références pour les courants différentiels du MMC.

La nouvelle approche englobe toujours les fonctionnalités précédentes telles que la capacité de régulation de l'énergie indépendamment pour chaque bras du convertisseur, mais elle présente l'avantage supplémentaire d'assurer une puissance constante aux bornes DC. En outre, deux modes de fonctionnement sont analysés: I) courant de circulation différentiel constant et II) somme d'énergie par phase constante pour la réduction des fluctuations des tensions de condensateur du MMC. Une première tentative a été présentée dans [C11] et [C9], néanmoins la puissance aux bornes DC n'était pas exactement constante, malgré une réduction significative des oscillations. En effet, la contrainte de courant continu constant dans la formulation d'optimisation était en conflit avec la contrainte supplémentaire concernant la différence d'énergie entre les bras supérieure et inférieure, affectant négativement les performances souhaitées.

L'amélioration de ces travaux a fait l'objet des publications [J3] et [C15]. Il est également expliqué comment la référence primaire de puissance pour le MMC peut être fournie. Lorsque la référence primaire de puissance est utilisée pour le calcul de la référence du courant de réseau côté AC, la référence de puissance pour la référence du courant différentiel doit être fournie par un contrôleur qui permettra d'équilibrer l'énergie totale stockée dans le MMC, et vice-versa. Il a été observé un découplage plus efficace lors de transitoires AC entre les puissances lorsque la référence primaire de puissance est utilisée pour le calcul du courant différentiel de référence.

Une étude fournissant un aperçu des performances d'une stratégie de commande du courant de réseau en coordonnées de phases "abc" pour le MMC, avec une stratégie de commande de courant différentiel pour prévenir les oscillations en puissance du côté courant continu, manquait. Par conséquent l'évaluation de la performance de la stratégie de commande du courant différentiel présenté ici sous des stratégies de commande de courant de réseau avec trois objectifs comble ce manque : 1) puissance active constante avec des courants de réseau sinusoïdales, 2) les courants de réseau équilibrés et 3) la puissance réactive constante avec des courants de réseau sinusoïdales. Ainsi, l'influence des différentes stratégies de commande du réseau sur l'énergie stockée et les oscillations de tensions des condensateurs en conditions déséquilibrées est analysée.

Un système alternatif de commande pour réguler les courants différentiels des convertisseurs modulaires multiniveaux en coordonnées de phase ("abc"), basé la méthode des multiplicateurs de Lagrange, a été proposé dans ce manuscrit de thèse. Une telle procédure permet d'obtenir l'expression an un que le flux d'énergie constant côté DC, non-oscillant même dans des conditions déséquilibrées du réseau AC. La condition du flux de puissance non-oscillatoire côté DC du convertisseur peut être réalisée soit avec somme d'énergie capacitive constante soit avec courant différentiel constant par phase. Dans ces deux cas, la stratégie de commande du courant différentiel proposée pour le MMC est capable d'empêcher, en cas de déséquilibre entre phases, la propagation côté DC des oscillations de puissance. De plus, il a été montré qu'en établissant la référence primaire de puissance aux bornes de courant continu du MMC au moyen de la somme des courant différentiels, au lieu d'établir la référence de puissance primaire au point de couplage commun du réseau via les courants de

ligne, les oscillation en puissance en état d'équilibre et les fluctuations transitoires ou perturbations du réseau n'ont pas d'influence sur la puissance aux bornes DC du MMC tant que le fonctionnement du convertisseur est maintenu dans ses conditions nominales. Ainsi, le MMC peut être commandé pour agir comme une source constante de courant continu, qui pourrait être d'un intérêt particulier pour interfacer le MMC avec un convertisseur type source de courant, comme par exemple dans les applications HVDC hybrides. Dans les deux cas, il a été montré le potentiel du MMC à agir comme un "pare-feu d'oscillation de puissance" pour découpler efficacement le flux d'énergie entre AC et DC. Une telle opération du MMC peut être particulièrement pertinente pour les systèmes HVDC (multi-terminaux) où les fluctuations de puissance et donc des fluctuations de tension DC sont à éviter, car elles vont influencer négativement d'autres convertisseurs connectés au même réseau.

Les performances de chaque stratégie de commande sont très différentes et doivent être prises en compte dans le processus de sélection de la commande pour chaque application en particulier. Plus précisément, il a été observé que commander le MMC avec puissance réactive instantanée constante pendant un déséquilibre réduit les oscillations de la tension des condensateurs du MMC, permettant d'optimiser leur dimensionnement.

Stabilité du MMC: stabilisation basé sur la théorie de la passivité

L'intérêt de commander le MMC dans ses coordonnées naturelles se justifie afin

d'être en mesure de réguler d'une manière simple, directe et explicite l'énergie stockée dans chaque phase et bras de la topologie du MMC. La stratégie de commande proposée dans cette thèse s'avère être robuste grâce à sa nature en boucle fermée, son indépendance aux paramètres du système, et sa bonne performance dynamique. Pourtant, une telle stratégie est basée sur des contrôleurs linéaires, alors que le système est fortement non-linéaire, ne permettant pas d'assurer la stabilité asymptotique globale. La question de la stabilité asymptotique globale a été étudiée au moyen des critères de stabilité de Lyapunov dans [31, 88]. Il a été possible de démontrer la stabilité asymptotique du MMC en boucle ouverte, mais deux questions sont soulevées :

- celle de l'influence de la précision de l'estimation du point d'équilibre de de la sensibilité aux paramètres et aux perturbations extérieures;
- l'impossibilité de garantir de manière incrémentale la stabilité de l'interconnexion de multiples convertisseurs MMC différents: la validité de la preuve de la stabilité asymptotique globale de Lyapunov pour les contrôleurs en boucle ouverte ne vaut que pour le système sous étude et doit être redémontrée pour chaque nouveau système lors de l'ajout de convertisseurs.

De toute évidence, la croissance d'éventuels réseaux HVDC sera "organique", l'état final de celui-ci demeurant inconnu car en constante évolution. En outre, dans l'objectif d'interconnecter des sources d'énergie à travers le continent, il est fort probable que les caractéristiques de chaque convertisseur seront variables. Par conséquent il semble d'un grand degré de complexité d'assurer la stabilité asymptotique globale d'un réseau multi-source croissant en utilisant une approche globale. Une approche modulaire pour assurer la stabilité globale d'un réseau interconnecté est nécessaire et doit être simple à

mettre en œuvre indépendamment de la complexité de la démonstration mathématique.

La théorie de la passivité est un candidat adaptée puisqu'elle permet d'assurer la stabilité asymptotique globale d'un système [89]. De plus, une telle propriété basée sur le critère de stabilité de Lyapunov est plus puissant que le critère de Lyapunov lui-même. En effet, la passivité inclut une propriété plus forte: l'interconnexion de systèmes passifs reste passif, et donc stable. De plus, il est possible d'utiliser un régulateur PI pour rendre le système globalement asymptotiquement stable grâce à la passivité, ce qui simplifie la mise en œuvre comme cela a été fait dans [90, 91, 92, 93]. Ces contrôleurs sont connus pour être simples et robustes.

Cependant, le travail effectué dans [90, 91, 92, 93] exige que les variables d'état souhaités dans l'état d'équilibre (c'est-à-dire, les valeurs de référence du système), soient des valeurs constantes. Ceci est naturellement contradictoire avec l'objectif initial de commander le MMC en coordonnées "abc,". Par conséquent, un tel problème ne peut pas être considéré comme un problème de régulation lorsque le point d'équilibre du système est représenté par un point, mais il se transforme en un problème de traçabilité, car l'état d'équilibre devient une orbite ou une trajectoire. Par conséquent, l'extension du régulateur PI basé sur la passivité de [90, 91, 92, 93] du problème de régulation au problème de la traçabilité est nécessaire. Résoudre un tel problème a été possible grâce à la coopération avec le professeur Romeo Ortega du Laboratoire des Signaux et Systèmes, une branche de l'institut de recherche gouvernementale française CNRS. L'extension de la preuve mathématique complexe a été faite par le professeur Ortega lui-même, et a été présenté dans [C16].

La nouvelle technique de commande, nommée traçabilité globale avec un contrôleur PI basé sur la passivité, est appliquée au MMC dans cette thèse. Cependant, la mise en œuvre de cette nouvelle stratégie de commande nécessite la connaissance préalable des variables d'état et de contrôle du MMC à l'état stationnaire. Ces variables d'état stationnaire doivent être estimés, le système ne pouvant pas être résolu analytiquement. Un estimateur en boucle fermée utilisant un modèle virtuel de l'énergie du MMC sur la base des résultats précédents est proposé, permettant de contrôler de manière indépendante chaque phase du MMC et d'empêcher la propagation côté DC d'oscillations de puissance provoquées par un déséquilibre du réseau AC.

La performance de la commande a été vérifiée par des simulations. Bien que le contrôleur ait montré des résultats prometteurs, certaines erreurs dans le processus d'estimation ont été observées, principalement causées par la non prise en compte d'harmoniques d'ordre élevé et la saturation de la commande. Cela étant, de bonnes performances ont été obtenues, démontrant un certain degré de robustesse. Un autre problème est l'estimation à partir d'un modèle, qui peut être la source d'incertitudes lors de la mise en œuvre pratique.

La technique d'estimation proposée est capable de tenir compte des pertes de puissance causées par les harmoniques fondamentaux de chaque courant dans la résistance interne du MMC, souvent négligé dans les approches de "boucle ouverte". Le contrôleur assure la passivité du système ainsi que la stabilité asymptotique globale. Cette contribution est une première étape vers le contrôle de systèmes multi-terminaux basés sur les MMC

assurant la stabilité globale avec des contrôleurs locaux.

Conclusions

Deux contrôleurs sont proposés, un linéaire et un non-linéaire. Le premier contrôleur est très robuste car basé sur les contrôleurs en boucle fermée qui régulent l'énergie du MMC indépendamment des paramètres du modèle. Le second contrôleur peut être utilisé pour assurer la stabilité asymptotique globale du MMC à l'aide d'un régulateur PI basé sur la passivité.

1

Introduction

The purpose of this introductory chapter is to provide a short overview of the Thesis and present the main objectives, scope and contributions

FOLLOWING Europe's 2020 growth program, the *Energy Roadmap 2050* launched by the European Commission (EC) has officially set a long term path for a low-carbon economy, assuming a reduction of at least 80% of greenhouse gas emissions by the year 2050. Meeting such ambitious requirements will imply a major change in paradigm, including the electricity grid infrastructure as we know it. The shape of the future electricity network, will inevitably be characterized by its suitability for large-scale renewable energy integration, from offshore energy sources such as multi-megawatt wind parks, or large-scale onshore renewable generation including photovoltaic and concentrated solar power plants, geothermal, etc. Furthermore, it is expected that European electricity networks will interconnect with neighboring power grids (e.g. Northern Africa, the Middle-East, Russia, etc.) to facilitate access to renewable energy sources in both directions. Last but not least, the penetration of distributed energy sources will play a crucial role in defining the final appearance of the medium to long-term electricity grid.

Even with the advent of more decentralized power systems within the *smart grid* context, it is highly expected that large and centralized high voltage transmission grids will still play a crucial role, as they will enable the possibility of transferring large-scale clean energy over long distances to important consumer centers, such as most major European cities. It is therefore highly expected that neither architecture will prevail over the other; instead they will combine in an optimal manner.

At the transmission level, the pan-European grid or *SuperGrid*, is no longer unattainable as High Voltage-Direct Current (HVDC) links based on Voltage Source Converter (VSC) technology have enabled this possibility. Currently, the main transmission grid projects agreed upon by network stakeholders and supported by EU legislative and financial instruments can be grouped into four clusters [4]:

- North Sea Offshore Grid,

- Southwestern Europe and Mediterranean area,
- Central and Southeastern Europe,
- Baltic Energy Market Interconnection Plan.

The breakthroughs in semi-conductor technology and the advances in power electronics topologies and control have added momentum to the on-going process of turning the *SuperGrid* into a reality. Perhaps the most recent breakthrough occurred in 2003, when Prof. Marquardt introduced the Modular Multilevel Converter (MMC or M2C) which is now the preferred power electronic topology that is starting to be used in VSC-HVDC stations. This is not by chance, since the MMC offers numerous advantages over its predecessors, such as lower switching losses, modular structure facilitating operation and maintenance, its suitability for HVDC, and low filtering requirements, to name a few. It does however, introduce a number of rather complex challenges such as “additional” circulating currents within the converter itself, causing extra losses and potentially unstable operation. In addition, the MMC will be required to properly balance the capacitive energy stored within its different *arms*, while transferring power between the AC and DC grids that it interfaces.

The present Thesis project aimed to design adequate “high-level” MMC control strategies suited for HVDC applications, under balanced and unbalanced AC grid conditions. The resulting control strategy is derived with a “top-to-bottom” design approach, inherent to optimization strategies, where the desired performance of the MMC results in the control scheme that will be applied. More precisely, the *Lagrange multipliers* optimization methodology is used to calculate the minimal MMC circulating current reference signals in phase coordinates, capable of successfully regulating the capacitive *arm* energies of the converter, while reducing losses and voltage fluctuations, and effectively decoupling any power oscillations that would take place in the AC grid and preventing them from propagating into the DC grid.

1.1 Objectives

1.1.1 General objective

The main objective of this Thesis is to propose a control scheme adapted for the modular multi-level converter for high voltage direct current applications.

1.1.2 Specific objectives

- To develop a control strategy capable of regulating the average value of the capacitive energy stored in the MMC independently by arm.
- To reduce power losses caused by the second order harmonics of the MMC internal currents and individual capacitor voltages.
- To perform closed loop control with fast dynamics and reduced harmonic sensitivity.
- To prevent power oscillations caused by unbalanced grid operation from flowing into the multi-terminal DC grid.
- To gain some insight on how the MMC acts under unbalanced grid conditions.

- To find a local approach to ensure stability for the larger and more complex scenario of MMC-based multi-terminal HVDC grid.
- To construct an experimental prototype to provide proof of concept.

1.2 Main contributions

The main contribution of this Thesis are:

- Novel MMC control approach: This first contribution aims to design a method for controlling the circulating current of the MMC such that the average values of the capacitive energies stored in each of its arms are regulated at all time while reducing power losses. Previous control strategies have been based on Park and Clarke transformations, which imply dqo or $\alpha\beta o$ coordinates, that fail to access and effectively regulate the average values of the MMC variables *independently by phase*, at least in a simple and direct manner. This Thesis presents a new circulating current control approach entirely in abc coordinates: the current reference is calculated by means of mathematical optimization using Lagrange multipliers, power losses are minimized and the objective function is subject to energy regulating constraints independently by phase and arm.
- Dynamic improvements via Adaptive filters: Implementation of the resulting control strategy that yielded from mathematical optimization has suffered from sensitivity to harmonic distortion of the input control signals, especially when the MMC has a low number of levels. Moreover, the controller has experienced slow dynamics caused by its dependence on average value calculations of sinusoidal variables via low pass filters. In this Thesis, it was demonstrated that the performance of the proposed control strategy can be improved by means of adaptive filters based on second order generalized integrators for processing the system variables needed as inputs for calculating the circulating current references.
- Constant DC power control under unbalanced conditions: A second optimization formulation has been defined and solved once more by means of the Lagrange multiplier methodology resulting in an alternative circulating current control reference able to cope with unbalanced AC grid voltages.
- Establishing the system primary power reference with the circulating currents: The new circulating current equation offered the possibility of establishing the converters primary power reference at the DC terminals of the converter by means of the circulating current (via P_{dc}^{ref}), instead of imposing it at the AC point of common coupling using the grid currents (via P_{ac}^{ref}). By using this new alternative, the MMC is able to act as a “power oscillation firewall” by using its distributed capacitance for preventing *both* 1) the power fluctuations that result from unbalanced operation of the AC grid from propagating into the DC grid, as well as 2) any type of transitory perturbations.
- Local stability approach: Passivity is a characterization of the system behavior based on energy, and it can be used to asses the stability of a single system. Most importantly, the negative feedback combination of two passive systems results in a passive and stable interconnection. A contribution of this manuscript is the use of local passivity-based controllers to ensure global stability of the entire MMC-based multi-terminal system as a whole.

- MMC Passivity-based PI Controller: A novel non-linear global *tracking* controller was applied to the MMC. It consists of a linear PI that regulates two constructed signals with respect to which the incremental model of the MMC becomes passive.
- Estimation of the equilibrium trajectories of the MMC state and control variables in steady state: A closed-loop estimator was proposed to estimate the MMC variables in steady state needed as input for the non-linear controller. Such an estimator consists of a virtual MMC energy model and both of the circulating current reference equations yielded from mathematical optimization using Lagrange multipliers.

1.3 Scope

The research in this Thesis was developed considering two main paradigms: the need of a new control philosophy for the MMC entirely in *abc* coordinates and a method for ensuring global asymptotic stability aiming at multi-terminal applications. Both of them pose significant new challenges for the control and safe operation of the future *SuperGrid*. Indeed, it is not expected to completely solve all these challenges in just one PhD Thesis. Therefore, the focus was placed on 4 main tasks:

- Optimal current reference calculation via Lagrange multipliers in *abc* coordinates.
- Dynamically performing linear closed-loop current control of the system.
- Operating the MMC as a *power oscillation firewall*.
- Stabilization of the MMC via passivity.

The general approach of this research consists of a theoretical investigation, complemented with simulations with Matlab/Simulink, EMTF and OPAL-RT, and validated with an experimental prototype.

1.4 List of publications

The publications resulting from this Thesis project are listed below. The main contributions presented in this Thesis manuscript are based on the two journal papers [J1] and [J3], and the four conference papers [C16], [C15], [C12] and [C10]. Although the remaining publications are not directly related to the main results, they paved the way for obtaining the findings presented here.

Journal papers:

- [J3] G. Bergna, J.A. Suul, E. Berne, P. Egrot, J.-C. Vannier, A. Arzandé, M. Molinas, "MMC Differential Current Reference Calculation in ABC Frame by means of Lagrange Multipliers for Ensuring Constant DC Power under Unbalanced Grid Conditions," *IEEE Transactions on Power Electronics*, UNDER REVIEW.

- [J2] S. Sánchez, R. Ortega, R. Griño, **G. Bergna**, M. Molinas, "Conditions for Existence of Equilibria of Systems with Constant Power Loads," *IEEE Transactions on Circuits and Systems, Circuits and Systems I: Regular Papers*, IEEE Transactions on , vol.61, no.7, pp.2204,2211, July 2014.
- [J1] **G. Bergna**, A. Garcés, E. Berne, P. Egrot, A. Arzandé, J.-C. Vannier, M. Molinas, "A Generalized Power Control Approach in ABC Frame for Modular Multilevel Converter HVDC Links based on Mathematical Optimization," *Power Delivery*, IEEE Transactions on , vol.29, no.1, pp.386,394, Feb. 2014
- [J0] **G. Bergna**, E. Berne, P. Egrot, P. Lefranc, A. Arzandé, J.-C. Vannier, M. Molinas, "An Energy-based Controller for HVDC Modular Multilevel Converter in Decoupled Double Synchronous Reference Frame for Voltage Oscillation Reduction," *IEEE Transactions on Industrial Electronics*, vol. 60, no.6, pp.2360,2371, June 2013.

Full papers in conferences with oral presentation:

- [C16] R. Cisneros, R. Ortega, M. Pirro, G. Ippoliti, **G. Bergna**, M. Molinas, "Global Tracking Passivity-based PI Control for power converters: An application to the Boost and Modular Multilevel converters," *Industrial Electronics (ISIE), 2014 IEEE 23rd International Symposium on* , vol., no., pp.1359,1365, 1-4 June 2014.
- [C15] **G. Bergna**, J.A. Suul, E. Berne, P. Egrot, J.-C. Vannier, A. Arzandé, M. Molinas, "MMC circulating current reference calculation in ABC frame by means of Lagrange Multipliers for ensuring constant DC power under unbalanced grid conditions," *Power Electronics and Applications (EPE'14-ECCE Europe), 2014 16th European Conference on* , vol., no., pp.1,10, 26-28 Aug. 2014.
- [C14] **G. Bergna**, S. Sánchez, E. Berne, J.-C. Vannier, M. Molinas, "Frequency Scanning of Power Electronic-based Smart Grids: The Modular Multilvel Converter Application," *IET PEMD Conference, Manchester 2014. 16th European Conference on Power Electronics and Applications (EPE), 2014*.
- [C13] A. Jaafar, **G. Bergna**, P. Lefranc, "Energy Concept-based Nonlinear Stabilization and Control for Modular Multilevel Converters for Voltage Oscillation Reduction," *Power Electronics and Applications (EPE'14-ECCE Europe), 2014 16th European Conference on* , vol., no., pp.1,10, 26-28 Aug. 2014.
- [C12] **G. Bergna**, J.-A. Suul, E. Berne, P. Egrot, J.-C. Vannier, M. Molinas, "Improving the Dynamics of Lagrange-based MMC Controllers by means of Adaptive Filters for Single-phase Voltage, Power and Energy Estimation," *IECON 2013-39TH Annual Conference of IEEE Industrial Electronics Society*, 10-13 Nov. 2013.
- [C11] **G. Bergna**, J.-A. Suul, E. Berne, P. Egrot, J.-C. Vannier, M. Molinas, "Analysis of Modular Multilevel Converters under Unbalanced Grid Conditions with different Load Current Control Strategies and Lagrange-based Differential Current Control," *International Future Energy Electronics Conference (IFEEEC), 2013*, 3-6 Nov. 2013.
- [C10] **G. Bergna**, E. Berne, A. Garcés, P. Egrot, J.-C. Vannier, M. Molinas, "A generalized power control approach in ABC frame for modular multilevel converters based on Lagrange multipliers," *15th European Conference on Power Electronics and Applications (EPE), 2013*, vol.,no.,pp.1,8, 2-6 Sept. 2013.

- [C9] **G. Bergna**, J.A. Suul, E. Berne, P. Egrot, J.-C. Vannier, M. Molinas, "Generalized ABC frame differential current control ensuring constant DC power for modular multilevel converters under unbalanced operation," *15th European Conference on Power Electronics and Applications (EPE)*, 2013, vol.,no.,pp.1,10, 2-6 Sept. 2013.
- [C8] S. Sánchez, R. Ortega, R. Grió, **G. Bergna**, M. Molinas, "Conditions for Existence of Equilibria of Systems with Constant Power Loads," *52nd IEEE Conference on Decision and Control (CDC)*, Firenze 2013.
- [C7] **G. Bergna**, J.A. Suul, E. Berne, P. Egrot, P. Lefranc, J.C. Vannier, M. Molinas, "Mitigating DC-side power oscillations and negative sequence load currents in Modular Multilevel Converters under unbalanced faults - First approach using resonant PI," *IECON 2012 - 38th Annual Conference on IEEE Industrial Electronics Society*, vol., no., pp.537,542,28-28 Oct. 2012.
- [C6] **G. Bergna**, E. Berne, P. Egrot, P. Lefranc, J.-C. Vannier, A. Arzandé, M. Molinas, "A generalized power control approach in ABC frame for modular multilevel converters based on mathematical optimizations," *Energy Conference and Exhibition (ENERGYCON)*, 2012 *IEEE International*, vol.no.,pp.158-165, 9-12 Sept. 2012, Florence, Italy.
- [C5] **G. Bergna**, J.-C. Vannier, P. Lefranc, A. Arzandé, E. Berne, P. Egrot, M. Molinas, "Modular Multilevel Converter leg-energy controller in rotating reference frame for voltage oscillations reduction," *Power Electronics for Distributed Generation Systems (PEDG)*, 2012 *3rd IEEE International Symposium on*, vol., no., pp.698-703, 25-28 June 2012, Aalborg, Denmark.
- [C4] **G. Bergna**, E. Berne, P. Lefranc, M. Molinas, "Modular Multilevel Converter-Energy Difference Controller in Rotating Reference Frame," *European Power Electronics - Power Electronics and Motion Control (EPE-PEMC) 2012*, Novi Sad, Serbia.
- [C3] **G. Bergna**, P. Egrot, E. Berne, J.-C. Vannier, M. Molinas, "HVDC links using the modular multilevel converter: Dynamic Response using Different Simulation Models," *CIGRE Colloquium 2012*, San Francisco, U.S.A.
- [C2] **G. Bergna**, M. Boyra, J.H. Vivas, "Novel Control Strategies for Modular Multilevel Converters (MMC) - An Evaluation and Comparison of control and modulation schemes." *CIGRE Symposium 2011*, Bologna, Italy.
- [C1] **G. Bergna**, M. Boyra, J.H. Vivas, "Evaluation and proposal of MMC-HVDC control strategies under transient and steady state conditions," *Power Electronics and Applications (EPE 2011)*, *Proceedings of the 2011-14th European Conference on*, vol.,no,pp.1-10, Aug. 30 2011-Sept. 1 2011, Birmingham, U.K.

Posters and presentations

- [P1] E. Berne, **G. Bergna**, P. Egrot, P. Monjean, J. Lacoste, "Full-bridge modular multilevel converters: simulation of a three-terminal HVDC link using EMTP-rv," *CIGRE-EPREI HVDC & FACTS Conference*, Palo Alto 2013.

Book chapters

- [B1] R. Torres-Olguin, A. Garcés, **G. Bergna** "HVDC Transmission for Offshore Wind Farms," *Large Scale Renewable Power Generation, Green Energy and Technology*, DOI: 10.1007/978-981-4585-30-9_11, © Springer Science+Business Media Singapore 2014

Broad audience magazines

- [M2] G. Bergna, M. Boyra, J.-L. Thomas, "Les technologies de liaisons à courant continue pour l'interconnexion des réseaux électriques," *La Revue 3E.I*, N73-Juillet 2013
- [M1] J.-L. Thomas, M. Boyra, G. Bergna, "Les technologies à courant continue pour l'interconnexion des réseaux électriques du pourour méditerranéen," *REE-Revue de l'électricité et de l'électronique*-N5 2011

1.5 Layout of the Thesis

The Thesis is organized as follows:

Chapter 2 introduces the MMC topology and derives its respective dynamic equations. The modulation strategy of the converter is analyzed, and a classification system is proposed. Furthermore, eight MMC models with different degrees of simplification are detailed, studied, compared and validated with respect to a reference model. The chapter ends by discussing some of the control schemes that were found in the literature when this project was undertaken. A review of these schemes justified the need for a new circulating current control strategy.

In chapter 3 a new control scheme to achieve *phase independent control* of the MMC in *abc* reference frame based on mathematical optimization by means of Lagrange multipliers is presented. The main findings of this chapter are based on [J1] and [C10].

In chapter 4, which is an extension of the findings of [C12], the dynamics of the proposed control are improved and the harmonic sensitivity reduced by means of adaptive filters based on second order generalized integrators to estimate single-phase voltage, power and energy variables. In addition, an experimental setup is used to validate the proposed control strategy.

Based on the main findings of [J3] and [C15], chapter 5 extends the results to include the unbalanced grid case scenario yielding an alternative control strategy able to ensure constant power at the DC terminals of the MMC. The method is also derived using mathematical optimization by means of Lagrange multipliers.

In chapter 6 the MMC is stabilized via a novel global tracking passivity-based PI controller along with a closed loop estimator based on a virtual energy model of the MMC, as presented in [C16]. This strategy stems from the need for a local approach to ensure stability of complex interconnections such as the future *SuperGrid*.

A summary of the Thesis with concluding remarks and an outline of possible topics for further research based on the presented results is given in chapter 7.

Appendix A gives the formal theoretical derivation and proof of the *Global Tracking Passivity-based PI Controller* for a general class of bi-linear systems. This control strategy has been applied to the MMC in chapter 6. Furthermore, in appendix B, Lyapunov's global asymptotic stability proof is reviewed for the MMC under open loop control, and extended to the 3-phase/VSC case.

2

The Modular Multilevel Converter

In this chapter, the overall topology of the MMC is described, its Sub-Module (SM) operating principle is analyzed, its balancing algorithm is briefly introduced, and its expected behavior in a grid connected configuration is studied. Furthermore, the main analytical equations that described the converter dynamics are derived, and a modulation strategy classification is given for the sake of clarity. Finally, the chapter concludes by highlighting the benefits of controlling the MMC circulating current, providing an overview of existing control schemes, and identifying the need for a new proposal.

2.1 Introduction

MULTI-TERMINAL High Voltage Direct Current (HVDC) grids seem to be one of the most viable solutions for massive integration of renewable energy to the power grid, especially for societies with an already highly developed AC Grid. This so-called SuperGrid will serve as a transcontinental highway for renewable energy, [1], allowing for geographical smoothing effects which will help to minimize the disadvantages inherent to the intermittent nature of renewable sources. The Modular Multilevel Converter (MMC) proposed by Prof. Marquardt [2] has emerged as the the most suitable power converter for such an application, since it has several advantages with respect to its predecessors.

The MMC topology allows a smooth and nearly ideal sinusoidal output voltage which requires little or no filtering, when many levels are used. It is able to operate at lower switching frequencies; hence the converter losses are more similar to those of the LCC technology [5]. It presents a modular design which may lead to a reduced production cost and easier maintenance. Moreover, it has high scalability allowing a simple adjustment to the maximum voltage by increasing or reducing the number of SMs; and finally it has the ability to continue its operation despite module failure [6].

Several studies have explained the dynamics of the converter [7, 8] and have efficiently modeled it [9, 10, 11].

This chapter starts by a brief overview of HVDC developments from the late 18th century to the current date in section 2.2. The MMC converter topology is introduced and its operating principles are analyzed in detail in section 2.3. Based on such an analysis, a step-by-step derivation of the equations that can accurately represent the dynamics of the converter is given in section 2.4, based on the work presented in [7].

Since the converter is designed for high voltage/high power applications, the number of SMs is expected to be relatively high, which will slow down the simulation time in electromagnetic transient programs. Therefore, an overview of fast simplified models is given in section 2.5.

The need for a control strategy for the circulating current is briefly discussed in section 2.7. The main focus of this Thesis is mainly related to the proposal of an improved control scheme for the MMC. Therefore, section 2.9 presents a brief overview of the different circulating current control strategies that were found in the literature when this project took place in 2011, to highlight the need for a different control option which will be the subject of the next chapters.

2.2 HVDC technology

2.2.1 Beginings

High Voltage - Direct Current transmission systems were first used in 1954 with the first commercial transmission link between Gotland island and the Swedish mainland. This took place about half a century after the so called "war of currents," where Edison strongly advocated the use DC current whereas Westinghouse, Tesla and Steinmetz advocated the use of AC current instead. DC technology almost disappeared in the power transmission sector because of the usefulness of rotating magnetic fields produced by AC currents coupled with the low cost of transmission resulting from increases in AC voltages thanks to the development of transformers; that is until the 1950s when the mercury-arc valve had a high enough capacity to convert high AC voltage to high DC voltage and vice-versa [12].

Since the Gotland island-Swedish mainland project, HVDC technology has advanced dramatically, and more than 100 HVDC transmission systems have been installed around the world [13]. In the 1970s, the ever reliable and industry successful thyristor was used to replace the mercury-arc valves, which were susceptible to failure. The high availability and low maintenance requirements of thyristors compared to mercury-arc valves, and the fact that they enabled new circuit configurations, led to the gradual replacement of the mercury-arc valves with thyristor valves [12]. Thyristors and mercury arc schemes are current source stations, therefore an inductance on the DC side acts as the energy storage element [14]. Thyristors and mercury-arc rectifiers control the instant at which one AC phase could start to take over conduction from another of the phases, yet the actual commutation is undertaken by the AC voltages of the system. Therefore, such systems are referred to as Line-Commutated Converters (LCC), and require a strong AC network as well as large amounts of reactive power [14]. A large amount of low-order harmonics are introduced due to the low-frequency commutation process. Large filters are therefore required for mitigating the low-order harmonics as well as for compensating the reactive power consumption of the station, yielding in large space requirements for the LCC stations [12, 14].

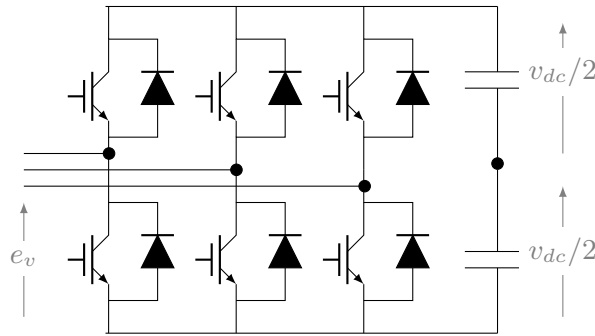


Figure 2.1: 2-level VSC topology

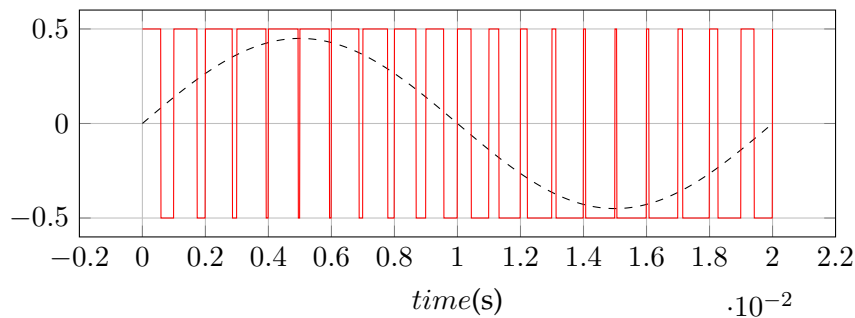


Figure 2.2: 2-level VSC typical waveform

2.2.2 The revolution: VSC technology

The Insulated Gate Bipolar Transistor (IGBT) was introduced as the main building block of the HVDC converter valves in the late 1990s. In contrast with thyristors, the IGBT is capable of “turning-off” whenever it is required to do so, independently of the AC voltage of the system. This seemingly small difference has completely revolutionized the world of HVDC, announcing the start of a new era in HVDC technology [12]. Furthermore, the IGBT required a complete change in the way that HVDC stations were designed and controlled, as the implementation of a Voltage Source Converter (VSC) HVDC station was now possible. As the devices are “self-commutating” they do not need a strong AC grid offering the possibility of black-start capability. Moreover, VSCs may switch at higher frequencies (1-2 kHz). This implies lower space requirements compared to LCCs, as smaller filters are now required to mitigate significantly smaller high-frequency harmonics [14]. In addition, the VSC has the inherent capability to control active and reactive power [12] adding an important degree of flexibility in power systems.

VSCs have gone through a distinct series of transformations. The first generations of VSCs, illustrated in Fig. 2.1, were based on two-levels ($+v_{dc}/2$, $-v_{dc}/2$) using Pulse Width Modulation (PWM) techniques with high switching frequencies as depicted in Fig. 2.2, resulting in large converter losses (3%) [13]. The two level PWM-based VSC topology, was first commercialized by ABB under the name “HVDC-Light 1st Generation” in 1997. ABB’s second generation of VSC was based on both the Three-level Neutral Point Clamped (NPC) converters, reducing total losses from 3% to 1.8% [14]. Their 3rd generation of VSCs that appeared in 2006 decreased the losses even further (1.4%) by returning to the two-level version using an optimized PWM.

The most recent VSC topology breakthrough is however the Modular Multilevel Converter (MMC) based on the proposal of Prof. Marquardt [2]. It was first commercially introduced by Siemens in 2010 under the name “HVDC Plus” in the “Trans Bay Cable” Project in the United

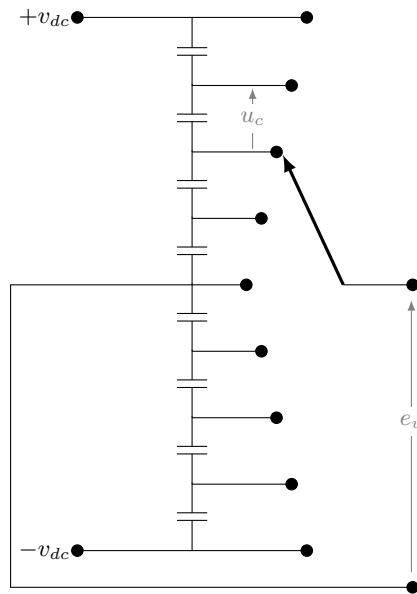


Figure 2.3: Principle of operation of the multilevel converter

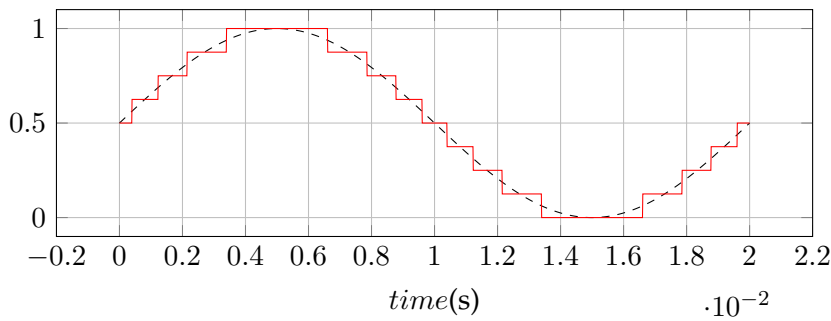


Figure 2.4: MMC typical waveform

States, operating at 400 MW and ± 200 kV. It is estimated that the MMC is able to produce even lower losses than its predecessor (between 0.9% and 1%) and has almost no filtering requirements. Alstom’s “HVDC MaxSine” as well as ABB’s “HVDC Light 4th Generation” have introduced similar concepts based on the MMC in 2014 and 2015, respectively [13].

The MMC approach offers theoretically no limit on the number of modules [12] thanks to its modular property. Each of the individual SMs is controlled to generate a small voltage step, acting as a discrete voltage source, as illustrated in Fig. 2.3 and Fig. 2.4. By incrementally controlling each step, a nearly sinusoidal voltage is generated at the AC output of the “multi-valves,” which substantially reduces the need for any filtering.

2.3 Basic structure and functionality of the MMC

A general phase of the MMC topology is depicted in Fig. 2.5. The converter topology is synthesized by connecting several SMs in series to constitute one “multi-valve”. Two of these multi-valves are present in each phase, one on the upper part or *arm* of the converter and one in the lower one, denoted by the sub-indexes *u* and *l* respectively. The number of the SMs in series usually depends on the application, however it is possible to generalize the analysis by assuming *N*

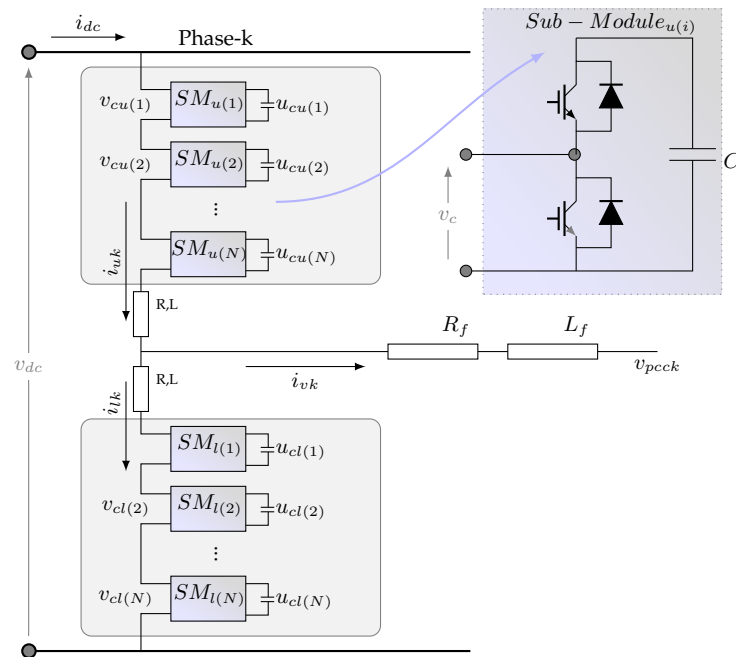


Figure 2.5: Topology of a general phase of the modular multilevel converter

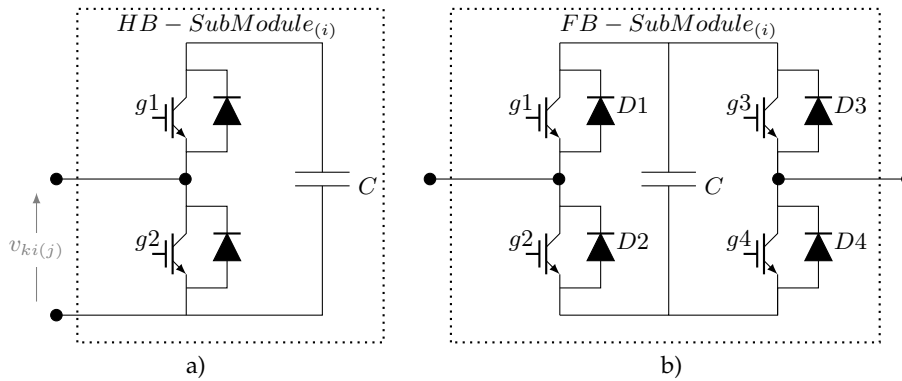


Figure 2.6: Two most common basic structures of a SM: a) half-bridge structure, b) full-bridge structure

SMs in each arm, equivalent to $2N$ per phase. An individual SM is formed by a capacitor, IGBTs and their corresponding free-wheel diodes. The two most common SM configurations found in literature are the Half-Bridge (HB) SM and the Full-Bridge (FB) SM, as illustrated in Fig. 2.6-a) and 2.6-b). The FB-SM version of the MMC has twice as much semiconductor devices than the HB version, which results in higher losses, but confers certain advantages as well [15, 16]. For the present analysis, and throughout the Thesis in general, the MMC under study is considered to be based on HB-SMs (Fig. 2.6-a)).

The multi-valve formed by the series connection of the N SMs of a single arm are connected to a filter inductor. This will allow for the parallel connection between the DC bus voltage v_{dc} and the voltage output of both arm multi-valves, as the inductor will cope with all voltage differences between them.

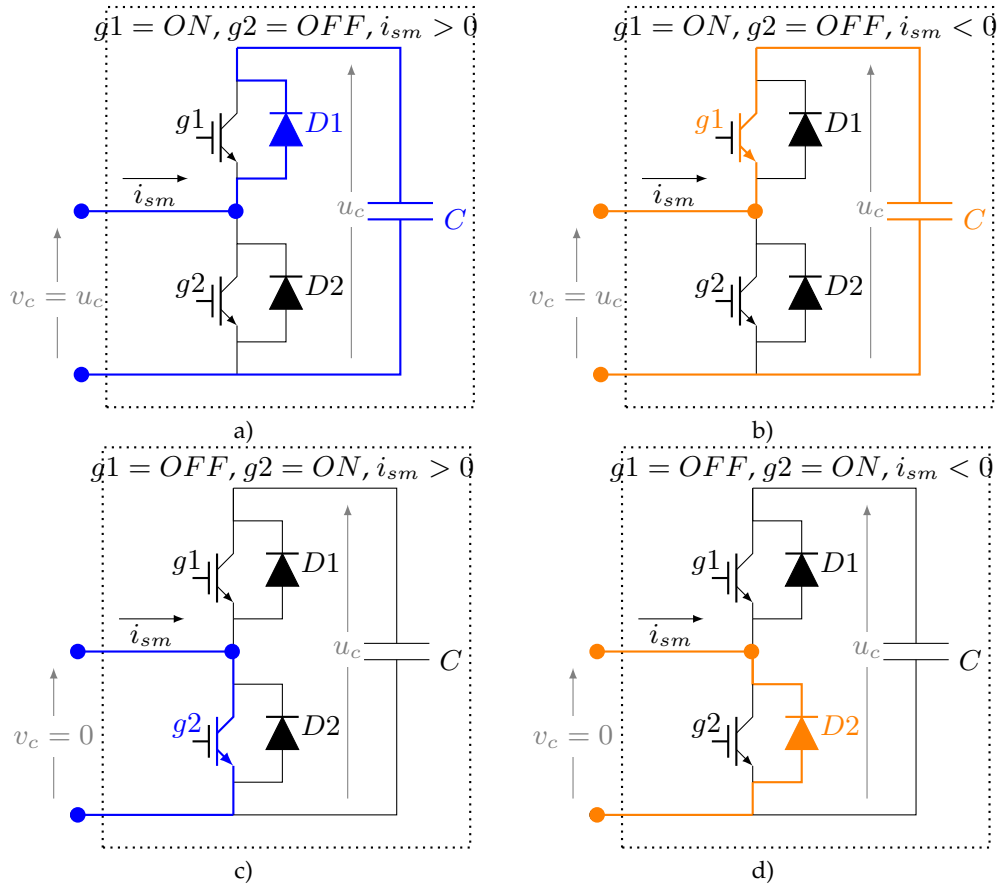


Figure 2.7: Current flowing in the SM semiconductor devices in normal operation: a) active SM and positive current, b) active SM and negative current, c) bypassed SM and positive current, d) bypassed SM and negative current

2.3.1 Sub-module analysis

In order to properly understand the basic operating principles of the MMC, it is necessary to start the analysis by its main power electronic building block or SM.

This SM structure has three possible states (without short-circuiting the capacitor) usually labeled as:

- **Active state:** In this case the IGBT g_1 is turned *ON* while the IGBT g_2 is turned *OFF*. This will result in two different electrical paths, depending on the sign of the current that is entering the SM. For a positive current $i_{sm} > 0$, that is to say, when the current is flowing into the SM, the capacitor will *charge* through the diode D_1 , as illustrated in Fig. 2.7-a). On the other hand, for a negative current $i_{sm} < 0$; i.e., when the current is leaving the SM, the capacitor will *discharge* through the IGBT g_1 , as depicted in Fig. 2.7-b). For both cases, the output voltage of the SM v_c will be equal to the voltage of the capacitor u_c , hence the SM is considered in the *active* state, irrespective of the direction of the SM current.
- **Bypassed state:** In this case the IGBT g_2 is turned *ON* while the IGBT g_1 is turned *OFF*. Depending on the sign of the current, two electrical paths can be identified for this state as well. For positive currents $i_{sm} > 0$, the current flow will pass through IGBT g_2 as shown in Fig. 2.7-c), whereas for negative currents will circulate through the diode D_2 as can be

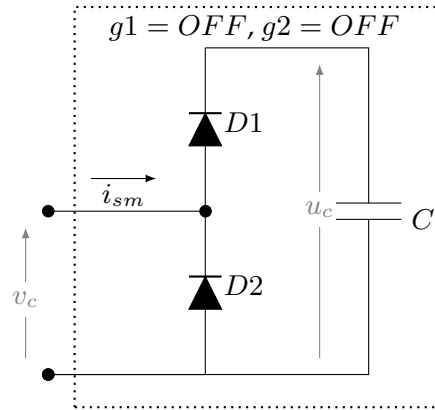


Figure 2.8: SM equivalent representation for blocked operation

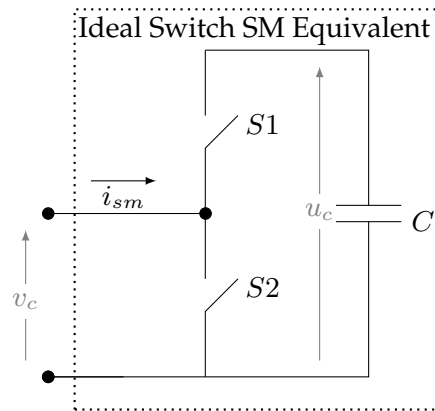


Figure 2.9: Ideal Switches SM Equivalent Representation for Normal Operation

seen in Fig. 2.7-d). This case is referred to as the *bypassed* state, since the voltage output of the SM v_c will be zero irrespective of the direction of the current, and the capacitor will neither charge nor discharge since it is “isolated” from the rest of the system.

- Blocked state: In this case, both IGBTs g_1 and g_2 are turned *OFF* resulting on the equivalent circuit depicted in Fig. 2.8. As can be seen, for this configuration, only the free wheel diodes take part in the operation of the SM, and a quick analysis is enough to conclude that the capacitor can never be discharged in this state, yet it can be charged through D_1 for positive currents if $v_c > u_c$, so this state will not be used in normal operation. In addition, it is important to note that the diode D_2 offers a path for negative currents, even if the SM is *blocked*.

Based on the above discussion, an equivalent circuit can be derived for when the SM is in normal operation. Since the active state, as well as the bypassed state work irrespective of the direction of the current entering the SM, it is then possible to model the IGBTs g_1 and g_2 and their corresponding free wheel diodes D_1 and D_2 as bidirectional ideal switches S_1 and S_2 , as depicted in Fig. 2.9. Moreover, the output voltage v_c of a general SM i can be defined as a function of the product between the SM *insertion index* n and the voltage of the capacitor u_c , as expressed in equation (2.1).

$$v_{c(i)} = n_{(i)} u_{c(i)} \quad (2.1)$$

Where the insertion index n will have only two possible values:

- $n = 1$, when S_1 is turned *ON* and S_2 is turned *OFF* resulting in $v_c = u_c$,
- $n = 0$, when S_1 is turned *OFF* and S_2 is turned *ON* resulting in $v_c = 0$.

Based on this definition, it is possible to write the SM capacitor voltage dynamics as in (2.2).

$$C \frac{d}{dt} v_{c(i)} = n_{(i)} i_{sm} \quad (2.2)$$

Note that since within an arm, the SMs are connected in series, the SM current i_{sm} will be equal to either the upper arm current i_u or the lower arm current i_l .

2.3.2 Balancing algorithm

The balancing algorithm is a low-level control strategy that is continuously sorting the individual capacitor voltages within an arm and selecting the most appropriate SM capacitors to be inserted required by the upper level control strategy. The number of SM that need to be inserted at a given instant can be defined by adding up the N instantaneous insertion indexes defined in (2.1). This is expressed by (2.3):

$$n_{arm} = \sum_{i=1}^N n_{(i)} \quad (2.3)$$

Equation (2.3) contains the information of the number of SM that are required to be inserted into the system and can vary from 0 SM to N . A degree of freedom may be observed at this point since different combinations of the individual SM can add up to form the required number of levels n_{arm} . A clever way of selecting the appropriate combination is to do so in a way such that all capacitor voltages $u_c(i)$ within the same arm have approximately the same waveform.

Ideal balancing algorithm

By analyzing the voltage dynamics of the individual capacitors using equation (2.2), it is possible to see that the sign of the arm current that will be flowing through the arm at that given instant will play a major role since if it is positive, the inserted capacitors will increase their voltages. In the same way, the capacitor voltages will decrease for negative currents. Therefore, if the current is positive, it is convenient to select the n_{arm} number of capacitors (out of N) with the lowest voltage to be inserted, whereas if the arm current is negative the n_{arm} number of capacitors with the highest voltage will be selected instead. If this process is implemented over and over again at a frequency high enough, all capacitors at the same arm will have almost exactly the same voltage trend. It is also worth mentioning that the performance of this strategy will be strongly linked to the sorting algorithm used to determine the n_{arm} most or least charged capacitors.

An example of the performance of this so-called *balancing algorithm* implemented at a high frequency $f = 50\mu s$ is illustrated in Fig. 2.10. In such figure, the capacitor voltage waveforms of a 6-level MMC containing 10 capacitors in each phase, which implies five capacitors per arm

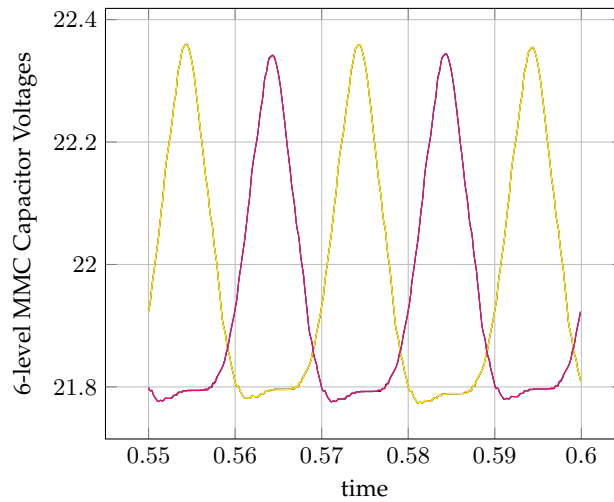


Figure 2.10: 6-level MMC individual capacitor waveforms using an ideal balancing algorithm

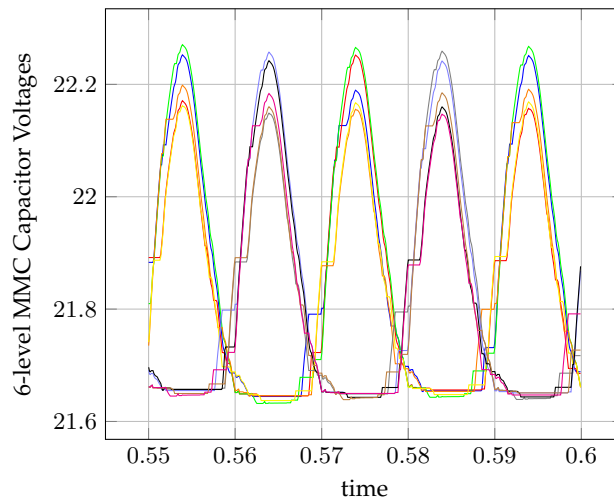


Figure 2.11: 6-level MMC individual capacitor waveforms using a more efficient balancing algorithm

($N = 5$). In this illustrative example, the $2N = 10$ voltage waveforms are plotted yet only two of such waveforms can be identified due to the high frequency of the balancing algorithm. In reality the two observed waveforms are two groups of 5 waveforms; one group representing the the upper arm and the other belonging to the lower arm of the MMC.

Since the focus of this Thesis was not the finding of more efficient balancing algorithms, the high-frequency balancing algorithm was used for its easy implementation and good results. Nonetheless, it is important to clarify that such algorithm is far from being efficient in terms of losses and has a high computational requirements, especially for MMC with high number of levels.

On more efficient balancing techniques

An almost ideal balancing technique such as the one described above, will imply a significantly high number of switching events, increasing the losses of the converter. To reduce this effect, it is possible to apply more efficient balancing algorithms, such as the one proposed in [17], where

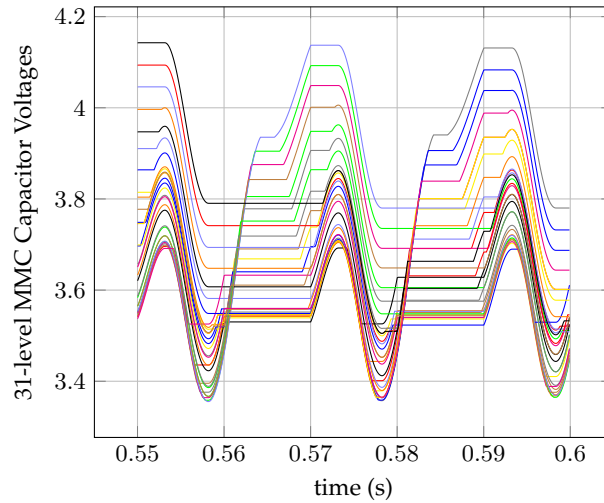


Figure 2.12: 31-level MMC upper arm individual capacitor waveforms sorting at 100Hz

the the sorting will not be performed every single integration step as the previous case, yet it will only be done if the new value of the aggregate insertion index is different from its previous one; i.e., $n_{arm}(t) \neq n_{arm}(t - \Delta T)$. This reduces the total number of switching events yielding in lower switching losses. The effect that this balancing algorithm has on the 10 capacitors of the same 6-level MMC used as an example is depicted in Fig. 2.11. In this case, it is possible to identify the 10 individual voltage waveforms since the balancing effect has been deteriorated in order to reduce the losses.

It is possible to reduce the switching losses even further. For instance, when the number of levels is increasing; i.e., $n_{arm}(t) > n_{arm}(t - \Delta T)$, the $n_{arm}(t - \Delta T)$ previously inserted SMs shall be left in the system, and the remaining $n_{arm}(t) - n_{arm}(t - \Delta T)$ required are added from the bypassed SMs. Similarly, when the number of levels is decreasing; i.e., $n_{arm}(t) < n_{arm}(t - \Delta T)$, the $N - n_{arm}(t - \Delta T)$ previously bypassed shall remain bypassed, and the $n_{arm}(t - \Delta T) - n_{arm}(t)$ SMs that are required to be bypassed are selected from the inserted SMs.

Reduced sorting frequency balancing algorithm

Finally, it is possible to reduce the sorting frequency of the balancing algorithm up to twice the grid's frequency (100Hz) for MMCs with high number of levels, while leaving the insertion frequency at higher values. The interest behind this is the reduction of the computational effort, since as the number of levels in the MMC increases, the sorting procedure will be more and more computationally demanding. In addition, the insertion frequency of the SMs needs to stay relatively high so that the quality of the output waveform of the multi-valves is not reduced, and all the desired levels may still appear.

To illustrate this case, a MMC with 30 SMs per arm is taken as an example. In Fig. 2.12, the 30 capacitors in the upper arm of the MMC are plotted. For this case, the difference between the SMs voltages $u_c(i)$ is much more significant than the previous cases. However it is still possible to operate the MMC with a high quality multi-valve voltage v_c , as illustrated in Fig. 2.13-a).

A consequence of sorting at such low frequencies is pointed out in Fig. 2.13-a) and amplified in Fig. 2.13-b): the occurrence of a voltage jump in the wrong direction.

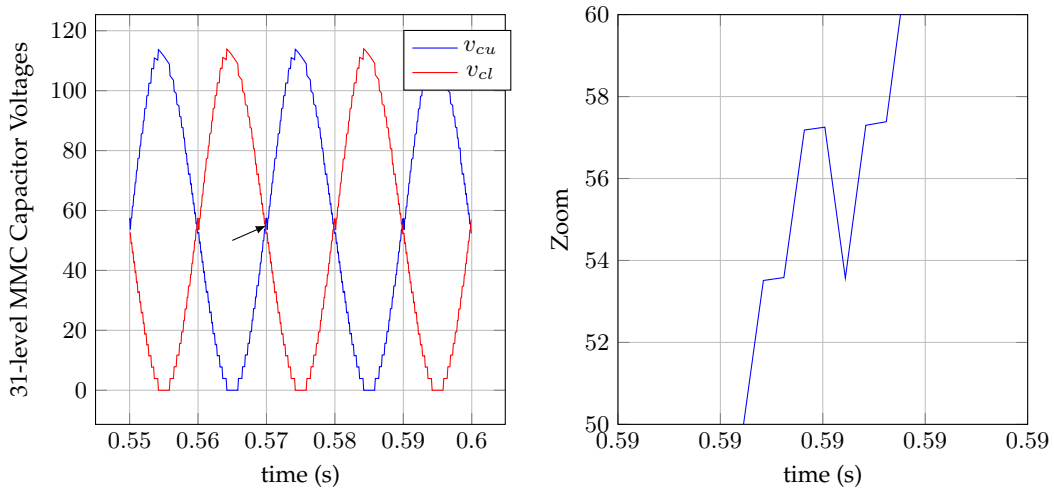


Figure 2.13: 31-level upper and lower MMC multi-valve voltage outputs

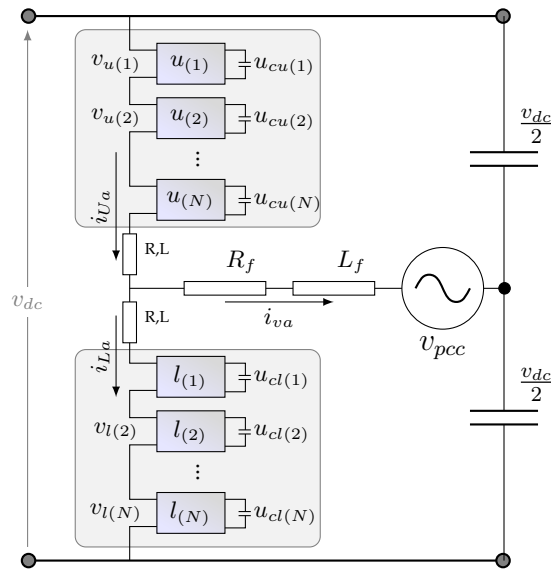


Figure 2.14: Topology of a grid-connected single-phase modular multilevel converter

2.3.3 Grid connected MMCs

Description

A single-phase MMC converter connected to the grid is depicted in Fig. 2.14. The output voltage of the MMC is measured between the middle point of both arm inductors and the middle point between the two capacitors (or DC voltage sources). The capacitors are used to create the neutral point needed for the grid current return. The three-phase version of the grid-connected MMC is shown in Fig. 2.15. This time, the central DC-capacitor is not necessary and in the figure it serves to indicate the DC-link voltage midpoint m , but due to the distributed energy storage of each SM, the MMC does not require the presence of such a centralized capacitor.

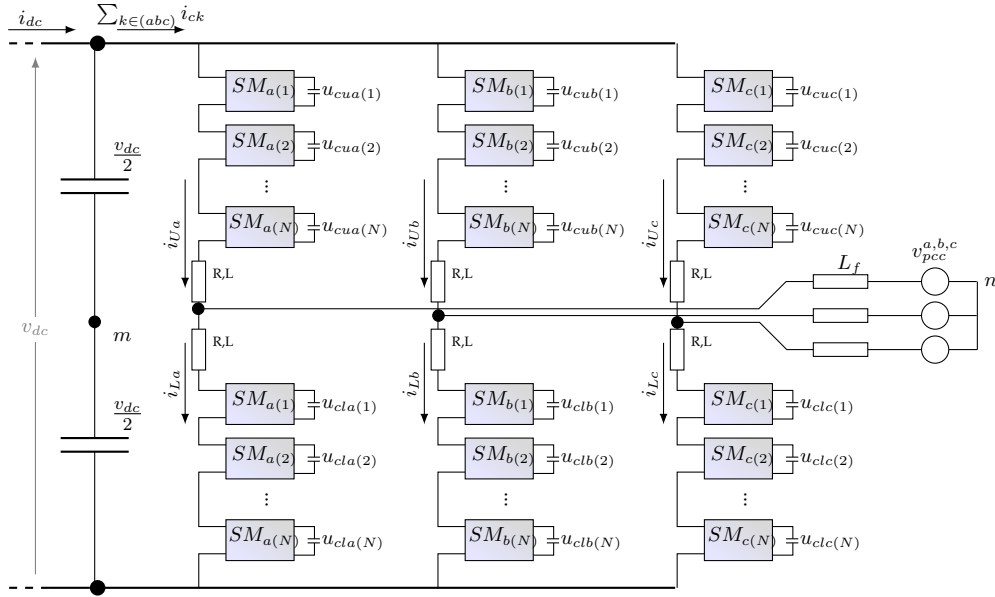


Figure 2.15: Topology of a grid-connected three-phase modular multilevel converter

Basic principles of multi-valve control

Let the equivalent output voltage of the multi-valve as a whole be $v_{cu,l}$ and the output voltage of the MMC converter that will be applied at the grid filter inductor be v_{mmc} . By applying Kirchhoff voltage equation to the upper and lower loops of the MMC in Fig. 2.14 results in (2.4)

$$\begin{aligned} -\frac{v_{dc}}{2} + v_{cu} + L \frac{d}{dt} i_u + R i_u + v_{mmc} &= 0 \\ -\frac{v_{dc}}{2} + v_{cl} + L \frac{d}{dt} i_l + R i_l - v_{mmc} &= 0 \end{aligned} \quad (2.4)$$

A quick analysis regarding the ideal shape of the multi-valve voltage can be made by neglecting the voltage drop on both inductors, and solving (2.4) for v_{mmc} . This results in (2.5).

$$\begin{aligned} v_{mmc} &\approx +\frac{v_{dc}}{2} - v_{cu} \approx \hat{v}_{mmc} \sin(\omega t + \varphi) \\ v_{mmc} &\approx -\frac{v_{dc}}{2} + v_{cl} \approx \hat{v}_{mmc} \sin(\omega t + \varphi) \end{aligned} \quad (2.5)$$

Since v_{mmc} is the ac output of the MMC, it should consist mainly of a sinusoidal signal at the same frequency of the grid to which it is connected as suggested with the right part of equation (2.5). Therefore the following observations can be drawn from such approximation:

- Both, multi-valve voltages v_{cu} and v_{cl} are to be controlled to have a DC component approximately equal to $v_{dc}/2$, so that the resulting output voltage of the MMC v_{mmc} shall be offset-free.
- Both multi-valve voltage outputs fundamental components amplitude are to be controlled approximately at \hat{v}_{mmc} .

- The lower multi-valve voltage output v_{cl} is to be controlled so that its fundamental AC component is in phase with the desired output of the MMC v_{mmc} whereas the upper multi-valve fundamental AC component is to be controlled in counter-phase.
- Taking into account that no negative voltage values are possible at both multi-valve outputs (for the HB-SM version of the MMC), the maximum output voltage is approximately v_{dc} in order to comply with the first observation.
- As a direct consequence of the above observation, the individual capacitor voltages is usually charged around v_{dc}/N in order to equally distribute the charge, although it can be charge at higher voltages.
- By adding up both equations presented in (2.5), it can be seen that at any given time $v_{cu} + v_{cl} = v_{dc}$. This implies that approximately half of the SM of a phase are inserted at any given instant.

2.4 Equations representing the operation of the MMC

The MMC topology is known to have several advantages with respect to modularity, scalability and availability as briefly introduced in [18, 6]. However, the converter structure also implies additional dynamics and complexity of the control compared to conventional two-level or multi-level VSCs. This is mainly because the MMC has additional degrees of freedom in the sense that the internal currents circulating between the upper and lower arms of one leg, and by that the voltage (or energy) of the capacitors in each arm can be controlled independently from the output AC currents. It is of course necessary to get familiarized with the mathematical model of the MMC so that an appropriate control strategy can be design to exploit the full potential of the converter. This section is devoted to the mathematical modeling of the converter. A step-by-step derivation of the converter equations is carried out in section 2.4.1, whereas the state equations of the MMC in matrix form are presented in section 2.4.2.

2.4.1 Step by step derivation of the MMC main equations

Voltage and current dynamics

With the sign conventions indicated in Fig. 2.15 and using Kirchhoff's current law, the output AC current, or *grid current* can be expressed by (2.6), and will be denoted as i_{vk} .

$$i_v(t) = i_u(t) - i_l(t) \quad (2.6)$$

In addition, the *circulating or differential current* is defined as the mean value between the upper and lower currents, and is denoted i_c , expressed in equation (2.7) [3, 7]:

$$i_c(t) = \frac{i_u(t) + i_l(t)}{2} \quad (2.7)$$

These relations can also be used to give explicit expressions for the upper and lower arm currents as function of the AC current and the circulating current as given by (2.8) and (2.9) respectively.

$$i_u = \frac{i_v}{2} + i_c \quad (2.8)$$

$$i_l = -\frac{i_v}{2} + i_c \quad (2.9)$$

The individual capacitor voltage dynamics of the upper arm of the MMC can be described as a function of the upper arm current and the individual insertion index of the corresponding SM.

$$\begin{aligned} C \frac{d}{dt} u_{cu}(1) &= n_u(1) i_u \\ C \frac{d}{dt} u_{cu}(2) &= n_u(2) i_u \\ &\vdots \\ C \frac{d}{dt} u_{cu}(N) &= n_u(N) i_u \end{aligned} \quad (2.10)$$

Similarly, the individual lower arm individual capacitor voltage dynamics can be obtained:

$$\begin{aligned} C \frac{d}{dt} u_{cl}(1) &= n_l(1) i_l \\ C \frac{d}{dt} u_{cl}(2) &= n_l(2) i_l \\ &\vdots \\ C \frac{d}{dt} u_{cl}(N) &= n_l(N) i_l \end{aligned} \quad (2.11)$$

The voltage output of an individual SM $v_{cu,l}(i)$ located in the upper (u) or lower (l) arm will be defined as the product of the voltage of its capacitor times its corresponding insertion index, as in (2.12).

$$v_{cu,l}(i) = n_{u,l}(i) u_{cu,l}(i) \quad (2.12)$$

It is indeed useful to define the voltage output of an arm or “multi-valve” as the sum of the individual voltage outputs of the SMs in the same arm. This yields in equation (2.13):

$$\begin{aligned} v_{cu} &= \sum_{i=1}^N n_u(i) u_{cu}(i) \\ v_{cl} &= \sum_{i=1}^N n_l(i) u_{cl}(i) \end{aligned} \quad (2.13)$$

At this point, it is interesting to make the assumption that *all voltages within an arm have the same waveform*. This is possible if a low-level balancing algorithm is implemented to equally distribute the charge of the arm SMs. The accuracy of the approximation will depend directly on the effectiveness of the balancing algorithm implemented. More detail on the balancing algorithm will be given in section 2.3.2. Therefore, by considering that $u_{cu,l}(1) = u_{cu,l}(2) = \dots = u_{cu,l}(N) = u_{cu,l}$, equation (2.13) can be written as in (2.14).

$$\begin{aligned}
 v_{cu} &= \sum_{i=1}^N n_u(i) u_{cu} = N n_u u_{cu} = n_u u_{cu}^{\Sigma} \\
 v_{cl} &= \sum_{i=1}^N n_l(i) u_{cl} = N n_l u_{cl} = n_l u_{cl}^{\Sigma}
 \end{aligned} \tag{2.14}$$

Where $n_{u,l}$ is the insertion index of the multi-valve, normalized between 0 and 1, defined as in (2.15); and u_c^{Σ} is the aggregate capacitor voltage of the upper (u) or lower (l) arm.

$$\begin{aligned}
 n_u &= \frac{\sum_{i=1}^N n_u(i)}{N} \\
 n_l &= \frac{\sum_{i=1}^N n_l(i)}{N}
 \end{aligned} \tag{2.15}$$

This insertion index is then expressing the ratio between the number of inserted SMs in one arm and the total number of SMs.

Since it is now assumed that all capacitors have the same waveform, the equations (2.10) and (2.11) that represent the dynamics of the capacitor voltages can be simplified into an aggregate equivalent. By adding up all individual equations in the upper arm, it is possible to obtain an equivalent equation for the arm aggregate capacitor voltage, expressed in (2.16).

$$C \frac{d}{dt} \sum_{i=1}^N (u_{cu}(i)) = \sum_{i=1}^N n_u(i) i_u \tag{2.16}$$

The same can be done for the lower arm, resulting in (2.17).

$$C \frac{d}{dt} \sum_{i=1}^N (u_{cl}(i)) = \sum_{i=1}^N n_l(i) i_l \tag{2.17}$$

By replacing the definition of the multi-valve insertion index into equations (2.16) and (2.17), one obtains (2.18).

$$\begin{aligned}
 \frac{C}{N} \frac{d}{dt} u_{cu}^{\Sigma} &= n_u i_u \\
 \frac{C}{N} \frac{d}{dt} u_{cl}^{\Sigma} &= n_l i_l
 \end{aligned} \tag{2.18}$$

By replacing the upper and lower arm currents of (2.18) by equations (2.8) and (2.9), results in (2.19).

$$\begin{aligned}
 \frac{C}{N} \frac{d}{dt} u_{cu}^{\Sigma} &= n_u \left(\frac{i_v}{2} + i_c \right) \\
 \frac{C}{N} \frac{d}{dt} u_{cl}^{\Sigma} &= n_l \left(\frac{-i_v}{2} + i_c \right)
 \end{aligned} \tag{2.19}$$

It can also be useful to define the total capacitance in one arm, as given by the series connection of all the capacitors, according to (2.20) [3].

$$C_{arm} = \frac{C}{N} \quad (2.20)$$

$$v_{c,u,l}(t) = n_{u,l}(t) \cdot u_{c,u,l}^{\Sigma}(t) \quad (2.21)$$

Assuming perfectly balanced capacitor voltages, the sum energy stored in the capacitors of each arm can be expressed by (2.22) [3, 7].

$$w_{c,u,l}(t) = \frac{1}{2} \frac{C}{N} (u_{c,u,l}^{\Sigma}(t))^2 \quad (2.22)$$

From the conventions indicated in Fig. 2.15 and the inserted voltages, it is also convenient to define the total capacitor voltage and the imbalance between the capacitor voltages in the upper and lower arms as given by (2.23) and (2.24) respectively.

$$u_c^{\Sigma}(t) = u_{cu}^{\Sigma}(t) + u_{cl}^{\Sigma}(t) \quad (2.23)$$

$$u_c^{\Delta}(t) = u_{cu}^{\Sigma}(t) - u_{cl}^{\Sigma}(t) \quad (2.24)$$

Similarly, the sum capacitor energy on one phase leg, and the energy unbalance can be defined by (2.25) and (2.26) respectively.

$$w_c^{\Sigma}(t) = w_{cu}(t) + w_{cl}(t) \quad (2.25)$$

$$w_c^{\Delta}(t) = w_{cu}(t) - w_{cl}(t) \quad (2.26)$$

Applying Kirchhoff's voltage law to the MMC, it is possible to come up with equations (2.27) and (2.28).

$$-\frac{v_{dc}}{2} + v_{cu} + Ri_u + L \frac{d}{dt} i_u + v_{out} = 0 \quad (2.27)$$

$$-\frac{v_{dc}}{2} + v_{cl} + Ri_l + L \frac{d}{dt} i_l - v_{out} = 0 \quad (2.28)$$

Adding up equations (2.27) and (2.28) yields in (2.29).

$$-\frac{v_{dc}}{2} + v_{cu} + v_{cl} + R(i_u + i_l) + L \frac{d}{dt} (i_u + i_l) = 0 \quad (2.29)$$

Rewriting (2.29) as a function of the circulating current using (2.7) yields (2.30).

$$u_c(t) = Ri_c(t) + L \frac{d}{dt} i_c(t) \quad (2.30)$$

Where u_c is the internal voltage of the MMC that drives the circulating current and is equal to (2.31):

$$u_c(t) = \frac{v_{dc}}{2} - \left[\frac{v_{cu}(t) + v_{cl}(t)}{2} \right] = \frac{v_{dc}}{2} - \left[\frac{n_u(t) u_{cu}^\Sigma(t) + n_l(t) u_{cl}^\Sigma(t)}{2} \right] \quad (2.31)$$

A similar procedure may be now repeated for the grid current: the difference between equations (2.27) and (2.28) results in (2.32):

$$v_{cu} - v_{cl} + R(i_u - i_l) + L \frac{d}{dt}(i_u - i_l) + 2v_{out} = 0 \quad (2.32)$$

Equation (2.32) can be expressed as a function of the grid current by means of (2.33):

$$e_v(t) = \frac{R}{2} i_v(t) + \frac{L}{2} \frac{d}{dt} i_v(t) + v_{out}(t) \quad (2.33)$$

Where e_v is the internal voltage of the MMC that drives the grid current and is equal to (2.34):

$$e_v(t) = \frac{v_{cl}(t) - v_{cu}(t)}{2} = \frac{n_l(t) u_{cl}^\Sigma(t) - n_u(t) u_{cu}^\Sigma(t)}{2} \quad (2.34)$$

An interesting feature of this converter can be observed at this point. The circulating and grid currents i_c and i_v are driven by the MMC voltages u_c and e_v defined in equations (2.31) and (2.34) respectively. While the circulating current driving voltage u_c depends on the sum of both multi-valve voltage outputs, the grid current driving voltage e_v depends on their difference. This means that the voltages can be assumed practically independent from one another, which in turn signifies that the circulating and grid currents can also be controlled independently, yielding in a additional degree of freedom for the converter under study.

MMC energy dynamics

The energy dynamics of an arm can be assessed by calculating the product between the arm current and the output voltage of the multi-valve as defined in (2.35) and (2.36):

$$p_u = v_{cu}(t) i_u(t) \quad (2.35)$$

$$p_l = v_{cl}(t) i_l(t) \quad (2.36)$$

These equations are conveniently transformed from upper and lower "coordinates" into sum and difference values:

$$p_\Sigma(t) = v_{cu}(t) i_u(t) + v_{cl}(t) i_l(t) \quad (2.37)$$

$$p_\Delta(t) = v_{cu}(t) i_u(t) - v_{cl}(t) i_l(t) \quad (2.38)$$

Rewriting the upper and lower currents as a function of the circulating and grid currents using (2.6) and (2.7), and similarly rewriting the multi-valve output voltages and as a function of v_{cu} and v_{cl} by means of (2.31) and (2.34) yields in the MMC arm energy dynamics equations [3, 7]:

$$p_{\Sigma}(t) = \dot{w}_{\Sigma}(t) = -e_v(t) i_v(t) + (v_{dc} - 2u_c(t)) i_c(t) \quad (2.39)$$

$$p_{\Delta}(t) = \dot{w}_{\Delta}(t) = \frac{i_v(t)}{2} (v_{dc} - 2u_c(t)) - 2e_v(t) i_c(t) \quad (2.40)$$

2.4.2 Two mathematical models in matrix representation for the MMC

Based on the step-by-step derivation described above, it is possible to obtain two different mathematical models of the MMC, expressed matrix representation. These are referred to as:

1. State equations model
2. Energy equations model

Throughout this Thesis, both models have been used for different purposes; for instance in section 2.5 of this chapter, it is described how the circuit model of the MMC has been simplified by means of the mathematical model in *state equations*. The control scheme contribution of this Thesis, detailed in chapters 3, 4 and 5 are based on the MMC *energy equations*. Chapter B relies once again on the *state equations* model of the MMC in order to analyze stability while in chapter A, both the *energy equations* as well as the *state equations* model of the MMC are used, for different purposes, in order to successfully synthesize the non-linear control proposal. Due to the important role that both mathematical models played in this work, they are therefore described in the following lines for a generalized MMC phase k .

State equation mathematical representation of the MMC

The state equations model requires the representation of the state variables of the MMC; i.e., the circulating and grid currents and the upper and lower aggregate voltage of the MMC capacitors $\rightarrow [i_{ck}, i_{vk}, u_{cuk}^{\Sigma}, u_{clk}^{\Sigma}]$.

The circulating current dynamic equation may be obtain by rewriting (2.30), and replacing u_c by its definition (see equation (2.31)), as shown in (2.41).

$$L \frac{d}{dt} i_{ck} = -R i_{ck} + \frac{v_{dc}}{2} - \frac{n_{uk} u_{cuk}^{\Sigma} + n_{lk} u_{clk}^{\Sigma}}{2} \quad (2.41)$$

In a similar fashion, the grid current dynamics can be obtained by rewriting (2.33) as in (2.42).

$$\frac{L}{2} \frac{d}{dt} i_{vk} = -\frac{R}{2} i_{vk} + e_{vk} - v_{out} \quad (2.42)$$

Considering that MMC is connected to a strong grid, by means of a filter inductor, as shown in Fig. 2.15, and replacing e_{vk} by its definition (see equation (2.34)) yields in (2.43).

$$L' \frac{d}{dt} i_{vk} = -R' i_{vk} + \frac{n_{lk} u_{clk}^\Sigma - n_{uk} u_{cuk}^\Sigma}{2} - v_{pcck} \quad (2.43)$$

Where L' and R' are the equivalent grid inductance and resistance defined as $L' = \frac{L}{2} + L_f$ and $R' = \frac{R}{2} + R_f$.

Finally, the upper and lower arm capacitor voltage sum (u_{cuk}^Σ & u_{clk}^Σ) dynamic equations are given in (2.19). By writing equations (2.19), (2.41) and (2.43) in matrix form yields (2.44).

$$\frac{d}{dt} \begin{bmatrix} i_{ck} \\ i_{vk} \\ u_{uk} \\ u_{lk} \end{bmatrix} = \begin{bmatrix} -\frac{R}{L} & 0 & -\frac{n_{uk}}{2L} & -\frac{n_{lk}}{2L} \\ 0 & -\frac{R'}{L'} & -\frac{n_{uk}}{2L'} & -\frac{n_{lk}}{2L'} \\ \frac{Nn_{uk}}{C} & \frac{Nn_{uk}}{2C} & 0 & 0 \\ \frac{Nn_{lk}}{C} & -\frac{Nn_{lk}}{2C} & 0 & 0 \end{bmatrix} \begin{bmatrix} i_{ck} \\ i_{vk} \\ u_{uk} \\ u_{lk} \end{bmatrix} + \begin{bmatrix} \frac{v_{dc}}{2L} \\ \frac{v_{pcck}}{L'} \\ 0 \\ 0 \end{bmatrix} \quad (2.44)$$

An additional way of representing the MMC in its *state equations* is using the sum and difference representation of the aggregate capacitors defined in (2.23) and (2.24), instead of their “upper-lower” equivalents. The dynamic equation in this new representation is obtained directly by adding and subtracting both equations presented in (2.19). This yields in (2.45)

$$\begin{aligned} \frac{C}{N} \frac{d}{dt} u_c^\Sigma &= n_\Sigma i_c + n_\Delta \frac{i_v}{2} \\ \frac{C}{N} \frac{d}{dt} u_c^\Delta &= n_\Delta i_c + n_\Sigma \frac{i_v}{2} \end{aligned} \quad (2.45)$$

Where n_Σ and n_Δ are defined as the sum and difference of the upper and lower insertion indexes n_u and n_l , as in (2.46).

$$\begin{aligned} n_\Sigma &= n_u + n_l \\ n_\Delta &= n_u - n_l \end{aligned} \quad (2.46)$$

Combining equations (2.46), (2.23) and (2.24) with the circulating and grid currents dynamic expressions given by (2.41) and (2.43) results in (2.47).

$$\begin{aligned} L \frac{d}{dt} i_{ck} &= -R i_{ck} + \frac{v_{dc}}{2} - \frac{n_{\Sigma k} u_{c\Sigma k} + n_{\Delta k} u_{c\Delta k}}{4} \\ L' \frac{d}{dt} i_{vk} &= -R' i_{vk} - \frac{n_{\Sigma k} u_{c\Delta k} + n_{\Delta k} u_{c\Sigma k}}{4} \end{aligned} \quad (2.47)$$

By writing the currents and voltage equations in their $\Sigma - \Delta$ representation, results in (2.48).

$$\frac{d}{dt} \begin{bmatrix} i_{ck} \\ i_{vk} \\ u_{c\Sigma k} \\ u_{c\Delta k} \end{bmatrix} = \begin{bmatrix} -\frac{R}{L} & 0 & -\frac{n_{\Sigma k}}{4L} & -\frac{n_{\Delta k}}{4L} \\ 0 & -\frac{R'}{L'} & -\frac{n_{\Delta k}}{4L'} & -\frac{n_{\Sigma k}}{4L'} \\ \frac{N}{C} n_{\Sigma k} & \frac{N}{2C} n_{\Delta k} & 0 & 0 \\ \frac{N}{C} n_{\Delta k} & \frac{N}{2C} n_{\Sigma k} & 0 & 0 \end{bmatrix} \begin{bmatrix} i_{ck} \\ i_{vk} \\ u_{c\Sigma k} \\ u_{c\Delta k} \end{bmatrix} + \begin{bmatrix} \frac{v_{dc}}{2L} \\ -\frac{v_{pcck}}{L'} \\ 0 \\ 0 \end{bmatrix} \quad (2.48)$$

Energy representation of the MMC

The energy representation is divided into two subsystems, one for the the grid and circulating currents $\rightarrow [i_{ck}, i_{vk}]$, whereas a second one for the energy stored in the capacitor arms in its common mode and differential representation $\rightarrow [w_{\Sigma k}, w_{\Delta k}]$. This model is based on the general premise that the bi-linear dynamics between the insertion indexes $n_{u,l}(t)$ and the upper and lower capacitor voltages $u_{cu,l}^{\Sigma}(t)$ are not considered. Moreover, such insertion indexes do not participate in the model at all. This implies that the control action is considered to be produced directly by u_c and e_v (the driving voltages of the circulating and grid currents), neglecting their “internal” non-linear behavior, yielding a simplified system as was first proposed in [3].

The circulating and grid currents in matrix representation can be written by means of equations (2.30) and (2.33), which results in (2.49).

$$\frac{d}{dt} \begin{bmatrix} i_{ck} \\ i_{vk} \end{bmatrix} = \begin{bmatrix} -\frac{R}{L} & 0 \\ 0 & -\frac{R'}{L'} \end{bmatrix} \begin{bmatrix} i_{ck} \\ i_{vk} \end{bmatrix} + \begin{bmatrix} \frac{u_{ck}}{L} \\ \frac{e_{vk} - v_{pcck}}{L'} \end{bmatrix} \quad (2.49)$$

Under the aforementioned approximation, this first subsystem turns out to be linear and can be controlled independently of the capacitive energy stored in the MMC arms. This is of course, because the non-linear dynamics contained in the control variables u_{ck} and e_{vk} have been neglected.

The second subsystem represents the capacitive energy of the MMC, and its matrix representation is found by rearranging equations (2.39) and (2.40), resulting in (2.50).

$$\frac{d}{dt} \begin{bmatrix} w_{\Sigma k} \\ w_{\Delta k} \end{bmatrix} = \begin{bmatrix} v_{dc} - 2u_{ck} & -e_{vk} \\ -2e_{vk} & \frac{1}{2}(v_{dc} - 2u_{ck}) \end{bmatrix} \begin{bmatrix} i_{ck} \\ i_{vk} \end{bmatrix} \quad (2.50)$$

By analyzing (2.50), it is possible to see that the regulation of the capacitive energy stored in the MMC can (under the aforementioned approximations) be done by adequately controlling the MMC currents. Moreover, taking into account that the currents can be controlled independently from the energies, as suggested by equation (2.49), the idea of implementing a cascaded control strategy may come to mind. In such control strategy, there would be an “inner” current control loop that will regulate the currents to the desired reference. In turn, such current reference should be the output of an “outer” energy control loop, that ensures that energy stored in the MMC is regulated at all times. The control strategy synthesized in chapters 3, 4 and 5 is based on this way of thinking.

2.4.3 Considerations for controlling the capacitive energy

The energy representation of the MMC is a suitable starting point for analyzing and understanding the various frequency components in the capacitor voltages and the circulating currents. The following points are worth noticing [3, 7]:

- From (2.39) it can be seen that the DC-component of the circulating current i_c multiplied with the DC-link voltage v_{dc} must balance the average power delivered to the AC side by the grid current i_v . This term must also cover the average losses inside the converter.

- The DC-component of i_c has no impact on the energy difference i_c as long as there are no DC-components in e_v or i_c . Thus, the DC-component of the circulating current can be used to control the total energy sum w_Σ .
- From (2.40), it can be seen that any fundamental frequency component of i_c will influence the energy difference w_Δ between the upper and lower arm, since the product of two fundamental frequency components will result in a DC-component and a second harmonic component. Thus, a fundamental frequency AC component in the circulating current can be used to change the energy difference between the upper and lower arms.

These considerations can be used as a starting point for designing strategies for control of the differential voltage (and by that the circulating current) on basis of the capacitive energy sum and difference. In section 2.9, an overview of several controls schemes is presented, where such considerations are often used.

2.5 Circuit modeling approaches for the modular multilevel converter

Modular multilevel converters usually contain a high number of insulated-gate bipolar transistors (IGBT). Using detailed models that represent the converter with a high degree of fidelity will require large computation time in order to simulate the MMC, especially for converters with a large amount of levels. The excessive computational burden required by high-fidelity models has led to the search for more efficient modelling techniques. Simplified and averaged models have been proposed in the literature to reduce this computation time without compromising significantly the accuracy of the results. In this section, some of the most promising modelling techniques for the MMC are reviewed. These are the followings:

- The detailed circuit-based model of the MMC, including explicit representation of all IGBTs and diodes, that will be used as the reference model
- A model based on circuit reduction, where the switching is represented by ON/OFF resistors [11].
- Simplified circuit-based models of the MMC that replace the circuit model of the SMs by their mathematical representation. These models are referred to as “Controlled Voltage Sources-based Model” or “Semi-Analytical Model,” since they combine the electrical interface of the simulation programs with mathematical representation of the SMs. The following three types of models are derived using this modelling technique:
 1. Explicit SM - Controlled Voltage Sources-based Model: This case considers explicitly the representation of every SM.
 2. Single equivalent SM - Controlled Voltage Sources-based Model: As opposed to the previous one, a single SM equivalent is used instead.
 3. Averaged Controlled Voltage Sources-based Model: Besides considering a single SM equivalent as the previous model, this “average” model will have only continuous control inputs; i.e., no switching modulation is used (e.g. PWM, SVM, etc).
- An entirely mathematical representation of the MMC without using any type of electrical circuit modelling technique. This model is referred to as “Analytical Mode.” As the former modelling technique, the analytical model may be divided in three different models using the exact same criteria:

1. Explicit SM - Analytical Model.
2. Single equivalent SM- Analytical Model.
3. Averaged Analytical Model.

2.5.1 Detailed or high-fidelity model of the MMC

This is the reference model where the entire MMC topology is represented in detail, including each of the IGBTs with their corresponding free-wheeling diode, requiring small numerical integration time steps to represent accurately fast and multiple simultaneous switching events [19]. The computational time increases exponentially with the number of levels, and taking into account that the implementation of the MMC requires up to two orders of magnitude more switches than the 2 or 3 level converters, more efficient models are required [19].

2.5.2 Reduced circuit modelling based on ON/OFF resistors

This method was proposed by Gnanarathna et al. in [11] in order to decrease the computation time of high-fidelity models. Electromagnetic transient (EMT) programs create an admittance matrix which has a size equal to the total number of nodes in the network subsystem. This admittance matrix must be inverted, and this might occur several hundred times in a cycle [11]. When such matrix becomes very large the inversion process becomes computationally very inefficient, as it is the case for the MMC intended for HVDC applications. Gnanarathna et al. have overcome this computational burden by converting a multi-node network into an exact but computationally simpler electrical equivalent using the Thévenin's theorem. Their methodology is based on the "Nested Fast and Simultaneous Solution" of [20] where the main network (the MMC) is partitioned into smaller sub-networks (MMC SMs) and the admittance problem is solved independently for each one of them [11]. Even though this procedure increases the number of steps to attain the solution, it reduces significantly the size of each of the admittances matrices compared to the one of the full network, yielding in a reduction in time simulation. In addition, they have managed to simplify the problem one step further by obtaining in a very straightforward way the Thévenin's circuit equivalent of each SM, drastically reducing the computations by avoiding unnecessary admittance matrices inversions.

Thévenin's equivalent circuit for the MMC SM

The two IGBTs (with their corresponding diodes) are treated as two state resistive devices: high resistance when the IGBT is "OFF" and a low resistance when the IGBT is "ON". Furthermore, the capacitor is represented as an equivalent voltage source and a resistor by means of the trapezoidal integration method [11]. This is expressed in (2.51) and (2.52).

$$v_c(t) = \frac{1}{T} \int_0^t i_c(t) dt \approx v_c(t - \Delta T) + \frac{1}{C} \left(\frac{i_c(t - \Delta T) + i_c(t)}{2} \right) \Delta T \quad (2.51)$$

hence,

$$v_c(t) = R_c i_c(t) + V_{cEq}(t - \Delta T) \quad (2.52)$$

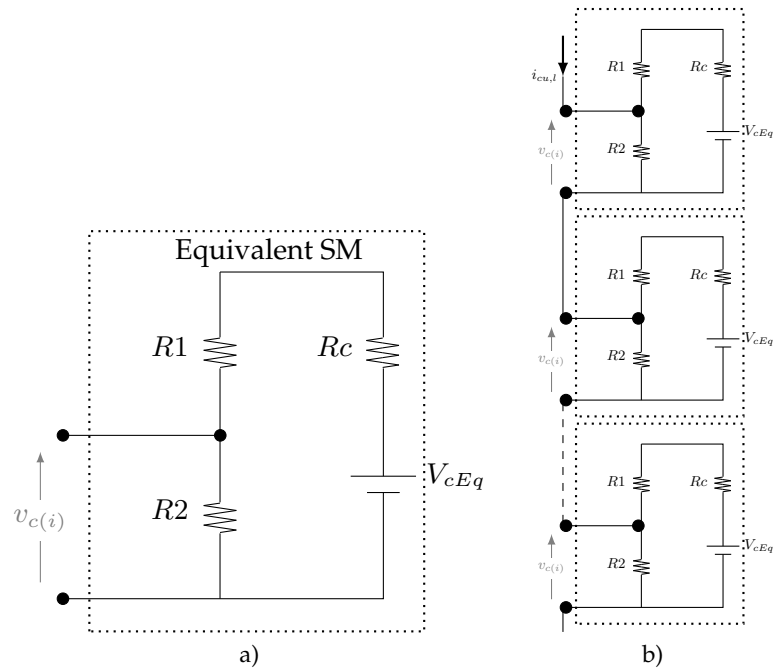


Figure 2.16: Reduced circuit model based on ON/OFF resistors: a) SM equivalent representation, b) equivalent multi-valve

where

$$Rc = \frac{\Delta T}{2C}$$

$$V_{cEq}(t - \Delta T) = \frac{\Delta T}{2C} i_c(t - \Delta T) + v_c(t - \Delta T)$$

Using this mathematical representation of the capacitor, and modeling both IGBT+diodes as “ON”/“OFF” resistors ($R1$ and $R2$), the equivalent circuit of a SM may be represented as it is shown in Fig. 2.16-a). Furthermore, by chaining the individual SMs depicted in Figure 2.16-a), the equivalent circuit of the multi-valve is constructed and depicted in Fig. 2.16-b). Its resulting admittance matrix is sparse and has a banded diagonal, making its inversion more computationally efficient. Nonetheless, the Thévenin’s equivalent of such circuit can be easily determined (refer to [11] for the complete proof) and is depicted in Fig. 2.17. By doing so, each arm of the MMC will have only two ports (A & B) instead of N , drastically reducing the computational time.

FPGA-based simulations for real-time implementation of MMC in EMT programs

Field programmable gate arrays (FPGA) are increasingly becoming a mainstream implementation platform for real-time power systems simulators, due to their highly parallel structure, the presence of dedicated high-performance DSP blocks, their inherent capability to support customized hardware designs, and their versatile programmable interconnect structure [21]. There has been a tendency of implementing the aforementioned model in FPGA-based real time simulator to augment the capabilities of a processor-based simulator to enable the real-time simulation of MMC-based systems: while the FPGA-based simulator is used to simulate the MMC, the processor-based simulator simulates the rest of the power system [21, 22, 23].

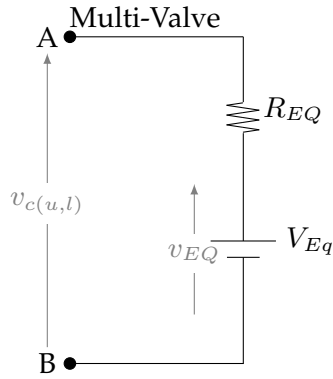


Figure 2.17: Multi-valve Thévenin's equivalent based on ON/OFF resistors

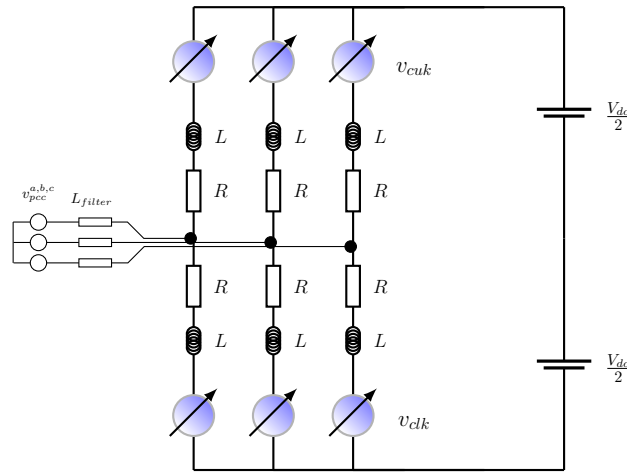


Figure 2.18: Controlled voltage sources-based MMC model representation

2.5.3 Controlled voltage sources-based models

Model considering explicit analytical representation of each SM capacitor

Description of the model

This model results as a combination of the MMC circuit model and analytical equations describing its dynamics. More precisely, the 3-phase MMC six multi-valves (two per phase) are replaced by six controlled voltage sources as depicted in Fig. 2.18. The output of these voltage sources will correspond to the multi-valve output voltages $v_{cu,l}$ as a function of their corresponding normalized insertion index $n_{u,l}$ and the sum of the capacitor voltages $u_{cu,l}^\Sigma$ of the corresponding arm for each phase, as expressed by (2.53).

$$\begin{aligned} v_{cu,k} &= n_{u,k}(t) u_{cu,k}^\Sigma(t) \\ v_{cl,k} &= n_{l,k}(t) u_{cl,k}^\Sigma(t) \end{aligned} \quad (2.53)$$

Where $u_{cu,k}^\Sigma$ and $u_{cl,k}^\Sigma$ are calculated as the sum of the individual capacitor voltages, given by (2.54).

$$\begin{aligned}
 u_{cu,k}^{\Sigma}(t) &= \sum_{i=1}^N u_{cu,i,k}(t) \\
 u_{cl,k}^{\Sigma}(t) &= \sum_{i=1}^N u_{cl,i,k}(t)
 \end{aligned} \tag{2.54}$$

Furthermore, the insertion indexes $n_{u,k}(t)$ and $n_{l,k}(t)$ are calculated as the sum of the individual insertion indexes as expressed in (2.55):

$$\begin{aligned}
 n_{u,k}(t) &= \frac{\sum_{i=1}^N n_{u,i,k}(t)}{N} \\
 n_{l,k}(t) &= \frac{\sum_{i=1}^N n_{l,i,k}(t)}{N}
 \end{aligned} \tag{2.55}$$

In turn, the individual capacitor voltages are calculated by (2.56).

$$\begin{aligned}
 u_{cu,i,k}(t) &= \frac{1}{C} \int_0^t n_{u,i,k}(t) i_{u,k}(t) dt \\
 u_{cl,i,k}(t) &= \frac{1}{C} \int_0^t n_{l,i,k}(t) i_{l,k}(t) dt
 \end{aligned} \tag{2.56}$$

whereas the individual capacitive currents are calculated by (2.57).

$$\begin{aligned}
 i_{cu,i,k} &= n_{u,i,k}(t) i_{u,k}(t) \\
 i_{cl,i,k} &= n_{l,i,k}(t) i_{l,k}(t)
 \end{aligned} \tag{2.57}$$

The individual insertion indexes $n_{u,i,k}(t)$ and $n_{l,i,k}(t)$ are taken as the direct outputs of the MMC balancing algorithm, while the upper and lower arm currents are measured directly from the circuit model of the MMC. These two variables are replaced in (2.56) to obtain the individual capacitor voltages, which in turn are used (along with the insertion indexes) to calculate the output of the controlled voltage sources, by means of (2.53).

This approach offers the following advantages:

- This model is significantly faster than the detailed model.
- It is particularly useful for testing control algorithms under balanced and unbalanced conditions.
- Since it is partly based on circuit modelling, it can easily cope with complex interconnections at the grid side, sometimes difficult to represent analytically (Y- transformers, different grounding techniques, short-circuits between phases, etc.).
- Despite its simplification, it retains the voltage and current information of all individual capacitors.

- It is easy to implement in Matlab/Simulink thanks to the individual SM information that may be managed by means of vectors; this means that only one equation is needed for the same variable for each arm.
- It is able to represent the blocking/de-blocking state of the MMC if such model is subject to some modifications described further on.

Model based on a single equivalent SM capacitor representation

Assuming that the capacitor voltages of each sum are balanced perfectly and neglecting the voltage differences between them, the waveforms of the individual capacitors are equal. This assumption allows deducing an equivalent capacitance $C_{arm} = \frac{C}{N}$. This yields in the following expression for the individual capacitor voltages:

$$v_{c1}(t) = v_{c2}(t) = \dots = v_{ci}(t) = \frac{v_c^\Sigma(t)}{N}$$

Where $v_c^\Sigma(t)$ represents the sum of all capacitor voltages in a specific arm of the MMC. The accuracy of this assumption increases when performing balancing algorithms are used, that are able to ensure almost identical waveforms between the capacitor voltages. However, this is not always desirable in since it will imply higher switching losses. The modelling method is basically the same as before except that the sum of all capacitor voltages in an arm is calculated directly by means of equation (2.58), instead of using (2.54) & (2.56) as was the case for the explicit model.

$$\begin{aligned} u_{cu,k}^\Sigma(t) &= \frac{N}{C} \int_0^t n_{u,k}(t) i_{u,k}(t) dt \\ u_{cl,k}^\Sigma(t) &= \frac{N}{C} \int_0^t n_{l,k}(t) i_{l,k}(t) dt \end{aligned} \quad (2.58)$$

The output of the controlled voltage sources will still be given by (2.53). Since this model does not use a capacitor balancing algorithm, for it assumes that all capacitors are balanced, the insertion indexes $n_{u,k}(t)$ & $n_{l,k}(t)$ are taken directly as the outputs of the modulation strategy (e.g., space vector modulation, PWM, etc).

This approach offers the following advantages and drawbacks: Indeed, the additional simplification of this model renders it even faster than the complete version of the model, since only six capacitor voltage state variables exist for a 3-phase MMC instead of $6N$. As the explicit SM capacitor version of the model, this simplified “equivalent SM” version of the model has an important electrical circuit part, which allows it to easily model “complex” AC grid connections. Of course, the inconvenience is that the individual capacitor voltage and current information is no longer available due the “ideal balancing” assumption.

2.5.4 Analytical models

It is of course possible to analytically model the MMC and not just its arm SMs as was the case for the “controlled voltage sources-based model”. Having an analytical model is always of interest

since in general, it is the fastest way to simulate systems, and especially if they are interconnected with other sub-systems. Since this model by definition does not contain any electrical circuit model, it is necessary to use the mathematical expressions of the converter grid/load and circulating current. The circulating and grid currents expressions used in this modelling technique are expressed in their discrete representation by (2.59) and (2.60). As can be seen from such equations, it is required that for the first iteration (t_0) both currents have to be initialized. The same requirement applies to the upper and lower capacitor voltages sum (u_{cuk}^Σ & u_{clk}^Σ) and the upper and lower insertion indexes (n_{uk} & n_{lk}).

$$i_{ck}(t_z + 1) = \left(1 - \frac{R\Delta T}{L}\right) i_{ck}(t_z) + \frac{\Delta T}{L} \left[\frac{v_{dc} - (n_{uk}(t_z) v_{cuk}^\Sigma(t_z) + n_{lk}(t_z) v_{clk}^\Sigma(t_z))}{2} \right] \quad (2.59)$$

$$i_{vk}(t_z + 1) = \left(1 - \frac{R'\Delta T}{L'}\right) i_{vk}(t_z) + \frac{\Delta T}{L'} \left[\left(e_{vk}(t_z) - \frac{1}{3} \sum_{k \in (abc)} e_{vk}(t_z) \right) - \left(v_{thk}(t_z) - \frac{1}{3} \sum_{k \in (abc)} v_{thk}(t_z) \right) \right] \quad (2.60)$$

with e_{vk} defined as

$$e_{vk}(t_z) = \frac{n_{lk}(t_z) u_{clk}^\Sigma(t_z) - n_{uk}(t_z) u_{cuk}^\Sigma(t_z)}{2} \quad (2.61)$$

ΔT is the discrete integration step and t_z is the discrete aggregate time interval. In addition, v_{thk} is the grid Thévenin's equivalent, R & L form the MMC arm impedance, while R' & L' form the equivalent impedance viewed from the grid equal to half the arm value plus the "external" filter impedance: $R' = \frac{R}{2} + R_f$ & $L' = \frac{L}{2} + L_f$ (refer to Fig. 2.5 for more details). Moreover, it is assumed that there is no 4th wire in the model, implying that no zero-sequence grid current can exist. Therefore, the zero sequence component of e_{vk} is calculated and extracted from its actual value as can be seen in (2.60).

As was the case for the "controlled voltage sources-based model," it is possible to consider explicitly the analytical representation of each of the MMC SMs, so that the capacitor voltage waveform information is available for each one of them by means of equation (2.54). Furthermore, it is also possible to obtain a more simplified model by only considering a single equivalent SM capacitor representation, if equation (2.58) is used instead.

This approach offers the following advantages and drawbacks: Both analytical models are theoretically the fastest way of simulating the MMC. However, for the case described above, a simple connection to the AC grid's Thévenin's equivalent was assumed. As was discussed before, more elaborated connections will require a non-neglectful effort in achieving their corresponding analytical model. Furthermore, since the diodes are not taken into account in the modelling, the model in its current form is not suitable for simulating the blocking/de-blocking state of the IGBTs during non-permanent DC short circuits.

2.5.5 Averaged MMC models

The simplified MMC model versions of the “controlled voltage sources-based model” and analytical model described in the previous sub-sections have the option of being turned into averaged models. This is achieved by eliminating the modulation block (e.g.: PWM, SVM, etc.) and hence giving a continuous insertion index as input to the multi-valve mathematical representation of (2.53).

2.6 MMC models comparison and validation

The accuracy of the eight models presented in section 2.5 is tested under balanced and unbalanced grid operation, as well as under a short-circuit between the DC terminals of the converter. The idea behind this is to validate each of the simplified models and to evaluate until what extent can they be used to provide accurate representation of the system under study.

The high-fidelity or detailed model has to be simulated to act as a reference for the other modelling techniques, and using this model can be extremely time consuming for converters with high number of levels. In this work a small number of levels was chosen for the comparison based on the premise that from a (robust) control design point of view this was enough, since the control results can be extended to MMC with higher number of levels. Validating the models with high number of levels was out of the scope of the Thesis, and the interested reader is referred to the work of Peralta *et al* presented in [10] for the simulation results of a 401-level MMC using a detailed model, as well as to the work from Saad *et al* presented in [19, 24, 25] where similar simplified models are evaluated to replace the 401-level MMC detailed model.

Since only 6 levels are used (5 SMs per arm), the pulse width modulation strategy selected is the Space Vector Modulation (SVM) for single phase multilevel converters from Leon *et al* in [26], instead of using the Nearest Level Modulation (NLM), which is usually more performing for MMCs with higher number of levels.

The high performing “ideal” balancing technique described in section 2.3.2 is used at the unrealistically high frequency of $100kHz$; or what is the same, at every $10\mu s$ time step of the simulation, the capacitors are sorted and balanced. Hence, all capacitors voltage waveforms within an MMC arm (obtained by the same modelling technique) are approximately equal. Therefore, only one individual voltage waveform is shown for each arm so simplify the comparison.

The system used to evaluate such models consists of a three-phase MMC converter connected to an ideal DC source for the direct-current side, and its AC terminals are connected to Thévenin’s grid equivalent by means of a filter inductor. The simulation parameters are given in Table 2.1.

The resulting waveforms of each one of the eight different MMC modelling techniques are plotted in the same figure to simplify the comparison, assigning different colors to each modelling technique waveform. The color legend used is given in Table 2.2 and is maintained throughout this section.

2.6.1 Comparison under balanced and unbalanced AC grid conditions

One second of the operation of the MMC was simulated yielding in Fig. 2.19. The converter reaches and stays in steady state between $t = 0s$ and $t = 0.4s$. At $t = 0.4s$, the Thévenin’s

Table 2.1: Simulation parameters for MMC models comparison and validation

Number of SM	5
DC voltage source	110V
Simulation time step	10 μ s
Space vector modulation frequency	2kHz
Grid frequency	50Hz
MMC arm resistance	0.01 Ω
MMC arm inductance	10mH
SM capacitance	1mF
Filter resistance	10 Ω
Filter inductance	10mH
Thévenin's grid equivalent resistance	10 Ω
Thévenin's grid equivalent inductance	10mH

Table 2.2: Waveform color legend for the 8 different MMC models

High Fidelity/Full detail Model	Blue
ON/OFF Resistors-based model	Magenta
Explicit Controlled voltage source-based model	Green
Aggregate Controlled Voltage Source-based model	Orange
Explicit Analytical Model	Yellow
Aggregate Analytical model	Gray
Controlled Voltage Source-based average model	Light blue
Analytical average model	Red

grid voltage phase “a” equivalent was brought to 0 Volts in order to simulate an extreme yet illustrative unbalanced grid condition. At $t = 0.6s$ the unbalanced event is removed, and the MMC retrieves its normal operation. Only the four main MMC state variables (u_{cu} , u_{cl} , i_v and i_c) are considered, one in each of the four plots forming the figure. All state variables are obtained from all the different models, in order to compare the divergence and accuracy with respect to the high-fidelity (or full detailed) model.

From such a broad perspective all models seem to agree quite well, although it is already possible to see some divergences, especially in the voltages. Nonetheless, the same overall behavior is being observed during steady state, and the transitory unbalanced case.

The waveforms are analyzed in depth in Fig. 2.20, where the previous plots have been zoomed in between $t=0.3s$ and $t=0.34s$, just enough to see a couple of oscillations. Furthermore, the case that is being analyzed occurs when the variables have reached steady state, before the unbalanced operation takes place.

At first sight, a significant divergence may be observed between both of the *averaged* models, and the rest of the models that take into account the modulation information.

The pulse width modulation strategy selected (Space Vector Modulation (SVM) [26]) seems to affect the circulating current the most. It is mostly in this variable that can be seen how the current harmonics are neglected in the averaged models. For the present simulation scenario, the peak of the circulating current obtained from the average models is approximately three to four times smaller with respect to the rest of the models. The absence of these harmonics in the average models will have a direct consequence in the rest of the variables as well. For instance, there is a non-neglectful phase shift in the grid current. This is because the averaged models will

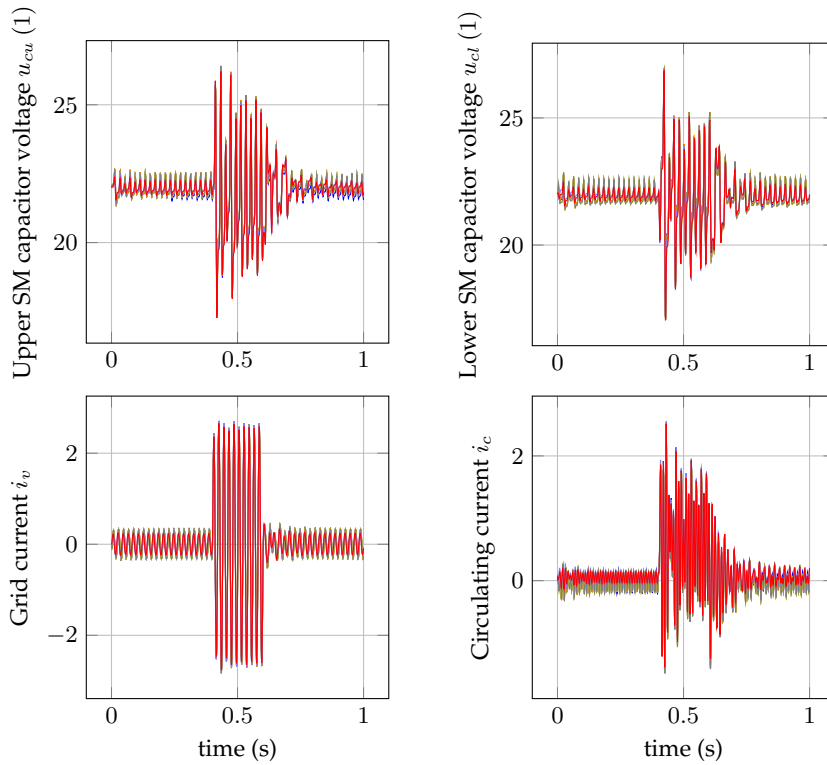


Figure 2.19: Models comparison and validation under balanced and unbalanced grid conditions

produce lesser losses, thus a different power is required from the grid, leading to a different grid current. This fact influences also the waveform trends of the upper and lower capacitors. Indeed, the error of the average models will be reduced for MMCs with higher number of levels.

The resulting upper 6-level multi-valve output waveform for all models is depicted in Fig. 2.22. As expected, the average models provide a continuous multi-valve waveform whereas the rest of the models successfully represent the discontinuous SVM effect.

Fig. 2.22 zooms in again, yet this time when the unbalanced event takes place; or more precisely, between $t=0.4s$ and $t=0.45s$. It can be seen, that the error between the averaged models has been significantly reduced. This occurs since during the unbalanced fault, much higher currents circulate through the converter, contributing to the increase of the losses in a more important degree than the losses due to the high order harmonics caused by the modulation, reducing the gap between averaged and non-averaged models.

- All models seem to converge quite well from a broad perspective for balanced and unbalanced grid operation.
- As expected, the most significant error occurs between the averaged models and the non-averaged models due to neglecting the high order harmonics introduced by the modulation in the formers. This error is expected to be reduced for MMC with larger number of levels.
- During the unbalanced condition, the error between averaged and non-averaged models is reduced due to the high currents.
- The analytical models are almost identical but the difference between them is expected to increase if the balancing algorithm is deteriorated.

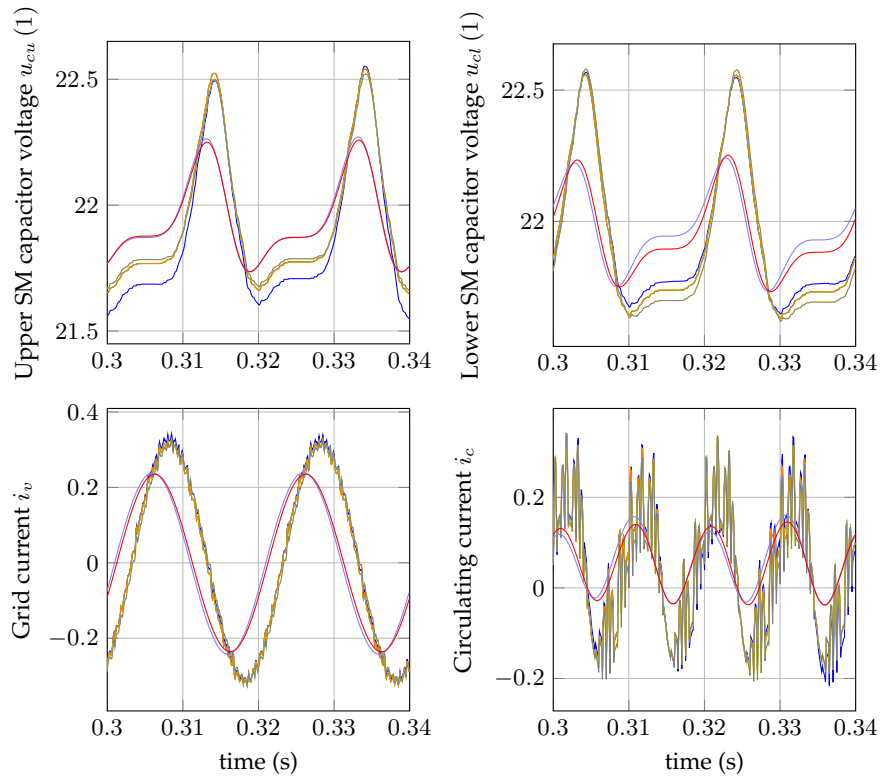


Figure 2.20: Zoom-in on balanced conditions for models validation

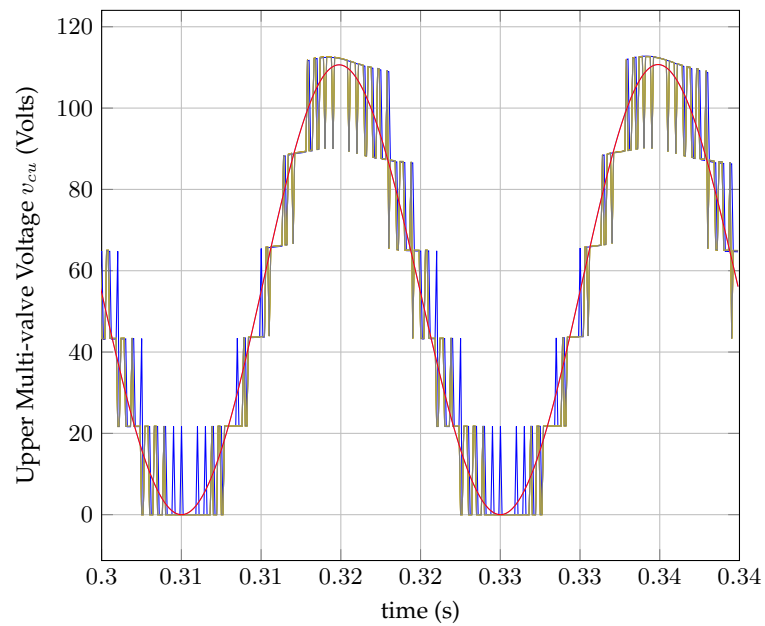


Figure 2.21: Model validation: upper and lower multi-valve outputs

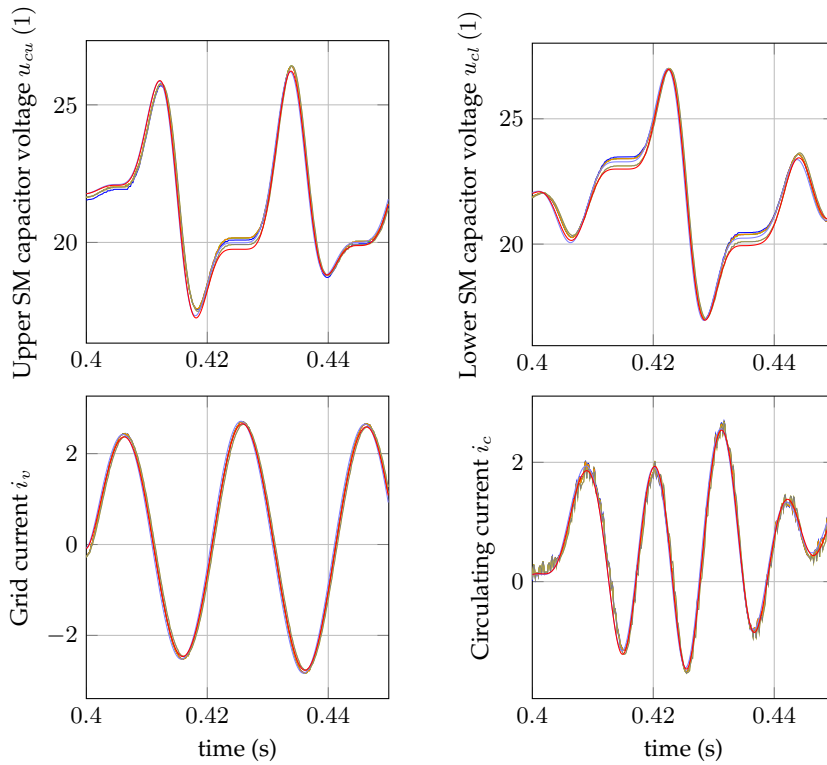


Figure 2.22: Zoom-in on unbalanced event for models validation

2.6.2 Models validation under DC short-circuits

The study of faults between the DC terminals of the MMC is a crucial issue for future power electronic based grids. Modelling the fault itself is rather simple and may be done without modifying significantly the previous models. However, the actual challenge lies within the successful modeling of the blocked state of the MMC; i.e., when all IGBTs are open, since the free-wheeling diode $D2$ (see Fig. 2.8) of each SM, offers a path for the DC fault current. Three cases are analyzed:

1. DC fault with no blocking state of the MMC
2. The IGBTs are blocked after a permanent fault
3. Non-permanent fault case

The first case does not require any additional changes in the models. The second case requires some slight modifications in the “controlled voltage sources-based model” and analytical models, whereas the third case is rather a challenging one as several modifications must be included in the circuit-based models in order to simulate the blocked state, while the entirely analytical models fail to do so. This is discussed in more depth in the following subsections.

DC fault with no blocking state of the MMC

As was mentioned earlier, this is the simplest case to model since no additional modifications are to be included in the models. In other words, the challenge lies in modeling the blocking state of

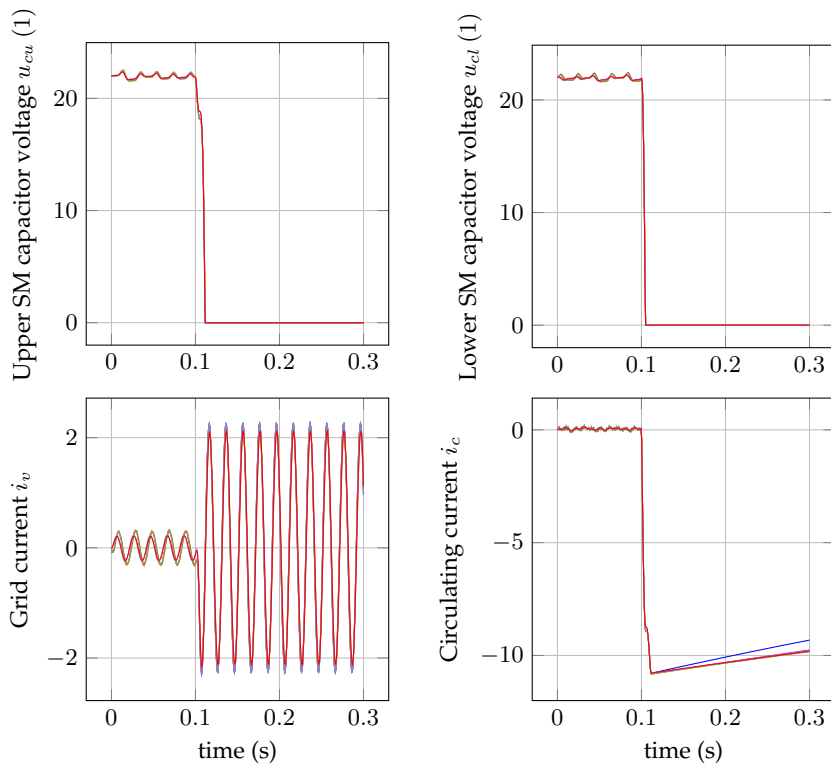


Figure 2.23: MMC models validation under a permanent DC fault with no blocking state

the IGBTs instead of the modeling of the fault itself. Therefore, for the “no blocking state” case, all of the eight models previously discussed represent the fault with great accuracy as is depicted in Fig. 2.23.

In such figure, the MMC is in steady state until a permanent DC fault occurs at $t = 0.1s$. Both the upper and lower capacitive voltage sums are brought to zero since they are feeding the fault. The grid current reaches approximately five times its original value, while the circulating current becomes ten times its original value after the fault. Needless to say, this case is to be avoided since all capacitors of the MMC are discharged and a high circulating current will be kept “trapped” inside the MMC. Therefore, there is a need of blocking the IGBT’s as soon as possible after the fault in order to avoid this scenario. This is analyzed in the following subsection.

Permanent fault: blocking state modelling of IGBTs

For this case, all of the eight models can be used again. However, some of them require some additional modifications for them to represent the blocking state accurately. More precisely, the models that require some modifications are the ones based on analytical equations: the “controlled voltage sources-based” models and the entirely analytical models, whether if they consider explicitly the SM capacitors representation, or not.

The modification of the mathematical representation of the SM basically requires the following two steps:

1. In the blocked state ($block = 0$), no must flow through the capacitors, thus the arm current is multiplied by the new variable “block.”

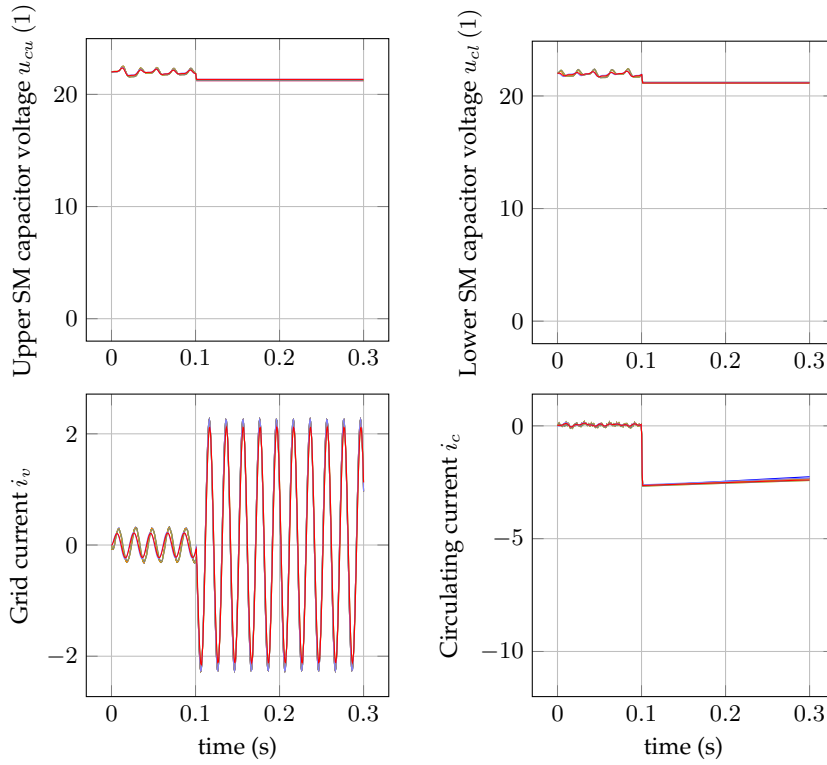


Figure 2.24: MMC models validation under a permanent DC fault

2. During the blocked state, the equivalent multi-valve output voltage is zero, hence a similar logic is applied.

For the explicit SM representation version, the equations are modified as in (2.62) for both controlled voltage sources-based models, as well as for analytical models. The aggregate SM representation can be done in a similar fashion.

$$\begin{aligned}
 i_{u,l}^f &= block \cdot i_{u,l} \\
 u_{cu,l}(i)^f &= f\left(n_{u,l}(i), i_{u,l}^f\right) \\
 v_{cu,l}^f &= \sum_{i=1}^N \left(n_{u,l}(i) u_{cu,l}(i)^f\right) \cdot block
 \end{aligned} \tag{2.62}$$

The waveform trends that yielded from simulating a permanent fault between the DC terminals of the MMC at 0.1 seconds, and blocking the IGBT's 0.001 seconds later are given in Fig. 2.24. It can be seen that all of the simplified models seem to converge with the reference. Unlike the previous case, the voltage of the MMC capacitors do not discharge and the short circuit current reaches lower amplitude directly related to the arm inductor and the fault detection / blocking time.

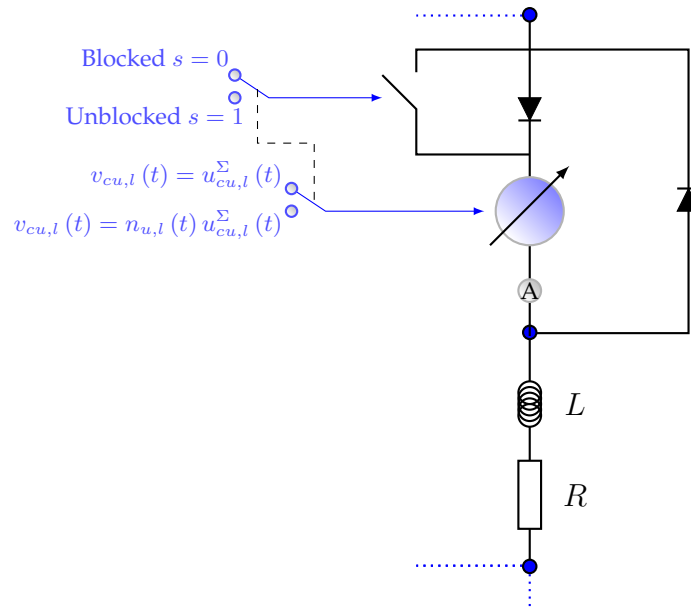


Figure 2.25: Modified version of the MMC controlled voltage sources-based multi-valve model suitable for representing the blocking/de-blocking action of the SMs

Non-permanent fault: blocking and de-blocking modelling of the IGBTs

A non-permanent DC fault will require the blocking of the IGBT's as well as their de-blocking state once the fault has been cleared. For this case only four simplified models out of the original eight models manage to effectively represent correctly the phenomenon.

Analytical models The analytical models require an extra logic that will enable them to represent the effect of the free-wheeling diodes, especially after the fault has been cleared and the system is reconnected. These models are yet to be developed and are not presented in this Thesis.

ON/OFF resistors-based model The ON/OFF Resistors-based model used is the one provided by OPAL-RT. Surprisingly, the version of the model used seems to fail to represent the reconnection or de-blocking case. However, this issue seems to be well known by a group of researchers in the field. In [19], Saad *et al* have presented an iterative solution in order to correct the limitation within an efficient model implementation. The solution presented there has not been implemented in this work, and the interested reader is referred to their article once again, were such solution is thoroughly described.

Controlled voltage sources-based model For this model, additional modifications are to be included in order to successfully model the reconnection of the MMC after the fault. Such modification was presented in [27] and is shown in Fig. 2.25. A diode is added in series with the controlled voltage source, with its respective bypass switch, so that it will only have an influence during the blocked state. This will prevent the discharge of the capacitors during the fault as was the case in the previous first scenario. Even though no current will flow through the capacitors during the blocked state, the circulating current that flows through the MMC internal inductors still needs a path in order to exist. Hence, a bypass diode is connected in parallel of the controlled voltage source and the in-series diode, to model this phenomenon. In addition, it can be seen that during the blocking state, the controlled voltage source will change its value from the original $v_c(t) = n(t) u_c^{\Sigma}(t)$ to only $v_c(t) = u_c^{\Sigma}(t)$. With this last modification, the capacitors can be charged through the in-series diode whenever $v_c(t) > u_c^{\Sigma}(t)$.

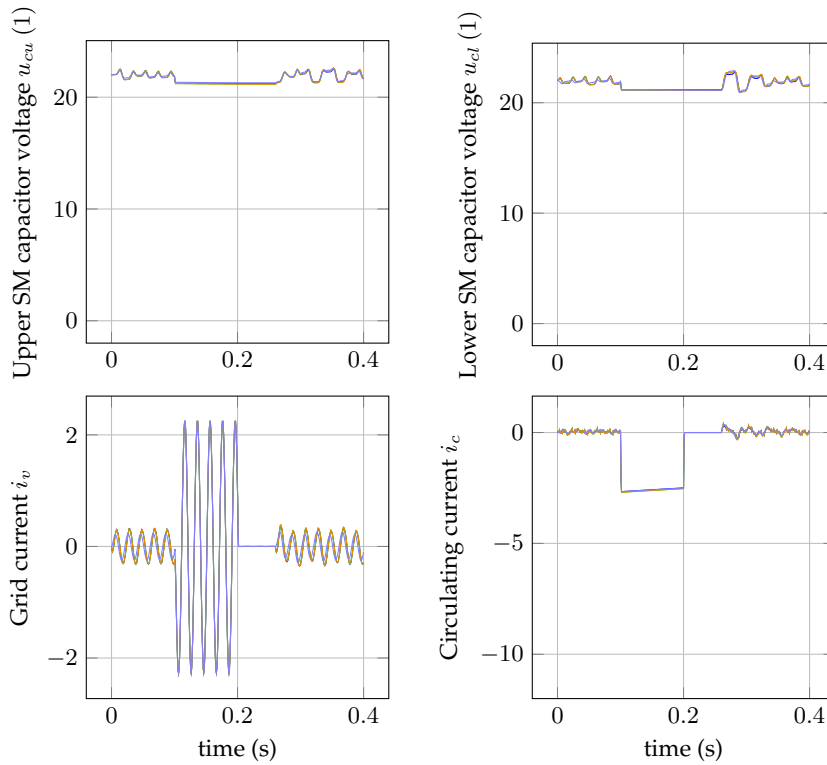


Figure 2.26: MMC models validation under a non-permanent DC fault

In Fig. 2.26, the MMC state variable waveforms of the reference high-fidelity model are plotted against the different types of models based on controlled voltage sources: 1) with explicit representation of the SM capacitors, 2) with a single equivalent SM capacitor representation and 3) averaged controlled voltage source-based model.

The simulation is left in steady state until a DC fault occurs at $0.1s$. After $t = 0.001s$, the IGBT's are blocked. Furthermore, the fault is cleared at $0.2s$, however the IGBT's remain blocked. The IGBTs are then "unblocked" at $t = 0.26s$, firing as they were doing before the fault. It can be seen how the simplified models seem to converge rather well with the reference high-fidelity model.

2.6.3 Concluding remarks on the MMC modelling techniques

As was discussed earlier, the eight models here analyzed seem to represent quite accurately the system under study. Averaged models neglect the harmonic losses and might lead to significant errors for low level MMCs. Analytical models may prove useful for simulating large system, but some extra effort is required to model the more complex grid interconnections. The simplified model based on ON/OFF resistors seems to be one of the best models though it might still need some improvements, particularly for the reconnection case after a DC short-circuit.

Finally the explicit and aggregate versions of the controlled voltage source-based model has proven to be quite fast, accurate and easy to implement, and can be used to study AC as well as DC faults. This last model was selected as the most appropriate, since besides the previously mentioned advantages, the scope of this Thesis was oriented more on designing an appropriate "high-level" control strategy suitable for the MMC. This implies that the overall or global be-

havior of the system was often more important than the details occurring in the individual SM. Hence most simulations were based on the averaged and discontinuous aggregate versions of the controlled voltage sources-based model.

2.7 On the need of a circulating current control

Back to when the converter was proposed, the circulating current seemed to be considered as one of the MMC main drawbacks, as its presence could hinder the successful operation of the converter. Indeed, the thought of having an uncontrolled current circulating through the MMC, potentially triggering unstable operation, as well as increasing the losses with its undesired natural second harmonic was certainly not appealing. Nonetheless, it did not take long to realize the great benefits that could be obtained by controlling such circulating current, which is now considered as a powerful extra degree of freedom, allowing for new features not seen until now in a VSC. A list of some of the advantages of controlling the circulating current is given in the following lines.

Avoiding resonances

If the circulating current is not controlled, there is a high risk of resonance since a resonant circuit is formed between the MMC inductances and the "variable capacitances" of the inserted SMs. In [28] the resonance frequency was analytically formulated for different harmonics n as a function of the modulation index \hat{m} as:

$$\omega_{rn} = \sqrt{\frac{N}{LC}} \sqrt{\frac{2(n^2 - 1) + \hat{m}n^2}{4n^2(n^2 - 1)}}, n = 3k \pm 1 \quad (2.63)$$

It is still possible to operate successfully the converter by avoiding the resonant behavior of the converter by parameter design, resulting in larger inductors and/or capacitors. On the other hand, if the circulating current is controlled at all time, it will be possible to regulate, and thus to limit its value at several frequencies, avoiding resonance phenomena via control yielding in a more compact version of the converter.

Reducing losses

It is well known that the second harmonic component of the uncontrolled circulating current will naturally appear in the converter. Since this harmonic does not contribute to the power transfer between the AC or DC side, it creates unnecessary Ohmic losses that should be avoided. This can be achieved by applying control actions such as the ones proposed in [17, 29], as well as the one proposed in this Thesis in chapter 3, in which the circulating current harmonics are suppressed, increasing the efficiency of the MMC.

Regulating independently the MMC arm average energies

Another important feature of the circulating current is that it can be controlled to independently regulate the average energy stored in each of the multi-valves, as will be shown in chapter 3.

It will be shown that by introducing a DC component in the circulating current reference, it was possible to regulate the average value of the sum between the upper and lower capacitive energies stored in a single phase of the converter; whereas by introducing an AC component, it was possible to regulate the average of the difference between them.

Power oscillation firewall during AC grid unbalanced conditions

The MMC extra degree of freedom provided by the circulating current can be controlled to use the distributed capacitance of the converter to absorb any power fluctuations coming from the AC grid during unbalanced operation in order to have a constant DC power at the output of the converter. In three-level VSC converters, this could also be achieved by controlling the grid currents. However, since the MMC is using the circulating current to cope with this issue, the grid current is relieved from that duty and can be controlled for other purposes such as to avoid current unbalances or to ensure constant reactive power in order to reduce the sizing of the capacitors. More detail on this feature is given in chapter 5.

2.8 Insertion index “continuous” modulation methods classification

In the present section, different methods of *continuous* modulation methods are discussed and a classification is proposed. It is important to stress that the insertion index modulation referred to in this section is a continuous one. This implies that it has not to do with Pulse Width Modulation (PWM) or Space Vector Modulation (SVM) techniques used to discretize the continuous insertion index. The different MMC *continuous modulations* studied in this section are related to the different methods of generating the continuous insertion indexes from the MMC voltage reference variables (u_c^* and e_v^*), which result from the control scheme used.

Note: For all methods, it will be assumed that there is an “ideal” sorting algorithm as discussed in section 2.3.2 [18, 6] included in the modulation scheme, ensuring that all SM capacitor voltages are equal within an arm.

As implied above, different techniques can be found in the literature regarding the generation of the MMC continuous insertion indexes $n_u(t)$ and $n_l(t)$. In an attempt to cover the different operating principles of these different techniques, they shall be classified in two broad groups, depending on whether they compensate or not the inherent non-linearity associated to the voltage capacitor sum:

1. Uncompensated modulation
2. Compensated modulation

This is explained in detail below.

In the section 2.4 were introduced the two currents of the MMC; that is to say, the grid current i_v and the circulating current i_c by equations (2.6) and (2.7). Moreover, it was also seen that the MMC is capable of driving independently these two currents by its two internal voltages e_v and u_c given in (2.34) and (2.31). Therefore, they will be given as references to the MMC e_v^* and u_c^* as expressed in (2.64) and (2.65). For instance, if a traditional current control scheme is applied, they may result as the outputs of PI controllers that regulate their respective currents to the desired value.

$$e_v^* = \frac{v_{cl}^* - v_{cu}^*}{2} \quad (2.64)$$

$$u_c^* = \frac{v_{dc}}{2} - \frac{[v_{cu}^* + v_{cl}^*]}{2} \quad (2.65)$$

Since both e_v^* and u_c^* are “artificial” variables, it is necessary to rewrite equations (2.64) and (2.65) in order to obtain their equivalent values of v_{cu}^* and v_{cl}^* . This results in the following equations:

$$v_{cu}^* = \frac{v_{dc}}{2} - e_v^* - u_c^* \quad (2.66)$$

$$v_{cl}^* = \frac{v_{dc}}{2} + e_v^* - u_c^* \quad (2.67)$$

At this point it is necessary to determine the value of the insertion indexes n_u and n_l from the upper and lower arm inserted voltage references v_{cu}^* and v_{cl}^* . According to (2.21), n_u and n_l may be calculated from v_{cu} and v_{cl} by respectively dividing each of the inserted voltages by the sum of the capacitor voltages in an arm (u_{cu}^Σ and u_{cl}^Σ). In consequence, the insertion indexes may be defined as a function of u_{cu}^Σ and u_{cl}^Σ as expressed in equations (2.68) and (2.69).

$$n_u = \frac{v_{cu}^*}{u_{cu}^\Sigma} = \frac{\frac{v_{dc}}{2} - e_v^* - u_c^*}{u_{cu}^\Sigma} \quad (2.68)$$

$$n_l = \frac{v_{cl}^*}{u_{cl}^\Sigma} = \frac{\frac{v_{dc}}{2} + e_v^* - u_c^*}{u_{cl}^\Sigma} \quad (2.69)$$

The type of waveform that is to be assigned to u_{cu}^Σ and u_{cl}^Σ will defined the type of modulation according to our classification (compensated or uncompensated modulation): If u_{cu}^Σ and u_{cl}^Σ include the oscillating component present in the MMC capacitor sum ($\tilde{u}_{c,u,l}^\Sigma$), in addition to its DC offset, as expressed in (2.70) and (2.71),

$$n_u = \frac{\frac{v_{dc}}{2} - e_v^* - u_c^*}{\tilde{u}_{cu}^\Sigma + \bar{U}_{cu}^\Sigma} \quad (2.70)$$

$$n_l = \frac{\frac{v_{dc}}{2} + e_v^* - u_c^*}{\tilde{u}_{cl}^\Sigma + \bar{U}_{cl}^\Sigma} \quad (2.71)$$

then the strategy will be classified as a compensated modulation. On the other hand, if in the insertion indexes generation equation, the oscillating components $\tilde{u}_{c,u,l}^\Sigma$ are neglected, and only a constant is used in the division, it will be referred to as uncompensated Modulation. Indeed, the difference between both of them will be if the nonlinear dynamic caused by the bi-linear product between the insertion index and the sum of the capacitor voltages in an arm is compensated or not.

Perhaps the most known uncompensated modulation strategy is the “direct modulation”[3]. In this case u_{cu}^Σ and u_{cl}^Σ of equations (2.68) and (2.69) are both approximated to the constant value of v_{dc} . In addition, $u_c^* = 0$ implying that there is no control of the circulating current under

this strategy. Examples of uncompensated modulation strategies with circulating current control ($u_c^* \neq 0$) are also found in the literature such as in [30] or [17], among others.

On the other hand, compensated modulation strategies may be found in the “closed loop control”[3] and the “open loop control”[29]. The first used the actual measurements of the sum of the capacitor voltages as input to equations (2.68) and (2.69): $u_{c.u,l}^\Sigma = u_{c.u,l}^{\Sigma,m}$. The second one used the estimated value of the variable: $u_{c.u,l}^\Sigma = \overline{v_{dc}} + u_{c.u,l}^{\Sigma,*}$. The “closed-loop control” presented instability issues and the authors claimed that it was caused by the division of the measured quantity, although results change if the circulating current internal control loop is used, as well as a saturation block to limit the transients from the measured variable from affecting the stability of the control system. On the other hand, the “open loop control” proved to have excellent results and global asymptotic stability was proven in [31].

In this Thesis, the uncompensated modulation strategy was implemented in the proposed control scheme detailed in chapters 3, 4 and 5, whereas the compensated modulation was used in the Lyapunov stability analysis of chapter B, and was implemented in the proposed non-linear controller of chapter A.

2.9 State of the art of circulating current control schemes

The objective of this Thesis is the proposal of what can be referred to as a *high level* control strategy for the MMC, in particular for regulating the inner dynamics of its circulating current and capacitive energy distribution. This section provides the state of the art of the main MMC control schemes that could be found in the literature back then when this project was undertaken at the beginning of the year 2011. Such control schemes provided a very influential starting point for this research project, and are therefore briefly reviewed. This section serves as the basis for the following one where the need for a new control scheme such as the one introduced and discussed in chapters 3, 4 and 5 is justified.

2.9.1 Direct Modulation

The simplest approach for modulation of the MMC will be to directly use a sinusoidal voltage reference as in a conventional VSC without considering the voltage fluctuations in the upper and lower arm capacitor voltages [3]. Assuming that the per unit voltage reference is given by (2.72), the equivalent output voltage behind the filter inductor of the MMC should then be given by (2.73) under ideal conditions with balanced capacitor voltages.

$$m(t) = \hat{m} \cos \theta_v = \hat{m} \cos \omega t \quad (2.72)$$

$$v_s(t) \approx \frac{v_{dc}}{2} m(t) \quad (2.73)$$

The voltage references for the upper and lower arms, or the corresponding insertion indexes, will then be given by (2.74).

$$\begin{aligned} v_{cu}^* &= \frac{v_{dc}(1-m(t))}{2} \longrightarrow n_u^* = \frac{(1-m(t))}{2} \\ v_{cl}^* &= \frac{v_{dc}(1+m(t))}{2} \longrightarrow n_l^* = \frac{(1+m(t))}{2} \end{aligned} \quad (2.74)$$

This approach is leaving the internal dynamics of the MMC to be uncontrolled, resulting in a large second harmonic circulating current [3, 7]. This uncontrolled circulating current might possibly cause unbalance and disturbances of other variables during transient events. However, it should be remembered, that the internal balancing of the SM capacitors is still ensured by the sorting algorithm used for the modulation. Since there is no feedback of the capacitor voltages, and the modulation is operated directly in open loop, the capacitor voltage dynamics will however remain around the intended voltage. Thus, control methods based on direct modulation will be self-stabilizing, and will not depend on additional control loops to stabilize the internal dynamics of the MMC. The MMC will therefore produce approximately the desired voltage on the AC output. Since the modulation signal will not be explicitly compensated with respect to voltage variations in the SM capacitors or any unbalance between the upper and lower arms, some un-intended harmonic components might however appear in the output voltage unless the SM capacitor is very large.

2.9.2 Open loop control based on estimation of stored energy

The MMC can be controlled on basis of open loop estimated energy in the converter arms instead of by using the measured sum voltage [29]. This approach is shown in Fig. 2.27 and allows for achieving the desired average energy distribution among the arms of the converter, without requiring the explicit measurement of the voltage at all the SM capacitors, even though such measurements are still required for the low-level balancing of the individual capacitors within an arm.

Using the classification method proposed in section 2.8, this control strategy belongs to the compensated modulation family. Therefore, the upper and lower insertion indexes are respectively obtain as the result of dividing their corresponding voltage references by the upper and lower capacitor voltage sum ($u_{cu,l}^\Sigma$) state variables (including their respective oscillating components). However, instead of using their measured values of $u_{cu,l}^{\Sigma,m}$, a steady-state estimated value $u_{cu,l}^{\Sigma}$ is used instead. This estimated value in steady state has to be in accordance with the MMC circulating and grid currents, that have to be estimated as well (i_{c^*} & i_{v^*}). The estimated currents information in steady state is placed in the insertion indexes equations (2.68) and (2.69) by means of their corresponding driving voltages e_{v^*} and u_{c^*} , as well as the estimated upper and lower arm capacitor voltages sum, giving rise to (2.75).

$$\begin{aligned} n_{u^*} &= \frac{\frac{v_{dc}}{2} - e_{v^*} - u_{c^*}}{u_{cu^*}^\Sigma} \\ n_{l^*} &= \frac{\frac{v_{dc}}{2} + e_{v^*} - u_{c^*}}{u_{cl^*}^\Sigma} \end{aligned} \quad (2.75)$$

Almost surprisingly, by applying the insertion indexes of (2.75) to the MMC, the “real” MMC state variables in steady $x \equiv [i_c, i_v, u_{cu}, u_{cl}]$ will converge to their estimated equilibrium $x \rightarrow x_*$

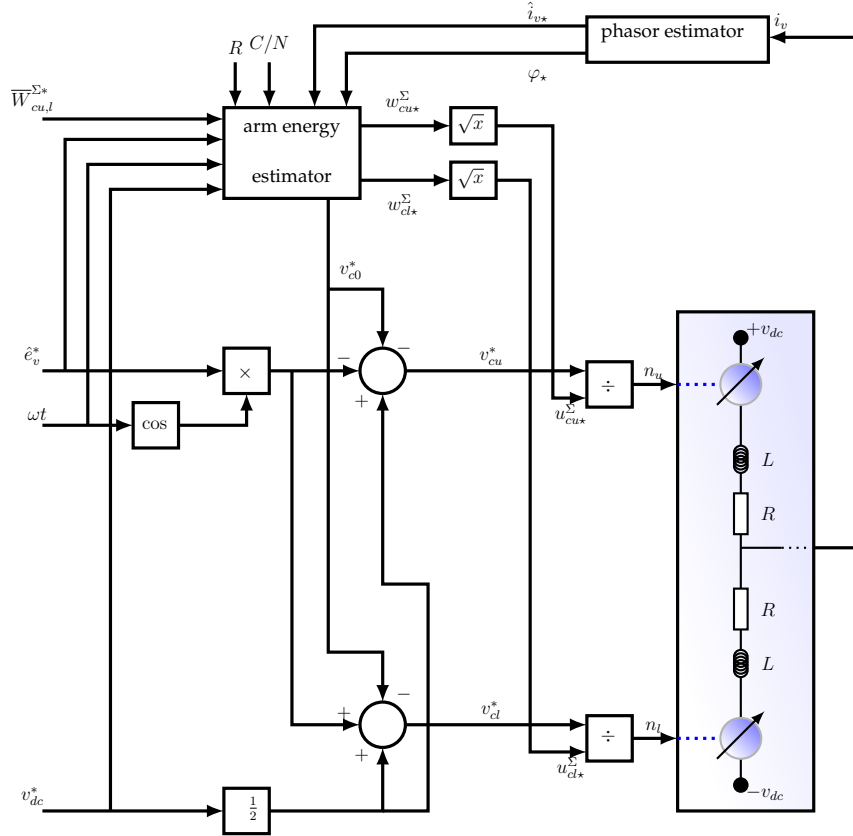


Figure 2.27: Open Loop Control Scheme

without the need of any current or voltage closed feedback measurement loop, hence the name of “open loop control.” The reason of this “self-stabilizing” property of this converter; i.e., x always converging to x_* , was proven some years later by the same research team in [31], by means of Lyapunov’s stability criteria. This proof is reviewed in appendix B so it will no longer be discuss in this section.

The starting point for the estimation method proposed by [29], is the calculation of the steady-state energy oscillations in the capacitors of the upper and lower arms on one MMC leg. This calculation can be started from the common-mode and differential energy distribution equations presented in (2.39) and (2.40); or more directly from the more natural “upper” and “lower” variables expressed in (2.76) and (2.77).

$$\frac{d}{dt}w_{cu*}(t) = i_{u*}u_{cu*} = \left(\frac{i_{v*}}{2} + i_{c*}\right) \left(\frac{v_{dc}}{2} - e_{v*} - u_{c*}\right) \quad (2.76)$$

$$\frac{d}{dt}w_{cl*}(t) = i_{l*}u_{cl*} = \left(-\frac{i_{v*}}{2} + i_{c*}\right) \left(\frac{v_{dc}}{2} + e_{v*} - u_{c*}\right) \quad (2.77)$$

The inputs of these equations are the estimated grid current i_{v*} , the MMC equivalent voltage that drives it e_{v*} , as well as the estimated circulating current i_{c*} and its respective driving voltage u_{c*} . The grid variables can easily be estimated based on the desired active and reactive power transfer between the AC/DC side. For the sake of generality, they are expressed as in (2.78) and (2.79).

$$e_{v\star} = \hat{e}_v \cos(\omega t) \quad (2.78)$$

$$i_{v\star} = \hat{i}_v \cos(\omega t + \varphi) \quad (2.79)$$

The circulating current can be calculated by means of the DC/AC power balance equation of the 3-phase MMC. Furthermore, the circulating current will be controlled constant since the sum of the instantaneous active power of each phase will give a constant as shown in (2.80).

$$i_{c\star} = \frac{P_{dc\star}}{3v_{dc}} \approx \frac{\sum_{k \in (abc)} e_{vk\star} i_{vk\star}}{3v_{dc}} \quad (2.80)$$

Note that in steady state, such current is produced by $u_{c\star} = R i_{c\star}$, where R is the MMC arm resistance.

Finally, the upper and lower capacitor voltage aggregate is estimated by means of (2.81).

$$\begin{aligned} w_{cu\star} &= \frac{1}{2} \frac{C}{N} (u_{cu\star}^\Sigma)^2 \longrightarrow u_{cu\star}^\Sigma = \sqrt{2w_{cu\star} \frac{N}{C}} \\ w_{cl\star} &= \frac{1}{2} \frac{C}{N} (u_{cl\star}^\Sigma)^2 \longrightarrow u_{cl\star}^\Sigma = \sqrt{2w_{cl\star} \frac{N}{C}} \end{aligned} \quad (2.81)$$

This method is very simple to implement and has low computational cost, since it is mainly based on estimating the desired equilibrium point in steady state, and does not need any measurements in the regulation process (although they are still needed for the capacitor balancing algorithm described in section 2.3.2). In addition, since the estimation is done in the natural “abc” coordinates, each voltage and current variable may be controlled independently by phase and by arm. Nonetheless, it is worth mentioning that this technique is model-dependent which implies that any change of the system parameters will lead to a error a different steady state equilibrium point. Furthermore, (2.80) or any equivalent way of obtaining the circulating current corresponding to the desired arm voltages, will involve some kind of approximations, such as neglecting the power losses and/or power fluctuations inside the converter. This is because the equation system that describes the dynamics of the MMC (refer to (2.44)) of the cannot be solved in order to find the desired x_\star .

2.9.3 Circulating current suppression controller

In [17] the authors have proposed a Circulating Current Suppression Controller (CCSC) so that the second harmonic component of the circulating current of the MMC may be suppressed. Such component does not contribute to the average power transfer at the DC terminals of the converter; yet it dissipates power since it circulates through the MMC internal resistances increasing the converter losses. Therefore, this current is aimed to be minimized so that it will only have a DC component.

The current controller, depicted in Fig. 2.28, is based on the double line frequency - negative sequence “dq” rotational reference frame. The three phase circulating currents are then decomposed into two DC components in the direct and in-quadrature axis by means of Park’s transform at 2ω and are both eliminated by a pair of proportional-integral controllers.

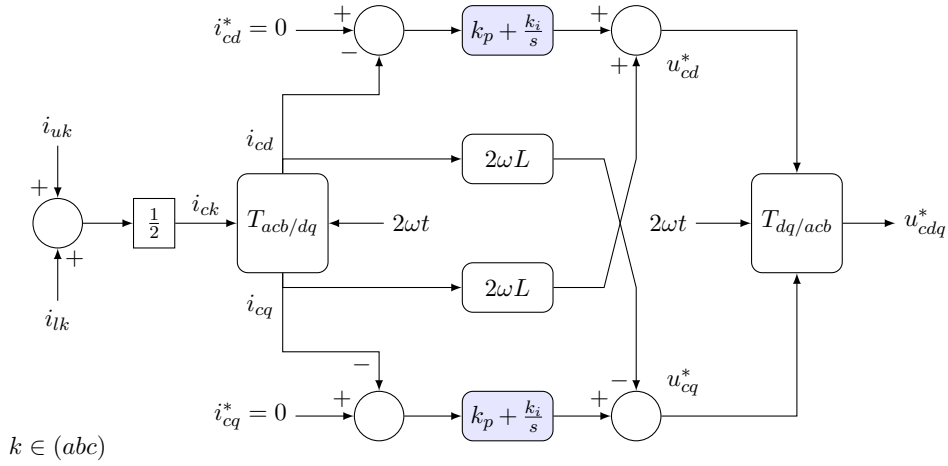


Figure 2.28: Circulating current suppression control scheme

A drawback of this converter is that since it is based on dq-coordinates, controlling independently the phase average values of the circulating currents is a rather complex task. This might be of interest in order to regulate phase-independently the average value of the capacitive energy of the MMC. In addition, by entirely suppressing the second harmonic component, there is no longer the possibility of reducing the capacitive energy fluctuations, as will be discussed in section 2.9.5. This control scheme can be easily enhanced to include the control of the zero-sequence component of the circulating current. A first approach is to set its reference to be a third of the DC current desired: $i_{co}^* = \frac{i_{dc}}{3}$. Nonetheless, it can be used to control the total capacitive energy of the converter $\sum_{k \in (abc)} w_{\Sigma k}$, which has proved particularly useful for operating the MMC under AC grid unbalances [32, 33, 34, 35, 36]. *The operation of the MMC under unbalanced grid conditions is further detailed in chapter 5, hence it will no longer be discussed here.*

2.9.4 Arm energy closed-loop control scheme in the “abc” frame

In [3], the authors proposed one of the first closed loop control for the MMC capable of regulating its internal capacitive energy independently by arm. The control scheme, depicted in Fig. 2.29, is based on the premise that capacitive energy sum $w_{\Sigma k}$ of one MMC leg can be regulated by controlling the DC component of the circulating current. Since the circulating current i_c is driven by u_c (see equations (2.30) and (2.31)) and depends on the MMC arm inductor impedance, a DC component of u_c will be sufficient for maintaining the total capacitor energy at the desired level. Thus, the sum energy control can be based on a simple PI-controller, as given by (2.82).

$$u_{co}^*(s) = [W_{\Sigma}^*(s) - w_{\Sigma}(s)] \cdot k_{po} \left(1 + \frac{1}{T_{io} \cdot s} \right) \quad (2.82)$$

The capacitive energy sum of one leg is then calculated as given by (2.84). The reference value for the sum energy is usually specified to be equal to the sum of the energy in the upper and lower arms when they are both charged to a sum voltage equal to the total, nominal, DC-link voltage, as given by (2.84).

$$w_{\Sigma}(t) = \frac{1}{2} \frac{C}{N} (u_{cu}^{\Sigma}(t))^2 + \frac{1}{2} \frac{C}{N} (u_{cl}^{\Sigma}(t))^2 \quad (2.83)$$

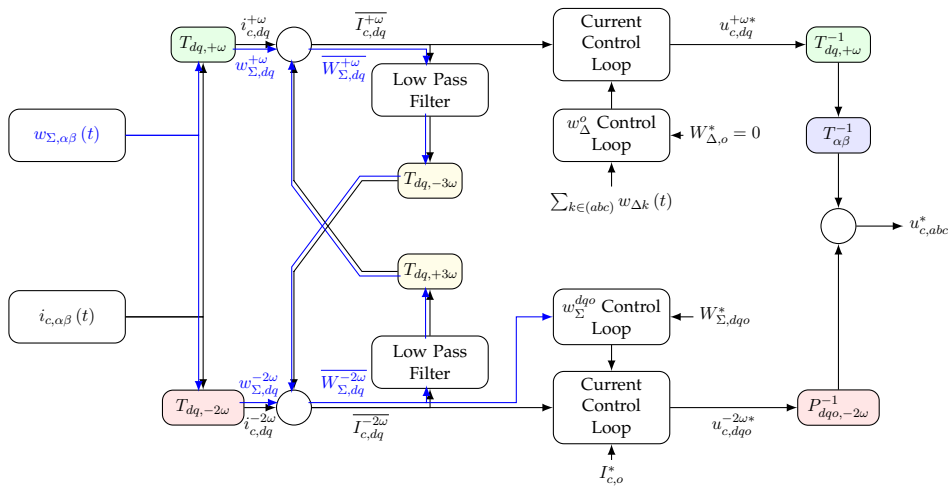


Figure 2.30: Decoupled double synchronous reference frame (DDSRF) control for 3-phase MMC

since hardly anything could be done to efficiently shape it. In addition authors claimed that dividing the insertion indexes by the measured voltages $\sum u_{cu,l}^{\Sigma}$ was a cause for instability and that such control scheme should be abandoned [7]. However, this strategy is reviewed since it played a rather important role in the development of the control proposal of this Thesis, also based on closed loop controllers.

2.9.5 Double decoupled synchronous reference frame (DDSRF) control for 3-phase MMC

An energy-based control scheme for three-phase MMCs in “dqo” coordinates was proposed as part of the work carried out during this PhD Thesis. The proposal of this control technique resulted in two conferences papers [C4]-[C5] and a journal paper [J0], where the interested reader is referred to. Only a brief review is presented in this Thesis manuscript as the approach used to obtain this control strategy is quite different from the one used to obtain what is considered to be the main contribution of this Thesis.

One advantage with this approach, illustrated in Fig. 2.30, is that the control of the various frequency components of the circulating current can be implemented in the appropriate synchronous reference frame.

The control strategy is divided into two main parts. The first one consists in transforming the capacitive energy sum w_{Σ} and the circulating current i_c of the MMC from the stationary abc frame, into the synchronous dqo reference frame. Due to the fact that the MMC energy and current variables have various frequencies, this task is not straightforward, and decoupling the MMC variables into its different frequency components becomes necessary. This is illustrated on the left of Fig. 2.30. The second part, will consist in deriving the energy and circulating current controllers that will regulate the MMC to the desired reference values, as illustrated in the right part of Fig. 2.30. Both of these parts are briefly described in the following lines.

Decoupling method for the MMC

The Double Decoupled Synchronous Reference Frame method proposed by Rodriguez *et al* in [37, 38] is applied to the circulating current of the MMC in the following way.

Assuming that the circulating current can be written as a DC component and its natural components at once and twice the grid frequency, as expressed in (2.88),

$$\begin{bmatrix} i_c^{abc} \end{bmatrix} = \frac{i_{dc}}{3} + i_c^{-2\omega} \begin{bmatrix} \sin(2\omega t + \gamma^{-2\omega}) \\ \sin(2\omega t + \gamma^{-2\omega} + \frac{2\pi}{3}) \\ \sin(2\omega t + \gamma^{-2\omega} - \frac{2\pi}{3}) \end{bmatrix} + i_c^{+\omega} \begin{bmatrix} \sin(\omega t + \gamma^{+\omega}) \\ \sin(\omega t + \gamma^{+\omega} - \frac{2\pi}{3}) \\ \sin(\omega t + \gamma^{+\omega} + \frac{2\pi}{3}) \end{bmatrix} \quad (2.88)$$

By applying Clarke's transform to (2.88) results in (2.89).

$$\begin{aligned} \begin{bmatrix} i_c^{\alpha\beta} \end{bmatrix} &= \frac{2}{3} \begin{bmatrix} 1 & -\frac{1}{2} & -\frac{1}{2} \\ 0 & \frac{\sqrt{3}}{2} & -\frac{\sqrt{3}}{2} \end{bmatrix} \cdot \begin{bmatrix} i_c^{abc} \end{bmatrix} = i_c^{-2\omega} \begin{bmatrix} \sin(2\omega t + \gamma^{-2}) \\ \cos(2\omega t + \gamma^{-2}) \end{bmatrix} \\ &+ i_c^{+\omega} \begin{bmatrix} \sin(\omega t + \gamma^{+1}) \\ -\cos(\omega t + \gamma^{+1}) \end{bmatrix} \end{aligned} \quad (2.89)$$

By defining $\begin{bmatrix} i_c^{dq+\omega} \end{bmatrix}$ and $\begin{bmatrix} i_c^{dq-2\omega} \end{bmatrix}$ as in (2.90) and (2.91):

$$\begin{bmatrix} i_c^{dq+\omega} \end{bmatrix} = \begin{bmatrix} i_{cd}^{+\omega} \\ i_{cq}^{+\omega} \end{bmatrix} = \begin{bmatrix} T_{dq}^{+\omega} \end{bmatrix} \cdot \begin{bmatrix} i_c^{\alpha\beta} \end{bmatrix} \quad (2.90)$$

$$\begin{bmatrix} i_c^{dq-2\omega} \end{bmatrix} = \begin{bmatrix} i_{cd}^{-2\omega} \\ i_{cq}^{-2\omega} \end{bmatrix} = \begin{bmatrix} T_{dq}^{-2\omega} \end{bmatrix} \cdot \begin{bmatrix} i_c^{\alpha\beta} \end{bmatrix} \quad (2.91)$$

where $\begin{bmatrix} T_{dq}^{-2\omega} \end{bmatrix}$ y $\begin{bmatrix} T_{dq}^{+\omega} \end{bmatrix}$ are expressed in (2.92) with $\theta = +1, -2$.

$$\begin{bmatrix} T_{dq}^{+\theta} \end{bmatrix} = \begin{bmatrix} \cos \theta & \sin \theta \\ -\sin \theta & \cos \theta \end{bmatrix} \quad (2.92)$$

Taking into account that $\begin{bmatrix} T_{dq}^{+\theta} \end{bmatrix}^{-1} = \begin{bmatrix} T_{dq}^{-\theta} \end{bmatrix}$, and replacing (2.89) in (2.90) and (2.91) yields in (2.93).

$$\begin{aligned} \begin{bmatrix} i_c^{dq+\omega} \end{bmatrix} &= \overline{\begin{bmatrix} i_c^{dq+\omega} \end{bmatrix}} + \begin{bmatrix} T_{dq}^{+3} \end{bmatrix} \cdot \overline{\begin{bmatrix} i_c^{dq-2\omega} \end{bmatrix}} \\ \begin{bmatrix} i_c^{dq-2\omega} \end{bmatrix} &= \overline{\begin{bmatrix} i_c^{dq-2\omega} \end{bmatrix}} + \begin{bmatrix} T_{dq}^{+3} \end{bmatrix} \cdot \overline{\begin{bmatrix} i_c^{dq+\omega} \end{bmatrix}} \end{aligned} \quad (2.93)$$

with

$$\overline{\begin{bmatrix} i_c^{dq+\omega} \end{bmatrix}} = i_c^{+\omega} \begin{bmatrix} \sin \gamma^{+1} \\ -\cos \gamma^{+1} \end{bmatrix} \quad (2.94)$$

$$\overline{[i_c^{dq-2\omega}]} = i_c^{-2\omega} \begin{bmatrix} \sin \gamma^{-2} \\ \cos \gamma^{-2} \end{bmatrix} \quad (2.95)$$

Equation (2.93) is used as the basis for this control scheme, as can be seen from the left part Fig. 2.30. By applying this method, both of the circulating current harmonic components have been obtained in their respective synchronous reference frames, and can be now used in the control of the MMC. A similar procedure is applied to determine the second harmonic component of the capacitive energy sum $[w_{\Sigma}^{dq-2\omega}]$, which only illustrated in Fig. 2.30.

Controller design

The controllers proposed in [39] are therefore based on the following considerations:

- The zero sequence of the sum energy for all the three phases can be controlled by the zero sequence of the circulating current. This quantity can be controlled to a constant value, and this will correspond to a DC-component of the zero sequence circulating currents. Thus the average power balance of the MMC can be ensured by the following approach:
 - The zero sequence DC-component of the sum energy can be controlled by a simple PI-controller providing a DC-component reference for the zero sequence circulating current as given by (2.96)-(2.97):

$$i_{co}^*(s) = [W_{co}^{\Sigma*}] \cdot K_{p,Wo} \left(1 + \frac{1}{T_{i,Wo} \cdot s} \right) + \frac{P_{vo} + P_{co}}{v_{dc}} \quad (2.96)$$

$$\begin{aligned} W_{co}^{\Sigma*} &= \frac{C}{N} \cdot v_{dc}^2 \\ P_{vo} &= \frac{1}{3} (e_{va}i_{va} + e_{vb}i_{vb} + e_{vc}i_{vc}) \\ P_{co} &= \frac{2}{3} (u_{ca}i_{ca} + u_{cb}i_{cb} + u_{cc}i_{cc}) \end{aligned} \quad (2.97)$$

- The zero sequence circulating current can be controlled by a simple PI-controller providing the DC-component of the circulating voltage as given by (2.98).

$$u_{co}^*(s) = [i_{co}^*(s) - i_{co}(s)] \cdot K_{p,i_{co}} \left(1 + \frac{1}{T_{i,i_{co}} \cdot s} \right) \quad (2.98)$$

- The individual capacitor voltage ripples of an MMC can be reduced by controlling the sum energy in one leg to a constant value. Without explicit control of the capacitive energy sum in one phase, it will however oscillate with a dominant frequency of two times the fundamental grid frequency. For a three-phase configuration, these oscillations of the capacitive energy sum $w_{\Sigma k}$ of the MMC can be interpreted as a negative sequence double frequency component, and can therefore be expressed as d- and q- axis components in a synchronous reference frame rotating at twice the fundamental frequency. Since the average sum energy of all the three legs of the converter will appear as a zero sequence component, constant sum energy per phase can be achieved by controlling the d- and q-axis components of the sum energy in the double frequency synchronous reference frame to zero. It has been

shown in [39] that this will limit the capacitor voltage oscillations to lower values than what is resulting from other methods. Thus the sum energy oscillations of the MMC, and the corresponding capacitor voltage oscillations can be reduced by the following approach:

- The d- and q-axis sum energy oscillations in the double frequency negative sequence synchronous reference sequence frame can be controlled to zero by using the controllers given in (2.99) and (2.100) to provide reference values for the circulating current control. It can be noticed that these equations are designed by using similar principles as for decoupled current controllers in synchronous reference frames. Therefore, the equations contain feed-forward terms originating from the power flow through the converter as well as decoupling terms based on the sum energy.

$$i_{cd}^{*-2\omega}(s) = [W_{\Sigma d}^{*-2\omega}(s) - w_{\Sigma d}^{-2\omega}(s)] \cdot K_{p,2w\Sigma} \left(1 + \frac{1}{T_{i,2w\Sigma} \cdot s}\right) + \frac{P_{vd}^{-2\omega} + P_{cd}^{-2\omega} - 2\omega w_{\Sigma q}^{-2\omega}}{v_{dc}} \quad (2.99)$$

$$i_{cq}^{*-2\omega}(s) = [W_{\Sigma q}^{*-2\omega}(s) - w_{\Sigma q}^{-2\omega}(s)] \cdot K_{p,2w\Sigma} \left(1 + \frac{1}{T_{i,2w\Sigma} \cdot s}\right) + \frac{P_{vq}^{-2\omega} + P_{cq}^{-2\omega} + 2\omega w_{\Sigma d}^{-2\omega}}{v_{dc}} \quad (2.100)$$

- The circulating current according to the references provided by (2.99) and (2.100), can then be controlled by decoupled current controllers implemented in the double frequency negative sequence reference frame. Thus the corresponding d- and q- axis differential voltage components can be expressed by (2.101) and (2.102) respectively.

$$u_{cd}^{*-2\omega}(s) = [i_{cd}^{*-2\omega}(s) - i_{cd}^{-2\omega}(s)] \cdot K_{p,i2\omega} \left(1 + \frac{1}{T_{i,i2\omega} \cdot s}\right) - 2\omega \cdot L \cdot i_{cq}^{-2\omega} \quad (2.101)$$

$$u_{cq}^{*-2\omega}(s) = [i_{cq}^{*-2\omega}(s) - i_{cq}^{-2\omega}(s)] \cdot K_{p,i2\omega} \left(1 + \frac{1}{T_{i,i2\omega} \cdot s}\right) + 2\omega \cdot L \cdot i_{cd}^{-2\omega} \quad (2.102)$$

- The capacitive energy difference between the upper and lower arms of the MMC w_{Δ} is associated with oscillations at the fundamental frequency, and can therefore be controlled in a corresponding synchronously rotating reference frame. However, there is a natural fundamental frequency component in the energy difference that is related to the active power transfer of the MMC. This implies that the instantaneous d- and q-axis components of the energy difference are therefore not suitable for controlling the energy difference. Therefore, only the zero sequence component of the energy difference should be controlled, since this term is directly linked to the average energy difference of all the three phases.

- With the conventions applied in [39], the reference value for the fundamental frequency circulating current components in the positive sequence reference frame can be shown to be expressed by (2.103) and (2.104).

$$i_{cd}^{*+\omega}(s) = 0 \quad (2.103)$$

$$i_{cq}^{*+\omega}(s) \approx [W_{\Delta o}^*(s) - w_{\Delta o}(s)] \cdot K_{p,w\Delta o} \left(1 + \frac{1}{T_{i,w\Delta o} \cdot s} \right) \quad (2.104)$$

- The circulating current according to the references provided by (2.103) and (2.104), can then be controlled by decoupled current controllers implemented in the fundamental frequency positive sequence reference frame. Thus the corresponding d- and q- axis differential voltage components can be expressed by (2.105) and (2.106) respectively.

$$u_{cd}^{*+\omega}(s) = [i_{cd}^{*+\omega}(s) - i_{cd}^{+\omega}(s)] \cdot K_{p,icw} \left(1 + \frac{1}{T_{i,icw} \cdot s} \right) + \omega \cdot L \cdot i_{cq}^{\omega} \quad (2.105)$$

$$u_{cq}^{*+\omega}(s) = [i_{cq}^{*+\omega}(s) - i_{cq}^{+\omega}(s)] \cdot K_{p,icw} \left(1 + \frac{1}{T_{i,icw} \cdot s} \right) - \omega \cdot L \cdot i_{cd}^{\omega} \quad (2.106)$$

- The resulting differential voltage to be used for modulation of the converter will be given by the sum of all the voltage components ($u_{cd}^{*-2\omega}$, $u_{cq}^{*-2\omega}$, $u_{cd}^{*+\omega}$, $u_{cq}^{*+\omega}$ and u_{co}^*) from after transformation back to the natural abc reference frame, as illustrated in Fig. 2.30.

The control method described above requires several reference frame transformations and corresponding filtering to extract the appropriate frequency components of the energies and currents of the MMC, but the resulting performance is good, as further discussed in [J0]. A detailed explanation of all the steps and transformations needed for the implementation is, however, outside the scope of this manuscript. To give an overview, the main structure of the resulting control systems, showing only the main lines of signal flows, is shown in Fig. 2.30.

2.10 Motivation for a new circulating current control scheme for the MMC

When this Thesis was undertaken back in 2011, only a handful of control schemes for the MMC could be found in literature. Section 2.9 reviews some of the most influential control schemes for the main contributions presented in this manuscript in chapters 3, 4 and 5. These control schemes are compared with the proposed control scheme of this manuscript in Table 2.3. This is further discussed in the following lines.

The direct modulation strategy [3] does not intend to control the circulating current in any way; therefore, this strategy is not a suitable candidate for controlling the MMC due to the risk of unstable operation and resonances. However, it provides a simplified yet powerful tool for analyzing the interaction of the different harmonics that occur in the MMC, and for sizing and adequately selecting the MMC storage parameters, as was successfully done by Ilves *et al* in [28] and in [40], respectively.

The open loop control scheme [3, 7] reviewed in section 2.9.2 was and continues to be one of the most attractive strategies for the control of the MMC. Potentially, its most important advantage is the simplicity of the implementation: the insertion indexes are calculated based only on the estimation of the equilibrium point x_* and implemented in an “open loop” fashion, excluding the need for any feedback loop. Furthermore, it was demonstrated using Lyapunov’s stability criteria in [31] that the MMC with its open loop controller is globally asymptotically stable. However, this is a quite common phenomenon that can be found in nature; i.e., a great deal of systems

are globally asymptotically stable in open loop, yet there is still strong interest to close the loop in order to ensure robustness with respect to any perturbations, errors in the estimation process of the equilibrium point x_* , and parameter uncertainty. The MMC seems to be affected by all these aspects, suggesting that a feedback loop for currents and voltages might prove to be a rather useful feature. In addition, the response time in open loop systems is imposed by the natural time constants of the system. By closing the loop, the dynamical performance can be changed by means of the closed loop control action.

The closed-loop control proposed in [3] and reviewed in section 2.9.4 did not perform to expectations, which might have led the authors to pursue the open loop approach discussed in the above paragraph. Two reasons may have caused such unexpected results:

1. In [3] only a feedback loop for the arm capacitor voltages was used, leaving the circulating current completely on its own.
2. The insertion indexes were determined using the *compensated modulation* strategy, according to the definition proposed in 2.9. This means that to calculate the insertion indexes, the reference arm voltages $v_{cu,l}^*$ are *not* divided by the constant value of v_{dc} but by the sum of the capacitor voltages in an arm $u_{cu,l}^\Sigma$. Now, if this is done using the estimated value of such variable as was the case for the open loop control strategy; i.e., $u_{cu,l}^\Sigma$, no unstable operation should take place. However, the measured values of $u_{cu,l}^\Sigma$ were used instead, and their transient behavior seemed to have caused unstable operation of the converter.

These two factors can be avoided in order to obtain a satisfactory performing closed loop control for the MMC as will be discussed in the following chapters.

Contrary to the closed-loop control of [3], the circulating current suppression control (CCSC) [17] reviewed in section 2.9.3 has a feedback loop only for the circulating current, leaving the capacitor arm voltages unregulated. Its feedback loop ensures robustness and good dynamic performance but the complete control scheme including the regulation of the missing MMC voltage variables had yet to be done. Such control was based on the “dqo” rotating reference frame, which has the inherent disadvantage of not providing direct and explicit control of the circulating current independently by phase.

The DDSRF control of the MMC proposed as part of the work carried out in this PhD Thesis in [J0] and reviewed in 2.9.5, is an attempt to extend the CCSC by including a feedback control loop in the arm capacitor energies of the MMC, while keeping the one for the circulating current to ensure good dynamical performance and robustness for all the converter variables. The main drawback of this control technique is its complexity: since the method is done in the “dqo” reference frame, several reference frame transformations are required at the different frequencies of the MMC, which in turn are naturally coupled. A second significant drawback of using “dqo” coordinates is the inability to control the average values of the energy sum $\overline{w_{\Sigma k}}$ and difference $\overline{w_{\Delta k}}$ independently by phase; instead only their zero-sequence values can be controlled. In other words, only the addition of the phase values can be controlled and not the phase values *per se*. This issue is not so important in classical three-phase VSC converters since the currents in each phase *do not have any DC components*. The MMC converter energy and circulating currents variables do however, present an important DC component in each phase, and successfully regulating it phase independently has proven to be advantageous.

To conclude, a new control scheme for the MMC was needed. Such a control scheme should be based on four feedback control loops; i.e. one for each of the MMC state variables to ensure

Table 2.3: Qualitative comparison between state of the art high level control schemes and justification of new proposal

	Good Dynamic Performance	Robustness/Parameter independent	Circulating Current Control	Capacitive Energy Control	SM Voltage Measurement independence	Phase Independent Control (abc frame)
Direct Modulation	✗	✓	✗	✗	✓	✗
Open Loop Control	✗	✗	✓	✓	✓	✓
Closed Loop Control	✗	✓	✗	✓	✗	✓
Circ. Current Suppr. Control	✓	✓	✓	✗	✓	✗
Double Decoupled Synchr. Control	✓	✓	✓	✓	✗	✗
Proposed Control	✓	✓	✓	✓	✗	✓

robustness. It should be done in the stationary “abc” frame to reduce the complexity of the implementation and to enable the control of the converter variables independently by phase. Last but not least, the controller must have a good dynamical performance, comparable to the well known “dqo”-based control techniques for three-level VSCs.

3

Optimization of the Circulating Current Signal for Phase Independent Energy Shaping and Regulation

The purpose of this chapter is to provide a novel control philosophy for the MMC in its natural abc reference frame that will enable stored capacitive energy to be regulated independently by phase and arms, while shaping the circulating current and transferring power between AC and DC terminals. This is achieved by replacing traditional control schemes based on the instantaneous pq-theory in d-qo or $\alpha\beta o$ coordinates by instantaneous abc-theory based on mathematical optimization using Lagrange multipliers. In addition, the implementation of such a current reference using multi-resonant controllers in a shunt configuration is discussed.

3.1 Introduction

SEVERAL studies have investigated the dynamics of the MMC, such as [3, 7, 8], and attempts have been made to efficiently model it [9, 10, 11, 27], as was described in the previous chapter. Although the MMC topology may appear quite simple, the task of regulating the capacitive arm energies w_Σ and w_Δ while performing a stable power transfer between both HVDC terminals is rather complex. This issue has awakened the interest of several researchers and has led to a number of publications such as the ones reviewed in chapter 2 [3, 29, 17, 39], as well as other important efforts such as [7, 3, 41, 42, 43, 29, 44, 45, 17, 39, 46] including predictive control [47, 48, 49, 50, 51, 52] and controllers for unbalanced faults [33, 32]. Most of the controllers proposed up until now have taken advantage of the fact that the MMC operates with two currents that are practically independent; i.e., the load or grid current i_v and the circulating current i_c . The grid current is typically used either to control the active power or to regulate the DC bus voltage. In addition, it may provide voltage support by adequately injecting the necessary reactive power

as a two or three-level voltage source converter. Meanwhile, the circulating current, which could be defined as a current that naturally circulates “inside” the MMC without directly interfering with the AC grid, has been used in several control propositions to balance and equally distribute the MMC total energy between each arm [3]. This current has also been controlled in such a way that it will not present its natural ripple at twice the grid frequency [17].

Previous publications [53]-[J0] have proposed a solution where a specific current component at twice the grid fundamental frequency is added to the circulating current in order to reduce voltage oscillations. Given the high number of capacitors in the MMC for HVDC applications ($n \geq 80$) and the fact that DC capacitor sizing is sensitive to AC voltage variations, the size of the converter can be significantly reduced. In order to do so, the capacitive stored energy in each phase must be maintained constant, while the average energy difference between the upper and lower multi-valves is maintained at zero. Some of the controllers that achieve this objective ([J0]) are obtained in one (or more) synchronous reference frames, which need mathematical transformations on the dqo frame in combination with the well known instantaneous power theory of [54]. This methodology complicates the accomplishment of this task, since a strong coupling exists between current and energy variables, and the decoupling is not always a straightforward task to perform as discussed in chapter 2. To overcome this obstacle, abc power theories are preferred instead.

Several authors have searched for appropriate instantaneous power theories in the abc frame to “shape” the current reference, including [55, 56, 57, 58]. Nevertheless, most of these theories do not necessarily find the optimal operating point. Therefore a generalized compensation approach based on mathematical optimization using the Lagrange multipliers method in ABC frame is preferred instead. This strategy, reviewed in [54] and generalized in [59], enhances the classical ABC theory [60] for reactive power compensation and active filtering. Due to the generality and versatility of the Lagrange’s multipliers ABC theory, it was possible to apply this optimization technique to the MMC, leading to its own general power control approach in the ABC frame. A first step of this method was published in [[C6]]. Nonetheless, the research was still at a very early stage. Subsequently, significant and clear improvements of the precedent work were made and the main findings were published in [J1] and [C10], since the entire mathematical optimization problem was reformulated leading to a simpler and more effective control scheme. This control scheme for the MMC based on mathematical optimization is the main contribution of this chapter.

The outline of this chapter is as follows: a review of the minimized current method based on Lagrange multipliers is provided in section 3.2 to set the basis for the rest of the chapter. In section 3.3 the mathematical optimization is applied to the internal dynamics of the MMC to control instantaneously the average capacitive energy sum and difference ($\bar{w}_{\Sigma k}$ & $\bar{w}_{\Delta k}$) stored in the MMC capacitors between the upper and lower multi-valves, while forcing the circulating current (section 3.3.1) or the instantaneous capacitive energy sum (section 3.3.2) to fluctuate as little as possible. Subsequently, in section 3.3.3, a generalized formulation including both results obtained in sections 3.3.1 and 3.3.2 is given, obtained by multi-objective optimization. Section 3.5 shows the simulated results of using this equation to control a 200 level MMC high efficiency model [11] in EMTP. More precisely, in section 3.5.3, a comparison between the proposed control approach with both the CCSC of [17] (section 3.5.3) and the Closed-Loop Control of [3] (section 3.5.3) is presented. Furthermore, in section 3.5.4, a two terminal MMC-HVDC system was simulated under both energy (section 3.5.4) and power (section 3.5.4) reference step changes in order to validate the proposed control approach for this kind of application. Finally, some chapter conclusions based on the results presented are described in section 3.6.

3.2 Introduction to the instantaneous abc theory

Using the classification proposed by Akagi *et al* in their well renowned book *Instantaneous Power Theory and Applications to Power Conditioning* [54], the instantaneous power theory can be separated into two groups depending on whether the power has been defined on the $\alpha\beta o$ -reference frame or directly using the instantaneous phase voltages and line currents; i.e., using the natural *abc* coordinates from the start. To contrast with *p-q theory*, which they use to define the first set of power definitions, they have suggested the term *abc theory* for the second group. The *abc theory* is also referred to as the *vectorial theory* due to the formulation presented by Peng [60].

The use of mathematical optimization was suggested for reactive power compensation in the work of [61, 62], and has been used to provide some power definitions, such as in the work of Willems *et al* [63]. In addition, a small number of publications have applied the mathematical optimization approach using the *abc theory*, such as those in [64, 65]. Furthermore, in a small section called “Active and Nonactive Current Calculation by Means of a Minimization Method” of the previously mentioned book by Akagi *et al* ([54]) published in 2007, the authors used the Lagrange Multiplier method to determine the required currents in the “abc” coordinates. However only a very particular case was addressed (instantaneously constant active power), without truly exploiting the versatility advantages of the optimization technique. Nonetheless, this represents an important contribution to this research field of this Thesis, and is therefore briefly reviewed in section 3.2.1.

In 2012, A. Garcés, M. Molinas and P. Rodriguez managed to fully exploit the versatility of the optimization method based on Lagrange multipliers, by generalizing the results of [54] for the case of active filters [59]. These two contributions are considered essential to the scientific proposal presented in this chapter, as the methodology was extended for the case of the MMC. For this reason, they are briefly reviewed in sections 3.2.1 and 3.2.2, respectively.

3.2.1 Active and nonactive current calculation by means of a minimization method

H. Akagi’s method, presented in [54], involves minimizing the three phase currents of a three phase system (e.g.: active rectifier) under the constraint that such currents should transfer the desired instantaneous active power. This means that the objective function f that is to be minimized should consist on the phase current i_k , where $k \in (abc)$, as expressed in (3.1).

$$\min \rightarrow f(i_k) = (i_k)^2, k \in (abc) \quad (3.1)$$

Equation 3.1 is subject to the following constraint: the dot product between the three phase currents with their corresponding voltages will give the desired instantaneous three-phase active power, as expressed in (3.2).

$$p_{3\varphi} = \sum_{k \in (abc)} v_k i_k \quad (3.2)$$

The Lagrange equation can be therefore written as a function of the current and the Lagrange multiplier λ , as shown in (3.3).

$$\mathcal{L}(i_k, \lambda) = (i_k)^2 + \lambda \left(\sum_{k \in (abc)} v_k i_k - p_{3\varphi} \right) \quad (3.3)$$

In order to find the minimized current, it is necessary to solve the equation system represented by (3.4).

$$\nabla_{i_k, \lambda} \mathcal{L}(i_k, \lambda) = 0 \quad (3.4)$$

Both of the resulting partial derivatives are expressed in equations (3.5) and (3.6).

$$\frac{\partial \mathcal{L}(i_k, \lambda)}{\partial i_k} = 2i_k + \lambda v_k = 0 \quad (3.5)$$

$$\frac{\partial \mathcal{L}(i_k, \lambda)}{\partial \lambda} = \sum_{k \in (abc)} (v_k i_k) - p_{3\varphi} = 0 \quad (3.6)$$

By multiplying equation (3.5) by v_k , adding up all three phase, combining the resulting equation with (3.6) and solving for λ gives:

$$\lambda = -\frac{2p_{3\varphi}}{\sum_{k \in (abc)} v_k^2} \quad (3.7)$$

Finally, the minimized current is obtain by replacing (3.7) in (3.5) and solving for i_k , yielding in (3.8).

$$i_k = \frac{p_{3\varphi}}{\sum_{k \in (abc)} v_k^2} v_k \quad (3.8)$$

Using Fryze's nomenclature, the resulting minimized current can be referred to as well as the instantaneous *active* current. Such a current can be considered as a part of the original instantaneous load current. The difference between the instantaneous original load current and the instantaneous active (minimized) current is often referred to as the *non-active* current. However, if a current controller is used as for the case of this Thesis, the instantaneous original load current can be forced to be equal to the active current.

3.2.2 Generalized compensation theory for active filters based on mathematical optimization

The method presented in the previous section only considered one particular case of power transfer. Garcés *et al* managed to extend these results by using the inherent versatility of Lagrange multipliers method. In [59], they calculated the minimized current necessary to achieve the following four cases:

1. Invariant instantaneous power,

2. Constant power,
3. Unity power factor,
4. Pure sinusoidal currents.

Each of these cases were the result of writing the optimization problem in different ways. The first case, for instance generalized Akagi's contribution as well as Fryze's similar proposal for a three-phase, four-wire system by including a second constraint to ensure that the fourth wire line current is eliminated. The Lagrange equation for this case for an active rectifier is expressed in (3.9).

$$\mathcal{L}(i_k, \lambda_P, \lambda_0) = (i_k)^2 + \lambda_P \left(\sum_{k \in (abc)} v_k i_k - p_{3\varphi} \right) + \lambda_0 \left(\sum_{k \in (abc)} i_k \right) \quad (3.9)$$

By solving $\nabla_{(i_k, \lambda_P, \lambda_0)} \mathcal{L}(i_k, \lambda_P, \lambda_0)$ using a similar procedure to what was presented in section 3.2.1 yields in:

$$i_k = \frac{p_{3\varphi}}{\sum_{k \in (abc)} v_k^2 - 3(v_o)^2} \cdot (v_k - v_o) \quad (3.10)$$

where $v_o = \frac{1}{3} \sum_{k \in (abc)} v_k$.

The minimized current expressed in (3.10) is a clear generalization of the one expressed in (3.8), since it includes the zero sequence current elimination property. It is important to stress here that this was done by modifying the Lagrange equation, or more particularly, by adding constraints.

Taking the unity power factor case of [59] as an other example (without ensuring zero line current in the fourth wire for simplicity), the Lagrange equation yields in (3.11).

$$\mathcal{L}(i_k, \lambda_P) = \frac{1}{T} \int_{t_o}^{t_o+T} (i_k)^2 dt + \lambda_P \left(\frac{1}{T} \int_{t_o}^{t_o+T} \sum_{k \in (abc)} v_k i_k dt - p_{3\varphi} \right) \quad (3.11)$$

By solving $\nabla_{(i_k, \lambda_P)} \mathcal{L}(i_k, \lambda_P)$, the minimized current for this case results in (3.12).

$$i_k = \frac{p_{3\varphi}}{\sum_{k \in (abc)} (V_k^{rms})^2} \cdot v_k \quad (3.12)$$

Where $V_k^{rms} = \sqrt{\frac{1}{T} v_k^2 dt}$.

Once again, the versatility of the methodology is highlighted since a different equation is found simply by reformulating the optimization problem. This versatility property of mathematical optimization, as well as obtaining the theoretical minimum current and the possibility of applying the method directly in the "abc" coordinates of the converter, were the determining factors of its extension to the MMC case.

3.3 MMC circulating current calculation for phase independent control

3.3.1 MMC constant circulating current

The goal of this section is to analytically calculate the circulating current *constant* reference that is able to control the average energy distribution inside the MMC (i.e., control of $\overline{w}_{\Sigma k}$ and $\overline{w}_{\Delta k}$). Immediately it is possible to suggest to pose as the objective function to be minimized, the instantaneous value of the circulating current oscillations; i.e., $\min \rightarrow \Delta(i_{ck})$, or for a more general result, to minimize the instantaneous value of the DC power phase contribution oscillations; i.e., $\min \rightarrow \Delta(v_{dc}i_{ck})$. Since usually v_{dc} is constant, the objective functions are almost equivalent for our purposes. Although the objective function is an instantaneous value, the optimization problem will be subject to two *averaged* constraint equations ((3.14) and (3.15)). The fact of having an instantaneous objective function and averaged constraints will complicate the analytical resolution of the problem. To avoid this complication, the instantaneous objective function is transformed into an averaged one as well, without losing the “instantaneous” information, by minimizing the average of the variable squared value instead, as shown in (3.13).

$$\min \rightarrow \frac{1}{T} \int_{t_0}^{t_0+T} (v_{dc}i_{ck})^2 dt \quad (3.13)$$

We now proceed to minimize such an objective function subject to the following constraints:

$$\frac{1}{T} \int_{t_0}^{t_0+T} (-e_{vk}i_{vk} + v_{dc}i_{ck}) dt = \overline{P_{\Sigma k}^{ref}} \quad (3.14)$$

$$\frac{1}{T} \int_{t_0}^{t_0+T} \left(\frac{i_{vk}}{2}v_{dc} - 2e_{vk}i_{ck} \right) dt = \overline{P_{\Delta k}^{ref}} \quad (3.15)$$

Where equation (3.14) is the average value of the energy sum dynamics $w_{\Sigma}(t)$ and equation (3.15) is the average value of the energy-difference dynamics $w_{\Delta}(t)$. Each of these two energy dynamics are forced to be equal to the references expressed in equations (3.16) and (3.17):

$$\overline{P_{\Sigma k}^{ref}} = \left[kp_{\Sigma} \left(W_{\Sigma k}^{ref} - \overline{w_{\Sigma k}} \right) + ki_{\Sigma} \int \left(W_{\Sigma k}^{ref} - \overline{w_{\Sigma k}} \right) dt \right] \quad (3.16)$$

$$\overline{P_{\Delta k}^{ref}} = \left[kp_{\Delta} \left(W_{\Delta k}^{ref} - \overline{w_{\Delta k}} \right) + ki_{\Delta} \int \left(W_{\Delta k}^{ref} - \overline{w_{\Delta k}} \right) dt \right] \quad (3.17)$$

Where $\overline{w_{\Sigma k}}$ and $\overline{w_{\Delta k}}$ are the average values of the energy sum and difference as a function of time, respectively. The ideal value of the left side of (3.14) and (3.15) would be zero, but then again, this would only ensure that the average value of $w_{\Sigma k}(t)$ and $w_{\Delta k}(t)$ would be any constant, and not the desired constant. Therefore, they are set at $P_{\Sigma k}$ and $P_{\Delta k}$ which are calculated in (3.16) and (3.17).

The Lagrange equation \mathcal{L} for this case is written in (3.18).

$$\begin{aligned} \mathcal{L}(i_{ck}, \lambda_{\Sigma}, \lambda_{\Delta}) = & \frac{1}{T} \int_{t_0}^{t_0+T} (v_{dc} i_{ck})^2 dt + \\ & \lambda_{\Sigma} \left(\overline{w_{\Sigma k}}(t) - \overline{P_{\Sigma k}^{ref}} \right) + \lambda_{\Delta} \left(\overline{w_{\Delta k}}(t) - \overline{P_{\Delta k}^{ref}} \right) \end{aligned} \quad (3.18)$$

Where $\overline{w_{\Sigma k}}(t)$ is given by the left side of (3.14) and $\overline{w_{\Delta k}}(t)$ is given by the left side of (3.15).

In order to find the circulating current, it is necessary to solve (3.19):

$$\nabla_{(i_{ck}, \lambda_{\Sigma}, \lambda_{\Delta})} \mathcal{L}(i_{ck}, \lambda_{\Sigma}, \lambda_{\Delta}) = 0 \quad (3.19)$$

The first derivative is expressed by the following equation:

$$\frac{\partial \mathcal{L}}{\partial i_{ck}} = \frac{1}{T} \int_{t_0}^{t_0+T} 2v_{dc}^2 i_{ck} dt + \lambda_{\Sigma} \frac{1}{T} \int_{t_0}^{t_0+T} v_{dc} dt - 2\lambda_{\Delta} \frac{1}{T} \int_{t_0}^{t_0+T} e_{vk} dt = 0 \quad (3.20)$$

Equation (3.20) can be re-written as (3.21) by cancelling out the integrating action.

$$\frac{\partial \mathcal{L}}{\partial i_{ck}} = 2v_{dc}^2 i_{ck} + \lambda_{\Sigma} v_{dc} - 2\lambda_{\Delta} e_{vk} = 0 \quad (3.21)$$

The solution to the other two derivatives are expressed in the following equations:

$$\frac{\partial \mathcal{L}}{\partial \lambda_{\Sigma}} = \overline{w_{\Sigma k}}(t) - \overline{P_{\Sigma k}^{ref}} = 0 \quad (3.22)$$

$$\frac{\partial \mathcal{L}}{\partial \lambda_{\Delta}} = \overline{w_{\Delta k}}(t) - \overline{P_{\Delta k}^{ref}} = 0 \quad (3.23)$$

Replacing $\overline{w_{\Sigma k}}(t)$ and $\overline{w_{\Delta k}}(t)$ by the left side of (3.14) and (3.15), respectively, and solving the three dimensional equation system formed by (3.21), (3.22) and (3.23), the solution for the circulating current reference is obtained, and it is given in (3.24).

$$i_{ck} = \left[\frac{\overline{P_{\Sigma k}^{ref}} + \overline{P_{vk}}}{v_{dc}^2} \right] v_{dc} + \left[\frac{-\overline{P_{\Delta k}^{ref}}}{2v_{dc}^2 (e_{vk,p.u.}^{rms})^2} \right] e_{vk} \quad (3.24)$$

Where:

$$\begin{aligned} \overline{P_{vk}} &= \frac{1}{T} \int_{t_0}^{t_0+T} e_{vk} i_{vk} dt \\ (e_{vk,p.u.}^{rms})^2 &= \frac{1}{T} \int_{t_0}^{t_0+T} \frac{e_{vk}^2}{v_{dc}^2} dt \end{aligned}$$

As can be seen, (3.24) has a mathematical structure similar to the structures of instantaneous power theories-based currents definitions; in this case, two conductances directly proportional to the two voltages e_{vk} and v_{dc} .

3.3.2 MMC constant energy sum

In this case, we are interested in operating the converter with constant capacitive energy in each phase in order to reduce the capacitor voltages oscillations (see [39]). In order to do so, the optimization problem will have the instantaneous energy sum dynamics $\dot{w}_{\Sigma k}$ as the objective function to be minimized. This is expressed in 3.25.

$$\min \rightarrow \frac{1}{T} \int_{t_0}^{t_0+T} (\dot{w}_{\Sigma k})^2 dt \quad (3.25)$$

The constraints of the optimization problem are the same constraints as the ones from the previous section, i.e., (3.14) and (3.15). This is no coincidence as it will be made obvious in section 3.3.3. Hence, the Lagrange equation may be written as in (3.26).

$$\begin{aligned} \mathcal{L}(i_{ck}, \lambda_{\Sigma}, \lambda_{\Delta}) = & \frac{1}{T} \int_{t_0}^{t_0+T} (\dot{w}_{\Sigma k})^2 dt + \lambda_{\Sigma} \left(\overline{w_{\Sigma k}}(t) - \overline{P_{\Sigma k}^{ref}} \right) \\ & + \lambda_{\Delta} \left(\overline{w_{\Delta k}}(t) - \overline{P_{\Delta k}^{ref}} \right) \end{aligned} \quad (3.26)$$

As the previous case, in order to find the circulating current control reference, the three partial derivatives (Equation 3.19) of the newly obtained Lagrange equation (Equation (3.26)) must be solved. The first derivative resulting in:

$$\begin{aligned} \frac{\partial \mathcal{L}}{\partial i_{ck}} = & \frac{1}{T} \int_{t_0}^{t_0+T} 2(-e_{vk}i_{vk} + v_{dc}i_{ck})v_{dc}dt + \lambda_{\Sigma} \frac{1}{T} \int_{t_0}^{t_0+T} v_{dc}dt \\ & - 2\lambda_{\Delta} \frac{1}{T} \int_{t_0}^{t_0+T} e_{vk}dt = 0 \end{aligned} \quad (3.27)$$

Canceling the integral action of (3.27) gives:

$$\frac{\partial \mathcal{L}}{\partial i_{ck}} = 2(-e_{vk}i_{vk} + v_{dc}i_{ck})v_{dc} + \lambda_{\Sigma}v_{dc} - 2\lambda_{\Delta}e_{vk} = 0 \quad (3.28)$$

Since the same optimization constraints are used in this case, the solution to the other two derivatives are given by (3.22) and (3.23). Solving this three-dimensional system formed by (3.28), (3.22) and (3.23), one may obtain the circulating current control reference:

$$i_{ck} = \left[\frac{\overline{P_{\Sigma k}^{ref}}}{v_{dc}^2} \right] v_{dc} + \frac{P_{vk}}{v_{dc}} + \left[\frac{-\overline{P_{\Delta k}^{ref}}}{2v_{dc}^2 \left(e_{vk,p.u.}^{rms} \right)^2} \right] e_{vk} \quad (3.29)$$

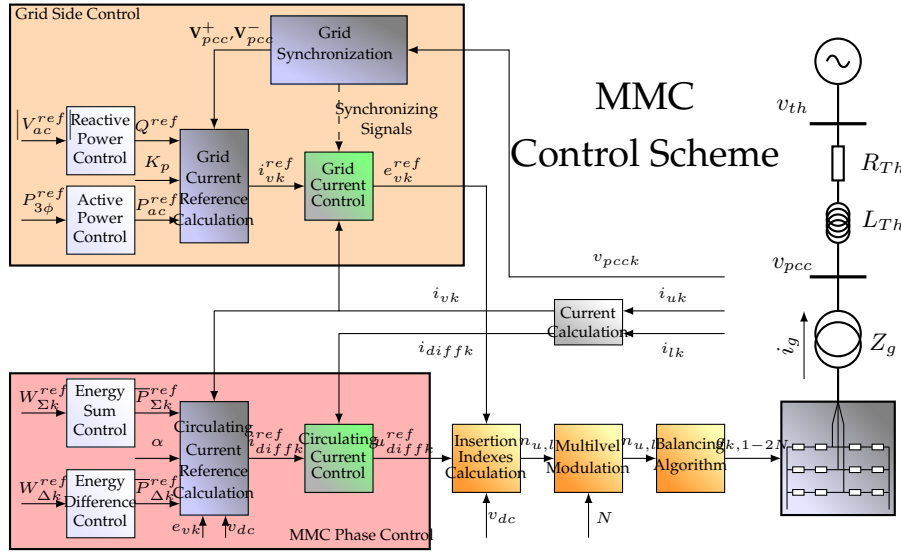


Figure 3.1: MMC phase control scheme

3.3.3 Generalized equation

By solving the following multi-objective optimization problem, it is possible to obtain a generalized circulating current reference equation that includes both results from sections 3.3.1 and 3.3.2.

$$\min \rightarrow \frac{1}{T} \int_{t_0}^{t_0+T} \left[\alpha (\dot{w}_{\Sigma k})^2 + (1 - \alpha) (v_{dc} i_{ck})^2 \right] dt \quad (3.30)$$

Note that α is a weighting factor and $\alpha \in [0, 1]$. The two frontier case are of course constant energy addition (when $\alpha = 1$), and constant circulating current (when $\alpha = 0$). Nevertheless, new intermediate states may appear, giving birth to potentially interesting points of operation (e.g.: $\alpha = 0.5$). The result of the optimization problem, subject to the constraints of (3.14) and (3.15), gives birth to the following generalized equation.

A solution to such an optimization problem is possible since the two selected constraints are compatible: i.e., from [3, 7] it is possible to see that the average value of the energy sum ($\overline{w_{\Sigma k}}$) depends on the DC component of the circulating current, while the average value of the energy difference ($\overline{w_{\Delta k}}$) depends on the grid fundamental frequency component of the circulating current. The restrictions alone will participate in the shaping of the circulating current reference, namely in its DC and in its grid frequency components. Nonetheless, there is still degrees of freedom regarding the component at twice the grid frequency. Such a component is directly associated to the objective functions, and will strongly depend on the weighting factor selected. The complete control scheme is depicted in Fig. 3.1.

$$i_{ck} = \frac{\overline{P_{\Sigma k}^{ref}} + (1 - \alpha) \overline{P_{vk}}}{v_{dc}^2} v_{dc} + \frac{\alpha P_{vk}}{v_{dc}} + \frac{-\overline{P_{\Delta k}^{ref}}}{2v_{dc}^2 (e_{vk,p.u.}^{rms})^2} e_{vk} \quad (3.31)$$

3.4 Implementation by means of stationary multi-resonant controllers

The circulating current reference obtained in the previous sections gives the theoretical optimal current capable of regulating the arm capacitive energies independently by phase. This section explains how the MMC circulating current is controlled to be equal to its previously calculated reference by means of current control. In general, different current control solutions for VSCs based on PWM techniques can be found in the literature, with their corresponding advantages and drawbacks. Based on the classification that M. Kazmierkowski and L. Malesani proposed in their survey article [66], current control techniques for VSC can be divided into two groups: 1) *Linear*, i.e., stationary, synchronous and predictive deadbeat controllers, and 2) *nonlinear*; i.e., hysteresis, DM, and on-line optimized controllers. The mentioned controllers are well suited for when the current reference has only one frequency component, yet this is not always the case for multi-frequency applications such as active filters. The multi-frequency application is of most interest since by analyzing the circulating current reference in (3.31), it is possible to see that it has three different harmonic components:

1. A DC component proportional to v_{dc}
2. A grid frequency component proportional to e_{vk}
3. A frequency component at twice the grid frequency proportional to P_{vk}

One *linear* control solution suitable for multi-frequency applications is the use of integrator-based regulators such as multiple synchronous frame PI controllers. However, they present shortcomings related to the need for multiple synchronous dq transformations requiring additional computational resources [67, 68, 69]. Furthermore, it would contradict the control philosophy adopted in this Thesis of controlling the MMC in its natural abc coordinates. Nonetheless, a similar approach also based on integrators is to use multiple stationary frame *resonant* controllers [70, 69]. The resonant controller has been widely presented as an interesting alternative to the use of synchronous PI regulators in order to avoid the computational load of the implementation of the synchronous reference frames [69].

The resonant controller is usually made up of a proportional and resonant term, which contains a double imaginary pole aimed at obtaining an infinite gain at the resonance frequency ω_o [69]. The continuous and its discrete equivalent representation are expressed in equations (3.32) and (3.33).

$$C_R(s) = k_p + \frac{2 \cdot k_i \cdot s}{s^2 + \omega_o^2} \quad (3.32)$$

$$C_R(z) = k_p + \frac{2 \cdot k_i \cdot T_s [z^2 - \cos(\omega_o T_s)z]}{z^2 - 2 \cos(\omega_o T_s)z + 1} \quad (3.33)$$

Equation (3.32) gives the ideal proportional-resonant (PR) controller with an infinite gain at the AC frequency of ω_o . However, to avoid stability problems associated with an infinite gain, a “non-ideal” PR controller can be used instead and its expression is given in (3.34). This controller has a finite, yet high enough gain for enforcing small steady state errors, as suggested in [67]. In addition, its bandwidth can be widened by setting ω_c appropriately, to reduce sensitivity towards slight frequency variations in the grid [67].

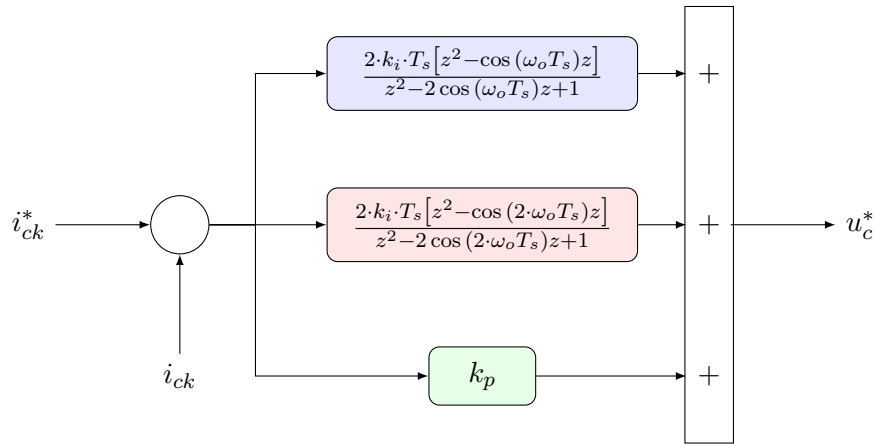


Figure 3.2: Multi-resonant shunt control structure for the circulating current

$$C_R(s) = k_p + \frac{2 \cdot k_i \omega_c \cdot s}{s^2 + 2\omega_c + \omega_o^2} \quad (3.34)$$

The multi-resonant controller structure implemented in this Thesis is depicted in Fig. 3.2. It consists on the direct addition of two single resonant controllers at once and twice the grid frequency with a unique proportional term (referred to as parallel or shunt configuration [69]). This structure corresponds to the *circulating current control* block of the complete control scheme, depicted in Fig. 3.1.

The design criteria of the multi-resonant control parameters was not considered in this research project and has been left as future work. Two interesting design techniques, that may serve as starting point, were presented by A. López de Heredia *et al* in [69] for this type of controllers, using frequency response analysis and a pole placement approach.

3.5 Simulation results

In this section, the performance of (3.31) has been validated as the control reference of the MMC circulating current control loop, depicted in Fig. 3.1. This has been done in four parts. Firstly, the MMC has been simulated in steady state with different values of α in section 3.5.1. Furthermore, the transient behavior of the converter using 3.31 with different energy (sum and difference) references per phase is studied in section 3.5.2. Moreover, a comparison with two existing MMC controllers was done in section 3.5.3. These controllers are the “d_{qo}” frame-based (CCSC) of [17], and the “abc” frame-based “closed loop control” of [3]. Finally in section 3.5.4, equation 3.31 was validated using the MMC-HVDC system depicted in Fig. 3.11, under both, MMC energy (section 3.5.4) and power (section 3.5.4) reference step changes. Table 3.1 shows the values of the MMC parameters used in simulation.

The MMC with the parameters of Table 3.1 was simulated in Matlab/Simulink in steady state and under unbalanced reference step changes, in order to prove the validity of (3.31).

Table 3.1: MMC Parameters

Number of SM	200
SM Nominal Voltage	1kV
SM Capacity	15mF
Arm Inductance	30mH
Arm Resistance	0.1 Ω

3.5.1 Steady state performance

Fig. 3.3 depicts the sum of the MMC capacitor voltages of each one of the six arms (u_{ck}^Σ), as well as their corresponding circulating current under the control scheme based on equation (3.31). More precisely, Fig. 3.3-a) and -b) show such a variables for the case in which $\alpha = 0$, whereas Fig. 3.3-c) and d) for the $\alpha = 1$ case.

Furthermore Fig. 3.4 depicts the energy variables of the MMC, which are the energy sum ($w_{\Sigma k}$) and difference ($w_{\Delta k}$) for each phase. As the previous figure, Fig. 3.4 -a) and -b) depict the energy variables for the case in which $\alpha = 0$, while Fig. 3.4 -d) and -c) do so for when $\alpha = 1$.

As can be seen, when using $\alpha = 0$, it is possible to successfully operate with constant circulating current in order to reduce the MMC internal resistive losses. On the other hand, if one choses to operate with $\alpha = 1$ instead, it is the capacitive energy stored in each phase of the converter ($w_{\Sigma k}$) that becomes constant, which has as consequence a significant reduction regarding the oscillations of the MMC capacitor voltages u_{ck}^Σ (see [39]), that implies a reduction on the capacitive losses. Yet, in order to achieve such a condition, it is required that the circulating current should have an important second harmonic component. It appears that the oscillations of the energy difference ($w_{\Delta k}$) are reduced as well when the operating with constant energy sum. Which one of the two border conditions should be used will depend of course on the MMC application and the parameters such as number of SMs and capacitance, and internal resistance. In addition, it is possible to operate with intermediate values between 0 and 1, which will yield interesting new operating points.

3.5.2 Operating under unequal arm energy references

One of the most significant features of (3.31) is its possibility of generating the desired references in "abc" coordinates, making it is possible to work with each phase independently. This subsection intends to demonstrate the fact that our proposed regulation is capable to successfully deal with unequal reference step changes.

The simulation consists of the following events: The simulation initializes at $t = 0s$. At $t = 0.2s$, the energy difference of each phase is given a different reference step change: from zero to $20kJ$, $60kJ$ and $100kJ$ for $\bar{w}_{\Delta a}$, $\bar{w}_{\Delta b}$ and $\bar{w}_{\Delta c}$ respectively. At $t = 0.4s$, they are all brought back again to $0kJ$.

At $t = 0.6s$ a reversal in the flow of the active power is done. This is reflected on the circulating current, depicted in the right side column of Fig. 3.5.

Finally, at $t = 0.8s$ the average value of the energy sum of phase "a" ($\bar{w}_{\Sigma a}$) receives reference step increment of 30%, the average value of the energy sum of phase "b" ($\bar{w}_{\Sigma b}$) remains unchanged, whilst the one of phase "c" ($\bar{w}_{\Sigma c}$) receives a reference step decrement of 30%. Subsequently, they are all brought back to the original value at $t = 1s$.

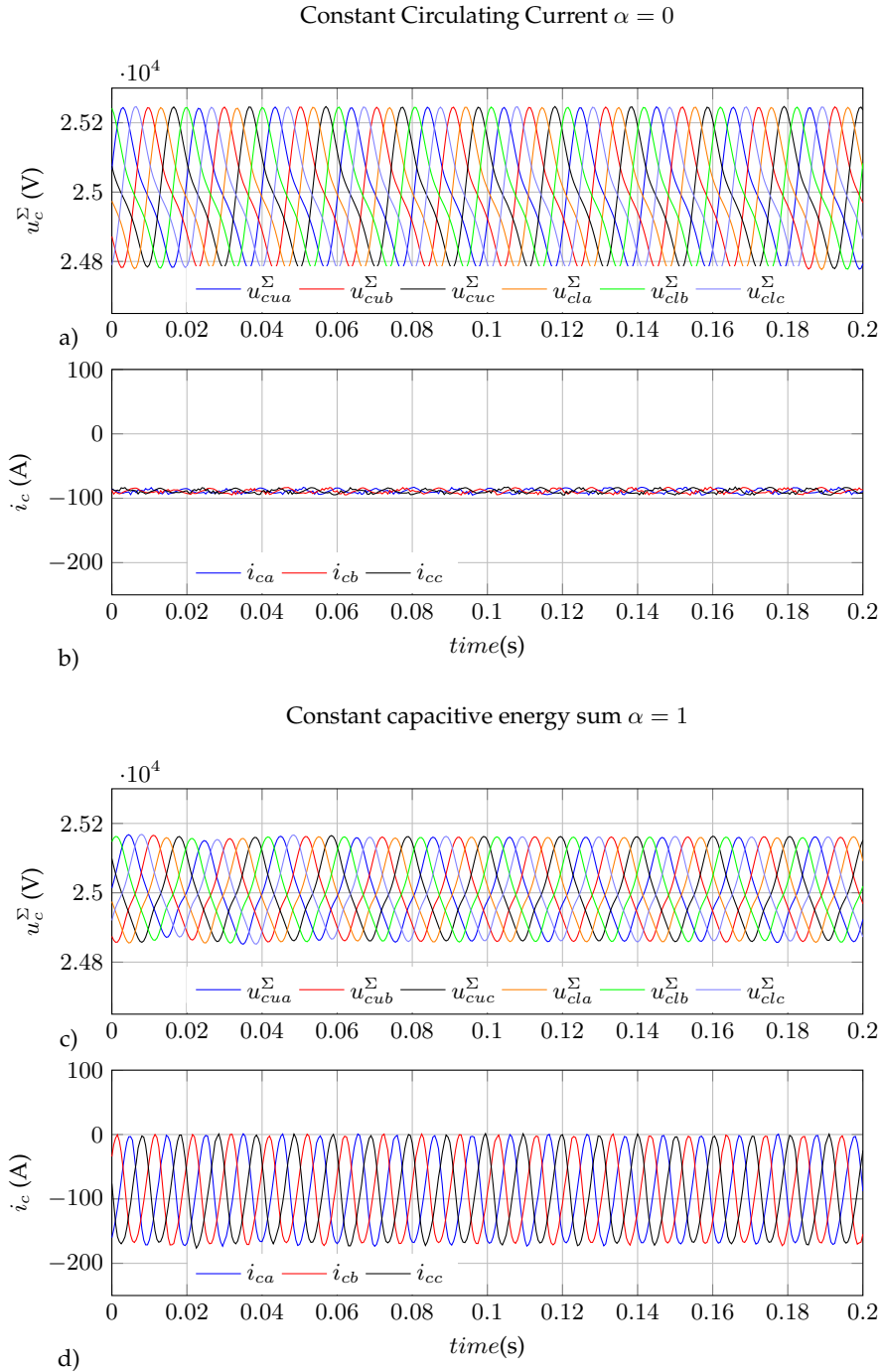


Figure 3.3: Steady state MMC variables: a) MMC arm capacitor sum and b) circulating current under the constant circulating current scenario $\alpha = 0$. c) MMC arm capacitor sum and d) circulating current under the constant energy sum scenario $\alpha = 1$

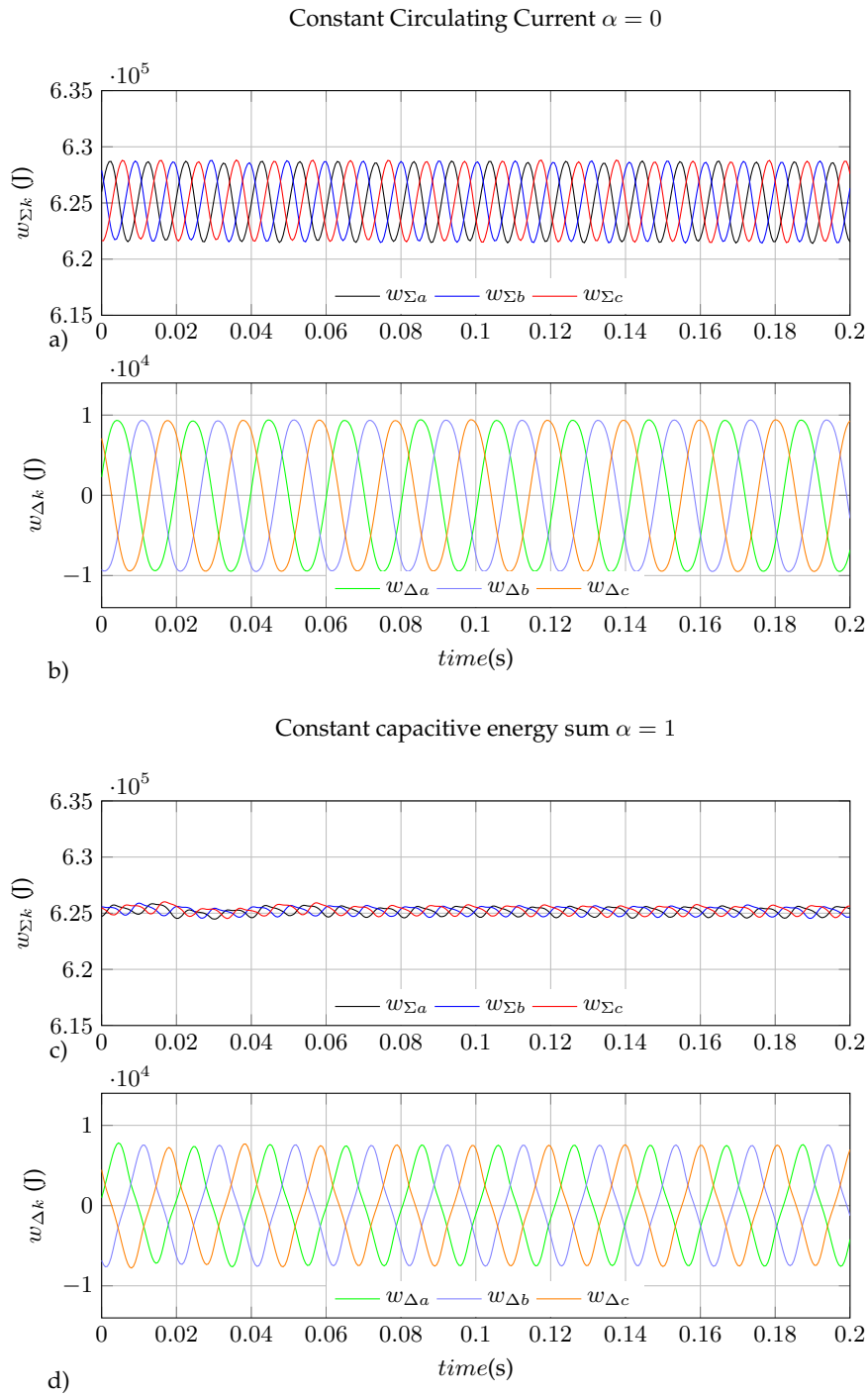


Figure 3.4: MMC capacitive energy variables: a) MMC capacitive energy sum and b) difference under the constant circulating current scenario $\alpha = 0$. c) MMC capacitive energy sum and d) difference under the constant energy sum scenario $\alpha = 1$

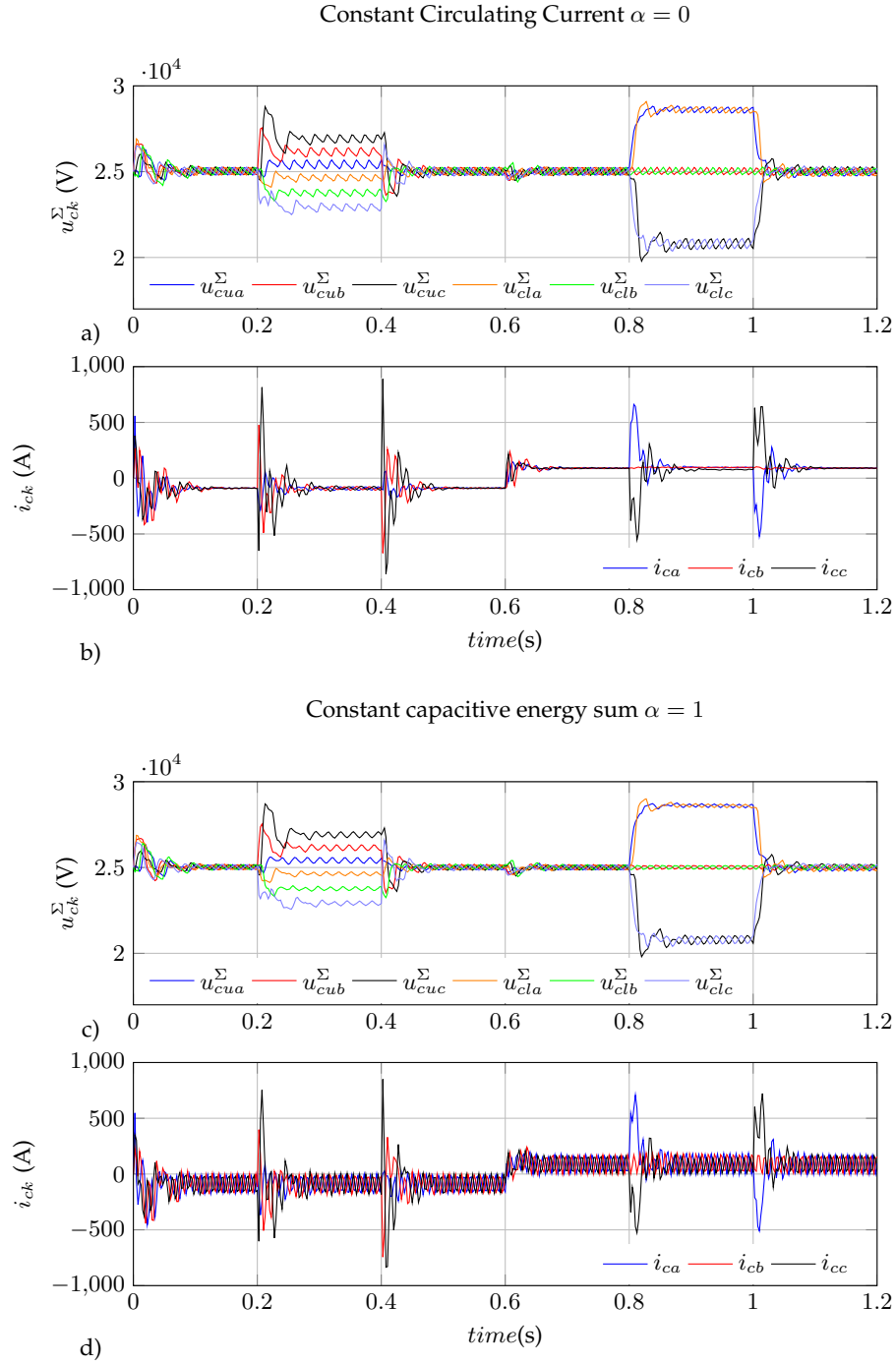


Figure 3.5: Dynamic performance of the MMC state variables: MMC capacitor voltages with a) $\alpha = 0$ and c) $\alpha = 1$. Circulating currents with b) $\alpha = 0$ and d) $\alpha = 1$.

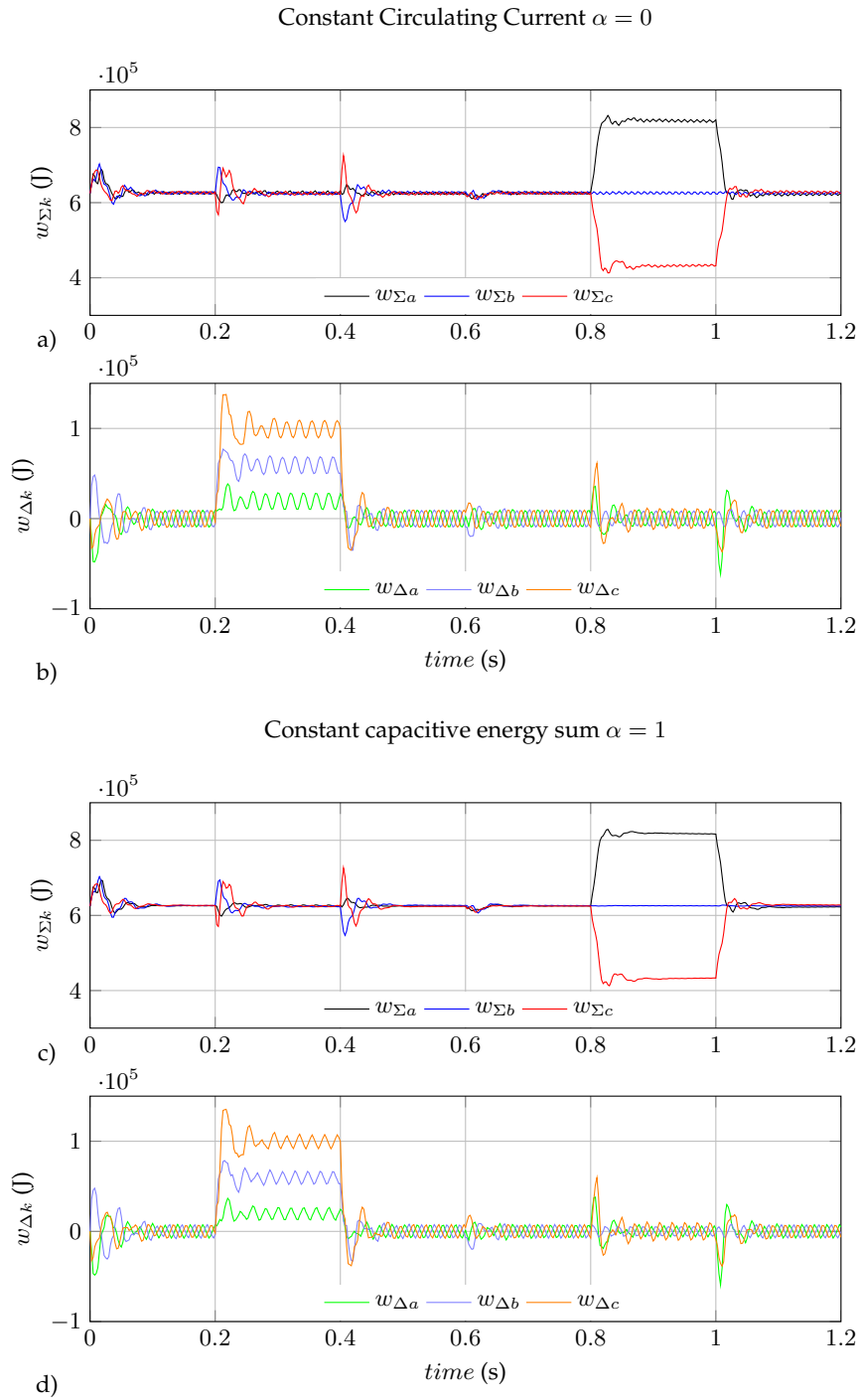


Figure 3.6: Dynamic performance of the MMC capacitive energy variables: energy sum with a) $\alpha = 0$ and c) $\alpha = 1$. Energy difference with b) $\alpha = 0$ and d) $\alpha = 1$.

Fig. 3.5-a) shows the behavior of the MMC capacitor voltages and while Fig. 3.5-b) shows the circulating currents, under the aforementioned events, for $\alpha = 0$. Similarly, 3.5-c) and d) show the same variables under the same events but with $\alpha = 1$.

The energy sum and difference waveform trends under both frontier values of α are depicted in Fig. 3.6. It is possible to see how the reference step changes in the average values of both energy values is reflected in the distribution of the arm voltages of the MMC, regardless of the value of the α . Moreover, such a distribution may be done independently for each phase, making it suitable for unbalanced operation. It can also be seen that the circulating currents, regardless of the value of α , have similar patterns during the transient state, even if they are different (constant vs. sinusoidal) during steady state.

3.5.3 Comparison with the existing controllers

Circulating current suppression controller

In Fig. 3.7 and 3.8, a first comparison is made against the CCSC since it is based on “dqo” frame, in order to highlight the advantages of controlling the MMC in the “abc” coordinates. In both figures, the CCSC technique is compared with the proposed control scheme (with $\alpha = 0$). Although the same MMC 3-phase capacitive reference $\sum_{k \in abc} w_{\Sigma k}^{ref}$ (or $3w_{\Sigma}^{ref} \phi$ in “dqo”) is given to the MMC, as can be seen in Fig. 3.7-a) and 3.7-b), the independent averaged energy values $\bar{w}_{\Sigma k}$ for the case of the CCSC, shown on Fig. 3.7-c), will be a third part of the total energy reference, yet the our control proposal offers infinite possibilities for the distribution of these independent phase energy levels (e.g.: Fig.3.7-d)) which may be useful, particularly when facing unbalanced conditions. In 3.8-a) & 3.8-b), the circulating currents for each controllers are depicted. For the CCSC, each phase circulating current has the same value at all time, for they are being controlled by their zero sequence $i_{c\phi}$ while forcing $i_{cd,q}$ to zero. However for the control proposal case, each circulating current adopts a different value, particularly during the transient state, in order to achieve different desired phase energy levels. Finally, in the last two rows of Fig. 3.8, the average value of the energy difference $\bar{w}_{\Delta k}$ is shown. It can be noticed that the proposed control strategy offers a better dynamic since the last term of equation (3.31) is constantly regulating this variable, while the CCSC does not give this possibility. Note that an extended version of the CCSC was proposed in [39], however the results of the comparison are approximately equivalent since it is still in “dqo” coordinates.

Closed loop control

Another interesting comparison is to contrast the proposed control strategy with another “closed loop” controller in the “abc” frame. For this case the closed loop control of [3] was chosen. In Fig. 3.9, the dynamics of the instantaneous value of the capacitive phase energy $w_{\Sigma k}$ are compared using the CLC (Fig. 3.9-a)) and the proposed control scheme (Fig. 3.9 -b) and -c)). As can be seen, between 2.2 and 2.6 seconds, $w_{\Sigma a}^{ref}$ is given a 20% step increment, $w_{\Sigma b}^{ref}$ remains unchanged, and $w_{\Sigma c}^{ref}$ decreases 20%.

It can be seen that for both values of α that the dynamic response of the proposed control is clearly improved with respect to the CLC for it uses an internal current control loop while the CLC does not. In Fig. 3.10, the respective circulating currents are depicted: the first row shows the circulating current associated to the CLC; the second row depicts the one related to the the present proposed technique with $\alpha = 0$, while the last row shows the case with $\alpha = 1$. It can

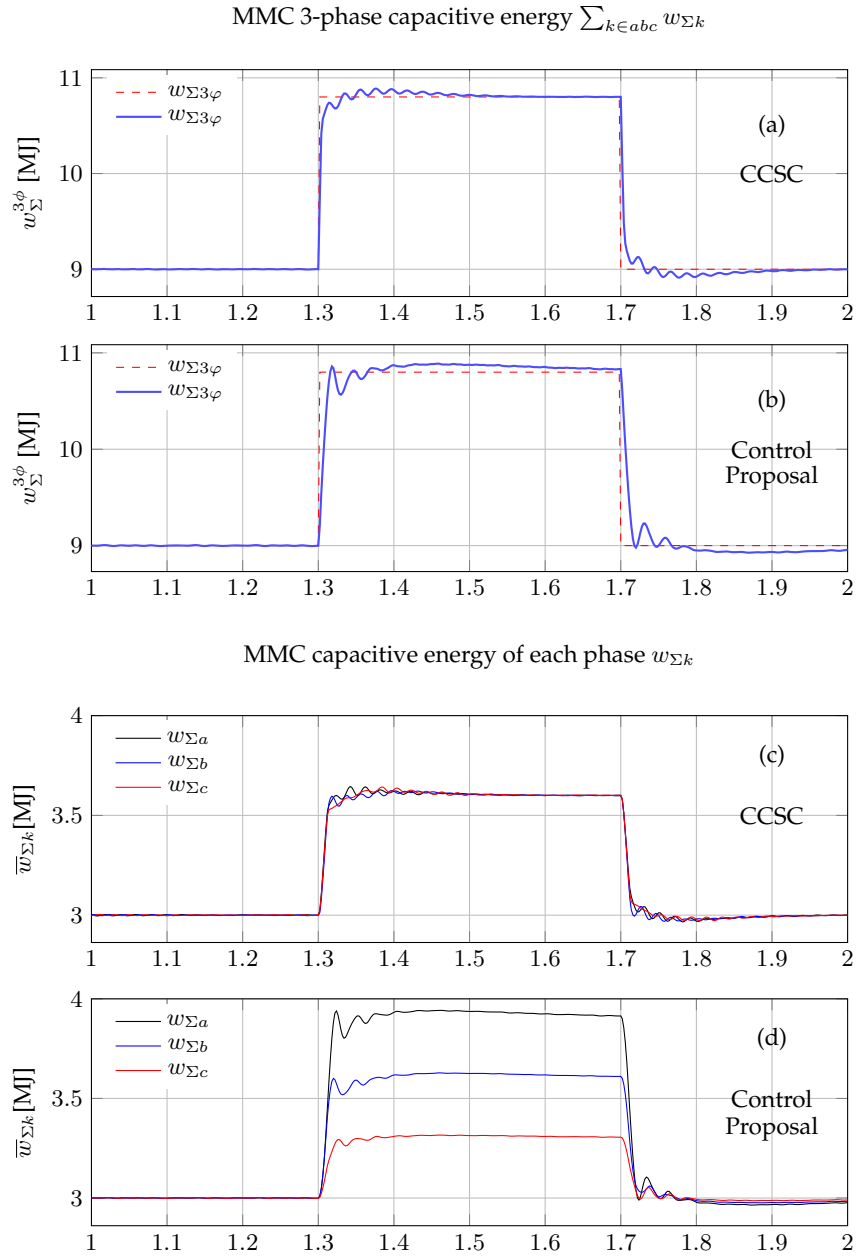


Figure 3.7: CCSC vs. proposed control strategy; Part I: (a-b) 3-phase MMC capacitive energy, (c-d) phase-independent average capacitive energy

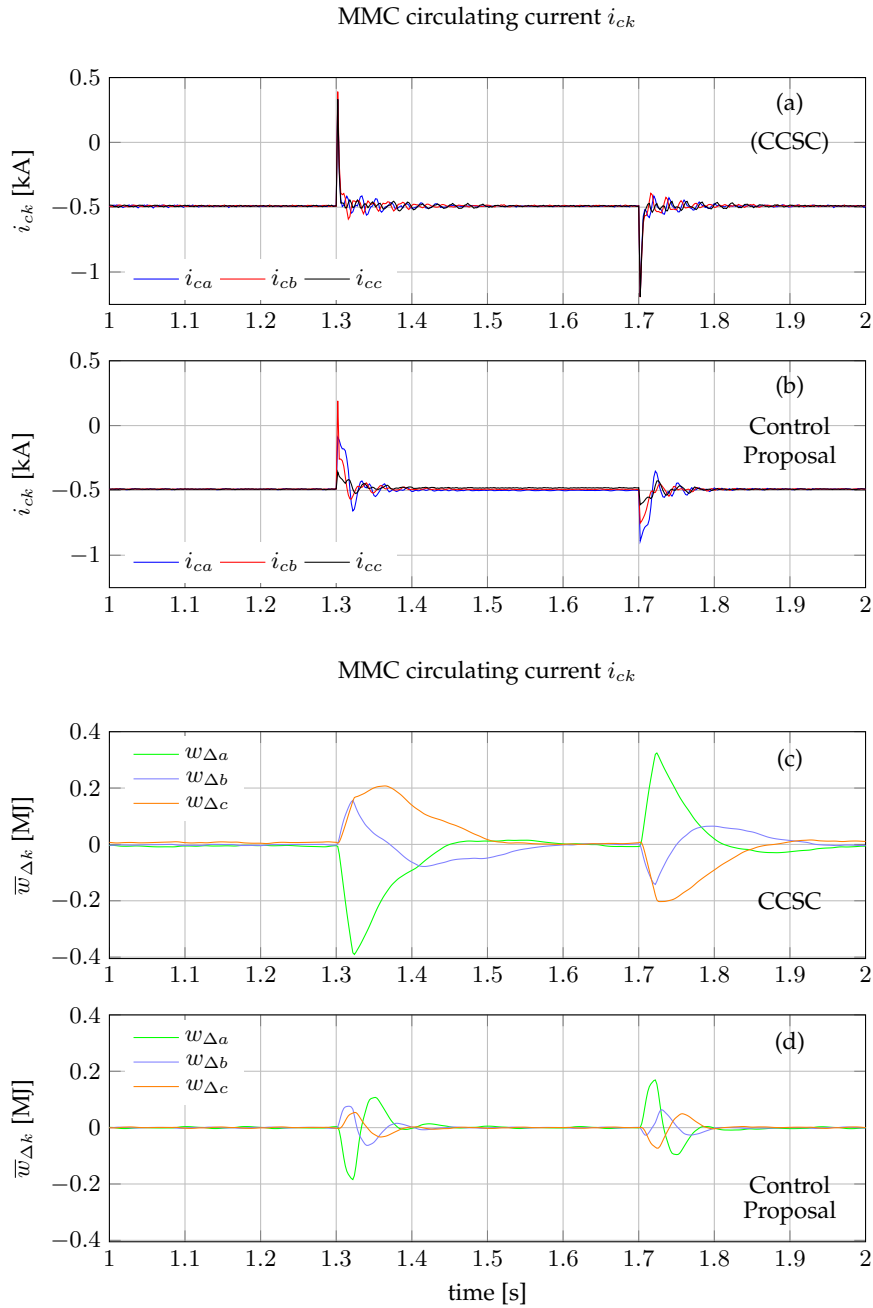


Figure 3.8: CCSC vs. proposed control strategy: (a-b) circulating currents, (c-d) average value of the phase energy difference between upper and lower arms

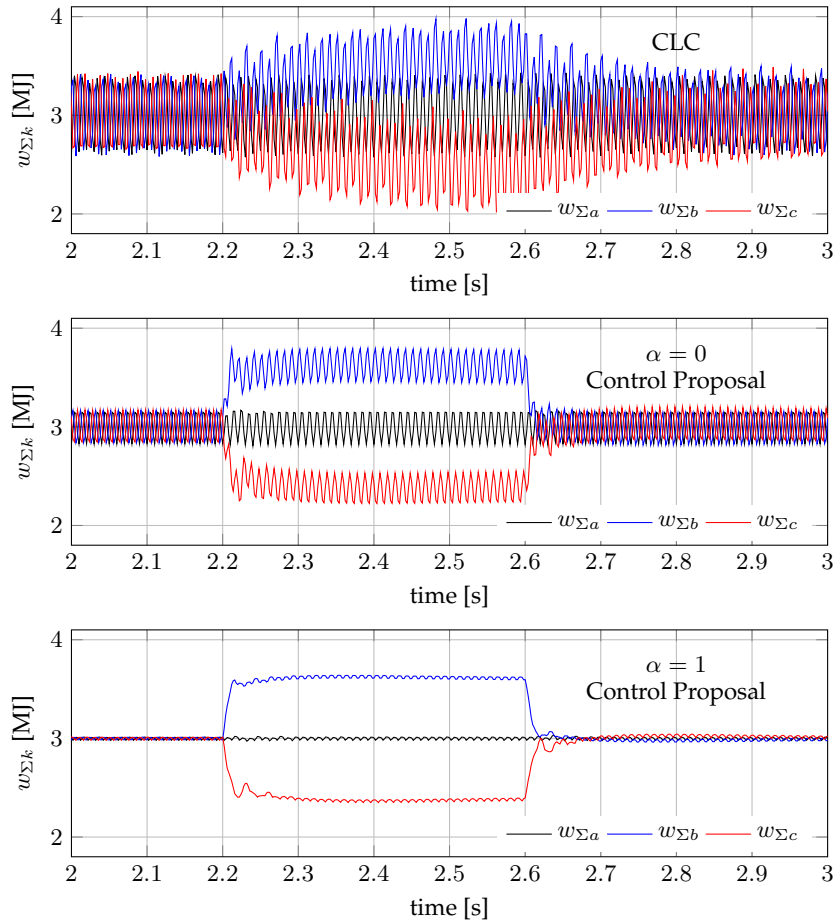


Figure 3.9: Capacitive energy sum by arm $w_{\Sigma k}$ under different step reference change per phase: closed loop control (CLC) [3] vs. control proposal

also be seen that the quality of the dynamics of the circulating currents is significantly improved with respect to the CLC. It can also be concluded that the second harmonic present in the CLC circulating current does not constantly the capacitive phase energy $w_{\Sigma k}$ while the second case of the control proposition does, reducing the capacitive losses.

3.5.4 MMC-HVDC simulation

This section validates the proposed controller based on equation (3.31), depicted in Fig. 3.1, via a two terminal MMC-HVDC system with the parameters shown in Tables 3.2. In section 3.5.4, the $\alpha = 0$ case (i.e.: constant circulating current) was simulated under step reference changes of the average values of the phase energy sum $\bar{w}_{\Sigma k}^{ref}$ and difference $\bar{w}_{\Delta k}^{ref}$. In section 3.5.4, the $\alpha = 1$ case (i.e.: constant $w_{\Sigma k}$) was simulated under DC voltage and AC power reference step changes.

Energy references step changes

In Fig. 3.12 are depicted the variables of the DC-Voltage controlling MMC-HVDC terminal, hereafter referred to as Station I; while Fig. 3.13 shows the variables corresponding to the AC Power controlling MMC-HVDC terminal, hereafter referred to as Station II.

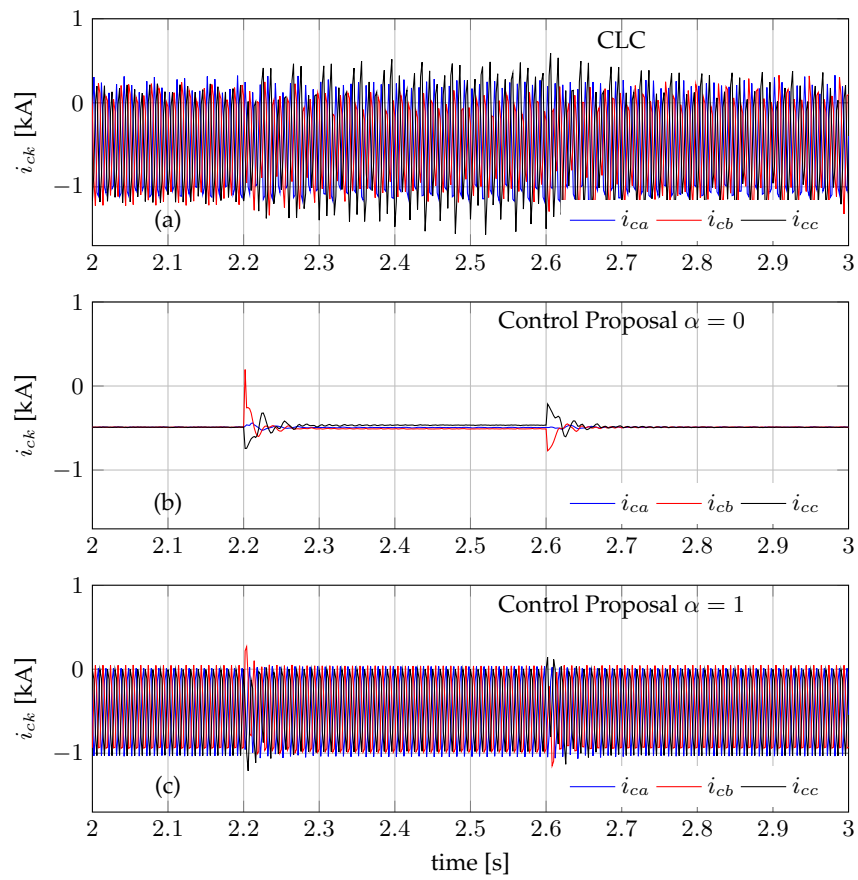


Figure 3.10: Circulating currents using a) close loop control and the control proposal with b) $\alpha = 0$ and c) $\alpha = 1$.

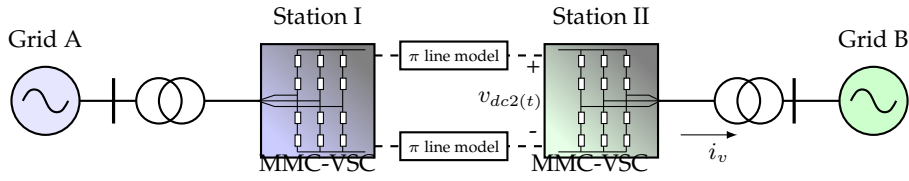


Figure 3.11: Schematic representation of an MMC-based HVDC system

Regarding Station I, the following energy reference step changes were made: between 0.5 and 0.9 seconds, the average energy difference reference $\bar{w}_{\Delta k}^{ref}$, originally at 0 MJoules, was placed at 0.6 MJoules. In addition, the average energy sum $\bar{w}_{\Sigma k}^{ref}$, originally set at 3 MJoules, was placed at +10% for $\bar{w}_{\Sigma a}^{ref}$, -10% for $\bar{w}_{\Sigma c}^{ref}$ while $\bar{w}_{\Sigma b}^{ref}$ remained unchanged, between 1.2 and 1.6 seconds, as can be seen from Fig. 3.12.

Regarding Station II: between 0.5 and 0.9 seconds, the average energy sum $\bar{w}_{\Sigma k}^{ref}$, originally set at 3 MJoules, was placed at +20% for $\bar{w}_{\Sigma a}^{ref}$, -20% for $\bar{w}_{\Sigma c}^{ref}$ while $\bar{w}_{\Sigma b}^{ref}$ remained unchanged. Furthermore, the average energy difference reference $\bar{w}_{\Delta k}^{ref}$, originally at 0 MJoules, was placed at 0.6 MJoules, between 1.2 and 1.6 seconds, as can be seen in Fig. 3.13.

For both stations, one can see how the MMC-HVDC system behaves properly under these reference changes: The first and second rows of Fig. 3.12 and 3.13 show the expected behavior of the capacitive energy sum ($w_{\Sigma k}$) and difference ($w_{\Delta k}$), respectively. The third row of both figures display the MMC capacitor voltages. In the fourth row, are depicted for each corresponding stations, the circulating currents. These currents appear to be practically constant, and have slightly different values when imposing $w_{\Sigma k}$ to have different values as well. They also adopt a sinusoidal waveform at 50Hz when imposing $\bar{w}_{\Delta k}^{ref} \neq 0$. Finally in the last row of Fig. 3.12 is depicted the DC voltage while in the last row of Fig. 3.13, the AC active power is displayed.

Power references step changes

In this simulation scenario, both stations are controlled by means of the proposed control strategy with $\alpha = 1$. The following power reference step changes take place: At 1.8 seconds, active power reversal occurs; i.e., from -300MW to +300MW. At 1.3 seconds the reactive power is taken from +30MVAR to -150MVAR. Finally at 1.4 seconds, the DC voltage is increased by 10%. Station I variables are depicted on Fig. 3.14 while Station II variables on Fig. 3.15.

The MMC-HVDC system behaves as expected: the first and second rows of Fig. 3.14 and 3.15 show the expected behavior of the capacitive energy sum ($w_{\Sigma k}$) and difference ($w_{\Delta k}$), respectively. In this case, since $\alpha = 1$, the capacitive phase energy variables ($w_{\Sigma k}$) are practically constant, inducing a reduction on the capacitor voltages ([39]), that are shown in the third row of both figures. In the fourth row are depicted for each corresponding stations, the circulating currents. As can be seen, these currents are sinusoidal at 100Hz, again since we are operating with $\alpha = 1$. The fifth row of Fig. 3.14 shows the DC voltage on the terminals of Station I, while the fifth row of Fig. 3.15 shows the AC active power measured on the PCC of Station II. Finally in the last row of both figures, the reactive power is displayed for each corresponding station.

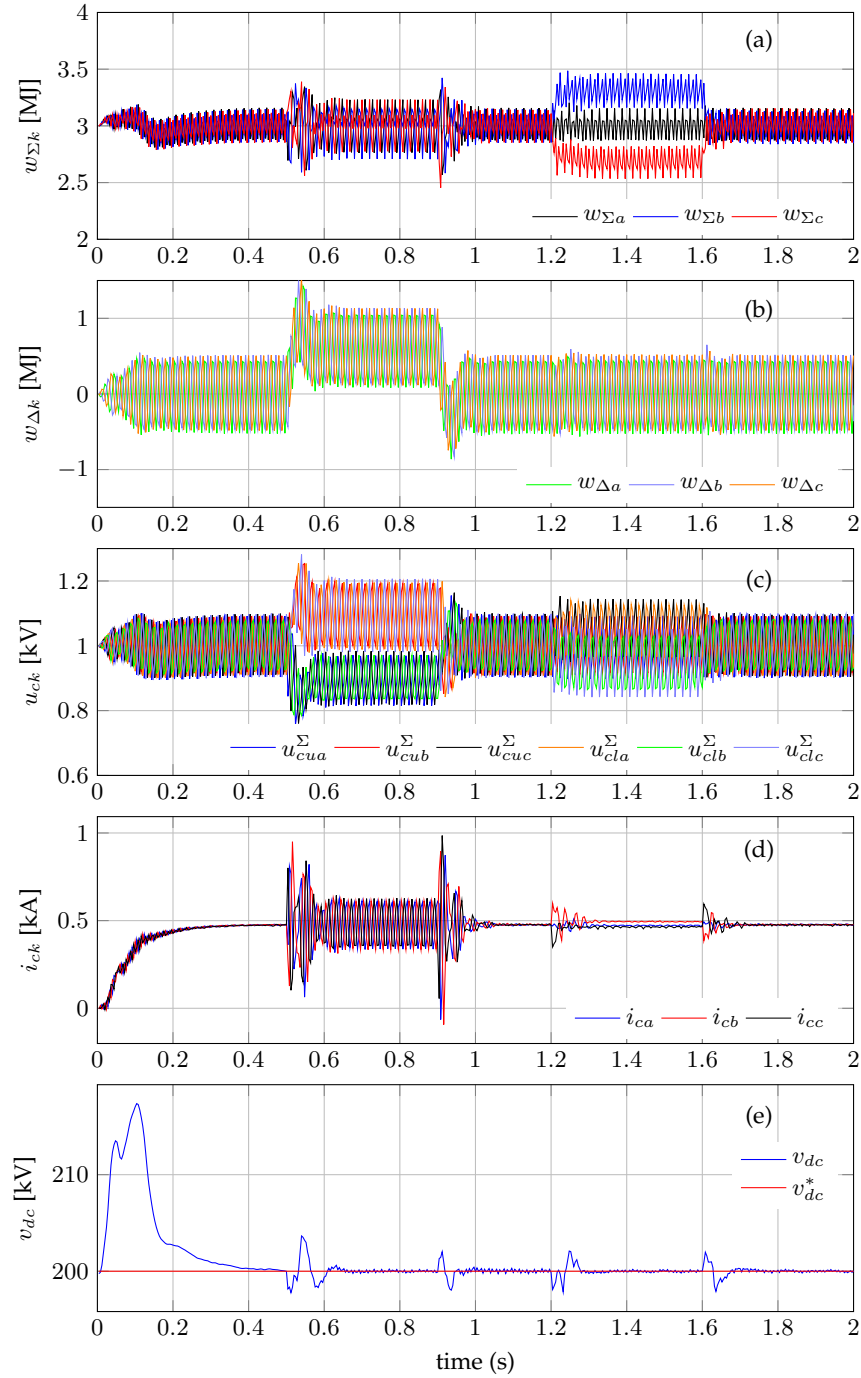


Figure 3.12: MMC-HVDC station I - energy references step changes. a) Energy sum, b) energy difference, c) MMC capacitor voltages, d) circulating currents and e) DC Link Voltage.

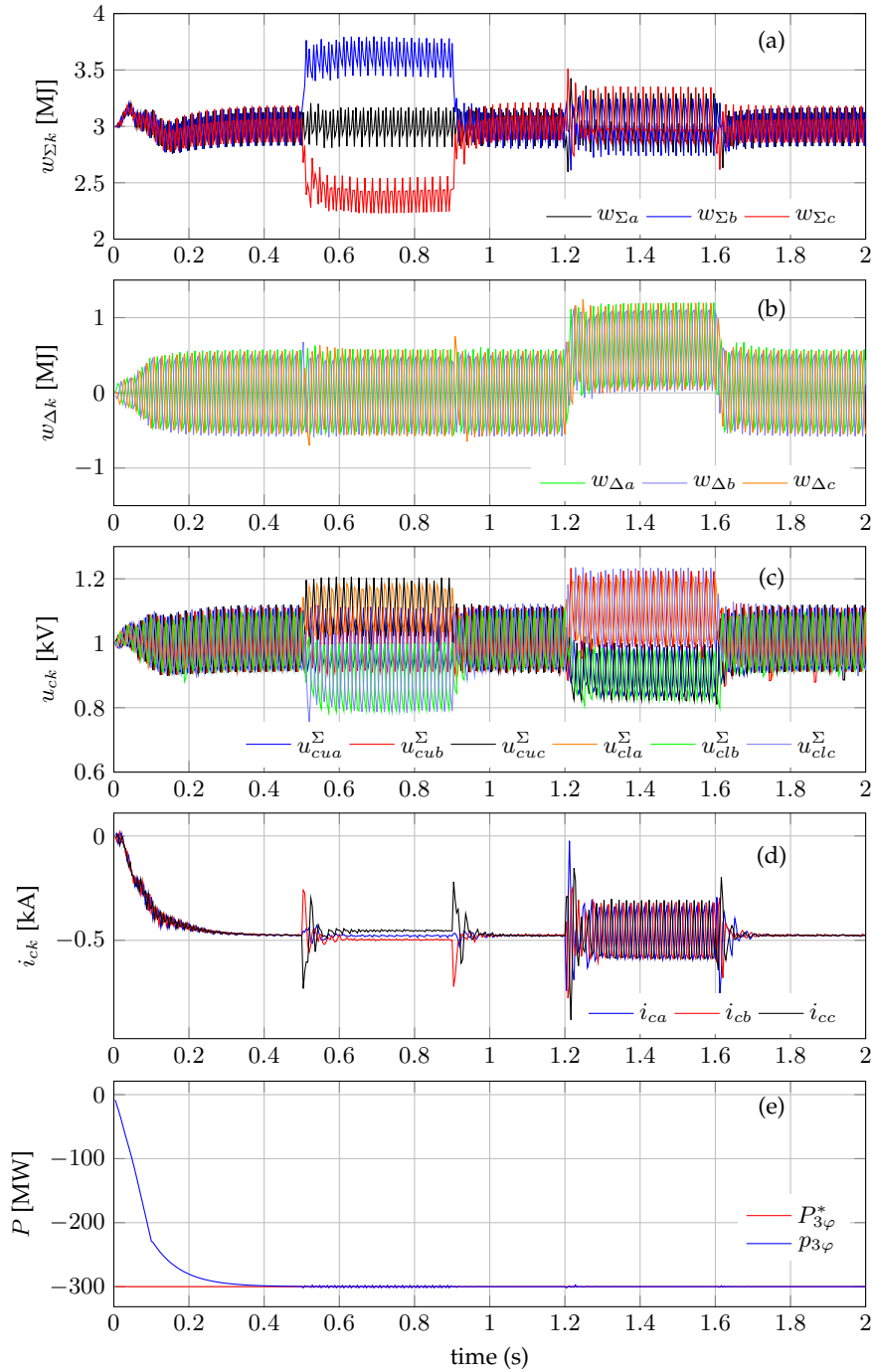


Figure 3.13: MMC-HVDC station II- energy references step changes. a) Energy sum, b) energy difference, c) MMC capacitor voltages, d) circulating currents and e) active power.

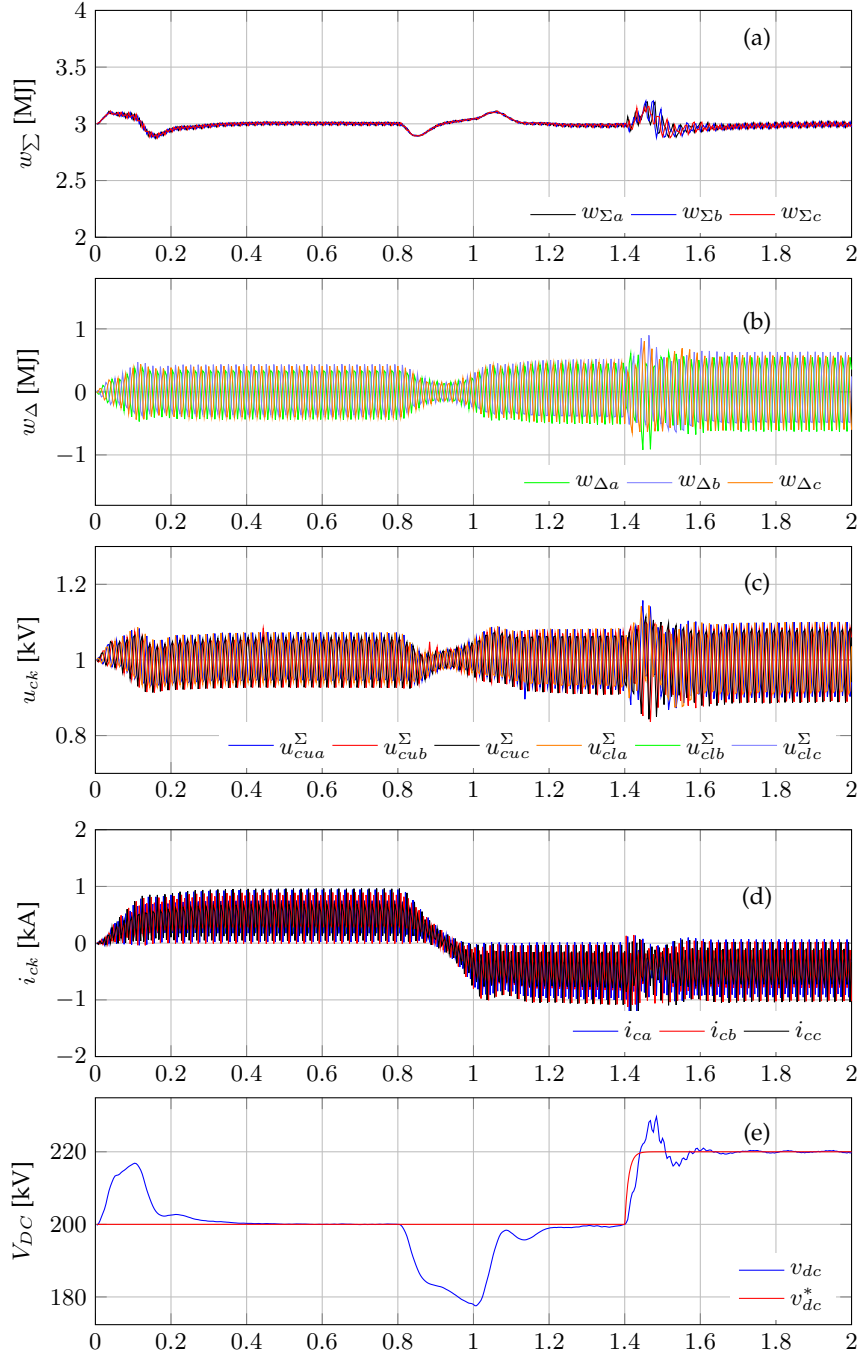


Figure 3.14: MMC-HVDC station I - Power references step changes. a) Energy sum, b) energy difference, c) MMC capacitor voltages, d) circulating currents and e) DC Link Voltage.

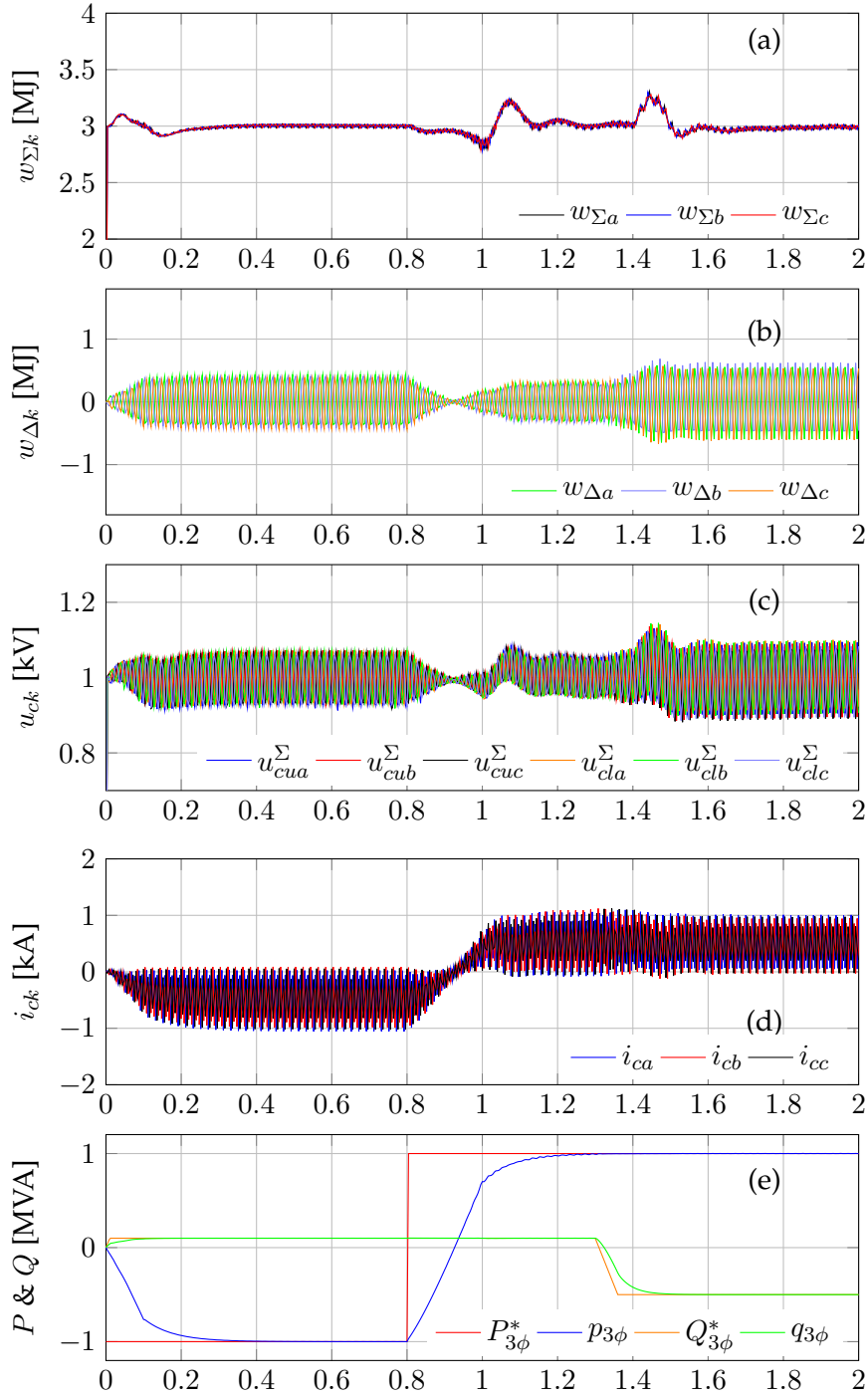


Figure 3.15: MMC-HVDC station II - Power references step changes. a) Energy sum, b) energy difference, c) MMC capacitor voltages, d) circulating currents, e) active and reactive power.

Table 3.2: HVDC Parameters

Apparent Power	300MVA
DC Nominal Voltage	200kV
TRX Voltage Primary Side	220kV RMS
TRX Voltage Primary Side	100kV RMS
TRX Connection	$Y_g\Delta$
DC Cable Resistance	1.0425Ω
DC Cable Inductance	$11.925mH$
DC Cable Capacitance	$17.325\mu F$

3.6 Conclusion

In this chapter, the compensation control approach for active filters based on Lagrange multipliers [59] is extrapolated to the MMC application. A control approach based on mathematical optimization in the abc frame suited for the MMC frame is proposed. The equation of the controller presents three main terms, one related to zero frequency, once and twice the grid fundamental frequency, by means of v_{dc} , e_{vk} and P_{vk} , respectively. Moreover, two variable conductances “adjust” the value of these contributions in a convenient way in order to create the desired circulating current control equation, with a structure similar to instantaneous power theories in the abc frame. The equation is generalized using multi-objective optimization so that by conveniently choosing the values of the weighing factor α , one could operate in constant circulating current mode, constant capacitive phase energy mode, or interesting intermediates states that will be left for future research. The control action was derived with a single circulating current reference, that resulted directly from the optimization process and was able to attain both control objectives. The advantage of operating such a converter in the abc in contrast to the dqo frame was also presented as a comparison with respect to the CCSC. Furthermore, since the proposed control strategy is based on internal circulating current and capacitive energy feedback loops, the resulting performance appears as robust with respect to parameter uncertainty. In addition, the controller was successfully implemented in both sides of a two terminal MMC-HVDC link, in order to demonstrate that it may be a potential candidate for this type of application.

4

Circulating Current Signal Estimation based on Adaptive Filters: Faster Dynamics and Reduced THD

The calculation of MMC circulating current reference signals in the abc-frame using the Lagrange multipliers method and its implementation via current multi-resonant controllers has been sensitive to the quality of the required input signals. More precisely, such a control approach has proven to be sensitive to the harmonic distortion of the required instantaneous signals when applied to systems with a low number of levels, and its dependence on average value calculations of sinusoidal variables, slowing down the dynamics of the control and making the tuning of the control system difficult under certain conditions. In this chapter it is demonstrated that such issues are solved by introducing adaptive filtering based on Second Order Generalized Integrators to estimate the voltage, power and energy variables needed for calculating the circulating current references.

4.1 Introduction

GENERATING the minimized circulating current reference signals by means of mathematical optimization in the systems natural abc reference frame, and its implementation using multi-resonant current controllers offers several advantages: Such a control scheme allows for independent regulation of the average values of the MMC capacitive energy stored in each arm in a direct and explicit way, while being able of shaping the circulating current and the capacitive energy sum waveforms. Besides independent phase regulation, the resulting circulating current reference in the system natural abc coordinates gives useful insight on the MMC behavior, that can be used to simply enhance the understanding of the converter or for estimating

MMC equilibrium points; e.g., for non-linear controllers design. Last but not least, the proposed control strategy is robust as it relies on four feedback loops by phase (i.e., two for the capacitive energies w_Σ, w_Δ ; and two for the currents i_c, i_v). This implies that within certain conditions, the control is not sensitive to the MMC parameters, errors in the estimation of the equilibrium point, or undesired perturbations.

Although this approach has shown to be very versatile and useful, the following two issues needed to be addressed to make such a control strategy truly competitive: 1) The implementation has in many cases suffered from relatively slow dynamics, since the mean value of sinusoidal variables used for the circulating current reference generation needed to be calculated and this was done by means of a simple Low Pass Filter (LPF). 2) Another inconvenience was found when the controller was applied to a MMC with low number of levels, which implied a higher THD in the AC output voltage. These resulting harmonics interacted with the controller and decreased its performance.

This chapter addresses both issues by applying adaptive filters based on Second Order Generalized Integrator (SOGIs) [71, 72] configured as Quadrature Signal Generators (QSG), for estimating the input variables needed for calculating the circulating current references, following the work published in [C12]. By doing so, the input variables will have an increased dynamical performance compared to the use of LPFs while the THD of the reference signals is simultaneously reduced. In addition to improved control dynamics and easier tuning of system controllers, the use of the adaptive filters provides inherent capability for operation under frequency variations, and is therefore suitable for control of MMCs operating in weak grids as well as for high- or medium-voltage motor drives.

The outline of this chapter is as follows: section 4.2 analyzes the circulating current reference equation that was proposed in chapter 3, and uses it to explain how the harmonic distortion, as well as low pass filtering techniques may negatively influence the MMC, as an attempt to justify the use of adaptive filters for estimating the required input signals. Furthermore, a brief introduction to the SOGI-QSG is given in section 4.3. Section 4.4 details the contribution of this chapter: an enhanced control scheme for calculating the circulating current reference based on the estimation of the MMC single-phase instantaneous and averaged inputs using 4 SOGI-QSGs. In addition, to prove the validity of the control scheme, simulation results are given in section 4.5; whereas in section 4.6.2, the enhanced proposed strategy is implemented in a single-phase 5-level MMC laboratory prototype. Finally, the chapter conclusions are drawn in section 4.7.

4.2 On harmonic sensitivity and slow dynamics of the circulating current reference signal generation based on Lagrange multipliers

The circulating current reference was calculated in chapter 3 using the Lagrange multipliers method, yielding in (3.31). Such an equation is presented again in this chapter in (4.1) to emphasize the harmonic sensitivity issue as well as the risk of operating with slow dynamics.

$$i_{ck} = \frac{\bar{P}_{\Sigma k}^{ref} + (1 - \alpha) \bar{P}_{vk}}{v_{dc}^2} v_{dc} + \frac{\alpha P_{vk}}{v_{dc}} + \frac{-\bar{P}_{\Delta k}^{ref}}{2v_{dc}^2 \left(e_{vk,p.u.}^{rms} \right)^2} e_{vk} \quad (4.1)$$

4.2.1 Harmonic sensitivity

One of the advantages of the MMC, or multi-level converters in general, is that they usually produce a voltage output with low Total Harmonic Distortion (THD). This is true of course, for converters with high-enough number of levels such as those aimed for HVDC applications. Nonetheless, MMC with lower number of levels do introduce a non-negligible harmonic content that negatively influence the overall performance of the controller. This fact cannot be disregarded since MMCs with low number of levels are expected for drive applications as well as for low voltage laboratory setups useful for validating control techniques. Indeed, the later was a significant motivation factor for ensuring that the control proposal would work irrespectively of the harmonic content.

Analyzing (4.1), and neglecting any harmonic content present in v_{dc} , it is possible to conclude that most of the harmonic influence will be introduced through the grid current driving voltage e_{vk} and in turn, through the instantaneous AC power input P_{vk} . The rest of the variables are averaged and are not significantly influenced by the THD.

As can be recalled from section 2.4, the driving voltage e_{vk} is a fictitious voltage definition and may be expressed as a function of the difference between the lower and the upper MMC multi-valve output voltages. This is reminded in (4.2).

$$e_{vk}(t) = \frac{n_l(t) u_{cl}^\Sigma(t) - n_u(t) u_{cu}^\Sigma(t)}{2} \quad (4.2)$$

As the number of levels of a MMC is reduced, the discontinuous insertion indexes $n_u(t)$ and $n_l(t)$ will look less to a perfectly continuous sinusoidal waveform, and present a more discrete and discontinuous shape. This is directly reflected on the multi-valve output voltages $n_u(t) u_{cu}^\Sigma(t)$ and $n_l(t) u_{cl}^\Sigma(t)$ which define the driving voltage of the grid current e_{vk} . As consequence, if this voltage is taken directly with no further processing as input for the circulating current reference signal generation, such a reference as well as its resulting current will be distorted causing unnecessary harmonic losses. Furthermore, the instantaneous AC power $P_{vk}(t)$ that is defined as the product between $e_{vk}(t)$ and the grid current $i_{vk}(t)$ will have a similar effect as it includes all the harmonic content introduced by both $e_{vk}(t)$ and $i_{vk}(t)$.

4.2.2 Risk of slow dynamics

Although working in the stationary abc -frame does introduce several advantages for the MMC as the ones discussed in the introduction of this chapter, it poses the risk of slow dynamic performance for the proposed control strategy. This will tend to occur when low pass filters are used to obtain the average values of the required sinusoidal input signals for the reference generation defined by (4.1). The average inputs are:

- The average AC power $\overline{P_{vk}}(t)$ defined in (4.3)
- The squared value of the RMS grid current driving voltage in per unit $\left(e_{vk,p.u.}^{rms}\right)^2$ as defined in (4.4)
- The averaged values of the capacitive energy sum $\overline{w_{\Sigma k}}(t)$ and difference $\overline{w_{\Delta k}}(t)$ between arms defined by (4.5), and introduced into the circulating current reference equation by means of the outputs of two PI controllers $\overline{P_{\Sigma k}}$ and $\overline{P_{\Delta k}}$ defined in (4.6).

$$\bar{P}_{vk} = \frac{1}{T} \int_{t_0}^{t_0+T} e_{vk} i_{vk} dt \quad (4.3)$$

$$(e_{vk,p.u.}^{rms})^2 = \frac{1}{T} \int_{t_0}^{t_0+T} \frac{e_{vk}^2}{v_{dc}^2} dt \quad (4.4)$$

$$\begin{aligned} \overline{w_{\Sigma k}}(t) &= \frac{1}{T} \int_{t_0}^{t_0+T} w_{\Sigma k}(t) dt \\ \overline{w_{\Delta k}}(t) &= \frac{1}{T} \int_{t_0}^{t_0+T} w_{\Delta k}(t) dt \end{aligned} \quad (4.5)$$

$$\begin{aligned} \overline{P_{\Sigma k}^{ref}} &= \left[kp_{\Sigma} \left(W_{\Sigma k}^{ref} - \overline{w_{\Sigma k}} \right) + ki_{\Sigma} \int \left(W_{\Sigma k}^{ref} - \overline{w_{\Sigma k}} \right) dt \right] \\ \overline{P_{\Delta k}^{ref}} &= \left[kp_{\Delta} \left(W_{\Delta k}^{ref} - \overline{w_{\Delta k}} \right) + ki_{\Delta} \int \left(W_{\Delta k}^{ref} - \overline{w_{\Delta k}} \right) dt \right] \end{aligned} \quad (4.6)$$

One might argue that it is possible to improve the dynamic response of the system by simply increasing the bandwidth of the low-pass filter. This is done of course at the expense of its required filtering performance; i.e., the resulting signal will not be as constant as desired. A direct implication of using LPFs is that the tuning of the controller parameters will become rather a complex task. In the following sections, it is shown how the slow dynamics inherent to LPFs can be avoided by using SOGI-QSG based adaptive filters to estimate all the required average signal inputs for calculating the circulating current reference using (4.1).

4.3 The second order generalized integrator configured as a quadrature signal generator

The Second Order Generalized Integrator has become well known as a building block used for sinusoidal signal integration in converter control systems and grid synchronization methods [73, 71, 72, 74, 75]. Configured as an on-line frequency-adaptive Quadrature Signal Generator as shown in Fig. 4.1, the SOGI can provide two output signals [73]: an in-phase, band-pass-filtered (α -axis) signal, and an in-quadrature low-pass-filtered (β -axis) signal. This configuration, labeled SOGI-QSG, has found widespread applications in grid synchronization methods, where 90 phase shifting can be utilized for implementing synchronous reference frames Phase Lock Loops (SRF-PLLs) in single-phase systems and for symmetrical component sequence separation under unbalanced three-phase conditions [73].

For single-phase applications, these two signals can be used for forming a virtual balanced two-phase system represented in the stationary $\alpha - \beta$ frame [38].

Steady-state characteristics and tuning of SOGI-QSG

Considering a constant resonance frequency ω' , the functions representing the in-phase and the in-quadrature signals of the SOGI-QSG that were presented in Fig. 4.1, can be expressed as in

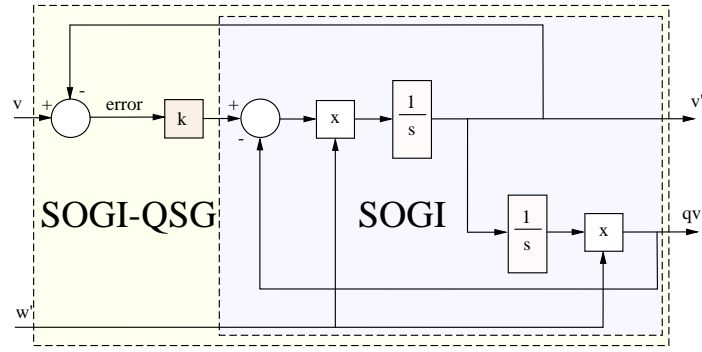


Figure 4.1: Explicitly frequency-adaptive SOGI-QSG

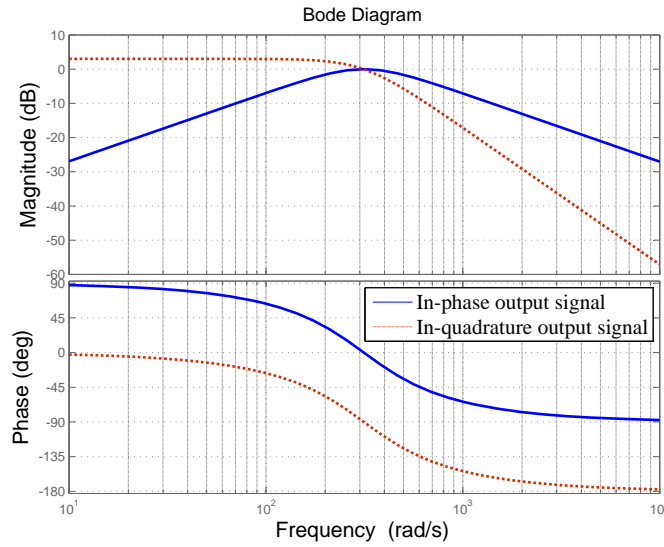


Figure 4.2: Frequency Response of SOGI-QSG

(4.7) and in (4.8), .

$$\mathbf{v}' = \mathbf{x}_\alpha = \frac{k \cdot \omega' \cdot s}{s^2 + k \cdot \omega' \cdot s + \omega'^2} \mathbf{v} \quad (4.7)$$

$$\mathbf{qv}' = \mathbf{x}_\beta = \frac{k \cdot \omega'^2}{s^2 + k \cdot \omega' \cdot s + \omega'^2} \mathbf{v} \quad (4.8)$$

The frequency responses of the transfer functions $v'(s)/v(s)$ and $qv'(s)/v(s)$ are shaped by the value of the gain constant k . Selecting k equal to $\sqrt{2}$ yields in a critically damped second order system, providing a good compromise between overshoot, settling time and rejection of high frequency harmonic components, as discussed in [73, 71, 76]. The value of k is therefore kept at $\sqrt{2}$ for the following research. The resulting frequency characteristics of the SOGI-QSG are shown in the Bode-diagram of Fig. 4.2 for a resonance frequency of $50Hz$.

The frequency response for the in-phase signal shows a band-pass characteristic with unity gain and zero phase shift at the fundamental angular frequency $\omega' = 2\pi \cdot 50Hz$, whereas the in-quadrature signal presents a low-pass characteristic with unity gain and -90 phase shift at the fundamental angular frequency.

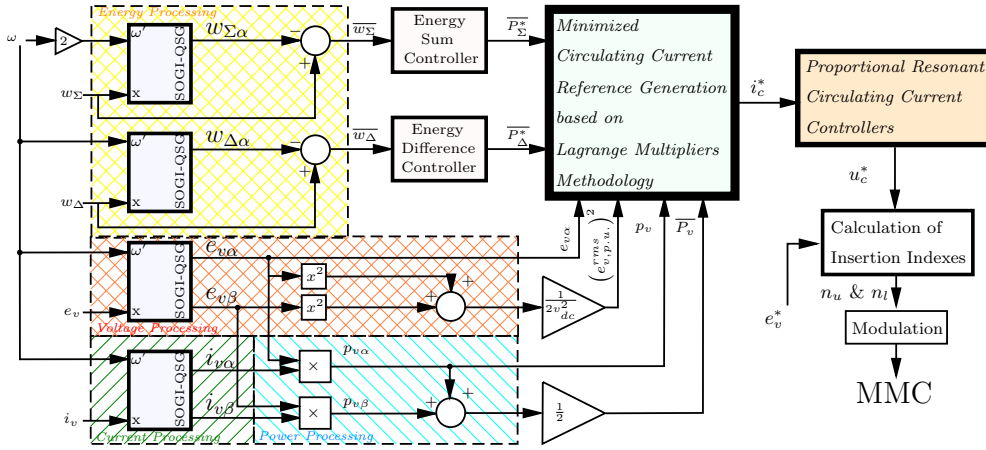


Figure 4.3: Generation of circulating current minimized reference using Power, Voltage and Energy Estimations based-on 4 SOGI-QSG

Based on Fig. 4.2 and on equations (4.8), the in-quadrature signal will have a DC gain equal to k . Nonetheless, the magnitude of such a DC component will be assumed negligible for the following discussions.

4.4 Circulating current reference calculation based on single-phase voltage, power and energy estimation for MMCs

Following the previous discussions, two main issues have to be addressed in order to improve the performance of the proposed controller:

1. The calculation of the mean values of the input signals needed for the current reference signal generation will require a fast and acceptable dynamical response.
2. Regardless of the number of SMs of the MMC, the total harmonic distortion (THD) introduced by the internal emf e_{vk} , and in turn by the instantaneous power P_{vk} , must not affect the quality of the circulating current reference.

Both aspects are solved by estimating the input parameters by means of adaptive filters based on SOGIs, as will be detailed in the following lines.

The enhanced control strategy is shown in Fig. 4.3. As can be seen, it is based on four SOGI-QSG building blocks as the one illustrated in Fig. 4.1. Two SOGI-QSG for processing the capacitive energies $w_{\Sigma k}$ and $w_{\Delta k}$, one for the driving voltage e_{vk} , and one for the grid current i_{vk} . The required single-phase voltage, power and energy input variables are then estimated by simple arithmetics and are introduced to the block named *Minimized Circulating Current Reference Generation based on Lagrange Multipliers Methodology*. The output of such a block is indeed the circulating current reference that will become the input for the *Proportional Resonant Circulating Current Controllers* block, yielding in the reference driving voltage u_c^* . The following subsections describe in detail the estimation process of each of the required inputs for the circulating current reference calculation.

4.4.1 Estimation of single-phase fundamental frequency voltage and power

For the estimation of the values of e_{vk} and P_{vk} , the approach is to use the SOGI-QSG as a band-pass filter, only by means of the “in-phase” α -axis signal. The estimated value of the MMC internal voltage is then:

$$\hat{e}_{vk} = e_{vk\alpha} = \frac{k \cdot \omega' \cdot s}{s^2 + k \cdot \omega' \cdot s + \omega'^2} e_{vk} \quad (4.9)$$

Where $\omega = 2\pi f_{grid}$. In turn, the estimated instantaneous power is the trivial:

$$\hat{P}_{vk} = e_{vk\alpha} i_{vk\alpha} \quad (4.10)$$

with $i_{vk\alpha}$ defined as:

$$i_{vk\alpha} = \frac{k \cdot \omega' \cdot s}{s^2 + k \cdot \omega' \cdot s + \omega'^2} i_{vk} \quad (4.11)$$

4.4.2 Estimation of the single-phase RMS voltage

To estimate the squared value of the MMC internal emf in per unit (p.u.); i.e., $\left(\hat{e}_{vk,p.u.}^{rms}\right)^2$, the β -axis signal will be used as well as the α -axis signal of (4.7) and (4.8). The estimate is provided in the following (4.12).

$$\left(\hat{e}_{vk,p.u.}^{rms}\right)^2 = \frac{e_{vk\alpha}^2 + e_{vk\beta}^2}{2v_{dc}^2} \quad (4.12)$$

Where $e_{vk\alpha}$ and $e_{vk\beta}$ are obtained by replacing e_{vk} in (4.7) and (4.8), respectively. The 90° phase-shift that exists between $e_{vk\alpha}$ and $e_{vk\beta}$, is turned to 180° when both variables are squared. Therefore, by simply adding $e_{vk\alpha}^2$ with $e_{vk\beta}^2$, the oscillating component at $100Hz$ present in each one of them cancels out, leaving only a DC component at twice the required value.

4.4.3 Estimation of the single-phase average power

An estimate for the instantaneous average power in the single-phase system may be calculated directly from the outputs of two SOGI-QSGs, one for the voltage signal and one for the current signal. The power in a virtual balanced two phase system can be calculated directly according to instantaneous power theory as:

$$p_{virtual-2ph} = \mathbf{v} \cdot \mathbf{i} = \hat{e}_{vk\alpha} \hat{i}_{vk\alpha} + \hat{e}_{vk\beta} \hat{i}_{vk\beta} \quad (4.13)$$

Where $\hat{e}_{vk\alpha,\beta}$ and $\hat{i}_{vk\alpha,\beta}$ is the result of replacing e_{vk} and i_{vk} in (4.7) and (4.8).

Then, since the β -axis is only a virtual auxiliary system, the power in the single phase system is given by half the power calculated in the two-phase system.

Table 4.1: Low number of levels MMC Parameters

Number of SM	5
SM Nominal Voltage	5kV
SM Capacity	3.3mF
Arm Inductance	10mH
Arm Resistance	0.1Ω
Nominal Power	2.5 MVA

$$\bar{P}_{vk} = \frac{p_{virtual-2ph}}{2} = \frac{1}{2} (e_{vk\alpha} i_{vk\alpha} + e_{vk\beta} i_{vk\beta}) \quad (4.14)$$

Here again, the resulting power is oscillation-free since the individual components at $100Hz$ of $e_{vk\alpha} i_{vk\alpha}$ and $e_{vk\beta} i_{vk\beta}$ are $180^\circ C$ phase shifted, and thus cancel out with each other. This is a natural consequence of using an auxiliary virtual system with a phase-shift of $90^\circ C$.

4.4.4 Estimation of the single-phase average values for the MMC energy sum and difference

Finally, to estimate the mean values of the MMC energy sum ($\bar{w}_{\Sigma k}$) and difference ($\bar{w}_{\Delta k}$), the SOGI-QSG is used again as a notch filter. The in-phase signal of the SOGI-QSG is used to estimate the sinusoidal oscillation in the signal; at fundamental frequency for the energy difference and at twice the fundamental frequency for the energy sum. The DC component is calculated as the difference between the original signal and the estimated (α -axis) signal, as follows.

$$\hat{\bar{w}}_{\Sigma k} = w_{\Sigma k} - w_{\Sigma k\alpha} \quad (4.15)$$

$$\hat{\bar{w}}_{\Delta k} = w_{\Delta k} - w_{\Delta k\alpha} \quad (4.16)$$

4.5 Simulation results

In this section the MMC was simulated in Matlab-Simulink using the enhanced control scheme presented in Fig. 4.3 where equation (4.1) is used to calculate the circulating current references signal using as inputs SOGI-QSG-based estimated single-phase voltage, power and energy values. As in the previous chapter, the implementation was done using proportional multi-resonant current controllers [69]. For the simulation study, a MMC with low number of levels is chosen since this would imply a more elevated THD, with the parameters of Table 4.1.

Harmonics reduction improvement

Figure 4.4 shows the MMC internal emf e_{vk} , both unfiltered and filtered by means of the described SOGI-based technique.

Fig. 4.5 depicts the circulating current reference obtained by replacing both unfiltered and filtered e_{vk} in 3.31, with $\alpha = 1$. The circulating current presented in Fig. 4.5-a) has clearly a

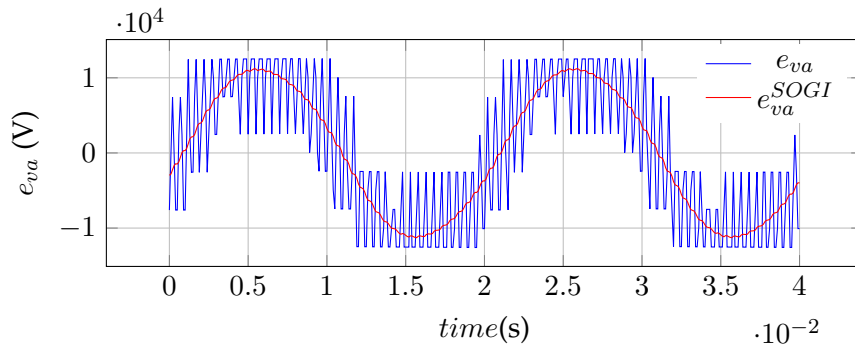


Figure 4.4: Internal emf (e_{vk}) for a 5-level MMC

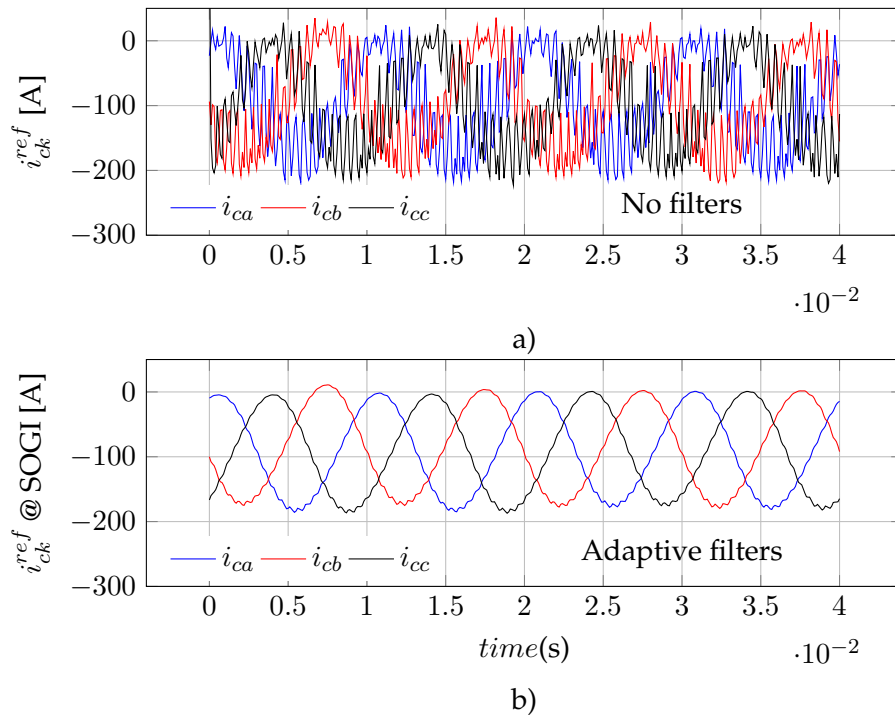


Figure 4.5: Circulating currents reference (i_{ck}^*): a) Without adaptive filters and b) with adaptive filters

much higher THD than the one presented in 4.5-b). However, it is possible to argue that a PI controller with low bandwidth could also filter such harmonics. Nonetheless, even if in Fig. 4.6 the harmonics of the resulting circulating current are reduced, it can be seen that the unfiltered case of Fig. 4.6-a) still presents a more distorted waveform than the case using the SOGI-QSG illustrated in Fig. 4.6-b). Hence the unfiltered case will lead to unnecessary harmonic losses.

Moreover, Fig. 4.7 shows the difference between the unfiltered instantaneous power with respect to the filtered case by means of the SOGI-QSG. As expected, the SOGI-based signal is significantly less distorted.

Average MMC single-phase power dynamics improvement

In this case scenario the mean value of the MMC single-phase power calculated by means of a simple LPF is compared to the one calculated in 4.14. In order to make clear the advantage of

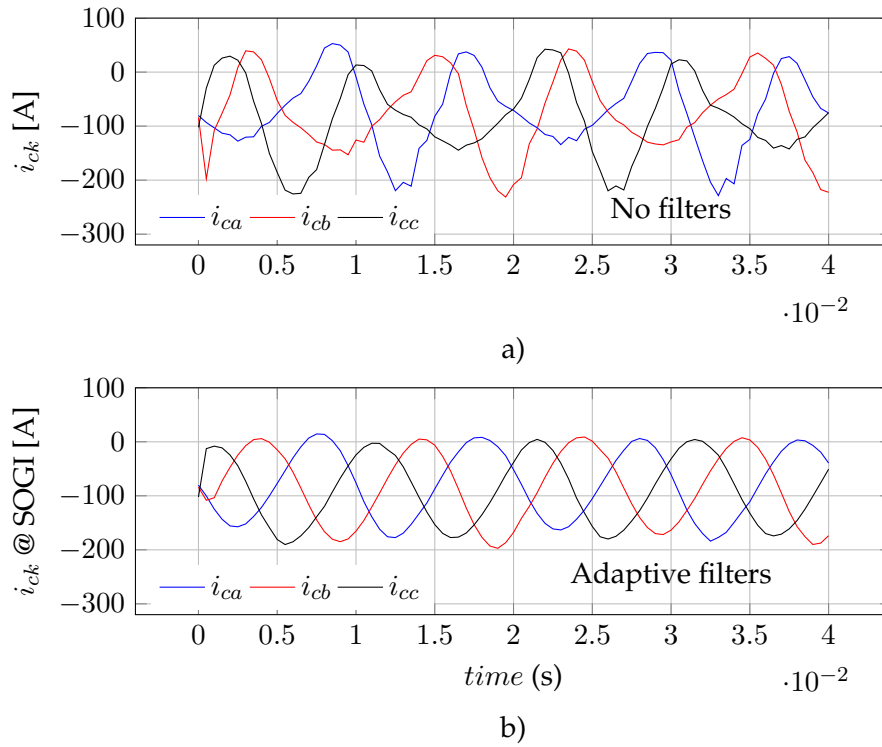


Figure 4.6: Resulting circulating currents (i_{ck}): a) Without adaptive filters and b) with adaptive filters

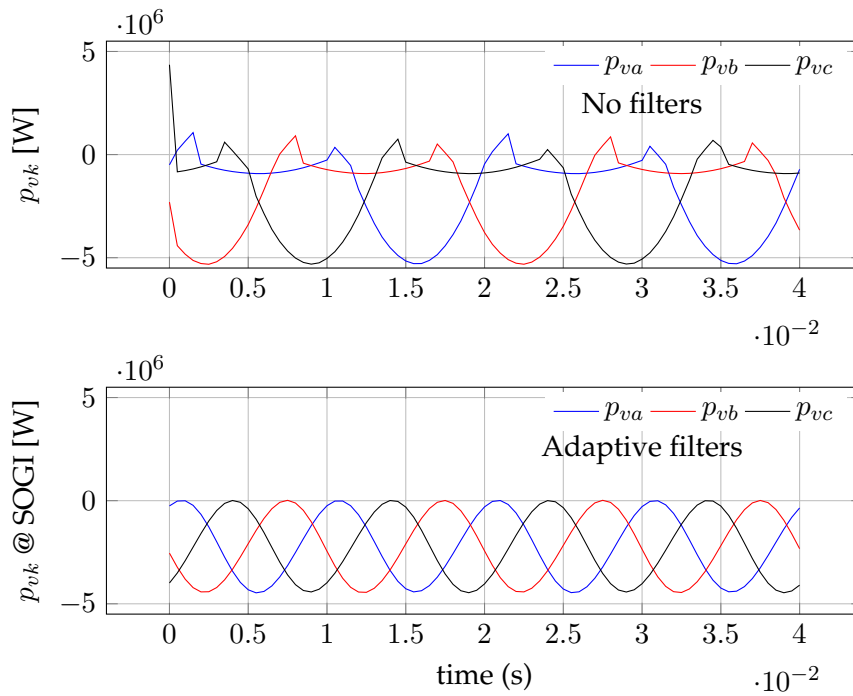


Figure 4.7: Instantaneous MMC single-phase power (p_{vk}): a) Without adaptive filters and b) with adaptive filters.

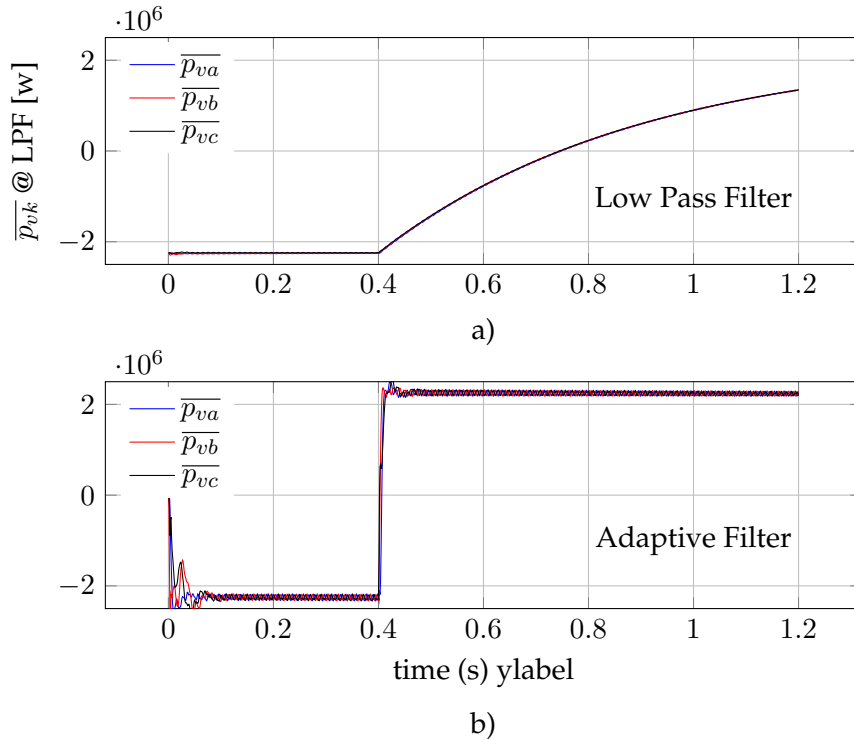


Figure 4.8: Average MMC single-phase power ($\overline{p_{vk}}$) calculated using a) Low Pass Filters (LPF) and b) SOGI-based adaptive filters.

the second one with respect to the first one, a power reversal is done at $t = 0.4s$. As can be seen in Fig. 4.8, the SOGI methodology used to calculate the average value offers a better dynamical performance in front of a power reference step changes.

Calculation of the MMC internal RMS voltage

Subsequently, the MMC internal voltage RMS calculated in 4.12 has a better dynamical performance than the one based on LPF, as can be inferred from Fig. 4.9.

Average capacitive energy values dynamics improvement

This section shows the gain in dynamical performance regarding the MMC average energy (sum and difference) regulation that is achieved by means of the use of SOGI-QSG as a notch filter, compared to a traditional low pass filter (LPF). For this case, a high number of SM is considered ($n \approx \infty$), and $\alpha = 0$ is considered in 3.31. In this case scenario, a 20% increment step change is given to the energy sum reference ($w_{\Sigma k}^{ref}$) at $t = 0.2s$, whereas at $t = 0.8s$ the energy difference reference, originally at $0kJ$, is given a step change of $40kJ$. In Fig. 4.10 and 4.11, the response of the energy sum and difference are depicted respectively, using LPF and SOGI-QSG.

When the LPF is used, it is possible to have poor dynamical performance as can be seen in the upper rows of Fig. 4.10 and 4.11, without mentioning the complication associated to the tuning of the PI parameters. On the other hand, the SOGI-QSG improves significantly such a dynamical issue, as depicted on the lower rows of the same figures. Fig. 4.12 shows the MMC capacitor

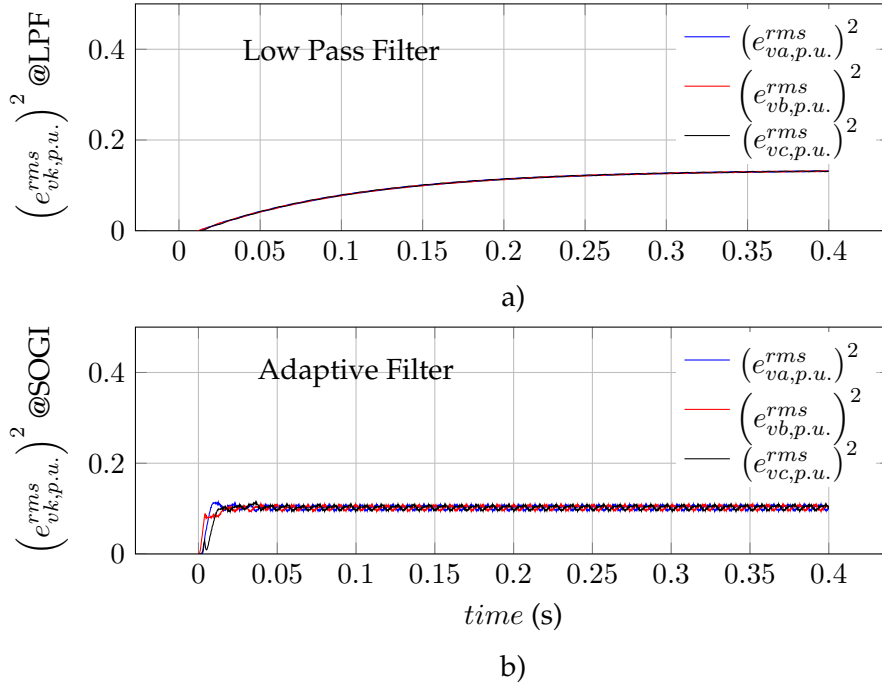


Figure 4.9: MMC Internal voltage RMS calculated using a) Low Pass Filters (LPF) and b) SOGI-based adaptive filters

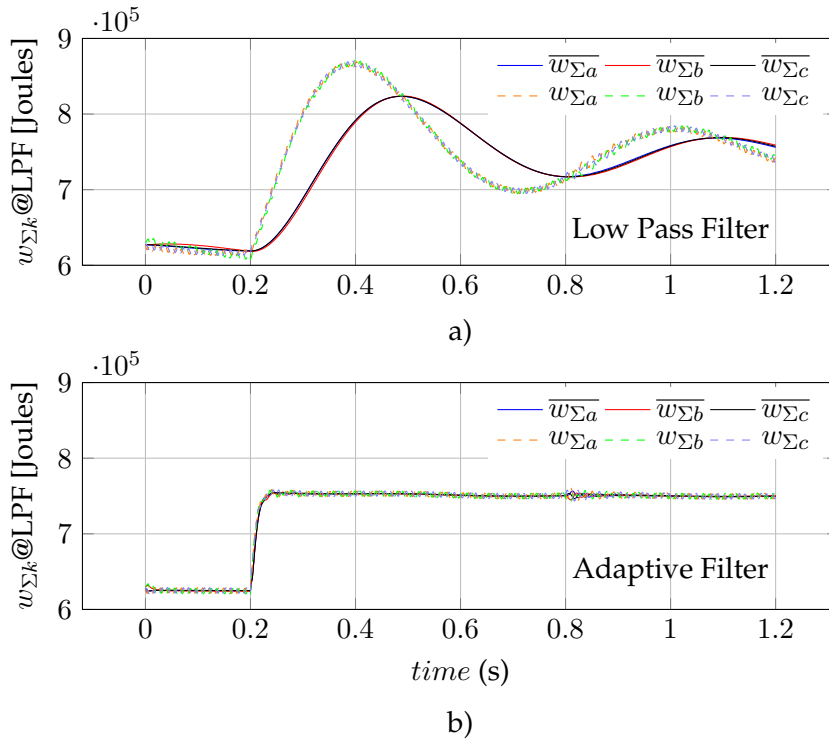


Figure 4.10: Capacitive Energy Sum between MMC arms $w_{\Sigma k}$ resulting from the proposed control strategy using a) low-pass filters and b) using SOGI-based adaptive filters

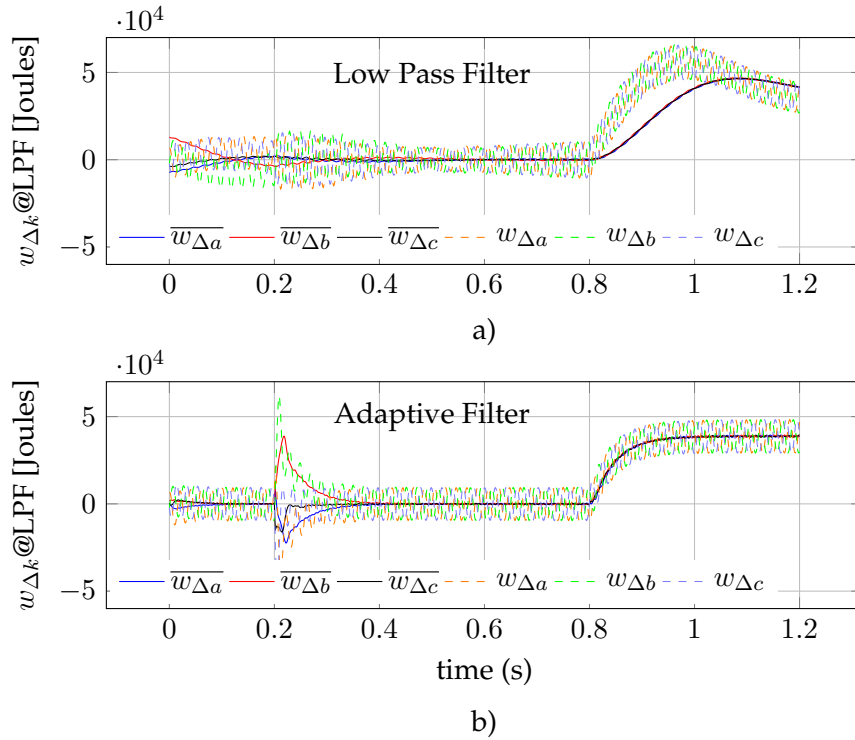


Figure 4.11: Capacitive Energy Difference between MMC resulting from the proposed control strategy using a) Low Pass Filters and b) Adaptive filters

voltages response under the same aforementioned energy reference step changes, while Fig. 4.13 does the same for the circulating currents.

Average capacitive energy sum and difference reference step changes

This last case scenario intends to demonstrate that by using the proposed circulating current reference calculation method combined with SOGI-QSG based adaptive filters, the MMC can be regulated phase-independently by exploiting the inherent properties of an abc frame control strategy while keeping high dynamical performance.

In Fig. 4.14-a) is depicted the upper and lower capacitor voltages, whereas in Fig. 4.14-b) the circulating currents. At $t = 0.2s$ $w_{\Delta k}^{ref}$ reference step change is given from 0kJ to 40kJ and brought back to 0kJ at $t = 0.4s$. Furthermore, at $t = 0.6s$, $w_{\Sigma a}^{ref}$ is increased by 20%, $w_{\Sigma b}^{ref}$ is increased by 30%, while $w_{\Sigma c}^{ref}$ is increased by 10%; they are brought by to their original values at $t = 0.8s$.

Fig. 4.14-a) shows the MMC capacitor voltages response to the aforementioned case-scenario while Fig. 4.14-b) the circulating currents. It can be seen that the controller successfully achieves the desired reference values with a performing dynamical response, in great part since the LPF were substituted by the SOGI-QSG based filtering scheme presented in this chapter.

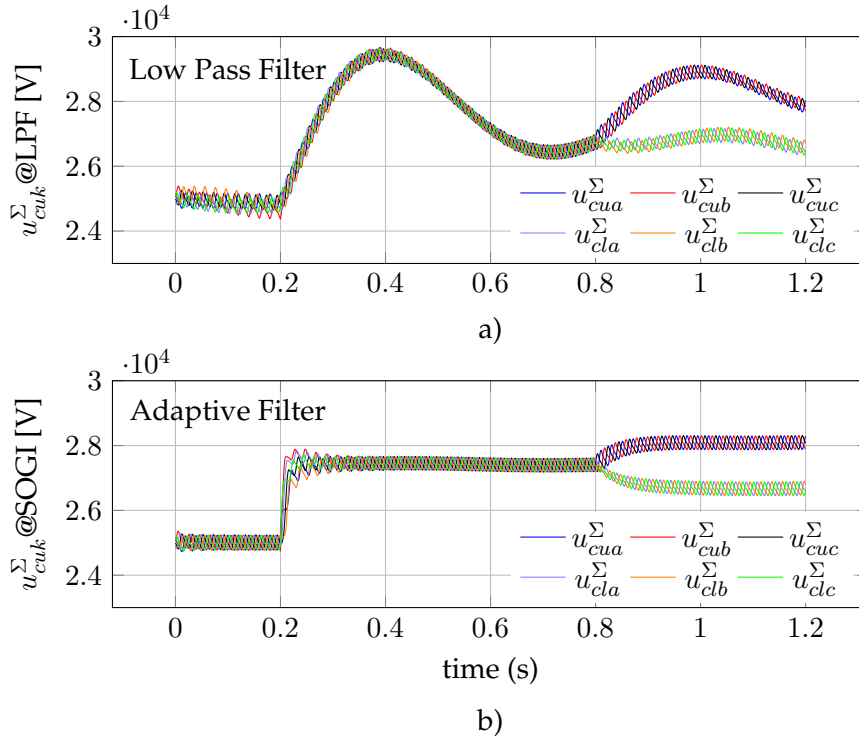


Figure 4.12: MMC Upper and Lower Capacitor Voltages Sum per phase (u_{ck}^{Σ}) resulting from the proposed control strategy using a) Low Pass Filters and b) Adaptive filters

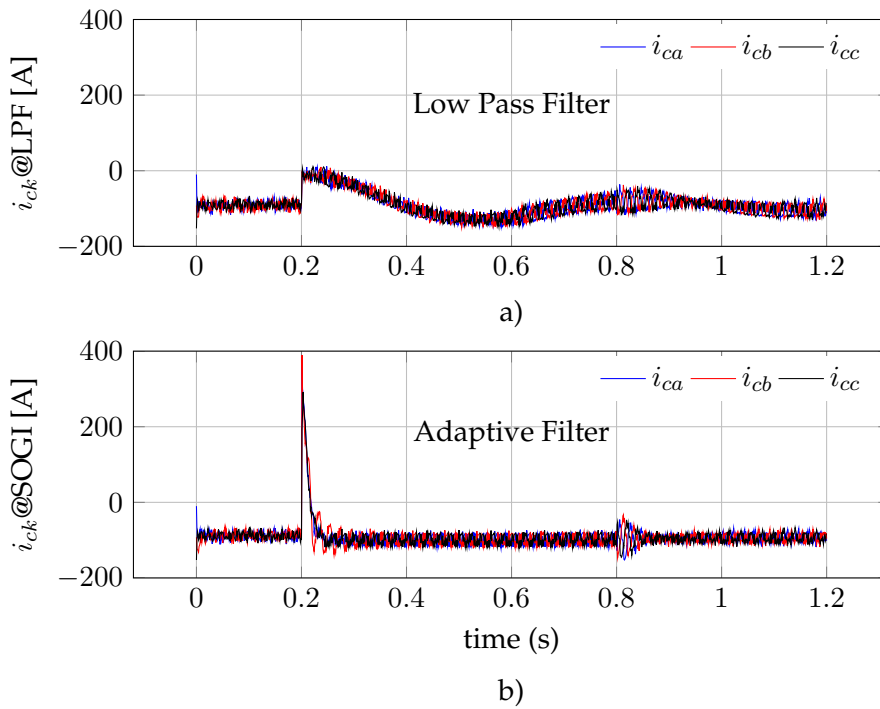


Figure 4.13: MMC circulating currents (i_{ck}) resulting from the proposed control strategy using a) Low Pass Filters and b) Adaptive filters

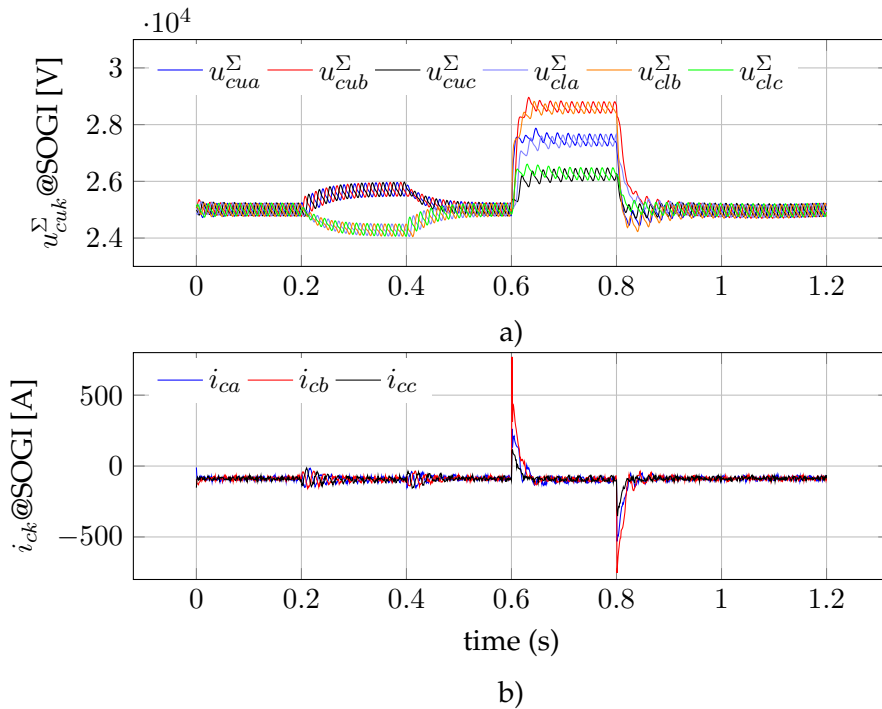


Figure 4.14: a) MMC arm capacitor voltage sum under unbalanced reference change and b) circulating currents, both resulting from the proposed control strategy using SOGI-adaptive filters. Behavior under different reference step changes per phase.

4.6 Proof of concept via lab experimental prototype

4.6.1 Experimental setup

The experimental setup for verification of the proposed control scheme based on mathematical optimization and multi-resonant controllers, is the single phase MMC depicted in Fig. 4.15. The power is provided by a controllable DC source of 150 Volts to the DC link capacitors through a diode, to ensure power flow in one direction (for grid connected applications). This controllable source is the limiting element in power. Therefore, the prototype in its current configuration was not able to be operated beyond 1 kVA, although the system has been designed to go further in power for future experiments. A passive load is considered in this setup, formed by an inductor and a resistor L_l and R_l , respectively. The MMC prototype is formed by five SMs in each arm yielding in a 6-level multi-valve voltage output. A resistor with high resistance is added in series to the arm inductor in order to be able to energize the capacitors through the DC source to their initial value, just before normal operation. The proposed circulating current reference calculation method was implemented on an OPAL-RT platform together with the multi-resonant controllers and balancing algorithm needed to operate the converter. The main parameters of the laboratory setup are listed in Table 4.2.

4.6.2 Experimental Results

A set of results showing the operation of the laboratory prototype using the proposed control is presented in this section.

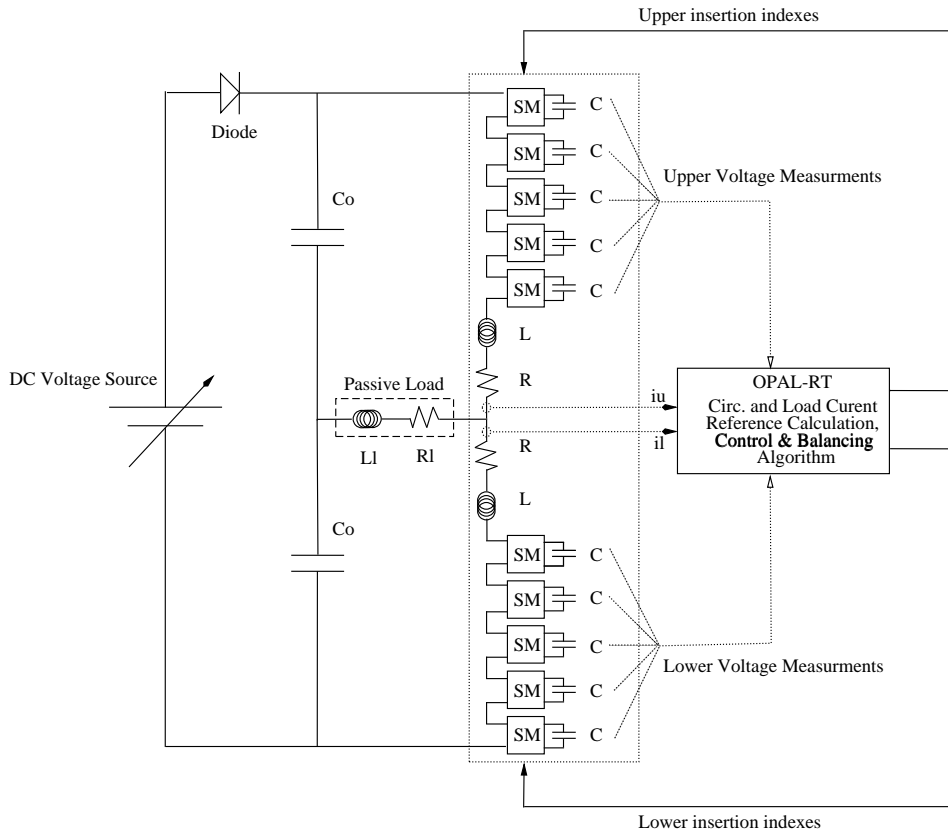


Figure 4.15: Overview of the laboratory setup for verification of the proposed control strategy

Table 4.2: Experimental setup parameters

Apparent Power	140VA
DC Nominal Voltage	140V
AC RMS Voltage	50V
Load Resistance	12Ω
Load Inductance	40mH
Arm Resistance	12Ω
Arm Inductance	10mH
Sub-Module Capacitance	3.3mF
Number of levels N	5
AC voltage frequency	50Hz
Balancing frequency	1kHz

Table 4.3: PI parameters

$w_{\Sigma k}$ PI	kp_{Σ}	88.885	ki_{Σ}	0.05^{-1}
$w_{\Delta k}$ PI	kp_{Δ}	48.885	ki_{Δ}	0.05^{-1}
i_{ck} PIR	kp	180	$ki, ki_{2\omega}$	$0.18^{-1}, 5000$
Active Power	kp	1.1	ki	0.0414^{-1}
Reactive Power	kp	0.37	ki	0.0114^{-1}
Active Power	kp	1.1	ki	0.0414^{-1}
DC Voltage	kp	3	ki	0.035^{-1}
i_{vk} PI	kp	5.0598	ki	0.003^{-1}

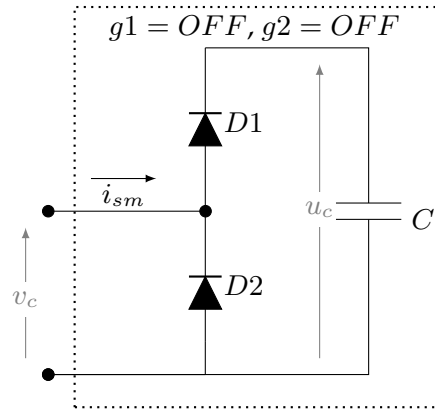


Figure 4.16: SM Equivalent Representation for Blocked Operation

Initializing the MMC and pre-charging the capacitors

Before entering normal operation in a simulation program, it is usually required to initialize each SM capacitor to a voltage of V_{dc}/N . To initialize the MMC lab prototype, the controllable DC source (depicted in Fig. 4.15) is brought from 0 to 150 Volts. As the MMC is still in its blocked state; that is, all $4N$ IGBTs are turned off, the resulting SM equivalent is as illustrated in Fig. 4.16. Therefore, each SM capacitor will be charged through “D1” to approximately $v_{dc}/2N$ which is half of the required initial voltage (v_{dc}/N). Thus an initialization strategy is required to double the voltages of every SM capacitor before entering normal operation. The strategy adopted is described in the following lines and was chosen based on its simplicity. However, this solution is not a good option for high-voltage MMCs connected to the grid and was only used so that the proposed control scheme could be tested.

- The controllable DC source is energized and the MMC is in blocked stated: All capacitors are brought naturally to v_{dc}/N .
- All $2N$ SMs are bypassed as in Fig. 4.17-a). In other words, both multi-valves will generate a *controlled* short-circuit. In order to protect the controllable DC source, and limit the resulting short-circuit current, the arm resistors R of the MMC are chosen sufficiently high. This is undesirable in high-voltage applications.
- Furthermore, only the capacitor of the *first* SM is inserted into the system, as in Fig. 4.17-b). The capacitor will then start charging from its initial value of $v_{dc}/2N$ to v_{dc} . However, a control action is required to interrupt this charging process when it reaches the desired value of v_{dc}/N .
- Once the first SM capacitor voltage reaches the desired v_{dc}/N voltage level, it is bypassed again.
- The same procedure is repeated with the second SM, and so forth until all $2N$ SM have been charged to the desired value.

The result of implementing such an initialization algorithm in the lab prototype is given in Fig. 4.18. It can be seen in Fig. 4.18-a), that all 10 ($2N$) capacitors have been charged in sequential order using this technique to 28 Volts (v_{dc}/N). In addition, the circulating current has its highest value before and after the charging process as the MMC is forcing a short-circuit operation. Indeed, the charging speed will depend on the values of the arm inductance and resistance.

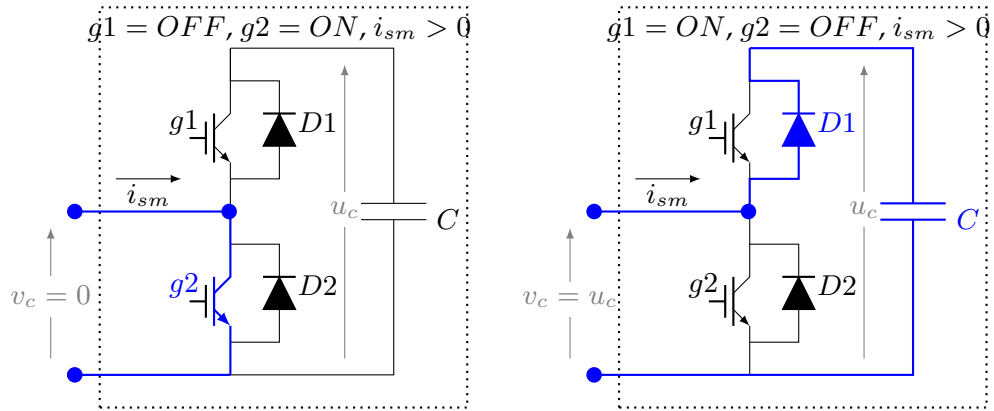


Figure 4.17: Current flowing in the SM Semiconductor devices in normal operation: a) Bypassed SM and Positive Current, b) Active SM and Positive Current

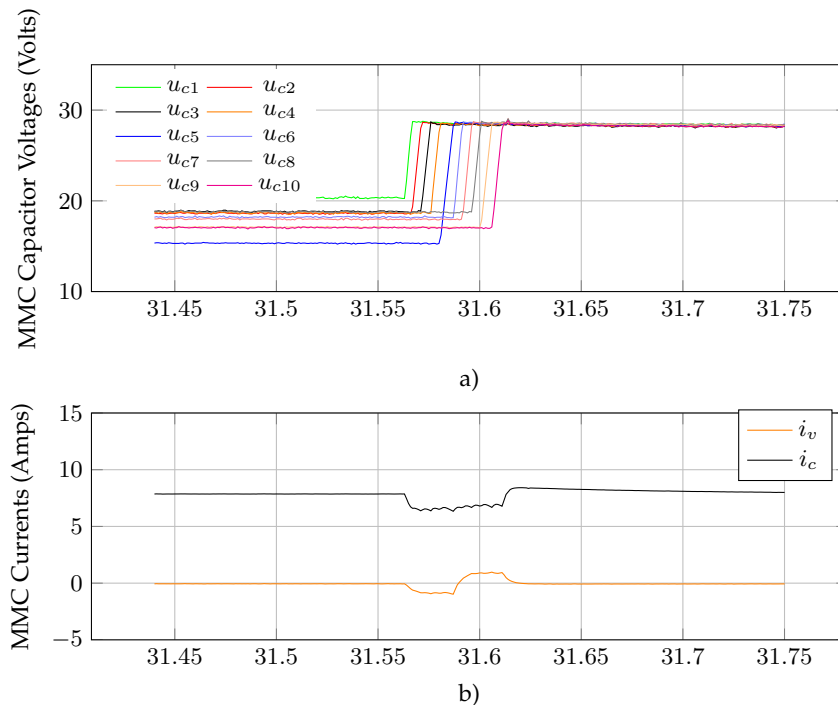


Figure 4.18: Pre-charging the SM capacitors of the single phase MMC lab prototype before normal operation: a) Sequential charging of SM capacitors, b) circulating and load currents

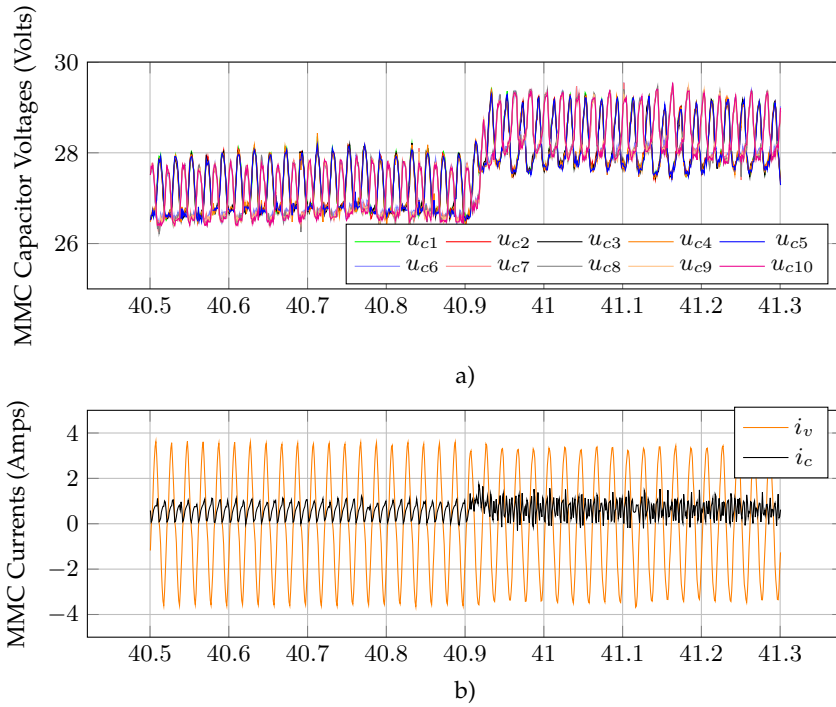


Figure 4.19: Turning on the proposed control strategy at $t=40.9$: a) MMC $2N$ SM Capacitors, b) Circulating and Load currents

Activating the proposed control scheme

Once the all 10 SM are brought to v_{dc}/N , the converter is ready to be operated. Since a passive load is used, no grid current control scheme was necessary and the reference for e_v is set to the desired output voltage of the MMC using equation 4.17.

$$e_v^* = \hat{v}_{ac} \cdot \sin \omega t \quad (4.17)$$

The converter is then controlled in using the *direct modulation* strategy [3] reviewed in section 2.9. In other words, the circulating current control is off, implying that $u_c^* = 0$.

The proposed control for the circulating current is activated manually a few seconds later. In Fig. 4.19, the moment when the proposed circulating current control strategy is activated for the lab prototype has been captured. For such an example, this occurs at $t = 40.9s$. The proposed strategy immediately brings the unregulated capacitor voltages average values to the reference value, given by $w_\Sigma^* = \frac{C}{N} v_{dc}^2$ and $w_\Delta^* = 0$ as depicted in Fig. 4.19-a).

In Fig. 4.19-b) the circulating and load currents are depicted. It can be seen that when the proposed control is turned on, additional harmonics appear in the circulating current. It was found that this is directly related to the controller gains, mostly of the current controller. Hence, the high order harmonic content can be reduced by reducing the gains. However, this was not carried out due to practical limitations of the prototype, discussed at the end of the section.

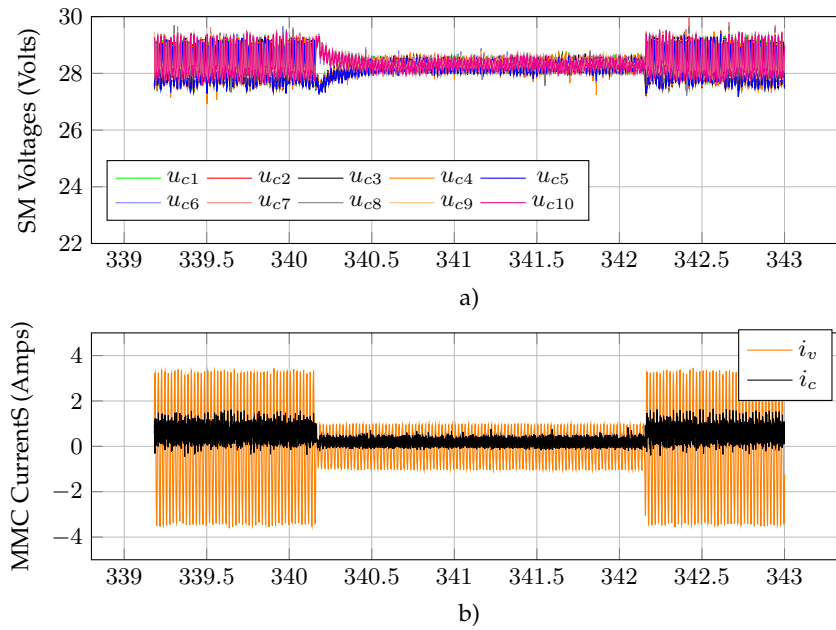


Figure 4.20: Load change: 10Ω to 60Ω, and back again: a) MMC SM capacitor voltages, b) MMC Circulating and load currents

Load step changes

The robustness of the proposed control scheme was tested under a sudden load change. In this case, the load resistance R_l was changed manually from 10Ω to 60Ω and back again to 10Ω. The resulting MMC currents and SM capacitor voltages under such a test are depicted in Fig. 4.20. It can be seen that regardless of the load change taking place, the proposed control scheme is able to keep the SM capacitors average voltages to the same values, fulfilling successfully its energy regulation feature.

Since a passive load is considered, no load current control is carried out. Therefore, when the resistance is increased from 10Ω to 60Ω, the load current is reduced accordingly as depicted in Fig. 4.20-b). The circulating current reduces its DC component as less power is consumed during the load change. Despite the changes in both MMC currents, the average value of the SM capacitor voltages remains at the same value, as can be seen from 4.20-a), thanks to the proposed control strategy. The robustness of the proposed control strategy against changes in the system is mainly attributed by the feedback loops of both the circulating current and capacitive energy variables.

Capacitive energy regulation

This section investigates whether the proposed strategy can effectively cope with both energy sum w_Σ and difference w_Δ reference step changes. The energy sum case is investigated in Fig. 4.21 while the energy difference case is illustrated in Fig. 4.22. For both cases, the effect of increasing the energy reference as well as decreasing it is considered.

In Fig. 4.21, the reference value of the energy sum is increased and decreased 30% of its original value. In Fig. 4.21-a) and c), such changes are reflected in the average value of the voltage being charged or discharged approximately 4 volts for each SM capacitor. By analyzing

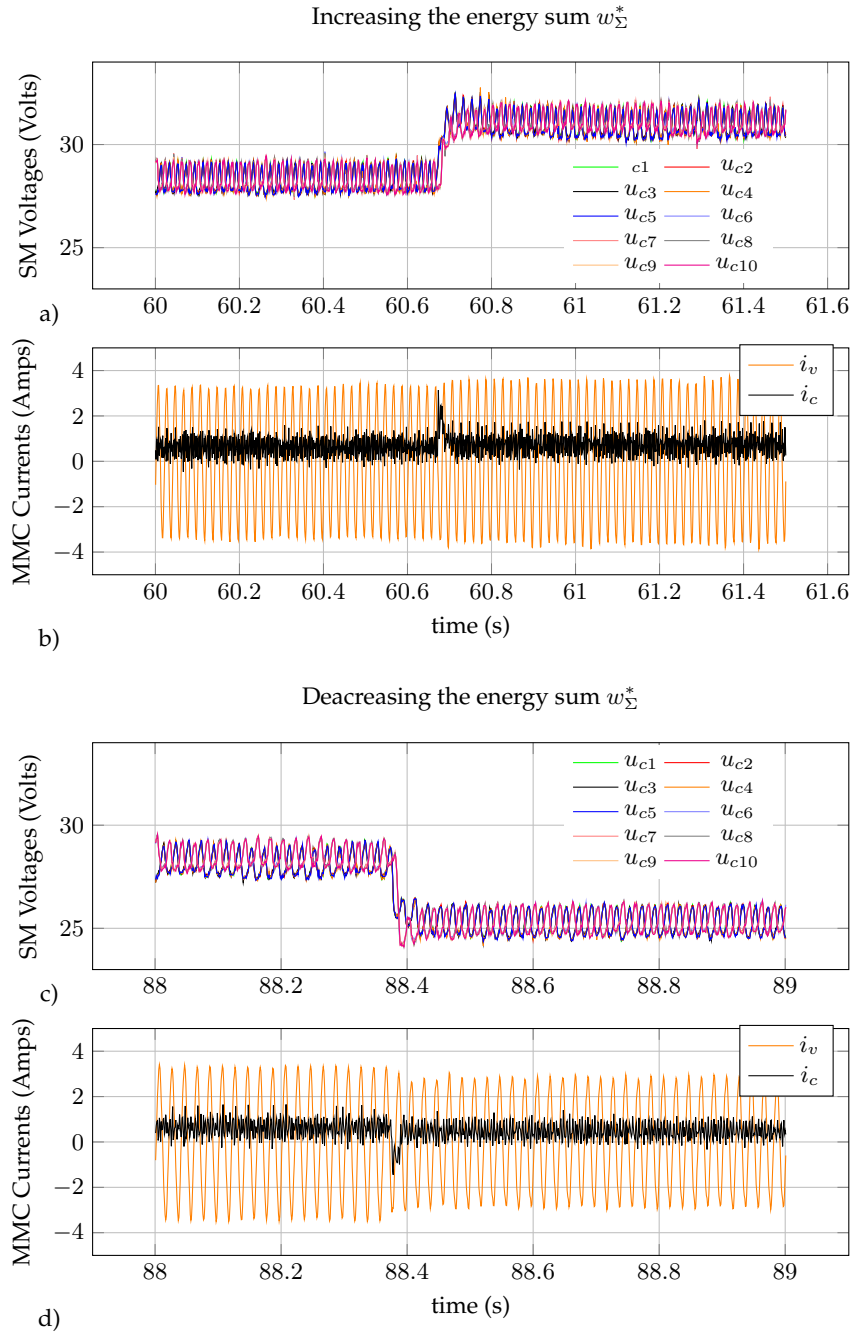


Figure 4.21: Energy sum reference step change: a) MMC SM capacitor voltages and b) circulating and load currents under a energy sum reference increase; c) MMC SM capacitor voltages and d) circulating and load currents under a energy sum reference decrease.

Fig. 4.21-b) and 4.21-d), it is possible to observe that the circulating current is clearly responsible for such an action, since a transient current peak appears with the same direction of the energy change.

A similar performance is found for the energy difference regulation, under both a 20% increase and reduction of the energy difference. In Fig. 4.22-a) and b), the energy difference reference is set at zero Joules, and is increased 20% at $t = 127.8s$. This is reflected by the approximately 3 volts voltage separation between the SMs of the upper arm and those on the lower arm. In the same way, Fig. 4.22-c) and d) start with a 20% energy difference between arms and the reference is brought back to zero Joules at $t = 137.6s$. Interestingly enough, the circulating current contribution is so small and that it can not be seen in the figures.

Low level SM balancing frequency effect under the proposed control

The objective of this section is to prove that within certain limits, the proposed control can operate successfully even if the performance of the balancing algorithm is reduced (see section 2.3.2). This is usually of interest since reducing the performance of such a low level control yields in smaller switching losses. The following three cases have been examined:

- “Infinite” Frequency case: In this case the frequency is as high as it can be: the sorting and balancing of the capacitors takes place at every time step. For this application: $20kHz$.
- Reduced switching frequency case: The frequency is reduced to $1kHz$.
- Efficient balancing algorithm: The algorithm will only take action if there has been a change in the value of the insertion index $n(t) \neq n(t - \Delta t)$.

The three cases operate with the proposed control, and only their steady state behavior is shown in the following set of figures. The SM capacitor voltages for all cases is shown in Fig. 4.23. Their corresponding load and circulating currents are depicted in Fig. 4.24 while the output voltage of the MMC v_{mmc} for each case is given in Fig. 4.25.

From Fig. 4.23, it is possible to see that for all cases the proposed control methodology is capable of operating successfully. As expected, the “infinite” frequency case is the one that has most uniform SM voltages per arm, whereas the efficient balancing strategy has the less balanced arm SMs. Moreover, it is possible to see that for this particular experimental setup, the infinite frequency case produces the most content of high order harmonics in the circulating current as can be seen from Fig. 4.24, while the other two strategies seem to give similar results. Finally, the output voltage waveform of the MMC in the “infinite” frequency case is drastically different from the other two cases, as shown in Fig. 4.25. In fact, the cases with reduced frequency seem to work with a *staircase modulation* strategy even if this is not the case. This is an issue encountered in this setup and is explained in the section entitled *Limitations of the laboratory experimental setup*. Nonetheless, it is still possible to conclude that the control strategy that has been developed in this Thesis is able to produce good regulatory performances in a small-scaled MMC laboratory prototype.

Limitations of the experimental setup

Despite the good results obtain in the lab by controlling the MMC prototype with the proposed control strategy, it is important nonetheless to mention some of the experimental setup limita-

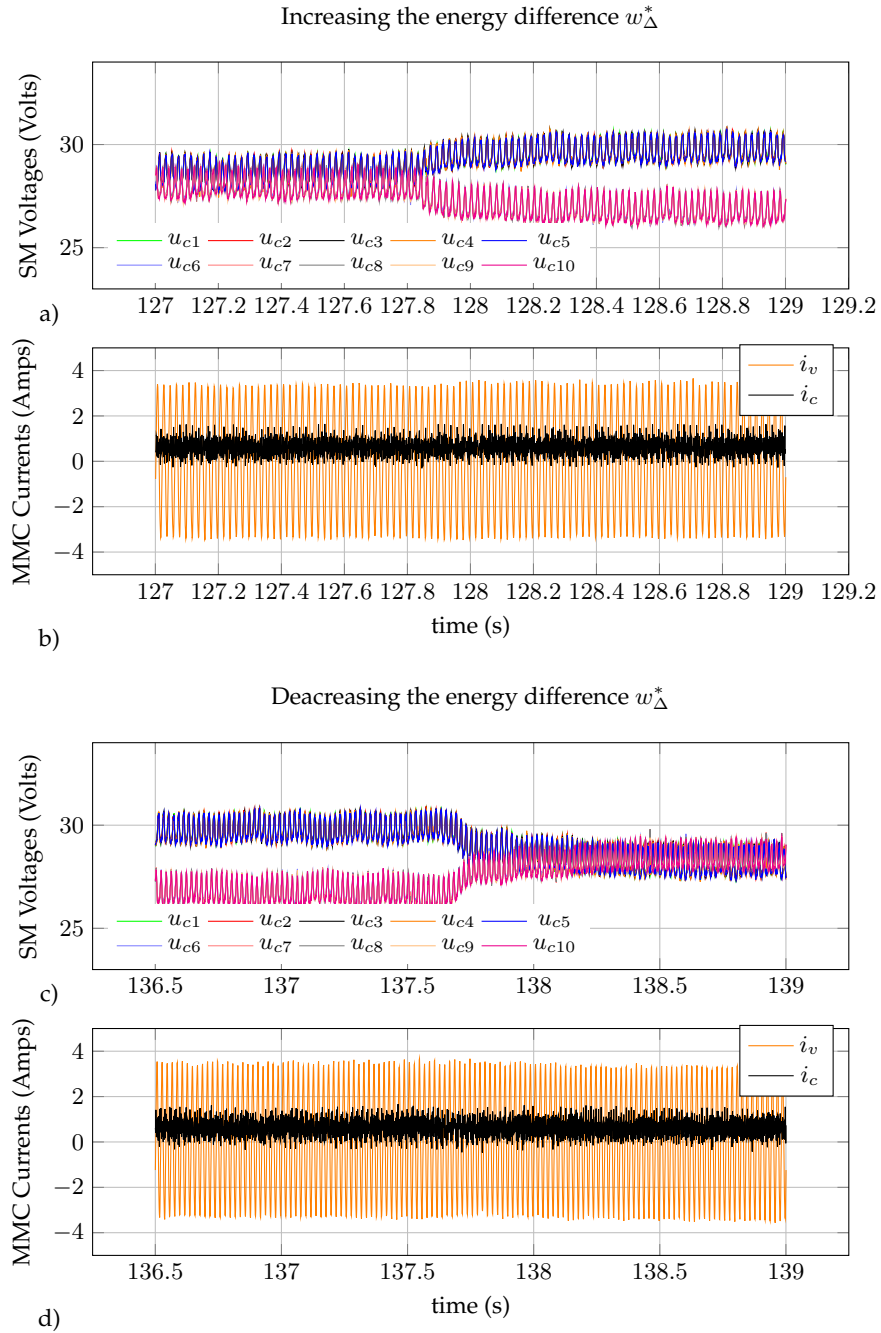


Figure 4.22: Energy difference reference step change: a) MMC SM capacitor voltages and b) circulating and load currents under a energy difference reference increase; c) MMC SM capacitor voltages and d) circulating and load currents under a energy difference reference decrease.

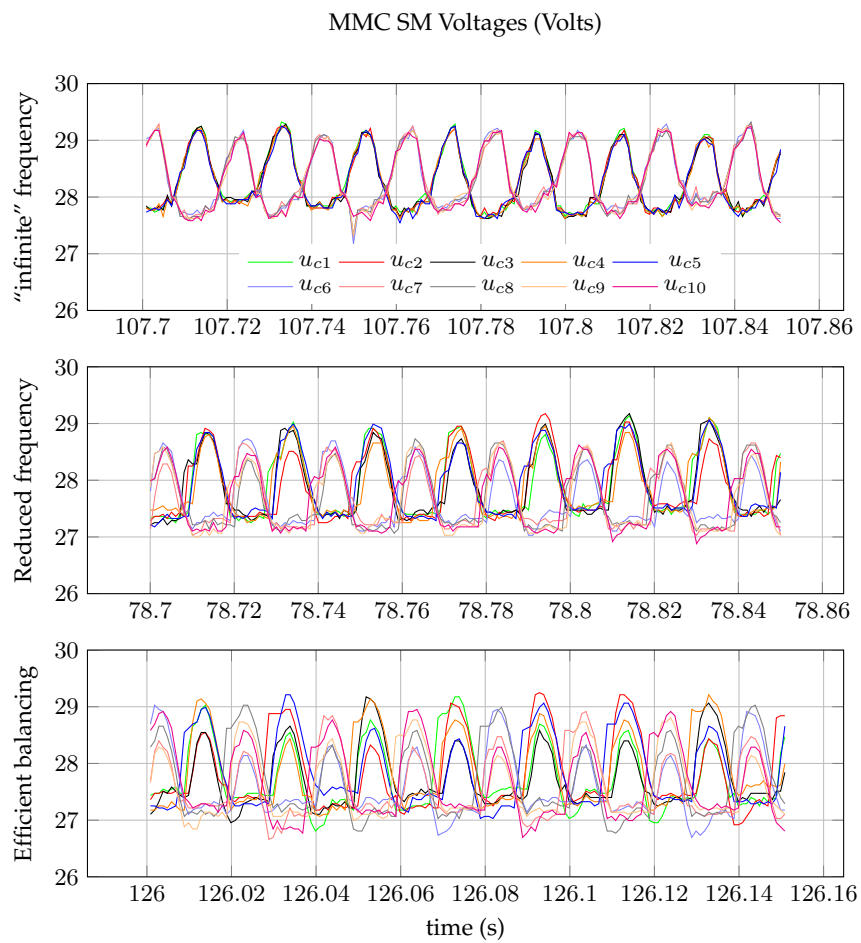


Figure 4.23: Effect of changing the balancing frequency in the SM capacitor voltages under the proposed control strategy

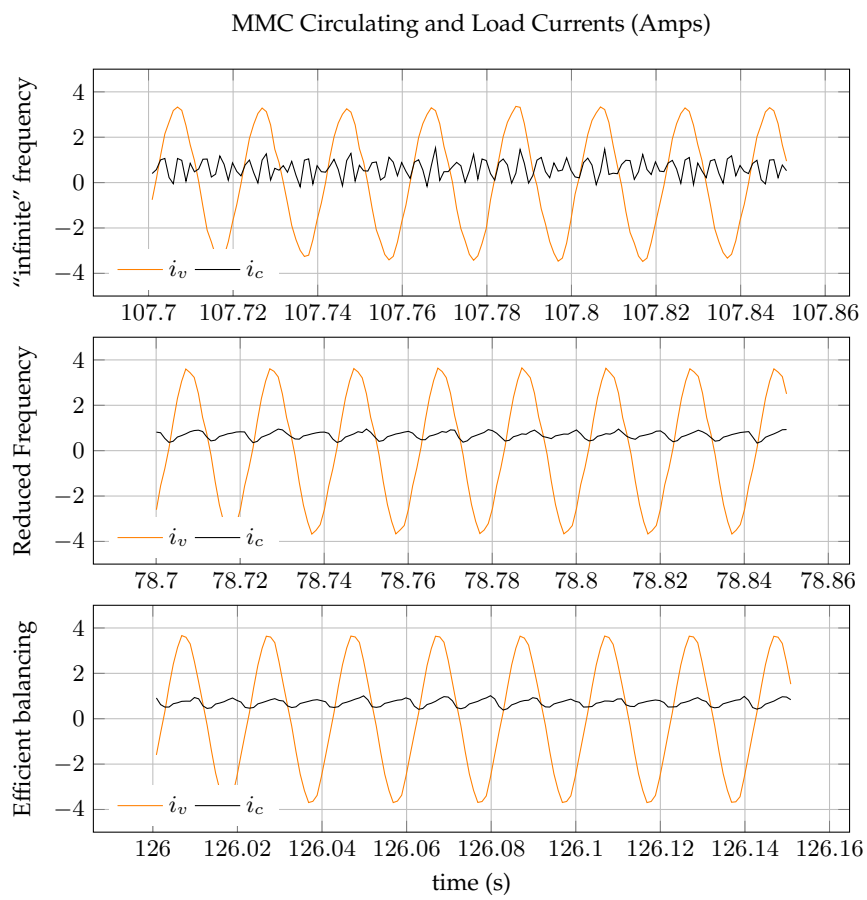


Figure 4.24: Effect of changing the balancing frequency on the MMC circulating and load currents under the proposed control strategy

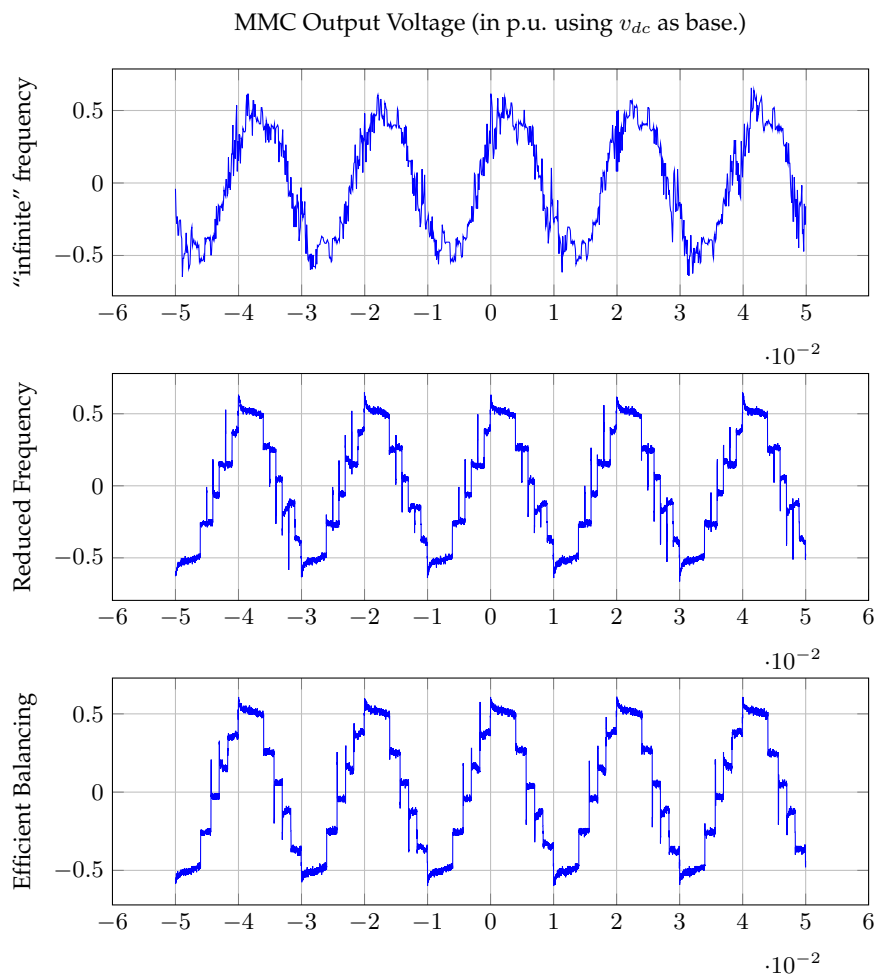


Figure 4.25: Effect of changing the balancing frequency on the MMC output voltage under the proposed control strategy

tions, so that it can be improved. A short list is provided in the following lines:

- An issue with the dead-time of the IGBTs modules was encountered. A direct consequence is that the dead-time was approximately 10 times higher than it should be. This has to do with how OPAL-RT generates the control signals and the driver that was used to give the gate signals to the IGBTs. The implementation problem was encountered in the final stage of this research project and has been taken care of. However, due to time limitations, the improved results with a smaller dead-time could not be included in the final version of this manuscript.
- The grid connection of the converter has been left as future work.
- The prototype that is considered here is a single-phase prototype. A three-phase version of the MMC has been constructed. However, results with the three-phase version of the prototype have not been included in this manuscript. The 3-phase prototype will be used in the ongoing research carried out at *Supélec* on the subject of MMC converters.

4.7 Conclusion

Adaptive filters based on SOGIs have been successfully used to enhanced the control strategy performance proposed in chapter 3, where mathematical optimization based on Lagrange multipliers yielded the circulating current reference signals in the abc frame for controlling the MMC. More precisely, four SOGI-based adaptive filters were used to estimate the fundamental frequency component and the amplitude of the instantaneous and RMS values of the MMC internal voltage (\hat{e}_{vk}), the instantaneous and average values of the output power (\hat{P}_{vk}), and the average values of the energy sum ($\hat{w}_{\Sigma k}$) and energy difference ($\hat{w}_{\Delta k}$), used as inputs to the circulating current reference generation equation. This has been shown to improve the dynamic performance of the controller, reduce the sensitivity to harmonic distortion of the control signals when applied to MMCs with low number of levels, as well as to ease the tuning of the controller parameters. The proposal was successfully validated using both simulation results as well as a single-phase 5-level MMC experimental setup in the laboratory. Since the SOGI-based filters are frequency adaptive, the proposed implementation is also suitable for application in weak grids and for control of electric drives. Thus, the presented control approach implementation seems suitable for controlling the internal dynamics of the MMCs in power system as well as drives applications, regardless of the voltage level and the number of SMs.

5

Circulating Current Signal for Constant Power under Unbalanced Grid Conditions: The MMC Energy Buffer

The work presented in this chapter extends the control contribution of this Thesis by calculating a general circulating current reference for the MMC suitable for operation under both balanced and unbalanced AC grid voltages. More precisely, the optimization problem is posed in a way such that power oscillations at the DC terminals of the converter will not take place, independently from the AC grid voltage conditions. The generation of the circulating current reference signals will therefore result from solving such an optimization problem using the Lagrange multipliers method once again. Furthermore, it is shown that the power flow in the DC side of the MMC is most effectively decoupled from transients in the AC grid by establishing the primary power reference of the system at the DC terminals of the converter instead of at the point of common coupling.

5.1 Introduction

FOR VSC-based HVDC systems, and especially for future multi-terminal systems, it will be of high importance to avoid that power oscillations caused by unbalanced conditions in the AC grid shall propagate into the DC system. For conventional 2- or 3-level VSC converters, this is a challenge that can only be met by controlling the converter grid currents so that the instantaneous three-phase power flow on the AC side is constant, as discussed in [77, 78, 79, 80, 81, 82, 38]. The MMC topology, with its distributed capacitive energy storage, is however allowing for more degrees of freedom in the control of the converter during unbalanced AC grid conditions. Thus, the MMC can be controlled to act as a *power oscillation firewall* during unbalanced events, by pre-

venting power oscillations on the AC side from propagating into the DC system. In addition, the MMC distributed capacitance can be controlled to meet the aforementioned task by controlling its circulating current. This implies that the grid currents of the MMC may be controlled for other purposes; e.g.: they can be kept balanced during unbalanced conditions [C7].

In [33, 34, 35, 36, 83] and [C7], circulating current control schemes were proposed to address this issue. Nonetheless, they were based on Clarke or Park transformations, significantly increasing the complexity of regulating independently the arm energies of the MMC.

The control approach proposal detailed in the previous chapters of this Thesis is based on the natural *abc* stationary frame. The optimization problem that was formulated resulted in the circulating current reference signal generation formula. Such an optimization procedure did however, consider the phases of the MMC as *completely independent*. This implies that it did not include the possibility for optimizing the operation of a three-phase converter under unbalanced conditions in the AC grid.

To achieve an adequate control approach for controlling the MMC to prevent DC power oscillations during unbalanced grid conditions, the work detailed in the present chapter aims to generalize the circulating current reference formula, previously presented in chapter 3, by including in the optimization problem formulation a constraint that will ensure a constant power output at the DC terminals of the converter. This will be shown to result in a single analytical formula for calculating the references for the MMC circulating currents.

The resulting control approach includes its previous features as the capability of regulating the capacitive energy independently for each arm of the converter, yet it presents the additional benefit of ensuring constant power at the DC terminals. Furthermore, two modes of operation are analyzed: I) constant circulating current (i_{ck}) and II) constant capacitive energy sum ($w_{\Sigma k}$) per phase for reduced fluctuations in the MMC capacitor voltages.

A first attempt was presented in [C11] and [C9], nonetheless the power at the DC terminals was not precisely constant even though the oscillations were reduced significantly. This is since the constant DC power constraint in the optimization formulation was then conflicting with the additional constraint regarding the energy difference between the upper and lower valves, affecting negatively the desired performance. The work presented in this chapter is a more robust and a clear improvement, which resulted in publications [J3] and [C15].

It is also discussed how the primary power reference for the MMC can be provided. When the primary power reference is used for the AC side current reference calculation, the power reference for the circulating current control should be provided from a controller that will balance the total energy stored in the MMC, and vice-versa. When using the primary power reference for the control of the circulating currents, it is however shown that the power flow in the DC side is most effectively decoupled from any transients in the AC grid, while the dynamic response to AC grid disturbances is only reflected in the control of the total stored energy in the MMC.

A study that provided insight on the performance of grid current control schemes in the “*abc*” frame for the MMC, along with a circulating current control strategy for preventing second harmonic DC power oscillations was missing. Therefore, this work evaluates the performance of the circulating current control scheme presented here under grid current control schemes with the following objectives: 1) constant active power with sinusoidal grid currents, 2) balanced grid currents and 3) constant reactive power with sinusoidal grid currents. Thus it will be shown and analyzed how the various grid control strategies are influencing the energy and voltage oscillations of the MMC under unbalanced conditions.

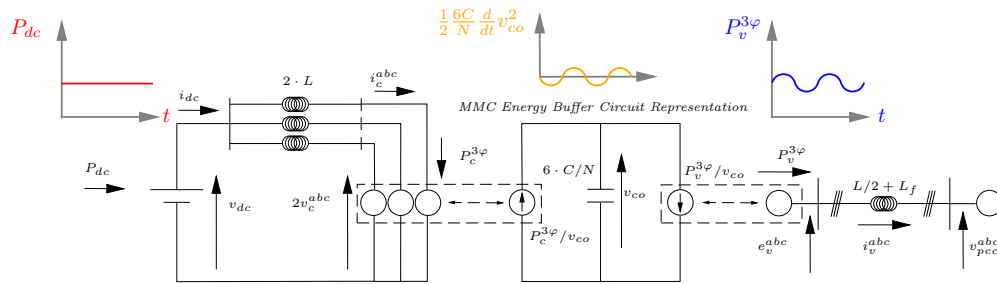


Figure 5.1: Reduced model of the MMC to emphasize its energy buffering capacity, view from a macroscopic perspective.

The outline of this chapter is as follows: The conceptual possibilities of the MMC under unbalanced conditions are investigated using a simplified macroscopic model of the converter in section 5.2. In section 5.3, the circulating current reference equation presented in chapter 3 (and in [30]) is generalized to cope with the unbalanced case. Subsequently, section 5.4 recalls the strategies applied for grid synchronization and for power control on the AC side of the MMC under unbalanced conditions, based on a generalized approach for current reference calculation with specifiable power control objectives. Section 5.5 discusses how the primary power reference for the MMC can be established, and the advantages of doing so with the circulating current at the DC terminals of the MMC. Section 5.6 shows the simulated results of using this equation to control the MMC. More precisely, in section 5.6.1, the performance of the circulating current reference equation presented in chapter 3 is evaluated via simulations. In section 5.6.2, the MMC is evaluated under the same conditions yet with the alternative formulation presented here, and section 5.6.3 illustrates the advantages of establishing the primary power reference at the DC terminals, instead of doing so at the point of common coupling. Finally, the chapter conclusions are drawn in section 5.7.

5.2 Investigating MMC conceptual possibilities under unbalanced operation using a simplified energetic macroscopic representation

A reduced model of the MMC is presented in Fig. 5.1 as an attempt to make clear its energy buffering features that are most useful for decoupling the AC from the DC side in terms of power oscillations. It is therefore necessary to start by introducing the simplifications that have been used to derive such a model.

Simplified model description

The circuit model is based on the following premises:

- The energy difference dynamics have been neglected, as it is assumed that from a macroscopic perspective, they do not participate in the AC/DC power balance equation.
- The MMC capacitive energy storage of all six arms has been represented by a single-equivalent aggregate capacitor equal to $6C/N$. This implies that only one state variable, defined as v_{co} , is representing the MMC total storage capacity.

This aggregate capacitive state variable of the reduced model of the MMC is defined as expressed in (5.1).

$$\frac{1}{2} \frac{C}{N} \sum_{k \in (abc)} \left[(u_{cuk}^{\Sigma})^2 + (u_{clk}^{\Sigma})^2 \right] = \frac{1}{2} \frac{C}{N} 6v_{co}^2 \quad (5.1)$$

Therefore, the equivalent circuit model of v_{co} is found by adding up the capacitive energy sum $w_{\Sigma k}$, defined in equation (2.39), for all three phases. This is expressed in (5.2).

$$\dot{w}_{\Sigma}(t) = \frac{1}{2} \frac{C}{N} 6 \frac{d}{dt} v_{co}^2 = -P_v^{3\varphi} + P_c^{3\varphi} \quad (5.2)$$

Where both 3-phase powers are defined as: $P_v^{3\varphi} = \sum_{k \in abc} e_{vk} i_{vk}$ and $P_c^{3\varphi} = 2 \sum_{k \in abc} v_{ck} i_{ck}$. Such a power balance equation is represented in the model of Fig. 5.1 by the *Energy Buffer Circuit*.

On conceptual possibilities of the MMC under unbalanced operation

One of the interest of the simplified model of the MMC represented in Fig. 5.1, is that it can easily be compared to its VSC predecessor. The 2 or 3-level VSC simplified circuit is formed only by two out of the three circuits depicted in Fig. 5.1; i.e., the circuit representing the AC grid interconnection (e_v, i_v), and the “energy buffer circuit” (v_{co}). Indeed, for the 2 or 3-level VSC, the capacitor voltage v_{co} is equal to v_{dc} . Therefore, if power fluctuations should appear in the AC side of the circuit at the point where e_v is represented, they will necessarily appear in v_{co} . As for 2 or 3-level VSC, the DC voltage v_{dc} is the same as v_{co} , such voltage and power fluctuations will propagate through the HVDC link. In such converters, this is usually avoided by controlling the grid currents in a way that no fluctuations will appear in the AC circuit. However, this will require the presence of unbalanced grid currents.

The MMC however, has an additional circuit represented on the left side of Fig. 5.1. This circuit represents the circulating current i_c of each phase, the dc current i_{dc} as well as the dc voltage v_{dc} . The first observation that can be made is that the voltage v_{co} is no longer the dc voltage v_{dc} as was the case for the 2- or 3-level VSC. Therefore, if power fluctuations were to appear at the AC grid side, the MMC distributed capacitance represented by the aggregate capacitor voltage v_{co} can be controlled as a true *energy buffer circuit* in order to absorb such oscillations, resulting in a oscillation-free power at the DC terminals of the MMC. Moreover, there is no longer the need of unbalanced grid currents as was the case for the classical VSC, implying that even during unbalanced operation the MMC can be controlled to have balanced grid currents as well as an oscillation-free power at its DC terminals.

Being the MMC model of Fig. 5.1 a simplified one, it is important to consider the arm energy independent regulation, as well as the possibility to shape the circulating current and energy sum when designing the control scheme for the full representation of the converter to cope with unbalances, as will be demonstrated in section 5.3.

On the possibility of controlling the MMC as a stiff DC current source

Using once again the simplified model of the MMC of Fig. Fig. 5.1 for the analysis, one can argue that by properly controlling the converter, the additional circulating current circuit as well as the “energy buffer” circuit of the MMC seem to be enough to completely decouple *any type* of undesired power fluctuations at the AC side from propagating into the DC side. In other words, there is no reason why such decoupling is only valid for steady state power oscillations at twice the grid frequency that take place under unbalanced grid operation. If the MMC is controlled properly, *any type* of power oscillations taking place at the AC-side, including most transients phenomena, power perturbations as well as the steady state oscillations during unbalanced operation, can be buffered and prevented from appearing at the DC terminals of the MMC. The MMC can be therefore controlled to act as a *stiff DC current source*, viewed from the rest of the DC grid system. It is expected that operating the MMC in such a way might be of interest for applications such as hybrid HVDCs, where the MMC is interfaced with a current source-type converter. The implementation of such a “stiff DC current source” behavior will be further discussed in section 5.5.

5.3 Circulating current reference adapted for unbalanced operation

In chapter 3, the minimized circulating current reference formula was calculated by means of mathematical optimization in phase (“abc”) coordinates, using the Lagrange multipliers method. The resulting equation yielded from formulating the optimization problem recalled in (5.3), subject to the two energy constraints (5.4) and (5.4).

$$\min \rightarrow \frac{1}{T} \int_{t_0}^{t_0+T} \left[\alpha (\dot{w}_{\Sigma k})^2 + (1 - \alpha) (v_{dc} i_{ck})^2 \right] dt \quad (5.3)$$

$$\frac{1}{T} \int_{t_0}^{t_0+T} w_{\Sigma k} dt = \overline{P_{\Sigma k}^{ref}} \quad (5.4)$$

$$\frac{1}{T} \int_{t_0}^{t_0+T} w_{\Delta k} dt = \overline{P_{\Delta k}^{ref}} \quad (5.5)$$

Solving the above optimization problem resulted in (5.6).

$$i_{ck} = \frac{\overline{P_{\Sigma k}^{ref}} + (1 - \alpha) \overline{P_{vk}}}{v_{dc}^2} v_{dc} + \frac{\alpha P_{vk}}{v_{dc}} + \frac{-\overline{P_{\Delta k}^{ref}}}{2v_{dc}^2 \left(e_{vk,p.u.}^{rms} \right)^2} e_{vk} \rightarrow \mathbf{I}_{ck}^{*Eq.5.6} \quad (5.6)$$

With $\overline{P_{\Sigma k}^{ref}}$ and $\overline{P_{\Delta k}^{ref}}$ defined by (5.7) and (5.8), respectively.

$$\overline{P_{\Sigma k}^{ref}} = \left[kp_{\Sigma} \left(W_{\Sigma k}^{ref} - \overline{w_{\Sigma k}} \right) + ki_{\Sigma} \int \left(W_{\Sigma k}^{ref} - \overline{w_{\Sigma k}} \right) dt \right] \quad (5.7)$$

$$\overline{P_{\Delta k}^{ref}} = \left[kp_{\Delta} \left(W_{\Delta k}^{ref} - \overline{w_{\Delta k}} \right) + ki_{\Delta} \int \left(W_{\Delta k}^{ref} - \overline{w_{\Delta k}} \right) dt \right] \quad (5.8)$$

Such a formula is recalled as it will be extended to cope with the unbalanced case.

As can be recalled from chapter 3, such a formula allows to control the capacitive energy independently by arm of the MMC; or in other words, offers the possibility to control the average values of the energy sum w_Σ and difference w_Δ independently by phase. In addition, by means of the weighting factor α , it allows for operating with minimized circulating current ($\alpha = 0$), minimized energy sum oscillations ($\alpha = 1$), or potentially interesting intermediate states.

Let $\mathbf{I}_{ck}^{*Eq.5.6}$ be the former circulating current reference equation expressed in 5.6. As was discussed earlier, the addition of the three circulating currents obtained by using such a reference is not being controlled to be constant as the optimization formulation considered each phase independently. Hence the DC power output will not be constant as well; i.e., $v_{dc} \sum_{k \in (abc)} \mathbf{I}_{ck}^{*Eq.5.6} \neq constant$. Therefore, the new circulating current control reference i_{ck} resulting from the Lagrange optimization problem needs the new following constraint:

$$v_{dc} \sum_{k \in (abc)} i_{ck} = P_{dc}^{ref} \quad (5.9)$$

Where P_{dc}^{ref} will be a constant power reference. How this constant power reference will be chosen is discussed in section 5.5.

Conflicting constraints

However, such a constraint is not compatible with the constraints used to determine $\mathbf{I}_{ck}^{*Eq.5.6}$, expressed in 5.4 and 5.5, since these ones are responsible for the DC component and the first harmonic component of the circulating current reference that are needed in order to achieve the desired energy regulation (of 5.7 and 5.8) and do not take into account the relation between phases. Moreover, the new constraint 5.9 is basically imposing a relation between phases, thus constraints 5.4 and 5.5 are conflicting with 5.9, and to overcome this issue one of them needs to be relaxed. Aiming for HVdc multi-terminal application, more weight was given to 5.9 since the suppression of the double frequency power oscillations at the DC terminals of the converter must be ensured. Furthermore, although the energy regulation provided by equations 5.4 and 5.5 is quite important to maintain the system stability, it can be relaxed in order to find the new circulating current control equation i_{ck} while avoiding the aforementioned obstacle. This is achieved by shifting such equations that were once constraints, to be now part of the new objective function.

Mathematical proof / derivation

The optimization problem is defined in the following way: The new circulating current i_{ck} will act *as much as possible* as $\mathbf{I}_{ck}^{*Eq.5.6}$; or what is the same, to instantaneously minimize the absolute value of the difference between i_{ck} and $\mathbf{I}_{ck}^{*Eq.5.6}$; subject to the constraint expressed in 5.9. In equations:

$$\mathcal{L}(i_{ck}, \lambda) = \left(i_{ck} - \mathbf{I}_{ck}^{*Eq.5.6} \right)^2 + \lambda \left(v_{dc} \sum_{k \in (abc)} i_{ck} - P_{dc}^{ref} \right) \quad (5.10)$$

A quick analysis is enough to conclude that the solution for this optimization problem is possible. Although one constraint appears, it does not define entirely the shape of the circulating current, yet it only ensures that the addition between phases (times v_{dc}) shall be constant. Therefore, there is a strong degree of freedom regarding the individual phase waveform, and it is here that the objective function will participate in its shaping.

Solving $\nabla_{(i_{ck}, \lambda)} \mathcal{L}(i_{ck}, \lambda) = 0$ yields both 5.11 and 5.12.

$$\frac{\partial \mathcal{L}}{\partial i_{ck}} = 2 \left(i_{ck} - \mathbf{I}_{ck}^{*Eq.5.6} \right) + \lambda v_{dc} = 0 \quad (5.11)$$

$$\frac{\partial \mathcal{L}}{\partial \lambda} = v_{dc} \sum_{k \in (abc)} i_{ck} - P_{dc}^{ref} = 0 \quad (5.12)$$

Multiplying 5.11 by $\frac{v_{dc}}{2}$, adding all three phases and combining the resulting equation with 5.12 yields:

$$\lambda = \frac{v_{dc} \sum_{k \in (abc)} \mathbf{I}_{ck}^{*Eq.5.6} - P_{dc}^{ref}}{\frac{3}{2} v_{dc}^2} \quad (5.13)$$

Replacing 5.13 in 5.11 yields the new circulating current reference formula, expressed in 5.14.

$$i_{ck} = \mathbf{I}_{ck}^{*Eq.5.6} + \frac{1}{3} \frac{P_{dc}^{ref}}{v_{dc}} - \frac{1}{3} \sum_{k \in (abc)} \mathbf{I}_{ck}^{*Eq.5.6} \quad (5.14)$$

Or in the more extended version, replacing $\mathbf{I}_{ck}^{*Eq.5.6}$ by 5.6:

$$\begin{aligned} i_{ck} = & \frac{\bar{P}_{\Sigma k}^{ref} + (1 - \alpha) \bar{P}_{vk}}{v_{dc}^2} v_{dc} + \frac{\alpha P_{vk}}{v_{dc}} + \frac{-\bar{P}_{\Delta k}^{ref} e_{vk}}{2v_{dc}^2 \left(e_{vk,p.u.}^{rms} \right)^2} \\ & - \sum_{k \in (abc)} \left(\frac{\bar{P}_{\Sigma k}^{ref} + (1 - \alpha) \bar{P}_{vk}}{v_{dc}^2} v_{dc} + \frac{\alpha P_{vk}}{v_{dc}} + \frac{-\bar{P}_{\Delta k}^{ref} e_{vk}}{2v_{dc}^2 \left(e_{vk,p.u.}^{rms} \right)^2} \right) + \frac{1}{3} \frac{P_{dc}^{ref}}{v_{dc}} \end{aligned} \quad (5.15)$$

It can be seen that the sum of the three phases of the circulating current regulation equation will always yield in $\frac{P_{dc}^{ref}}{v_{dc}}$, regardless of the phase independent energy regulation action that i_{ck} is performing. Moreover, by adequately choosing P_{dc}^{ref} , the output DC power of the converter may be controlled constant.

5.4 Grid current control strategies

As mentioned in the introduction, the performance of the MMC with the described circulating current reference calculation is evaluated under operation with different power control strategies

for controlling the AC-side grid currents. For simplicity, the investigation is limited to the case of active power control, and the corresponding three-phase current references are calculated according to the generalized equation given by [77]: equation (5.16) [78].

$$i_{vk} = \frac{P_{ac}^{ref}}{\|\mathbf{v}_{pcc}^+\|^2 + kp \cdot \|\mathbf{v}_{pcc}^-\|^2} \cdot \left(v_{pcc}^+ + kp \cdot v_{pcc}^- \right) \quad (5.16)$$

Where P_{ac}^{ref} is the power reference, and v_{pcc}^+ and v_{pcc}^- are the positive and negative sequence of the voltage of the point of common coupling of phase k . Three different cases are investigated, corresponding to the following objectives for controlling the power flow characteristics at the point of synchronization to the AC grid:

- Elimination of double frequency oscillations in the AC power flow while maintaining sinusoidal currents [77]: Current reference calculation by equation (5.16) with $kp = -1$
- Balanced sinusoidal AC currents [77]: Current reference calculation by equation (5.16) with $kp = 0$
- Elimination of double frequency reactive power oscillations at the point of synchronization to the grid [77]: Current reference calculation by equation (5.16) with $kp = +1$

The AC-side phase currents are controlled to follow the current references by using resonant controllers implemented in the stationary $\alpha\beta$ reference frame according to [84], providing the voltage references e_{vk}^{ref} as indicated in Fig. 5.2. The synchronization to the AC voltage at the Point of Common Coupling (PCC) and the detection of positive and negative sequence components grid voltage is based on Second Order Generalized Integrators configured as Quadrature Signal Generators according to [85].

5.5 Power references assignment

With the new circulating current control reference of 5.15, it is possible to access the DC power reference P_{dc}^{ref} . Furthermore, the 3-phase grid currents will impose the desired AC power reference P_{ac}^{ref} . With this new degree of freedom, two ways of controlling the MMC can be established.

Establishing the primary power reference of the system at the AC grid point of common coupling P_{ac}^{ref} via the grid currents

The first approach is the one closer to a classical VSC converter with only one degree of freedom; i.e., the desired power transfer; or in other words, the primary reference will be established by P_{ac}^{ref} by means of the grid currents, whereas the additional DC power reference P_{dc}^{ref} is used to regulate the average value of the capacitive energy of the MMC, by means of 5.17.

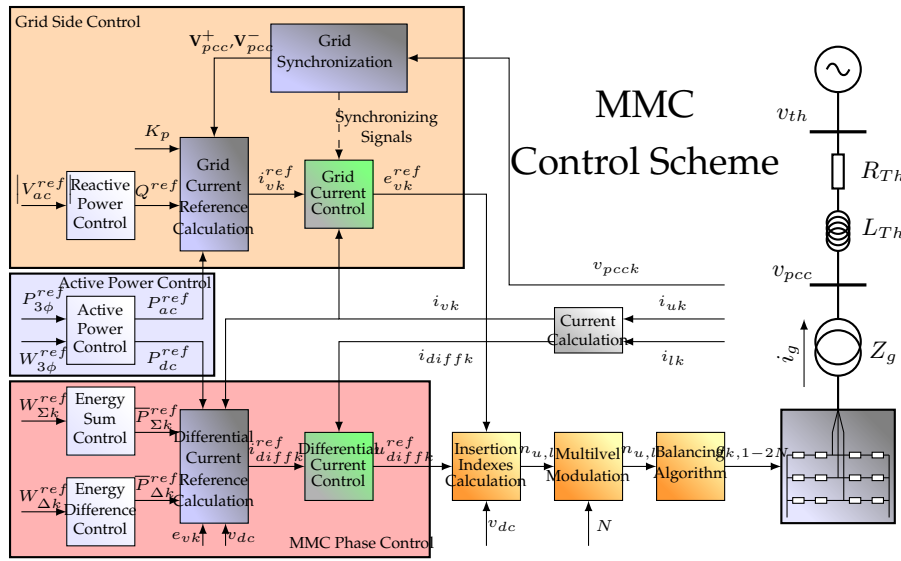


Figure 5.2: Schematic diagram of the proposed control

Establishing the primary power reference of the system at the DC terminals P_{dc}^{ref} via the sum of circulating currents

The second approach is to do the exact opposite of the previous case: the primary power reference will be established by means of the DC power reference P_{dc}^{ref} with the circulating currents; while the AC power reference P_{ac}^{ref} will behave as in 5.17. This case is of significant interest, since by doing so, the MMC will not only decouple the AC power fluctuations from the DC power fluctuations in steady state (as the previous case), yet it will additionally cope with the fluctuations in transient state as well, behaving as a *stiff DC current source*. This will be illustrated and further analyzed in section 5.6.3.

$$P_{(.)}^{ref} = \left(W_{3\phi}^{ref} - \overline{w_c^{3\phi}}(t) \right) \left[kp + \frac{ki}{s} \right] \quad (5.17)$$

In any case, (5.17) consists of a PI controller that will regulate the average value of the total energy stored in the capacitors of all phases of the converter ($\overline{w_c^{3\phi}}(t)$) to the desired value $W_{3\phi}^{ref}$.

The resulting control scheme is depicted in Fig. 5.2. As can be seen, the control of the active power $P_{3\phi}$ of the system is no longer necessarily a task of the grid currents, illustrated by the presence of the additional active power control block.

5.6 Results

In this section, the simulation results in steady state of the MMC of Table 5.1, are presented under an unbalanced condition. The simulation model used is based on the average version of the aggregate capacitor controlled voltage sources-based model, detailed in section 2.5.3. This is because the emphasis of this research was more on the proposed high-level control performance of the arm energies regulation and resulting currents, than the individual capacitors behavior within an arm. Therefore, the validity of the results presented in the following lines hold as long

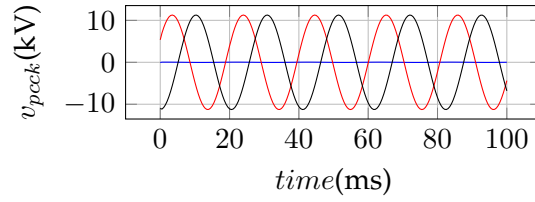


Figure 5.3: Thévenin's grid equivalent voltage

Table 5.1: MMC parameters

Parameter	Value
Number of SMs per arm	100
SM Nominal Voltage	5kV
SM Capacitance	5mF
Arm Inductance	3mH
Arm Resistance	0.1 Ω

as the performance of the balancing algorithm stays within acceptable operating limits.

The extreme case of when the phase "a" voltage of the Thevenin's equivalent representation of the grid is turned to zero, whereas phases "b" and "c" are kept with 25kV of amplitude (depicted in Fig. 5.3), is investigated. The complete control scheme used is depicted in Fig. 5.2. In addition, all the required input signals for the circulating current reference generation formula have been estimated using adaptive filters based on SOGI-QSG, as explained in chapter 4.

5.6.1 Former control equation for independent control per phase

Simulation results in steady state

The new control approach presented in this paper in (5.14) stems from the need of a more general equation, capable of ensuring constant power during unbalances. This section intends to briefly illustrate via simulations the limits of former equation (5.6), when unbalance grid voltage operation occurs. In Fig. 5.4 and 5.5 are depicted the MMC variables of the three-phase MMC topology facing an unbalance grid condition in the Point of Common Coupling. The former circulating current reference equation of (5.6) is used, the primary power reference of the system is established by P_{ac}^{ref} , and the grid current reference is calculated with (5.16) with $kp = 0$, to ensure balanced grid currents during the unbalanced operation.

Analysis

In Fig. 5.4 are shown the three phase grid currents, the instantaneous three-phase active power during the unbalance, the capacitive energy stored in each phase of the converter $w_{\Sigma k}$ and the instantaneous power at the DC terminals of the MMC. Moreover, Fig. 5.5 shows the sum of the capacitor voltages for each arm u_{ck}^{Σ} , the circulating currents i_{ck} , the energy difference between arms per phase $w_{\Delta k}$ and the instantaneous reactive power. Equation (5.6) is being used to control the converter with the two frontier values of α in order to evaluate the performance under both modes of operation: Constant circulating Current i_{ck} ($\alpha = 0$) and constant capacitive energy by

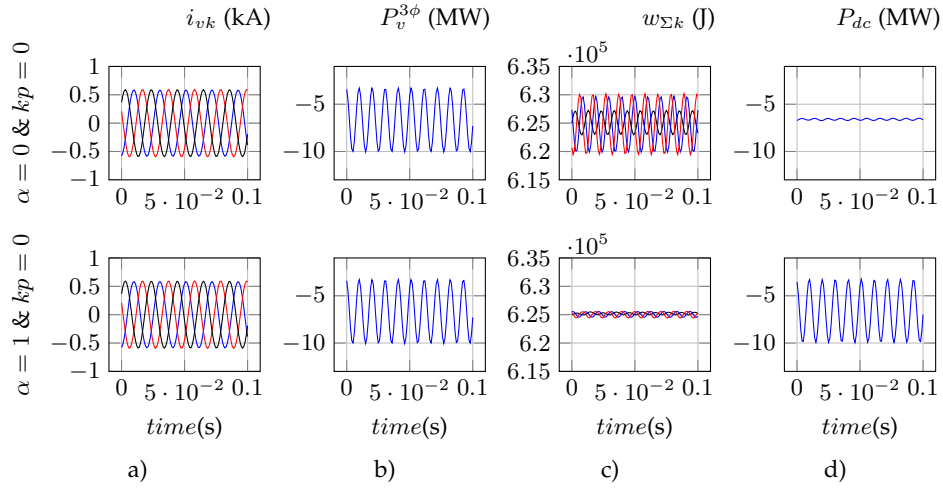


Figure 5.4: MMC variables during under unbalanced grid operation using the former circulating current reference formula. a) Grid currents, b) grid active power, c) MMC capacitive phase energy, d) power at the MMC DC terminals

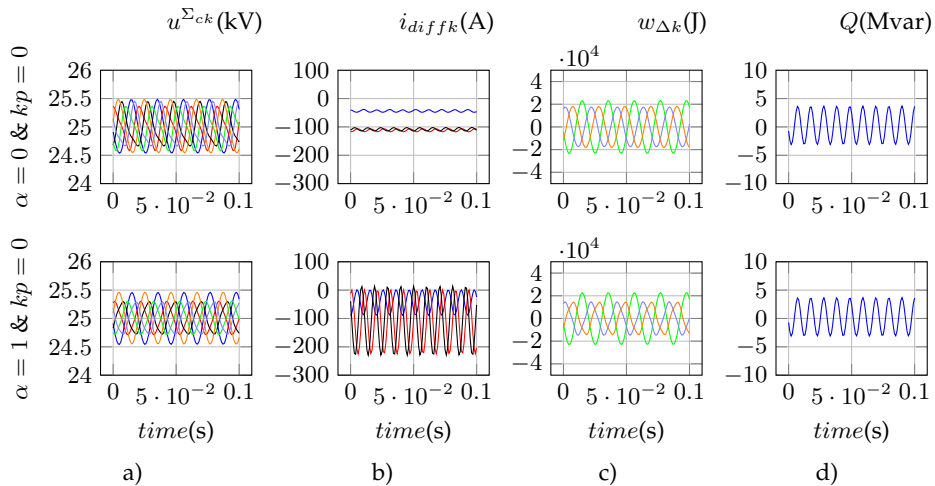


Figure 5.5: MMC variables during under unbalanced grid operation using the former circulating current reference formula. a) MMC capacitor voltages, b) circulating currents, c) energy difference between arms d) reactive power.

phase $w_{\Sigma k}$ ($\alpha = 1$).

Since there is an unbalanced grid operation, and the grid currents are being controlled to be balanced (and not to produce constant active power), the instantaneous active power at the grid side is highly fluctuating. When $\alpha = 1$; i.e., when operating with constant capacitive energy in the MMC, it can be seen how the power fluctuations that are at the grid side, can be found in the DC side as well. For this case it is clear that equation (5.6) is not enough to guarantee constant DC power when $\alpha = 1$. Nonetheless, when $\alpha = 0$, the circulating current is being minimized, therefore, they will become as constant as possible. The addition between them ($\sum_{k \in (abc)} i_{ck}$) will produce the DC current, that in turn will be responsible of the resulting DC power with its corresponding power fluctuations. Therefore, since there is a direct relationship between the circulating current fluctuations and the DC power fluctuations, the DC power oscillations are significantly smaller than the ones of the case of when $\alpha = 1$. However, even though the power fluctuations are small, they are still present. Another inconvenience of applying equation (5.6) under unbalanced grid conditions is that there is no way to establish a DC Power reference by means of the circulating current. Being able of controlling the DC Power reference and the AC (or grid-side) power reference at the same time offers interesting advantages as discussed in section 5.5.

5.6.2 Performance of the novel circulating current reference formulation adapted for unbalanced operation under different grid current control strategies

In this section, the new circulating current control equation is being evaluated under different grid current control strategies, which are: instantaneously constant active grid power, balanced grid currents and instantaneously constant reactive grid power. The aim of this section is two-fold: Firstly to validate (5.14) as an interesting control option for the MMC under unbalanced conditions and to give some insight on the performance of the MMC while combining such an equation with the different grid current control strategies already mentioned. In Fig. 5.6, a matrix of individual figures is shown representing the MMC grid currents, the active power at the grid, the energy stored in the capacitors in each phase, and the power at the DC terminals; for different values of $kp \in [-1, 0, +1]$ and $\alpha \in [0, 1]$. In Fig. 5.7, such a matrix is continued with the MMC capacitor voltages, circulating currents, energy difference between arms and the reactive power.

Several interesting remarks can be made by studying these figures:

Comparison between the former and novel circulating current reference equations

The first remark is that the instantaneous power at the DC terminals of the MMC controlled by (5.14) and depicted in Fig. 5.6 has a better performance in terms of the quality of the output waveform, than the one depicted in 5.4 independently of the value of α . This is since the constant DC power requirement was formulated as the only constraint in the optimization problem, and all other requirements regarding energy regulation and constant circulating current or phase capacitive energy were “relaxed” by making them part of the objective function. Similar conclusion can be drawn if we compare the performance of the newly obtained equation with the ones presented in [86], since what was presented in that occasion had more than one constraint, affecting the fluctuations of the DC power of the MMC. Another difference, is that with this new equation, when operating with $\alpha = 1$, the capacitive energy in each phase $w_{\Sigma k}$ presents

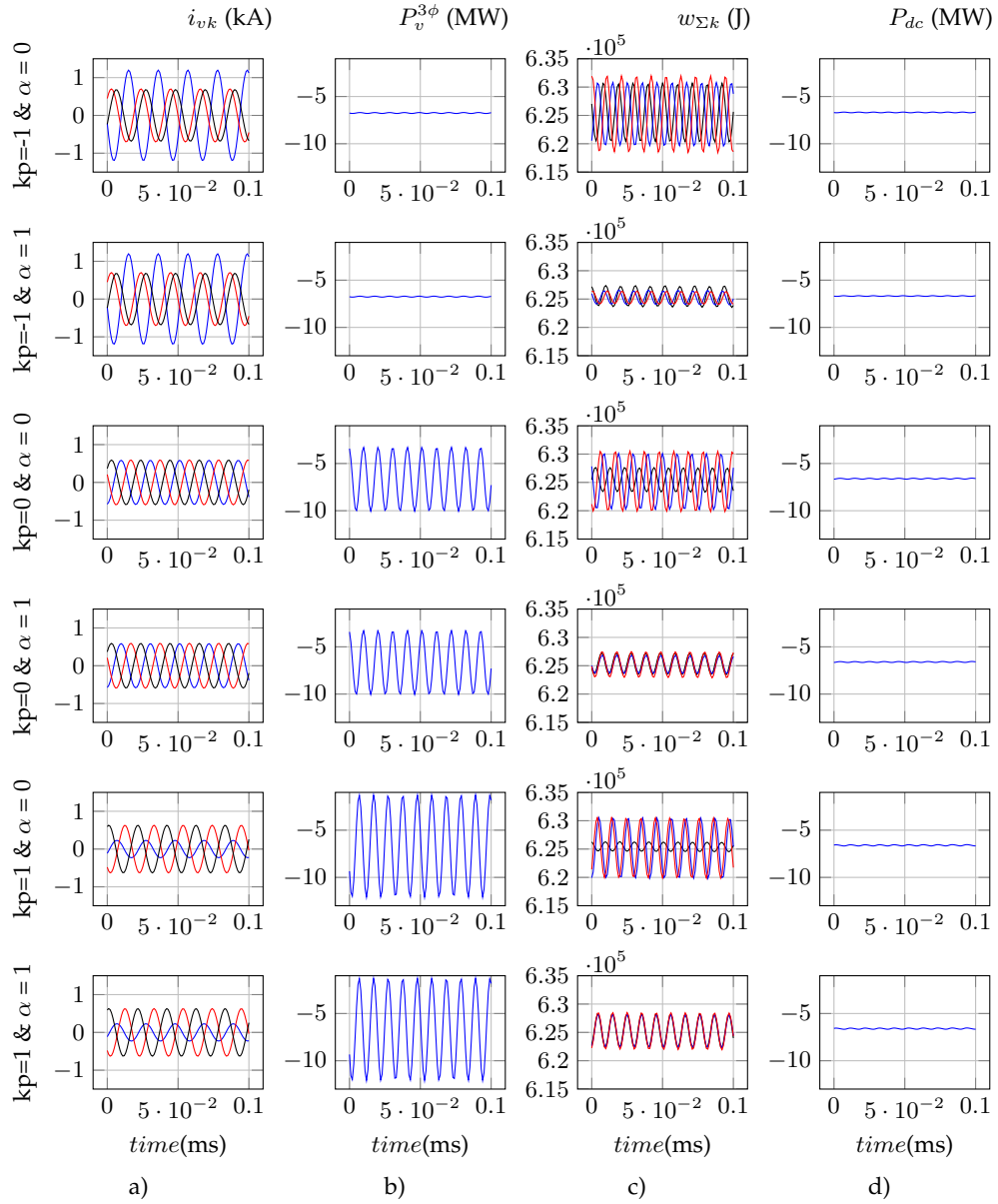


Figure 5.6: MMC variables during unbalanced grid operation. Part I: a) Grid Currents, b) Grid Active Power, c) MMC capacitive phase energy, d) power at the MMC DC terminals

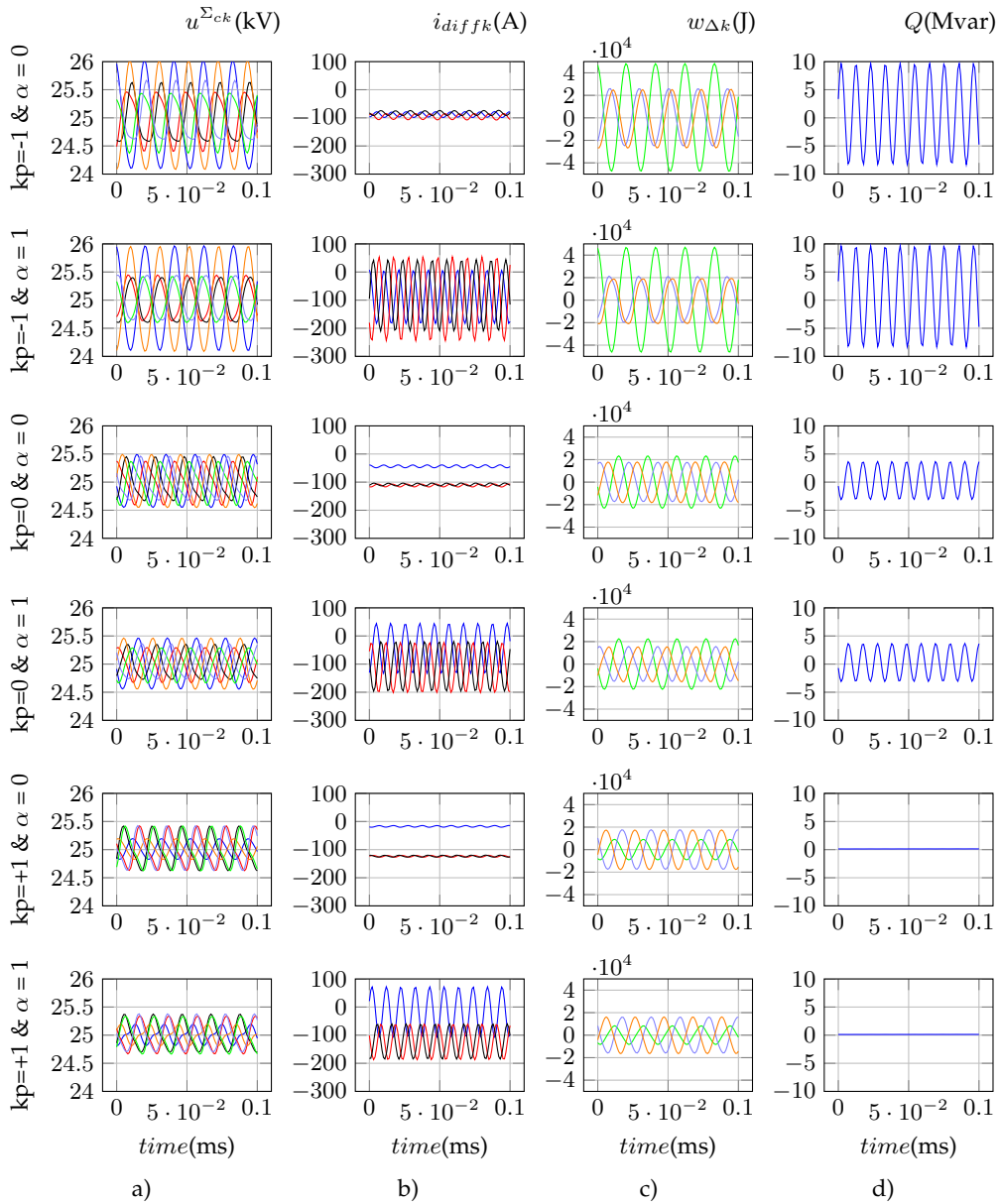


Figure 5.7: MMC variables during unbalanced grid operation. Part II: a) MMC capacitor voltages, b) circulating currents, c) energy difference between arms d) reactive power

more important oscillations than the one depicted in Fig. 5.4 since it needs to block the power fluctuations of the grid, yet it is as constant as possible.

Constant instantaneous grid active power with sinusoidal currents

When $kp = -1$ the AC power is constant at the PCC, and the DC power is constant as well. However, the stored capacitive energy inside the MMC has a zero-sequence oscillation component. This might seem strange at first since both AC and DC powers are constant, thus one might think that there should be no need for the MMC to compensate anything with such oscillations. To explain this phenomena, one must refer to the respective grid currents and notice that they have a strong negative sequence (in order to ensure constant AC Power). Note that, the sum of the squared values of balanced grid current is a constant ($\sum_{k \in abc} i_{vk}^2 = Constant$), yet when the currents are unbalanced, the sum of their squared values will fluctuate. Indeed, since these currents will flow through the inductors, the 3-phase instantaneous power of the inductances will have a zero-sequence oscillation. This is why the capacitive energy storage of the MMC has a zero-sequence (counter-phased) oscillation, in order to compensate the inductive energy fluctuation caused by $kp = -1$, whilst having constant AC and DC powers. This fact is certainly an advantage of the MMC with respect to the classic VSC, since the later needs accurate control of the power at the converter terminals to prevent power oscillations from entering into the DC system [82]. The corresponding power oscillations can be expressed in equations, by calculating the grid current contribution to the active power that will enter the MMC energy sum as the addition between active power at the Point of Common Coupling (P_{PCC}) and the active power in the inductors generated only by the grid current.

$$\begin{aligned} p_s &= p_{pcc} + r' |\mathbf{i}_v|^2 + \mathbf{i}_v L' \frac{d}{dt} \mathbf{i}_v \\ &= p_{pcc} + r' |\mathbf{i}_v^+|^2 + r' |\mathbf{i}_v^-|^2 + 2r' \mathbf{i}_v^+ \mathbf{i}_v^- + \omega L' 2\mathbf{i}_v^+ \mathbf{i}_{v\perp}^- \end{aligned} \quad (5.18)$$

Where “ \perp ” indicates a vector operation giving a -90 phase shift to the vector. Assuming that the resistance is negligible, this simplifies to [79]:

$$p_s \approx p_{pcc} + 2X'_L 2\mathbf{i}_v^+ \mathbf{i}_{v\perp}^- \quad (5.19)$$

Hence, the negative sequence current \mathbf{i}_v^- contributes to the oscillation in the three-phase active power that enters the MMC capacitive stored energy w_Σ .

Balanced sinusoidal currents

When $kp = 0$ (refer to the third and fourth rows of Fig. 5.6 and 5.7) the grid currents are being controlled to be balanced by means of (5.16) even under the presence of unbalanced AC grid voltage. The product between balanced grid currents and unbalanced AC grid voltages will give rise to a fluctuating power at the PCC. However, using the circulating current control proposed, the MMC will trap the power oscillations inside its distributed capacitors. In addition, and contrary to the previous case, there is no need to compensate any additional power oscillations in the inductances since the grid currents are balanced.

Constant instantaneous grid reactive power with sinusoidal currents

If constant reactive power is required during unbalanced conditions (i.e.: $kp = +1$, refer to the fifth and sixth rows of Fig. 5.6 & 5.7), it will be the case in which the MMC capacitive storing capability is required the most. In other words, the capacitive energy in the MMC $\sum_{k \in abc} w_{\Sigma k}$ fluctuates more than for the other cases ($kp = 0$ & $kp = -1$). This is easier to notice when $\alpha = 1$, than when $\alpha = 0$ since for the former case, the stored capacitive energies of each phase $w_{\Sigma k}$ are in phase with one another, and one can clearly see how the oscillations of the zero sequence of the energy sum reaches its highest value when $kp = +1$, its lowest when $kp = -1$, and an intermediate value when $kp = 0$ (When $\alpha = 0$, the same pattern may be found, by adding the three energy sums $w_{\Sigma k}$ of each phase). This is since the MMC is compensating for both “sources” of energy fluctuations: 1) Inductive energy fluctuations due to the unbalanced grid currents, and 2) the fluctuating AC power, which is significantly higher than for the other cases.

On reducing the sizing of the capacitors

The reactive power oscillation seems to affect significantly the energy difference between arms, and hence, the MMC capacitor voltages (u_{ck}^{Σ}) fluctuations as well. Note that when $kp = +1$, the energy difference oscillations and the MMC capacitor voltages are much lower than for the other values of kp , especially compared to the case of $kp = -1$ which presents the highest reactive power oscillations, and thus the highest oscillations of the energy difference and MMC voltage variables. Thus, ensuring constant instantaneous reactive power ($kp = +1$) during unbalances will tend to reduce the stress produced by the voltage oscillations in the capacitors, and therefore reduce their sizing.

Relationship between the circulating current and kp

Another interesting observation can be made by studying the mean value of the circulating currents for each case. For $kp = -1$, there is no significant difference between the mean value of i_{ca} , i_{cb} and i_{cc} . This is because constant 3-phase power is achieved by increasing the current in the phase with reduced voltage. Thus the AC side power control is ensuring equal average power in the three phases, which corresponds to equal DC - component of the circulating current. Nevertheless, when $kp = 0$, the mean value of i_{ca} is decreased compared to the other two phases, because this case does not ensure constant power per phase, but a power proportional to the voltage in the PCC. The difference observed between the phases is still more significant when $kp = +1$.

Advantages of the working directly in “abc” coordinates

For each case presented the mean values of the capacitive energy sum and difference stored in the arms of the MMC (i.e.: $\bar{w}_{\Sigma k}$ & $\bar{w}_{\Delta k}$) are kept at the desired value, a fact that is directly attributed to the control scheme (eq. (5.14)). Indeed, this would mean that the MMC capacitor voltages will have the desired average voltage value regardless of the unbalance and the grid current control method used to cope with it. Additionally, this average value may be controlled independently for each phase, thanks to the implementation in the “abc” reference frame [30, 87, 86].

The circulating current control reference of (5.14) will ensure that the sum of the circulating

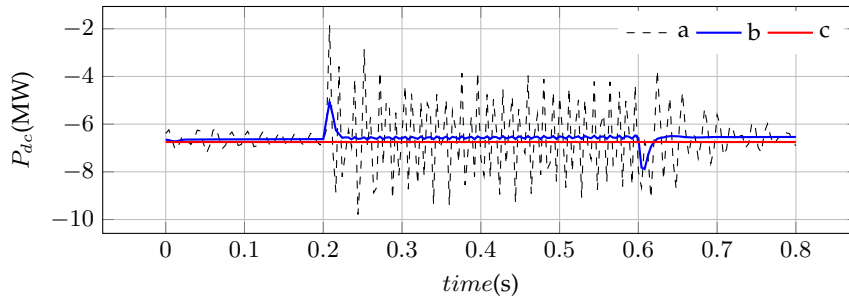


Figure 5.8: Power at the DC terminals of the MMC facing an unbalanced grid operation between $t = 200ms$ and $t = 600ms$, under the following control schemes: a) CCSC, b) control proposal with main power reference assignment by P_{ac}^{ref} c) control proposal with main power reference assignment by P_{dc}^{ref}

currents, and by that i_{dc} , will be constant, regardless of the value of α . Thus constant DC Power is ensured for every case. If the system is operated with $\alpha = 1$, the energy storing capacity of the MMC ($\sum_{k \in (abc)} w_{\Sigma k}$) will be in its most efficient scenario: Only zero-sequence will be present. This is not the case for $\alpha = 0$ since even though the same zero sequence appears (in order to compensate the same oscillations as before), one may observe the presence of positive and negative sequences as well.

General Observations

The presented results show that the MMC can always be controlled to prevent power oscillations from the AC side from entering the DC grid, thus the MMC can be controlled to act as a “power oscillation firewall,” as long as the capacitance is designed to handle the fluctuations. Controlling the power oscillations on the AC side can limit the energy sum ($w_{\Sigma k}$) oscillations. However u_{ck}^{Σ} is also related to the energy difference ($w_{\Delta k}$) which is highly dependent on the fluctuation of the reactive power at the AC side. Thus, constant instantaneous reactive power control can minimize the MMC SM capacitor voltage oscillations, during unbalanced operation.

5.6.3 Influence of the power reference assignment in transient state under unbalances

This section intends to show the difference between establishing the primary power reference of the system at the AC grid point of common coupling P_{ac}^{ref} via the grid currents, or at the DC terminals of the converter P_{dc}^{ref} via the sum of the circulating currents in section 5.5. The main advantage of establishing the primary power reference using P_{dc}^{ref} instead of P_{ac}^{ref} is made clear in Fig. 5.8. In this figure, it is possible to notice three instantaneous powers at the DC terminals of the MMC under an unbalanced grid conditions that takes place between $t = 0.2$ and $t = 0.6$. Each curve results from controlling the MMC in three different ways: a) Firstly, the Circulating Current Suppression Controller (CCSC) of [17] is used, only as a reference. This case has absolutely no control upon the zero sequence component of the circulating current (unlike [32]), and hence it is not capable of ensuring constant power. b) Moreover, the second curve shows the instantaneous power at the DC terminals of the converter resulting from applying the proposed control approach, and using P_{ac}^{ref} of (5.16) to establish the primary power reference. It can be seen how significantly the oscillations are reduced with respect to the reference case, yet during the unbalance, it is possible to notice a small fluctuating component that still exists and

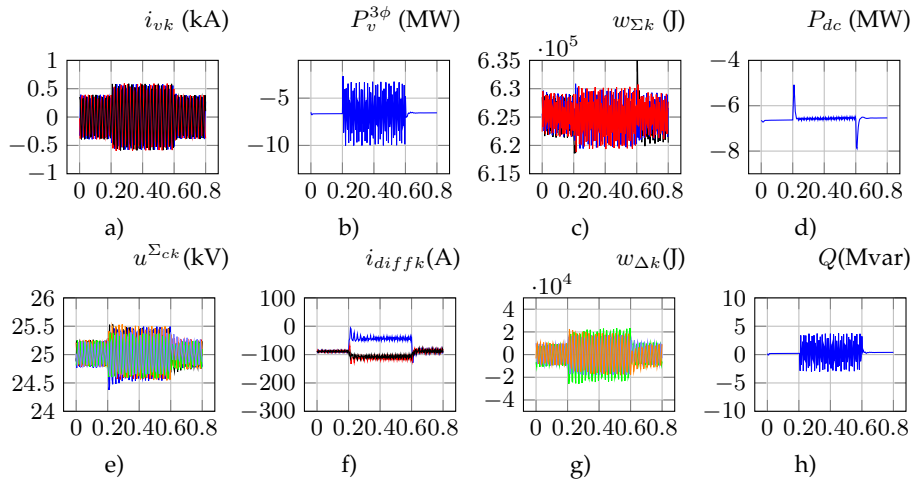


Figure 5.9: Establishing the main power reference at the AC grid PCC via P_{ac}^{ref} - MMC variables during an unbalanced grid operation between $t = 200ms$ and $t = 600ms$. a) grid currents, b) grid active power, c) MMC capacitive phase energy, d) power at the MMC DC terminals; e) MMC capacitor voltages, f) circulating currents, g) energy difference between arms h) reactive power.

that is introduced by P_{dc}^{ref} of (5.14) as a consequence of the PI parameters of (5.17) and/or the filtering technique that is being applied to extract the average value of the three phase energy $\overline{w_c^{3\phi}}(t)$. Furthermore, the transient can be clearly noticed in the same curve, both at $t = 0.2s$ and at $t = 0.6s$. These peaks are generated by equation (5.17), and since such an equation is the DC power reference P_{dc}^{ref} , it will appear in the instantaneous power at the DC terminals of the MMC. c) Finally, the third curve shows a perfect constant with no transitory peaks, and no small oscillations during the unbalanced operation, since for this case the proposed control approach is used yet the primary power reference is being established by the term P_{dc}^{ref} of equation (5.14). By doing so, all the inconveniences caused by the PI controller of (5.17) are shifted from P_{dc}^{ref} to the grid side of the converter, by means of P_{ac}^{ref} , leaving the DC side of the MMC absolutely decoupled from any kind of disturbances within its rated operating conditions.

In Fig. 5.9 and Fig. 5.10 the same case is shown for all MMC variables.

As was expected, the transitory peaks that were found in the power at the DC terminals of the MMC in Fig. 5.9-d) when establishing the primary power reference via P_{ac}^{ref} by means of the grid currents, are shifted into the distributed capacitive energy storage of the MMC, as shown in Fig. 5.10-c). It can also be seen in Fig. 5.10-a) and b), that such transients are also reflected in the AC side of the converter. In any case, the power at the DC terminals of the MMC presents a pure constant behavior.

5.7 Conclusion

An alternative control scheme for regulating the circulating currents of MMC based on Lagrange optimization in phase (“abc”) coordinates has been proposed in the present chapter of this Thesis manuscript. Such a procedure yields analytical expressions for the calculation of circulating current references for each phase of the MMC that will ensure constant, non-oscillatory, power flow at the DC side of the converter even under unbalanced conditions in the AC grid. The condition of non-oscillatory power flow at the DC-side of the converter can be achieved with

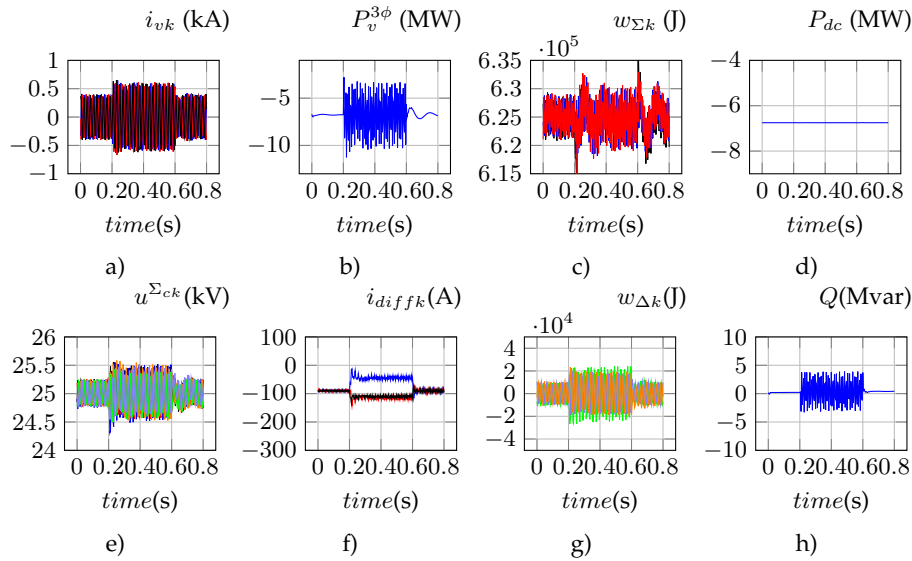


Figure 5.10: Establishing the main power reference at the DC terminals via P_{dc}^{ref} - MMC variables during an unbalanced grid operation between $t = 200ms$ and $t = 600ms$. a) grid currents, b) grid active power, c) MMC capacitive phase energy, d) power at the MMC DC terminals; e) MMC capacitor voltages, f) circulating currents, g) energy difference between arms h) reactive power. e) MMC capacitor voltages, f) circulating currents, g) energy difference between arms and h) reactive power.

either constant capacitive energy sum or with constant (pure DC) circulating current per phase. In both of these cases, the proposed circulating current control strategy for the MMC is capable of preventing steady state power oscillations at the AC side during unbalanced conditions from propagating into the DC side.

Moreover, it was shown that by establishing the primary power reference at the DC terminals of the MMC via P_{dc}^{ref} by means of the sum of the circulating current (i_{dc}), instead of establishing the primary power reference at AC grid point of common coupling via P_{ac} by means of the grid currents, both steady state and transient state power fluctuations or perturbations from the grid will not have any influence on the power at the DC terminals of the MMC as long as the operation of the converter is kept within its rated conditions. Thus, the MMC can be controlled to act as a stiff DC current source, which might be of special interest for interfacing the MMC with a current source converter, in hybrid HVDC applications. In both cases, it has been shown the “power oscillation firewall” or “energy buffer” potential of the distributed capacitance of the MMC topology to effectively decouple the power flow in the AC and DC sides, in terms of undesired energy fluctuations. Such an operation of the MMC can be especially relevant for (multi-terminal) HVDC systems where power fluctuations and thus DC voltage fluctuations are to be avoided, since they will negatively influence other converters connected to the same DC-network.

Furthermore, three different grid current control strategies for voltage source converters facing unbalanced AC grid voltage operation have been evaluated in conjunction with the proposed strategy. This analysis intends to give some insight into the operation of the MMC converter under unbalanced conditions when controlled to follow the circulating current references calculated using Lagrange multipliers for constant DC power. It was shown that, regardless of the grid current control strategy used, the circulating current can be controlled to use the MMC energy storing capacity to decouple the power oscillations of the AC side from the DC side. Nonetheless, the performance under each control strategy is quite different as it was demonstrated

in this contribution, and should be taken into account in the control selection process of each particular application. More precisely, it was seen how controlling the MMC with constant instantaneous reactive power during the unbalanced reduced the oscillations in the voltage of the MMC capacitors, which will have an important consequence in their sizing.

6

Stability of the MMC: Passivity-based Stabilization

In this chapter, a non-linear control technique based on the passivity theory is applied to the MMC. The purpose is twofold: to ensure global asymptotic stability for the MMC in closed-loop control, and to explore the conceptual possibilities of the local passivity controllers in large interconnected systems. The controller selected for the task is the global tracking passivity-based controller, that consists in a simple linear PI that regulates to zero an output signal that has been constructed respect to which the model under study becomes passive, ensuring global asymptotic stability of the system. The controller ensures the global tracking of the trajectories that have been estimated by means of the circulating current reference calculated by means of Lagrange multipliers in previous chapters of this manuscript along with an energy model of a virtual MMC.

6.1 Introduction

FORMER chapters 3, 4 and 5 have dealt with the reference signal generation and linear control issues of the MMC in its “abc”-coordinates instead of the commonly used “d_{qo}” or “ $\alpha\beta o$.” This interest arises in order to be able to regulate in a simple, direct and explicit way the energy stored in each phase and arm of the MMC. The control strategy proposed in the aforementioned chapters has proven to be robust thanks to its closed-loop nature and its independence to the system parameters, as well as it has presented a good dynamic performance. Yet, such a strategy is based on linear controllers, and since the system is highly non-linear, global asymptotic stability cannot be ensured.

In appendix B, the global asymptotic stability issue is investigated by means of Lyapunov’s stability criteria. In such an appendix the work from [31, 88] is reviewed and extended. Indeed, it was possible to demonstrate asymptotic stability of the MMC under open loop control, yet two

issues seem to appear:

- The first issue is the one related to robustness: As open loop controllers by definition do not present any closed feedback loops, they will be highly influenced by the accuracy of the estimation of the equilibrium point, parameter sensitivity and/or uncertainty and undesired perturbations. In addition, the time response of the system is fixed and cannot be modified.
- The validity of Lyapunov's global asymptotic stability proof for open loop controllers only holds for the system under study. This means that even if global asymptotic stability was independently proven for two different open-loop controlled MMC converters, the stability of the interconnection between these two systems is not ensured, and to prove it using Lyapunov's stability criteria one must consider the new and more complex system as a whole.

Clearly, since we are aiming at a multi-terminal HVDC systems which is supposed to grow "organically" in Europe, the final state of the *SuperGrid* is unknown since it will be continuously changing. Furthermore, the objective of this *SuperGrid* is to interconnect renewable energy all across the continent in order to take advantage of the geographical smoothing effect on these energy sources of intermittent nature. This means the multi-terminal HVDC system will be connected to different renewable energy subsystems, depending on the terminal.

With the complete picture in mind, it seems of a great degree of complexity to ensure global asymptotic stability of the ever growing multi-source *SuperGrid* using a global approach like the one used in appendix B. Therefore a modular approach for ensuring stability of the global interconnected system is needed. Last but not least, the required technique must be simple to implement regardless of the complexity of the proof.

From non-linear control theory, the *passivity* theory may ensure global asymptotic stability of a system [89]. Moreover, such a property based on Lyapunov's stability criteria is more powerful than Lyapunov's criteria itself. Passivity includes the stronger property of: *the interconnection of passive systems is passive*, and thus stable. Indeed, the modular approach required to ensure stability of the future multi-terminal HVDC systems might well be based on passivity.

Moreover, it is possible to use a PI controller to render the system globally asymptotically stable via passivity, simplifying the implementation as was done in [90, 91, 92, 93]. These controllers are known to be simple, robust and widely accepted by practitioners.

However, the work carried out in [90, 91, 92, 93] requires that the desired state variables in steady state that become the references values (x_*) of the system should be constant values, in order to solve this *regulation* problem. As mentioned earlier, the aim is to control the MMC in "abc" coordinates which implies that the reference state variables of the system, that is to say, the circulating and grid currents (i_{c*k} and i_{v*k}), and the upper and lower capacitor arm voltages sum (u_{cu*k}^Σ and u_{cl*k}^Σ) are not necessarily constants. Hence, such a problem cannot be considered as a *regulation* problem where the equilibrium of the system in steady state is represented by a *point*, yet it turns into a *tracking* problem instead, as the steady state equilibrium becomes an *orbit* or a *trajectory*.

Therefore, the extension of the passivity-based PI controller of [90, 91, 92, 93] from the *regulation* to the *tracking* case was required. Solving such a problem resulted from cooperating with Professor Romeo Ortega from the *Laboratoire des Signaux et Systèmes*, a branch of the french gov-

ernmental research institute CNRS. The extension of the complex mathematical proof was done by Prof. Ortega himself, and was presented in [C16], and it is here also reviewed in appendix A.

The new control technique, named *Global Tracking Passivity - based PI Control*, is applied to the MMC in this present chapter. However, the implementation of this new control strategy requires prior knowledge of the MMC state and control variables in steady state; i.e., x_* and u_* . An issue that arises, is that the steady state variables have to be estimated, as the system cannot be analytically solved for x_* and u_* . Such a crucial issue is thoroughly discussed, and a closed loop estimator using a virtual energy model of the MMC based on the results of chapters 3, 4 and 5 is proposed, capable for controlling the MMC in a phase-independent fashion as well as for preventing power oscillations caused in the unbalanced AC grid to flow to the DC side of the MMC.

The remainder of this chapter is organized as follows: The mathematical formulation of the controller is briefly presented and applied to the MMC in section 6.2. In section 6.3 it is discussed how to calculate the tracking references for phase independent control and for constant DC power during unbalanced grid conditions, considered the main contribution of this chapter. Simulations are performed with the proposed control scheme and their results are given in section 6.4. Finally, conclusions in Section 6.5 complete the chapter.

6.2 Global tracking passivity-based PI controller for modular multi-level converters

As mentioned in the introduction, the *Global Tracking Passivity - based PI Controller* is detailed in appendix A. The control proposition and proof are presented for a general class of bi-linear systems, with a mathematical rigor characteristic of the control theory scientific field. In this section however, a simplified description of the controller and its application to the MMC is given using a relatively less formal language as an attempt to clarify the proposed concept for non-control theorist/engineers. Therefore, the interested reader is referred to appendix A of this manuscript for a formal theoretical derivation of the controller.

6.2.1 Tracking problem for the MMC

The Modular Multilevel Converter dynamics, as well as a large class of bi-linear systems, can be represented using equation (6.1).

$$\dot{x}(t) = Ax(t) + d(t) + \sum_{i=1}^m u_i(t)B_i x(t) \quad (6.1)$$

Where x is the state vector, u the control vector, d the measurable disturbance vector and m the number of control inputs. For instance, consider the model of the MMC converter expressed in (6.2).

$$\frac{d}{dt} \begin{bmatrix} i_{ck} \\ i_{vk} \\ u_{c\Sigma k} \\ u_{c\Delta k} \end{bmatrix} = \begin{bmatrix} -\frac{R}{L} & 0 & -\frac{n_{\Sigma k}}{4L} & -\frac{n_{\Delta k}}{4L} \\ 0 & -\frac{R'}{L'} & -\frac{n_{\Delta k}}{4L'} & -\frac{n_{\Sigma k}}{4L'} \\ \frac{N}{C}n_{\Sigma k} & \frac{N}{2C}n_{\Delta k} & 0 & 0 \\ \frac{N}{C}n_{\Delta k} & \frac{N}{2C}n_{\Sigma k} & 0 & 0 \end{bmatrix} \begin{bmatrix} i_{ck} \\ i_{vk} \\ u_{c\Sigma k} \\ u_{c\Delta k} \end{bmatrix} + \begin{bmatrix} \frac{v_{dc}}{2L} \\ -\frac{v_{pcc}}{L'} \\ 0 \\ 0 \end{bmatrix} \quad (6.2)$$

Note that neither the voltages nor the insertion indexes of the state space representation of (6.2) are expressed in their upper and lower arm notation (u, l). Instead the common and differential notation (Σ, Δ) is used instead. Therefore, the voltage and control variables are expressed as:

$$\begin{aligned} n_{\Sigma} &= n_u + n_l \\ n_{\Delta} &= n_u - n_l \\ u_{c\Sigma k} &= u_{cu k}^{\Sigma} + u_{cl k}^{\Sigma} \\ u_{c\Delta k} &= u_{cu k}^{\Sigma} - u_{cl k}^{\Sigma} \end{aligned}$$

The dynamics of the MMC of (6.2), can be re-written in the form of general bi-linear system of (6.1), resulting in (6.3).

$$\begin{aligned} \frac{d}{dt} \begin{bmatrix} i_{ck} \\ i_{vk} \\ u_{c\Sigma k} \\ u_{c\Delta k} \end{bmatrix} &= \begin{bmatrix} -\frac{R}{L} & 0 & 0 & 0 \\ 0 & -\frac{R'}{L'} & 0 & 0 \\ 0 & 0 & 0 & 0 \\ 0 & 0 & 0 & 0 \end{bmatrix} \begin{bmatrix} i_{ck} \\ i_{vk} \\ u_{c\Sigma k} \\ u_{c\Delta k} \end{bmatrix} + \begin{bmatrix} \frac{v_{dc}}{2L} \\ -\frac{v_{pcc}}{L'} \\ 0 \\ 0 \end{bmatrix} \\ &+ \left(\begin{bmatrix} 0 & 0 & \frac{-1}{4L} & 0 \\ 0 & 0 & 0 & \frac{-1}{4L'} \\ \frac{N}{C} & 0 & 0 & 0 \\ 0 & \frac{N}{2C} & 0 & 0 \end{bmatrix} n_{\Sigma} + \begin{bmatrix} 0 & 0 & 0 & \frac{-1}{4L} \\ 0 & 0 & \frac{-1}{4L'} & 0 \\ 0 & \frac{N}{2C} & 0 & 0 \\ \frac{N}{C} & 0 & 0 & 0 \end{bmatrix} n_{\Delta} \right) \begin{bmatrix} i_{ck} \\ i_{vk} \\ u_{c\Sigma k} \\ u_{c\Delta k} \end{bmatrix} \quad (6.3) \end{aligned}$$

Then, using the notation of (6.1), the following definitions are derived for $x^{\top} = [i_{ck}; i_{vk}; u_{c\Sigma k}; u_{c\Delta k}]$ and $u^{\top} = [n_{\Sigma}; n_{\Delta}]$:

$$\begin{aligned} A &= \begin{bmatrix} -\frac{R}{L} & 0 & 0 & 0 \\ 0 & -\frac{R'}{L'} & 0 & 0 \\ 0 & 0 & 0 & 0 \\ 0 & 0 & 0 & 0 \end{bmatrix}, d = \begin{bmatrix} \frac{v_{dc}}{2L} \\ -\frac{v_{pcc}}{L'} \\ 0 \\ 0 \end{bmatrix} \\ B_{\Sigma} &= \begin{bmatrix} 0 & 0 & \frac{-1}{4L} & 0 \\ 0 & 0 & 0 & \frac{-1}{4L'} \\ \frac{N}{C} & 0 & 0 & 0 \\ 0 & \frac{N}{2C} & 0 & 0 \end{bmatrix}, B_{\Delta} = \begin{bmatrix} 0 & 0 & 0 & \frac{-1}{4L} \\ 0 & 0 & \frac{-1}{4L'} & 0 \\ 0 & \frac{N}{2C} & 0 & 0 \\ \frac{N}{C} & 0 & 0 & 0 \end{bmatrix}, \quad (6.4) \end{aligned}$$

The goal behind the *Global Tracking Passivity - based PI Controller* is to stabilize bi-linear systems that are defined as in (6.1), only by means of a simple PI controller, such that all state variables remain bounded and converge to their equilibrium orbit or trajectory x_* :

$$\lim_{t \rightarrow \infty} [x(t) - x_*(t)] = 0, \quad (6.5)$$

for all initial conditions.

However, this has been proven to be possible for only a limited class of bi-linear systems. Such a class, in which the MMC takes part in, is identified via the following assumption:

Assumption: There exists a symmetrical matrix $P \in \mathbb{R}^{n \times n}$ such that

$$\begin{aligned} \frac{1}{2} (PA + A^\top P^\top) &\leq 0 \\ \frac{1}{2} (PB_i + B_i^\top P) &= 0 \end{aligned} \quad (6.6)$$

where A and B_i have been defined for the MMC in (6.4), whereas matrix P is defined in the following subsection.

6.2.2 Passivity of the bi-linear incremental model

The state and control variables can be written in their *incremental* representation, such as:

$$\begin{aligned} \tilde{x} &= x - x_* \\ \tilde{u} &= u - u_* \end{aligned}$$

General theory

Consider the class of bi-linear systems under study; i.e., those that can be represented by (6.1), and that satisfy the assumption expressed by (6.6). For such a class of systems, in which the MMC takes part in, an output function y can be constructed with respect to which the system becomes *passive*.

Such an output function, also referred to as the *passive output* of the system, is defined as in (6.7)

$$y := \mathcal{C}(x_*)x \quad (6.7)$$

where \mathcal{C} is defined as

$$\mathcal{C} := \begin{bmatrix} x_*^\top B_1^\top \\ \vdots \\ x_*^\top B_m^\top \end{bmatrix} P \quad (6.8)$$

The operator $\tilde{u} \mapsto y$ is passive with storage function

$$V(\tilde{x}) := \frac{1}{2} \tilde{x}^\top P \tilde{x} \quad (6.9)$$

Thus, the system verifies the dissipation inequality

$$\dot{V} \leq \tilde{u}^\top y \quad (6.10)$$

MMC passive output

Matrix P can be defined in a straight forward way as the storage function (6.9) has a structure similar to the stored energy function of the system. Hence, for the particular case of the MMC, matrix P is defined as:

$$P = \begin{bmatrix} 2L & 0 & 0 & 0 \\ 0 & L' & 0 & 0 \\ 0 & 0 & \frac{C}{2N} & 0 \\ 0 & 0 & 0 & \frac{C}{2N} \end{bmatrix} \quad (6.11)$$

It follows that, defining $x^\top := [i_c \quad i_v \quad u_{C\Sigma} \quad u_{C\Delta}]^\top$, the passive output of the system is

$$\begin{aligned} y &= \begin{bmatrix} x_\star^\top B_\Sigma^\top \\ x_\star^\top B_\Delta^\top \end{bmatrix} P x \\ &= \frac{1}{2} \begin{bmatrix} i_{c\star} u_{C\Sigma} - i_c u_{C\Sigma\star} + \frac{1}{2} i_{v\star} u_{C\Delta} - \frac{1}{2} i_v u_{C\Delta\star} \\ i_{c\star} u_{C\Delta} - i_c u_{C\Delta\star} + \frac{1}{2} i_{v\star} u_{C\Sigma} - \frac{1}{2} i_v u_{C\Sigma\star} \end{bmatrix}. \end{aligned} \quad (6.12)$$

Note that both passive outputs of the MMC are constructed as a combination between the measured trajectories x , and the trajectories at the equilibrium point x_\star . Hence, prior knowledge of x_\star is required for the implementation.

In addition, the MMC has two passive outputs. The first one that results from the products of “directly” related variables; i.e., the product between the circulating current i_c and the voltage sum $u_{c\Sigma}$ on the one hand, and the product between the grid current i_v and the voltage difference $u_{c\Delta}$. Moreover, the second passive output consists on the product between variables that are not “directly related.” In other words, there seems to be quite a strong similarity between the structure of the passive outputs of the MMC, and the definitions of active and reactive power for 3-level VSC converters. This issue will be further explored in Appendix C.

6.2.3 A PI tracking controller

General theory

Consider again, the class of bi-linear systems that can be described by equation (6.1) that satisfy the assumption expressed in (6.6). In addition, if the passive output y of such a class of systems is forced to zero in closed loop with the PI controller

$$\begin{aligned} \dot{z} &= -y \\ \tilde{u} &= -K_p y + K_i z \end{aligned} \quad (6.13)$$

with positive PI gains K_p and K_i , then for all initial conditions the trajectories of the closed-loop system are bounded (global stability) and the *augmented passive output* y_a will tend to zero in steady state:

$$\lim_{t \rightarrow \infty} y_a(t) = 0, \quad (6.14)$$

where the augmented passive output y_a , is an extended version of y , and is defined as

$$y_a := \begin{bmatrix} \mathcal{C} \\ Q \end{bmatrix} \tilde{x}, \quad (6.15)$$

with $Q = -\frac{1}{2} (PA + A^\top P^\top)$.

At this point, the system global stability is ensured. Nonetheless, the global *asymptotic* stability ($\lim_{t \rightarrow \infty} x - x_\star = 0$) has not yet been proven. For this, one must verify the *detectability condition* of the system. This is done by checking if the inequality of expressed in (6.16) is satisfied.

Therefore, if

$$\text{rank} \begin{bmatrix} \mathcal{C} \\ Q \end{bmatrix} \geq n, \quad (6.16)$$

where n is the number of state variables, then global asymptotic stability is ensured; i.e., $\lim_{t \rightarrow \infty} x(t) - x_\star = 0$.

Detectability condition for the MMC

For the particular case of the MMC, detectability is given by the rank of the matrix

$$\begin{bmatrix} \mathcal{C} \\ Q \end{bmatrix} = \begin{bmatrix} -u_{C\Sigma\star} & -\frac{1}{2}u_{C\Delta\star} & i_{c\star} & \frac{1}{2}u_{C\Delta\star} \\ -u_{C\Delta\star} & -\frac{1}{2}u_{C\Sigma\star} & \frac{1}{2}i_{v\star} & i_{c\star} \\ 2R & 0 & 0 & 0 \\ 0 & R' & 0 & 0 \\ 0 & 0 & 0 & 0 \\ 0 & 0 & 0 & 0 \end{bmatrix}$$

which satisfies condition (6.16) whenever $i_{c\star}^2 - \frac{1}{4}i_{v\star}u_{c\Delta\star} \neq 0$.

6.2.4 MMC controller summary

To summarize, the application of the *global tracking passivity-based PI* theory to the MMC yields the following equations:

$$\begin{aligned} \dot{z} &= y \\ u &= -k_p y + k_i z + u_\star \\ y &= \frac{1}{2} \begin{bmatrix} i_{c\star}u_{c\Sigma} - i_c u_{c\Sigma\star} + \frac{1}{2}i_{v\star}u_{c\Delta} - \frac{1}{2}i_v u_{c\Delta\star} \\ i_{c\star}u_{c\Delta} - i_c u_{c\Delta\star} + \frac{1}{2}i_{v\star}u_{c\Sigma} - \frac{1}{2}i_v u_{c\Sigma\star} \end{bmatrix} \end{aligned} \quad (6.17)$$

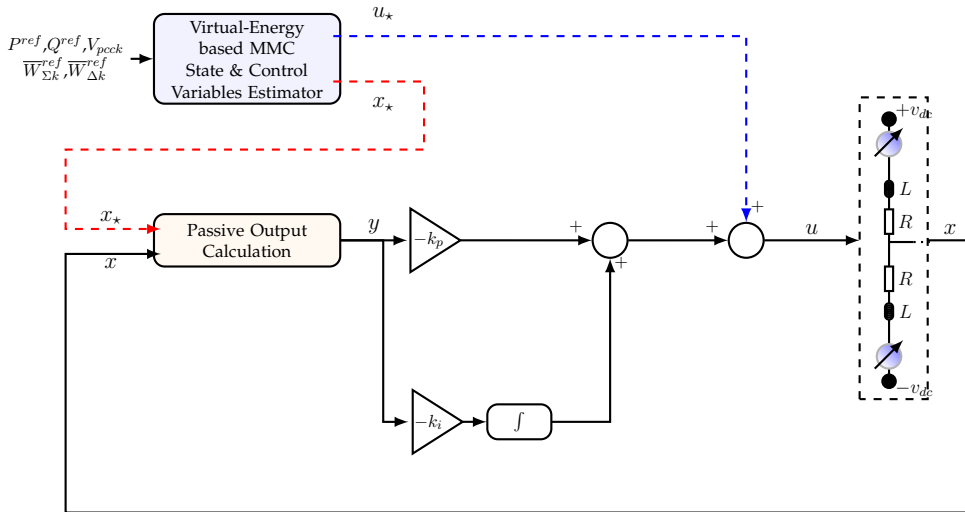


Figure 6.1: MMC control scheme: global tracking passivity-based PI with proposed virtual energy state and control variables estimator

where $u = [n_{\Sigma}; n_{\Delta}]^T$.

As can be seen from the set of equations in (6.17), it is necessary to have prior knowledge of the state and control variables in steady state; that is, x_* and u_* . As mentioned in the introduction, the MMC equation system cannot be solved analytically for x_* and u_* . Therefore, an estimation method is proposed, and described in the next section.

6.3 Generating the reference signals using a closed loop virtual energy estimator

In this section, an estimation method is proposed based on the minimized circulating current signal generation formula that has been discussed in previous chapters. The proposition consists of using such an equation, derived using the Lagrange multipliers optimization methodology, to estimate the steady state equilibrium trajectory x_* and u_* . The complete control scheme is therefore given in Fig. 6.1, where the proposed estimator is used along with the passivity-based PI to control the MMC and ensure its stability.

As two minimized circulating currents have been proposed in this Thesis; i.e., (3.31) in chapter 3, and (5.15) in chapter 5, two different configuration of such estimators have resulted. The first one, suitable for *phase independent energy regulation* whereas the second one useful for ensuring *constant DC power under unbalanced grid conditions*.

Both formulas (3.31) and (5.15), are based on PI controllers that allow for the internal energy regulation. However, as can be inferred from Fig. 6.1, the only “real” feedback loop is provided by the passive PI controller over x .

One possible solution is to neglect the influences of the PI controllers on equation (3.31) (or (5.15)), to avoid the use of feedback loops. This would yields in an *open-loop estimator*, similar to what has been proposed in [29], yet instead of applying it directly to control the MMC as in [29], it is only used to estimate x_* , leaving to the passive PI (in closed loop) the responsibility for the controlling the MMC. The control of the MMC using such an *open loop estimator* was an outcome

of the present PhD project, and was presented in [C16].

Nonetheless, the error introduced by the use of the open-loop estimator is non-negligible, especially for lower voltage MMCs (as the laboratory prototype) where the arm resistance losses have to be considered. Therefore, a *closed-loop estimator* is here presented instead. The loop is closed by means of a *virtual energy model* of the MMC; i.e., not the “real” MMC depicted in Fig. 6.1, yet the equations that model the energy dynamics of the converter are used for this purpose.

6.3.1 Phase independent energy regulation

As mentioned earlier, if the converter has a non-negligible internal resistance $R > 0$, a mismatch between the average values of powers $\overline{e_{vk}i_{vk}}$ and $v_{dc}i_{ck}$ will take place, making open-loop estimation no longer valid. As an attempt to overcome this issue, a *closed loop estimator* is proposed to calculate x_{\star} and u_{\star} , and is depicted in Fig. 6.2. The estimation technique is based on the application of equation (3.31) derived in chapter 3, and rewritten in (6.18) as a reminder, suited for *phase independent energy regulation*.

$$i_{ck\star} = \frac{\overline{P}_{\Sigma k\star}^{ref} + (1 - \alpha) \overline{P}_{vk\star}}{v_{dc}^2} v_{dc} + \frac{\alpha P_{vk\star}}{v_{dc}} + \frac{-\overline{P}_{\Delta k\star}^{ref}}{2v_{dc}^2 \left(e_{vk\star, p.u.}^{rms} \right)^2} e_{vk\star} \quad (6.18)$$

As discussed in chapter 3, equation (6.18) calculates the reference of the circulating current of the MMC. Such an equation contains two PI controllers represented by the terms $\overline{P}_{\Sigma k}^{ref}$ and $\overline{P}_{\Delta k}^{ref}$ that regulate the average values of the capacitive energy sum and difference stored in the arm of the converter ($\overline{w}_{\Sigma k}$ and $\overline{w}_{\Delta k}$). In the case that the MMC would have a non-negligible internal resistance R , the PI controller $\overline{P}_{\Sigma k}^{ref}$ (that was defined in equation (3.16)) will “add” the missing power that is neglected by “open-loop” estimation techniques. The difference between the proposition of chapter 3 and what is being proposed here, is that equation (3.31) will be applied to a *virtual MMC* instead of the real converter; that is to say that it will not participate directly in the control of the converter, yet it will generate the references needed for the control by means of the MMC state equations. The procedure is described in the following lines.

If the system is connected to a three-phased active grid ($V_{pcck} \neq 0$) then the grid current reference $i_{vk\star}$ is defined by equation (5.16) in chapter 5, written again as a reminder in (6.19).

$$i_{vk\star} = \frac{P_{ac}^{ref}}{\|\mathbf{v}_{pcc}^+\|^2 + kp \cdot \|\mathbf{v}_{pcc}^-\|^2} \cdot \left(v_{pcck}^+ + kp \cdot v_{pcck}^- \right) \quad (6.19)$$

Equation (6.19) calculates the grid current in steady state ($i_{v\star}$), as a function of the power reference established by the secondary control P_{ac}^{ref} , and the positive and negative voltage measurements of the point of common coupling (\mathbf{v}_{pcc}^+ and \mathbf{v}_{pcc}^-) from the *real* MMC, and a constant kp defined by the user (refer to chapter 5 for more details).

In order to calculate the circulating current reference in steady state ($i_{ck\star}$) equation 6.18 is used along with a *virtual energy model* of the MMC. Such a model contains the MMC energy sum and difference dynamics (\dot{w}_{Σ} and \dot{w}_{Δ})

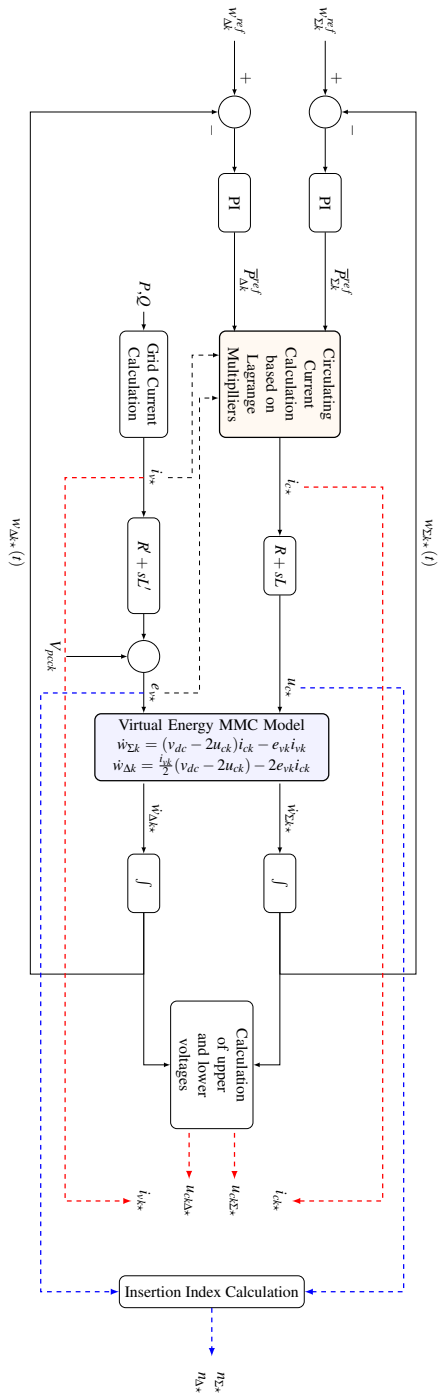


Figure 6.2: Proposed state and control variable estimator -based on virtual MMC energy model

$$\begin{aligned}
 \dot{w}_{\Sigma k^*} &= (-e_{vk^*}i_{vk^*} + (V_{dc} - 2u_{ck^*})i_{ck^*}) \\
 \dot{w}_{\Delta k^*} &= \left(\frac{i_{v^*k}}{2} (V_{dc} - 2u_{ck^*}) - 2e_{vk^*}i_{ck^*} \right) \\
 w_{\Sigma k^*} &= \int_0^t \dot{w}_{\Sigma k^*} dt \\
 w_{\Delta k^*} &= \int_0^t \dot{w}_{\Delta k^*} dt
 \end{aligned} \tag{6.20}$$

with e_{v^*k} and u_{c^*k} calculated as

$$\begin{aligned}
 u_{ck^*} &= Ri_{ck^*} + L \frac{d}{dt} i_{ck^*} \\
 e_{vk^*} &= R' i_{vk^*} + L' \frac{d}{dt} i_{vk^*} + V_{pcck}
 \end{aligned} \tag{6.21}$$

The average values of the $w_{\Sigma k^*}$ and $w_{\Delta k^*}$ are required to calculate $P_{\Sigma k^*}^{ref}$ and $P_{\Delta k^*}^{ref}$ expressed in (6.22) that are in turn needed for the calculation of i_{ck^*} by (6.18).

$$\begin{aligned}
 \overline{P_{\Sigma k^*}^{ref}} &= \left[kp_{\Sigma} \left(W_{\Sigma k^*}^{ref} - \overline{w_{\Sigma k^*}} \right) + ki_{\Sigma} \int \left(W_{\Sigma k^*}^{ref} - \overline{w_{\Sigma k^*}} \right) dt \right], \\
 \overline{P_{\Delta k^*}^{ref}} &= \left[kp_{\Delta} \left(W_{\Delta k^*}^{ref} - \overline{w_{\Delta k^*}} \right) + ki_{\Delta} \int \left(W_{\Delta k^*}^{ref} - \overline{w_{\Delta k^*}} \right) dt \right].
 \end{aligned} \tag{6.22}$$

In order to calculate the energy average keeping good dynamic performance, the average values of $w_{\Sigma k^*}$ and $w_{\Delta k^*}$ are calculated as in chapter 4 by:

$$\begin{aligned}
 \hat{\overline{w}}_{\Sigma k^*} &= w_{\Sigma k^*} - w_{\Sigma k^* \alpha}, \\
 \hat{\overline{w}}_{\Delta k^*} &= w_{\Delta k^*} - w_{\Delta k^* \alpha},
 \end{aligned} \tag{6.23}$$

where $w_{\Sigma k^* \alpha}$ and $w_{\Delta k^* \alpha}$ are the band-pass-filtered signals outputs of using a second order generalized integrator (SOGI) - quadrature signal generator, as discussed in chapter 4. Furthermore, u_{cuk^*} and u_{clk^*} are calculated via (6.24)

$$\begin{aligned}
 u_{cuk^*} &= \sqrt{\frac{N}{C}} [w_{\Sigma k^*} + w_{\Delta k^*}], \\
 u_{clk^*} &= \sqrt{\frac{N}{C}} [w_{\Sigma k^*} - w_{\Delta k^*}].
 \end{aligned} \tag{6.24}$$

Finally, $u_{c\Sigma}$ and $u_{c\Delta}$ are calculated as in 6.25. This concludes the estimation of x_* .

$$\begin{aligned}
 u_{ck\Sigma^*} &= u_{cuk^*} + u_{clk^*}, \\
 u_{ck\Delta^*} &= u_{cuk^*} - u_{clk^*}.
 \end{aligned} \tag{6.25}$$

In addition, the upper and lower insertion indexes are calculated by

$$\begin{aligned} n_{uk^*} &= \frac{\frac{V_{dc}}{2} - e_{vk^*} - u_{ck^*}}{u_{cuk^*}}, \\ n_{lk^*} &= \frac{\frac{V_{dc}}{2} + e_{vk^*} - u_{ck^*}}{u_{clk^*}}. \end{aligned} \quad (6.26)$$

Note that *compensated modulation* is being used in (6.26) according to the classification that was proposed in section 2.8, as the denominators are time varying signals. However, it is also possible to replace the denominators by a constant signal v_{dc} .

The control at the equilibrium point $u_* = [n_{\Sigma^*} \quad n_{\Delta^*}]^\top$ is therefore defined as

$$\begin{aligned} n_{\Sigma k^*} &= n_{uk^*} + n_{lk^*} \\ n_{\Delta k^*} &= n_{uk^*} - n_{lk^*}. \end{aligned} \quad (6.27)$$

6.3.2 Generation of references for constant DC power under unbalanced grid conditions

As discussed in chapter 5, i_{ck^*} determined by equation 6.18 is not able to successfully cope with unbalanced grid conditions, since it is the result of an analytical mathematical optimization that does not consider the relationship between the phases of the MMC. To be able to successfully handle unbalances, by preventing power fluctuations from the unbalanced AC side of the converter to pass its DC side, i_{ck^*} is calculated as shown in chapter 5 in (5.15). Such an equation is given as a reminder in 6.28.

$$\begin{aligned} i_{ck^*} &= \frac{\bar{P}_{\Sigma k^*}^{ref} + (1 - \alpha) \bar{P}_{vk^*}}{v_{dc}^2} v_{dc} + \frac{\alpha P_{vk^*}}{v_{dc}} + \frac{-\bar{P}_{\Delta k^*}^{ref} e_{vk^*}}{2v_{dc}^2 (e_{vk^*,p.u.}^{rms})^2} \\ &\quad - \sum_{k \in (abc)} \left(\frac{\bar{P}_{\Sigma k^*}^{ref} + (1 - \alpha) \bar{P}_{vk^*}}{v_{dc}^2} v_{dc} + \frac{\alpha P_{vk^*}}{v_{dc}} + \frac{-\bar{P}_{\Delta k^*}^{ref} e_{vk^*}}{2v_{dc}^2 (e_{vk^*,p.u.}^{rms})^2} \right) + \frac{1}{3} \frac{P_{dc}^{ref}}{v_{dc}} \end{aligned} \quad (6.28)$$

The estimator scheme is the same as the one presented in Fig. 6.2 case, yet equation (6.28) is used instead of (6.18).

Estimated control and state variables summary

To summarize, the state reference variables $x_* = [i_{ck^*} \quad i_{vk^*} \quad u_{c\Sigma k^*} \quad u_{c\Delta k^*}]^\top$ are defined by: i_{vk^*} in (6.19), i_{ck^*} in (6.18) for phase independent control and in (6.28) for constant DC power control; $u_{c\Sigma k^*}$ and $u_{c\Delta k^*}$ are defined by replacing (6.24) in (6.25).

In addition, the estimated control vector in steady state $u_* = [n_{\Sigma k^*} \quad n_{\Delta k^*}]$ is defined in (6.26) and (6.27).

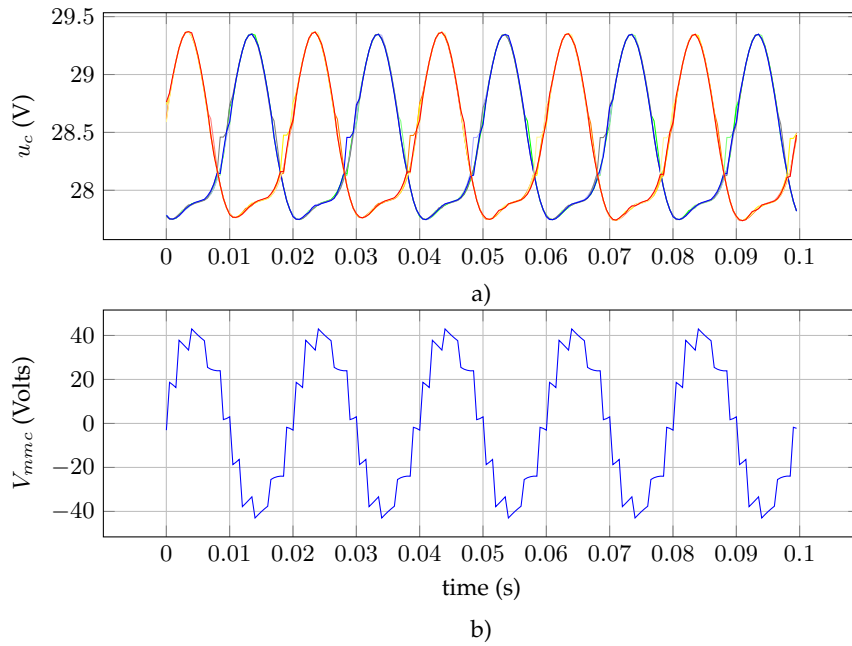


Figure 6.3: MMC $2N$ Individual Capacitor Voltages, b) MMC output voltage

6.4 Results

6.4.1 Phase independent control

First, a single-phase MMC simulation scenario has been set up in Matlab/Simulink to test the validity of the control. The considerations are the following : the converter has $2N = 10$ SMs, N in each arm. The input DC voltage is $V_{dc} = 140V$, the reference voltage e_{v^*} has an amplitude of $\frac{V_{dc}}{2}$ and a frequency set to $f = 50Hz$. The frequency of the balancing algorithm [3, 7] that balances the N capacitor voltages is set to $f = 20kHz$. The internal capacitance, resistance and inductance are respectively set to $C = 3.3mF$, $R = 12\Omega$ and $L = 10mH$. The load resistance and inductance values, respectively, are $R' = 12\Omega$ and $L' = 40mH$.

Figure 6.3-a) shows the $2N$ voltage trends of the MMC capacitors, whereas in 6.3-b) is depicted the AC output voltage multilevel waveform of the converter. Furthermore, the state references x_* as well as the measured state variable are depicted in Fig. 6.4. As can be seen from Fig. 6.4-a) and Fig. 6.4-b), the i_c and i_v converge to i_{c^*} and i_{v^*} . Nonetheless in Fig. 6.4-c) a non-negligible error between $u_{c_{u,l}^*}^{\Sigma}$ and $u_{c_{u,l}}^{\Sigma}$ of approximately one volt can be observed. Fortunately, $u_{c_{u,l}}^{\Sigma}$ is the sum all the N capacitors in the upper or lower arm, thus the error of the individual capacitor voltage one 0.2 volts.

The error occurs since there is still a remaining power mismatch, even after reducing it using the proposed closed loop estimator along with the *virtual* energy model. This occurs since the high frequency current harmonics caused by the modulation, and eventually by the saturation of the insertion indexes, were not considered in the model. These current harmonics produces losses when passing through the MMC resistances, and cause the error in the estimation.

Moreover, Fig. 6.5 shows the trends of the proposed control action applied to the single-phased MMC. More precisely, in Fig. 6.5-a) is depicted the passive output that is controlled to zero by means of the proposed controller. It is however still possible to identify steady state

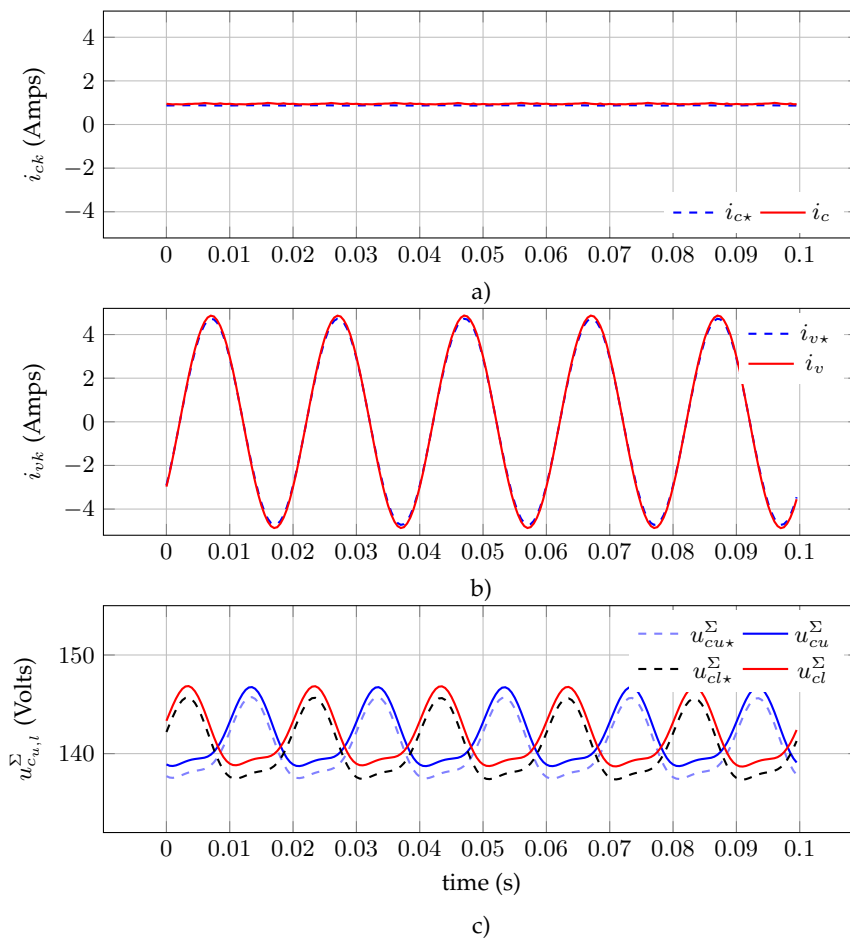


Figure 6.4: Phase-independent control of a single phased MMC: a) Circulating Current, b) Grid current and c) MMC Sum of capacitor voltages by arm.

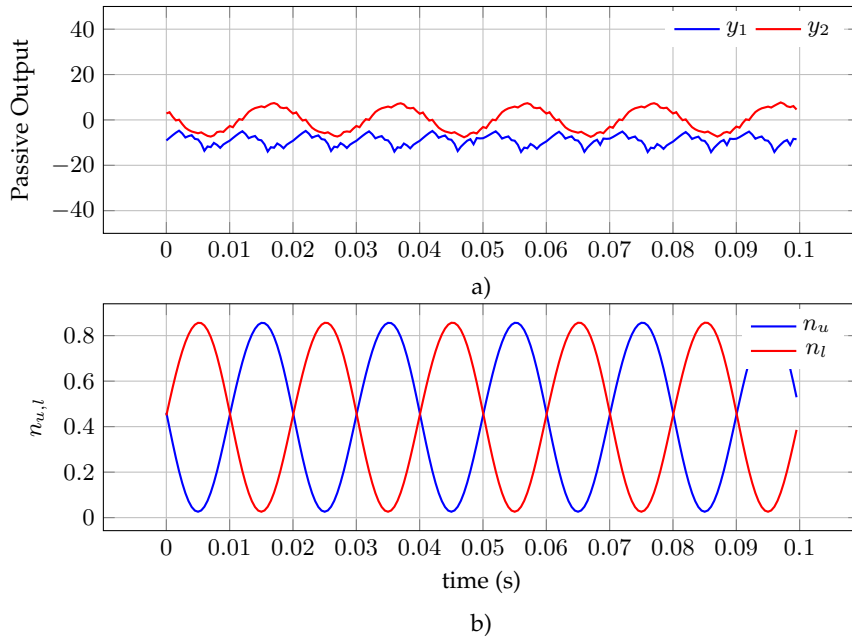


Figure 6.5: Phase-independent control of a single phased MMC: a) Passive output and b) Insertion Indexes.

Table 6.1: MMC Parameters

Parameter	Value
DC Voltage	150 Volts
Number of SM per arm	5
SM Nominal Voltage	30 Volts
SM Capacitance	3.3 mF
Arm Inductance	20 mH
Arm Resistance	6 Ω
Load Inductance	20 mH
Load Resistance	6 Ω

oscillations in the passive output that are caused by the power mismatch error when x_* , or more precisely when u_{cu*}^Σ and u_{cl*}^Σ are estimated. The insertion indexes are shown in Fig. 6.5-c).

6.4.2 Constant DC power control

In this section, a three-phased MMC converter connected to an active grid has been simulated under unbalanced conditions in order to test the proposed control along with the closed-loop estimator for constant DC power control. The simulation scenario was done by both : I) establishing the main power reference of the system at the AC grid via the grid currents, and II) establishing the main power references at the DC terminals of the MMC via the circulating currents (see chapter 5 for more details). The MMC parameters are given in table 6.1. This series of simulation analyzes the performance of the controller when at $t = 0.1s$ the voltage at the point of common coupling of phase “a” is reduced to 5% of its original value and remains at that value for a total time of $0.3s$, before returning to its original voltage level at $t = 0.4s$. This is depicted in Fig. 6.6.

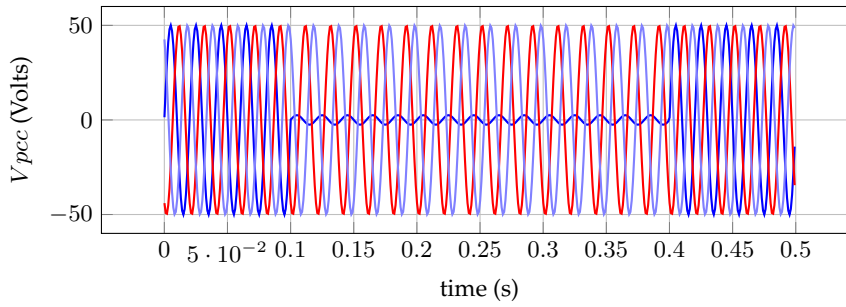


Figure 6.6: Voltage at the point of common coupling

In Fig. 6.7-a) and Fig. 6.8-a) are depicted the power at the point of common coupling P_{ac} and the power at the DC terminals of the MMC P_{dc} . It can be seen that during the fault P_{ac} starts fluctuating at twice the grid frequency. Nonetheless, the oscillations are blocked by the energy storing elements of the MMC, and do not appear at the DC side of the converter. Similar to the results obtained in chapter 5, when the main or primary power reference of the system is established at the DC side via the circulating currents, the power measured between the DC terminals of the converter does not see any perturbation whatsoever as shown in Fig. 6.8-a). This does not occur in Fig. 6.7-a), where the primary power of the system is established at the point of common coupling via the grid currents. Yet, absolute constant power at the DC terminals will require a more elevated energy and voltage stress to the MMC capacitors as can be seen in Fig. 6.7-b) and 6.7-c), and they will have to be oversized to withstand this scenario.

Figure 6.9 and 6.10 show the waveform trends of the estimated reference signals and the measured signals of the system (x_* and x), for both power ways of establishing the primary power reference of the system. A familiar result comes to mind: the grid and circulating currents are regulated quite well, whereas a stationary regulation error is found between reference and measurements of the capacitor voltages. The error is approximately of the order of 2%. Here again, it is caused by the power mismatch error in the estimation. Furthermore, the grid currents stay balanced in both cases since $k_p = 0$ is used in (6.19) [77, 78].

The passive output is regulated close to zero, however it does not converge perfectly to zero due to the estimation errors that yield in an erroneous passive output. Despite of that, the error does not seem to be significant and the system has proven to operate satisfactorily.

6.5 Conclusions

In this chapter, a passivity-based PI controller has been applied to the MMC in the ABC frame. Global asymptotic stability is ensured with a simple PI regulating the MMC passive outputs to zero. The obtained stability results are global and hold for all positive definite gains of the PI. The performance of the controller was tested by means of simulations. Although the controller showed promising results, some issues were observed during the implementation such as errors in the estimation process of x_* , mainly caused by neglecting the high order harmonics and physical limits including control saturation. Yet the converter showed good performance despite the estimation error, showing a certain degree of robustness. Furthermore, the estimation is model-based, which is usually a drawback during the practical implementation due to the parameters uncertainty.

The proposed estimation technique is capable of considering the power losses caused by the

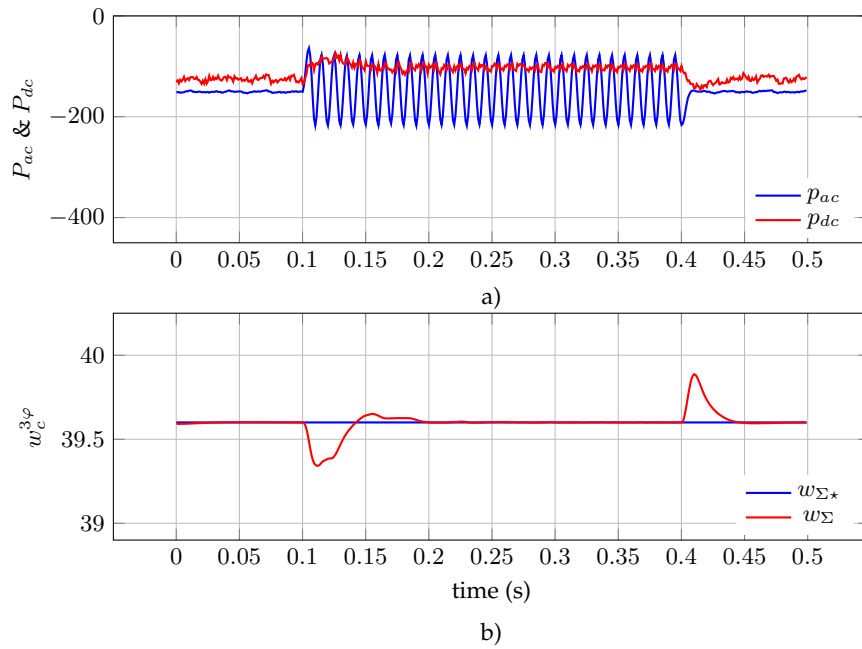


Figure 6.7: Power and energy trends establishing the primary power reference at the AC grid PCC, via the grid currents: a) Power at the dc terminals (in red) and at the PCC of the AC grid (in blue) and b) MMC 3-phase aggregate capacitive energy

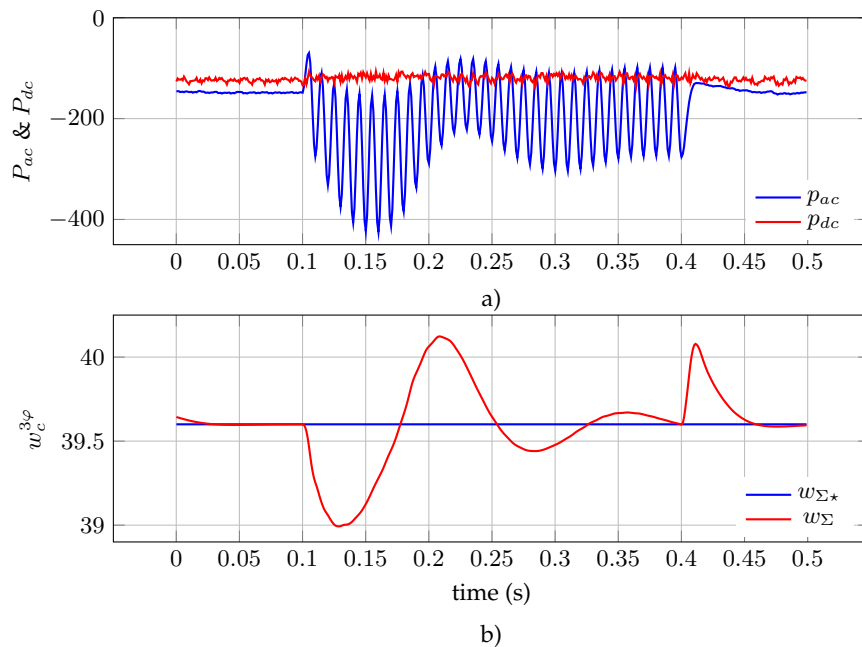


Figure 6.8: Power and energy trends establishing the primary power reference at the DC terminals of the MMC, via the circulating currents: a) Power at the dc terminals (in red) and at the PCC (in blue) and b) MMC 3-phase aggregate capacitive energy

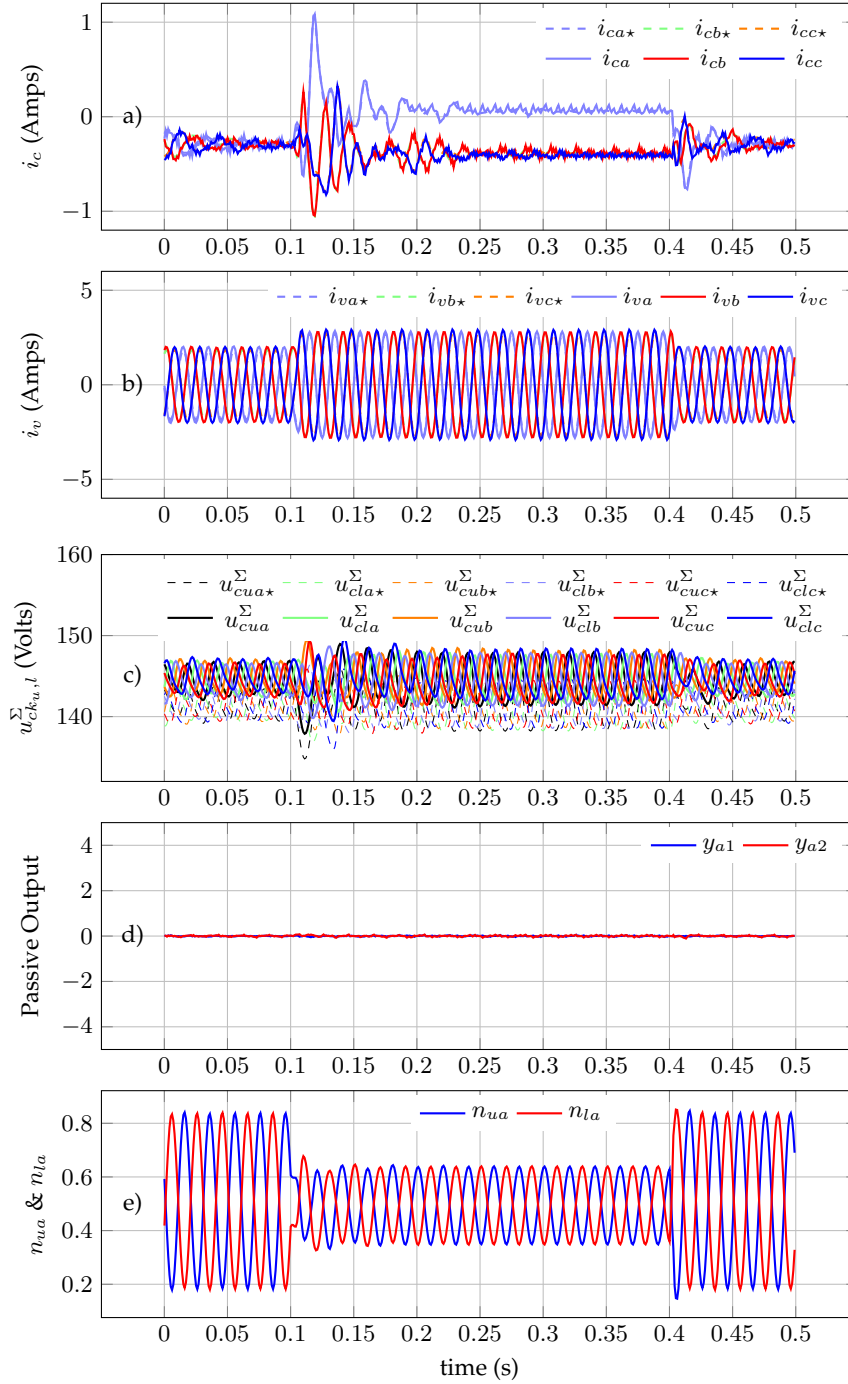


Figure 6.9: MMC state variables references and measures (x_* & x): a) circulating currents, b) grid currents and c) capacitor voltages sum per arm - phase "a" d) passive outputs and e) insertion indexes

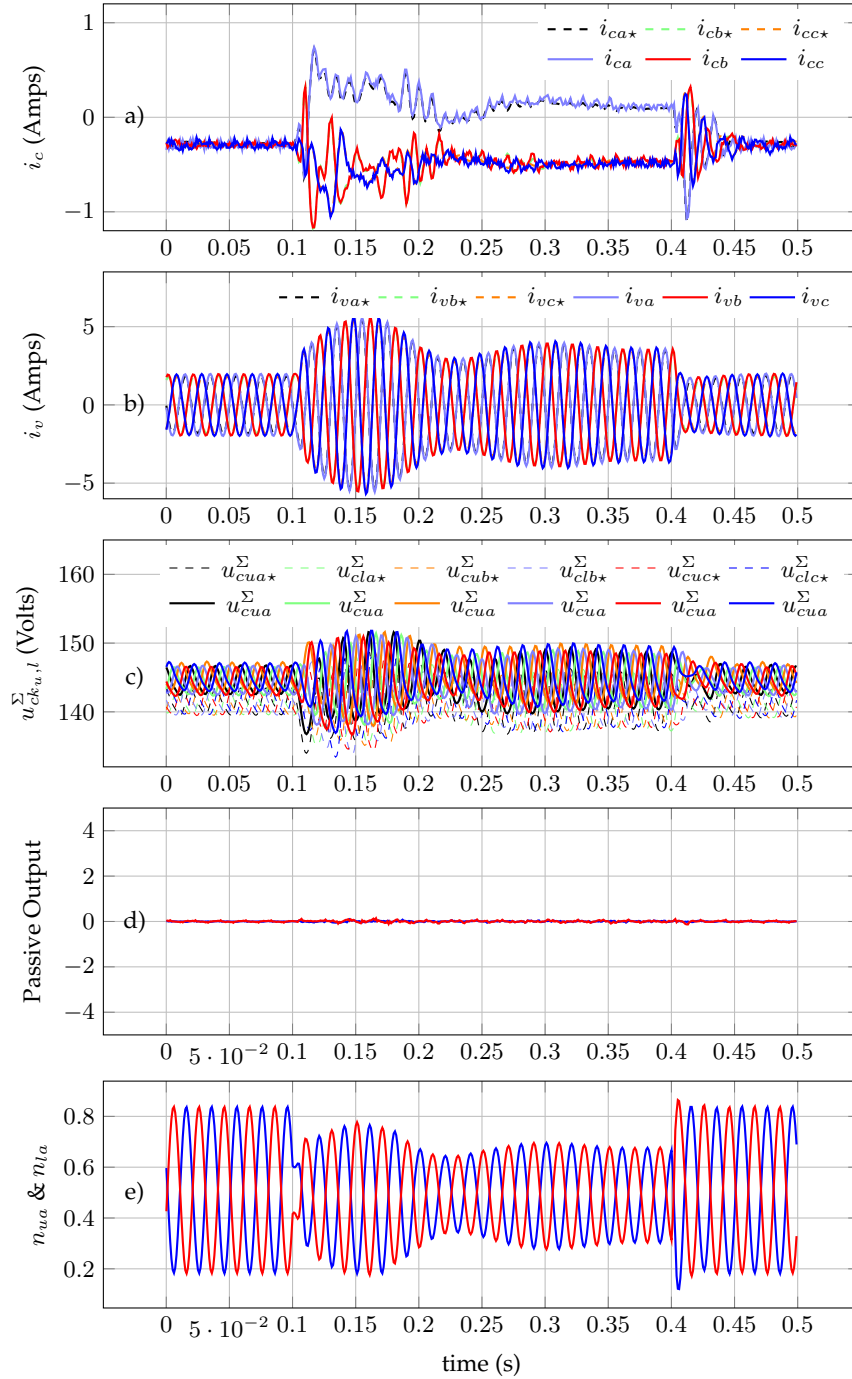


Figure 6.10: MMC state variables references and measures (x_* & x): a) circulating currents, b) grid currents and c) capacitor voltages sum per arm - phase "a" d) passive outputs and e) insertion indexes

fundamental harmonics of each current in the internal resistance of the MMC, usually neglected in “open loop” approaches. Furthermore, it can be used to generate the necessary references x_* for preventing power oscillations caused by an unbalanced grid from appearing at the DC terminals of the MMC.

The controller turns the system passive and global asymptotic stability is ensured. Moreover, passivity has the following useful property: “the interconnection of passive systems stays passive.” This approach, might be of high value for multi-terminal systems and SuperGrid applications, since it presents a modular approach of handling the stability problem, for very large and complicated interconnected systems. Hence, this chapter is but an initial step towards controlling MMC-based multi-terminal systems ensuring global stability with local controllers.

7

Conclusions and Future Research

This chapter recapitulates the mains results of this Thesis and presents some recommendations for further research.

TWO controllers are proposed. The first is linear whereas the second is non-linear. The first controller is quite robust since it is based on well known current closed-loop controllers, which regulate the energy of the MMC independently of the model parameters. The second controller may be used to ensure global asymptotic stability of the MMC by means of a passivity-based PI controller.

7.1 Conclusions

7.1.1 On the proposed control philosophy and linear control scheme

A simple closed loop control philosophy in the abc frame has been proposed as an alternative to dqo based strategies like [17], [J0] and [C7] that cannot directly control the arm energy distribution inside the converter without significantly increasing the controller mathematical complexity. Moreover, as the controller works with closed energy and current control loops along with proportional resonant controllers, it presents a high degree of robustness and it is not subject to uncertainty of the model parameters.

The proposed control strategy has been designed on a “top to bottom” approach inherent of optimization strategies, as the desired control objectives will shape the control scheme itself. The control strategy generates the minimal circulating current references capable of attaining the desired arm energy balancing objectives with the lowest theoretical losses. In this Thesis, the implementation of the current references was done with resonant controllers, yet it is possible to replace the control action with more advanced techniques, while maintaining the same circulating current reference signal generation. The proposed controller is the result of applying multi-objective mathematical optimization by means of the Lagrange multipliers methodology,

with the aim of minimizing independently by phase both: 1) the fluctuations of the power contribution of each circulating current to the power at the DC terminals ($v_{dc}i_{diffk}$) and 2) the fluctuations of the capacitive power “sum” of each phase ($\dot{w}_{\Sigma k}$). The first condition will result in constant circulating currents as long as the voltage at the DC terminals of the MMC stays constant, whereas the second one yields a constant capacitive energy sum in each phase ($w_{\Sigma k}$), that in turn results in a reduction in the oscillations of the MMC capacitor voltages (u_{ck}). Forcing the circulating current constant implies eliminating the power losses caused by its harmonics flowing through the internal resistance of the converter at twice the grid frequency. Similarly, reducing the voltage oscillations of the MMC capacitors implies a power loss reduction caused by the parasite resistance of the MMC individual capacitors. A weighting factor is used since both of the aforementioned objective functions are conflicting. In addition, the multi-objective optimization problem is subject to two energy regulating constraints; one constraint that regulates the average value of the capacitive energy sum ($\overline{w_{\Sigma k}}$), and a second one that regulates the average of the difference ($\overline{w_{\Delta k}}$). By doing so, the capacitive energy distribution is regulated at all times. With the optimization problem completely defined; i.e., objective functions and constraints are given, the Lagrange equation is written as the two objective functions with their corresponding weighting factors plus both energy constraints that are multiplied by two different Lagrange multipliers (λ_{Σ} and λ_{Δ}). Solving such an optimization problem yields the circulating current reference equation suitable for *phase independent control*, and is considered to be one of the main contributions of this Thesis.

It was found that for MMCs with low number of levels (or sub-modules), the circulating current reference signal generation was sensitive to harmonic distortion, mainly caused by the MMC inner voltage e_{vk} , and consequently, by the power flowing into the MMC coming from the grid $e_{vk}i_{vk}$. Furthermore, since the natural *abc* reference frame is used to control the converter, the MMC variables are mostly sinusoidal. In consequence, several input signals required for determining the circulating current reference calculated via Lagrange multipliers depend on the average value calculation of sinusoidal variables (i.e. $\overline{w_{\Sigma k}}$, $\overline{w_{\Delta k}}$ and $e_{vk,p.u.}^{2_{rms}}$), which slows down the dynamics of the control especially when first order filters are used, while additionally increasing the complexity of the tuning of the control system under certain conditions. Therefore, adaptive filters based on second order generalized integrators (SOGI) were used to estimate distortion-free MMC single-phase voltages, power and energy inputs required for the circulating current control reference equation, as well as their required average values improving significantly the controllers dynamic performance. In addition to improving control dynamics and facilitating the tuning of the system controllers, the use of the adaptive filters provides inherent capability for operation under frequency variations, and is therefore suitable for control of MMCs operating in weak grids as well as for high- or medium-voltage motor drives.

Indeed, the resulting control approach was suited for controlling independently by phase the MMC state variables in a robust and dynamically performing fashion; however, it failed to deal successfully with undesired power fluctuations at the DC terminals of the MMC caused by unbalanced grid conditions. This is because the relationship between phases was not considered in the optimization problem definition. Hence, a new optimization problem has been defined; the only constraint of this new formulation is the necessity to ensure constant power between the MMC DC terminals ($P_{dc} = const$) resulting from multiplying the voltage between the MMC terminals v_{dc} with the sum of the circulating currents of each phase $\sum_{k \in abc} i_{diffk}$. Moreover, the objective function is to minimize the difference between the new alternative circulating current

reference and the former one used for *phase independent control*. In other words, the performance of the new circulating current reference equation will resemble as much as possible that of the former one; i.e., it is capable of controlling phase independently the MMC state variables. However, the new circulating current reference will ensure constant power P_{dc} at all times, even if this means sacrificing fast *phase independent control* dynamics when unbalanced grid conditions take place. Although strategies that ensured constant P_{dc} could already be found in the literature [33, 32, 34, 35, 36, 94], they were based on dqo or $\alpha\beta o$ coordinates. This strategy stemmed from the need for achieving the same results in abc coordinates to be able to regulate the phase variables of the MMC while coping with unbalanced grid conditions.

This new circulating current reference formulation offers the new possibility of directly establishing the primary power reference of the system at the DC terminals of the MMC P_{dc}^{ref} using the circulating currents, instead of establishing it at the point of common coupling P_{ac}^{ref} by means of the grid current. This new possibility will prevent both steady state and transient state power fluctuations or perturbations from the grid from having any influence whatsoever on the power at the DC terminals of the MMC. Thus, the MMC can be controlled to act as a “power oscillation firewall” where the distributed capacitance of the MMC topology is controlled to effectively decouple the power flow in the AC and DC sides. Such operation of the MMC can be especially relevant for (multi-terminal) HVDC systems where power fluctuations and thus DC voltage fluctuations are to be avoided, since they will negatively influence other converters connected to the same DC network. Another potential application could lie in hybrid HVDC links; i.e., when the MMC is connected to a Current Source Converter (CSC), because the MMC is controlled as a stiff DC current source with this technique.

In addition, insight into the MMC operation was given through an analysis in which three different types of grid current control strategies were implemented along with the new circulating current control equation for *constant DC power control* obtained as a result of mathematical optimization. Such grid control strategies are capable of ensuring one of the following performances under unbalanced conditions: 1) balanced sinusoidal grid currents, 2) constant instantaneous active power with unbalanced sinusoidal grid currents, and 3) constant reactive power with unbalanced sinusoidal grid currents. The analysis showed that regardless of the grid current strategy used, the MMC controllability and distributed storage capacity were able to prevent the power fluctuations of the AC grid from appearing in the DC terminals of the converter. It was also proven that the oscillations in the voltage of the MMC capacitors were reduced the most when the constant reactive power grid current control strategy was implemented. This control strategy will therefore have an important consequence on the size of the capacitors.

To summarize, two circulating current reference equations in the abc frame are proposed with two different control objectives: *Phase Independent Control*, and *Constant DC Power Control* suitable for unbalanced grid conditions. Both strategies are able to regulate the capacitive energy in each arm in phase coordinates and result from solving two different analytical optimization problems using Lagrange multipliers. Proportional resonant controllers are used to successfully implement these references in the MMC. Moreover, the implementation of such a control strategy is independent of both the model and parameter uncertainties.

7.1.2 On stability issues and non-linear control proposal

An inconvenience of linear controllers, like the ones used to effectively implement the proposed circulating current reference, is that they fail to ensure global asymptotic stability; in other words the converter will always converge to its desired equilibrium independent of its operating point.

Nonetheless, [31, 88] proved using Lyapunov's stability criteria that the system under open loop control remains globally asymptotically stable. Such proof is reviewed in appendix B, and expanded to the case of three-phase MMC-VSC converters where neither DC voltage nor the grid currents were considered as perturbations; instead they were considered state variables, and the relationship between the phases was taken into account. Nonetheless, several issues seem to appear using open loop control for global asymptotic stability:

- Due to the inherent absence of feedback loops in a open loop control, the system performance is subject to parameter variations, error in the estimation process and perturbations of any type. In other words, the controller is not *robust*.
- The dynamics of the converter are set by the natural time constants of the system, also due to the absence of a feedback loop.
- Lyapunov's stability proof is only valid for the system under study. This directly implies that it will be very complicated to use Lyapunov's criteria to prove global asymptotic stability for large and complex interconnected systems such as the future *SuperGrid*.

Following the above discussion, a robust local approach over a global one was needed. In order to address this issue, passive system theory was used instead. Passivity is a characterization of the system behavior based on energy, and it can be used to assess the stability of a single system. Most importantly, the negative feedback combination of two passive systems results in a passive and stable interconnection. Therefore, the idea of making multi-terminal MMC-HVDC systems based on local passivity controllers for ensuring global asymptotic stability of the much larger system may be considered as one of the contributions of this manuscript.

A passivity-based controller was therefore needed for the MMC. The main priority was to facilitate the implementation of the controller regardless of the complexity of the proof; therefore, the passivity control technique selected was a simple PI controller, which is widely accepted by practitioners in the field. The PI controller will regulate two signals for which the incremental model of the MMC becomes passive, thus ensuring stability. Such a technique, presented in [90, 91, 92, 93], did not suffice since it was designed to solve a *regulation* problem; i.e., to regulate the state variables to a desired equilibrium point. Because of the *abc* control philosophy discussed and emphasized in this work, the desired equilibrium was not a point but an orbit or a trajectory, due to the sinusoidal nature of the signals in steady state. Hence, the passivity-based PI controller that solved the *regulation* problem was extrapolated to the *tracking* one thanks to the work carried out with Prof. Romeo Ortega from *Laboratoire des Signaux et des Systèmes (L2S)*.

In order to successfully apply the novel passivity-based PI controller to the MMC, one must estimate with great accuracy the equilibrium orbit that will act as the MMC state variable references. Such estimation depends on the system model, and thus will be subject to parameter uncertainties and the level of accuracy of the model. However, this work can be extended to overcome this feature using adaptive PI controllers following the procedure detailed in [93]. The estimation technique used in the well known Open Loop Control of [29, 31] neglects the losses in the MMC internal resistance, and hence fails to estimate the state variables of MMC when such resistance is not neglectful. The last contribution of this manuscript deals with this issue using a virtual energy model of the MMC along with both of the circulating current reference equations calculated via mathematical optimization for the linear controller to estimate the state variables of the MMC. Since any of the two equations can be used in the estimation process, the resulting non-linear controller may also address either *phase independent control* or *constant DC power control* suited for unbalanced conditions.

7.2 Future research

Several topics can be relevant for further studies and research based on the results presented in this manuscript. Some ideas are detailed in the following section.

7.2.1 Minimizing the energy difference during unbalances

As mentioned earlier, it was found that the least voltage fluctuations in the MMC $2N$ capacitors occurred when the grid currents were used to control constant the instantaneous reactive power during unbalanced AC grid conditions. A strong relationship between the voltage fluctuations and the oscillation of the energy difference was effectively seen, and can easily be demonstrated mathematically. A question that remains to be answered is the following: could voltage oscillations be reduced even further than for the case of constant reactive power? Indeed, the Lagrange multiplier technique can be applied again to answer this question, although this time it is used to calculate the grid current reference that will produce minimal energy difference fluctuations $\Delta w_{\Delta k}$ during unbalances under the power transfer constraint of $P_{ac}^{ref} = \sum_{k \in abc} v_{pck} i_{vk}$.

7.2.2 Perspectives on weak grid operation of MMCs

Indeed, the use of adaptive filters based on second order generalized integrators significantly improved the dynamics of the linear controller as well as dependence on the distortion for MMCs with a low number of sub-modules. Nonetheless, they offer the possibility of making the system frequency-adaptive, which is particularly useful when operating the MMC in weak grids. However, this has yet to be demonstrated.

7.2.3 Improving the MMC state estimation

One of the main obstacles for successfully implementing passivity controllers was believed to be the accurate estimation of the MMC variables in steady state (x_*). By using a virtual model and the circulating current equations obtained via mathematical optimization, it was possible to reduce the error caused by neglecting the internal resistance of the MMC. Nonetheless, neither the losses caused by harmonic distortion nor the physical limits and saturation were considered in the estimation process, and these factors remain a source of error. Future work in this area may include better estimation techniques or the use of observers to reduce the remaining error.

7.2.4 Adaptive PI stabilization of the MMC

As discussed above, the non-linear controller is sensitive to the estimation of the equilibrium point. Assuming that such error will always exist for the case of the MMC, an alternative is to extend the proof based on the passivity theory presented in chapter A by including the adaptive property of the PI controllers following the work of [93], in order to make this control truly robust.

7.2.5 Control by interconnection applied to the MMC

In order to fully take advantage of the passivity property, the MMC-based multi-terminal grid scenario needs to be addressed. In such a scenario, each converter shall be controlled locally by the proposed passivity-based PI controller and the interconnection of the global network will remain stable. The complexity of this scenario may be increased by connecting different renewable energy sources that are in turn controlled using passivity theory in order to demonstrate that passivity could be a powerful tool for ensuring stability for the future *SuperGrid* in a modular way.

Appendices



Global Tracking Passivity-based PI Controller

This appendix deals with the problem of trajectory tracking of a class of power converters, in which the MMC takes part. To analyze the stability of these systems it has been considered the bi-linear structure they admit. First, the theoretical framework for which it is possible to ensure global tracking of trajectories is proposed. To do so, a construction of an output signal respect to which the incremental model becomes passive is carried out. This leads to a simple linear PI controller for the plant.

A.1 Introduction

In the literature the tracking problem for converters has been addressed employing a variety of control techniques. In [95] a methodology to track periodic signals for non-minimum phase boost converters based on a stable inversion of the internal dynamics taking the normal form of an Abel ordinary differential equation was presented—see also [96]. There are also schemes involving sliding mode control, for example [97, 98, 99], and references therein. In [100] the well-known passivity property of [91] is used to address an “approximate” tracking problem for an inverter connected to a photovoltaic solar panel. However, one of the advantages of the present approach is the structure of the derived controller which is a PI.

The mathematical problem formulation is presented in Section A.2. The main result is contained in Section A.3, where a linear matrix inequality (LMI) condition is imposed to solve the tracking problem invoking passivity theory. Section A.4 is devoted to the synthesis of a PI controller where, under some detectability assumptions, ensures tracking trajectory. Finally, conclusions in Section A.5 complete this appendix.

A.2 Global tracking problem

Consider the bilinear system

$$\dot{x}(t) = Ax(t) + d(t) + \sum_{i=1}^m u_i(t)B_i x(t) \quad (\text{A.1})$$

where¹ $x, d \in \mathbb{R}^n$ are the state and the (measurable) disturbance vector, respectively, $u \in \mathbb{R}^m$, $m \leq n$, is the control vector, and $A, B_i \in \mathbb{R}^{n \times n}$ are real constant matrices.

Given an admissible, differentiable trajectory, that is a function $x_* : \mathbb{R}_+ \rightarrow \mathbb{R}^n$ verifying

$$\dot{x}_* = Ax_* + d + \sum_{i=1}^m u_i^* B_i x_* \quad (\text{A.2})$$

for some control signal $u_* : \mathbb{R}_+ \rightarrow \mathbb{R}^m$. Find, if possible, a dynamic state–feedback controller of the form

$$\dot{z} = F(x, x_*) \quad (\text{A.3})$$

$$u = H(x, x_*), \quad (\text{A.4})$$

where $F : \mathbb{R}^n \times \mathbb{R}^n \rightarrow \mathbb{R}^q$, $q \in \mathbb{Z}_+$, and $H : \mathbb{R}^n \times \mathbb{R}^n \rightarrow \mathbb{R}^m$, such that all signals remain bounded and

$$\lim_{t \rightarrow \infty} [x(t) - x_*(t)] = 0, \quad (\text{A.5})$$

for all initial conditions $(x(0), z(0)) \in \mathbb{R}^n \times \mathbb{R}^q$.

A set of matrices $\{A, B_i\}$ is characterized for which it is possible to solve the aforementioned global tracking problem with a simple *linear PI controller*. The class is identified via the following LMI.

Assumption 1 $\exists P \in \mathbb{R}^{n \times n}$, $P = P^\top > 0$ such that

$$\text{sym}(PA) \leq 0 \quad (\text{A.6})$$

$$\text{sym}(PB_i) = 0, \quad (\text{A.7})$$

where $\text{sym} : \mathbb{R}^{n \times n} \rightarrow \mathbb{R}^{n \times n}$ computes the symmetric part of the matrix.

To simplify the notation in the sequel we define the positive semidefinite matrix

$$Q := -\text{sym}(PA). \quad (\text{A.8})$$

A.3 Passivity of the bilinear incremental model

Instrumental to establish the main result of the previous section is the following lemma.

¹For brevity, in the sequel the time argument is omitted from all signals.

Lemma 1 Consider the system (A.1) verifying the LMI of Assumption 1 and an admissible trajectory x_* . Define the incremental signals

$$\tilde{(\cdot)} := (\cdot) - (\cdot)_*,$$

and the output function

$$y := \mathcal{C}(x_*)x \quad (\text{A.9})$$

where the map $\mathcal{C} : \mathbb{R}^n \rightarrow \mathbb{R}^{m \times n}$ is defined as

$$\mathcal{C} := \begin{bmatrix} x_*^\top B_1^\top \\ \vdots \\ x_*^\top B_m^\top \end{bmatrix} P.$$

The operator $\tilde{u} \mapsto y$ is passive with storage function

$$V(\tilde{x}) := \frac{1}{2} \tilde{x}^\top P \tilde{x}. \quad (\text{A.10})$$

Thus, the system verifies the dissipation inequality

$$\dot{V} \leq \tilde{u}^\top y.$$

Proof 1 Combining (A.1) and (A.2) yields

$$\dot{\tilde{x}} = \left(A + \sum_{i=1}^m u_i B_i \right) \tilde{x} + \sum_{i=1}^m \tilde{u}_i B_i x_*. \quad (\text{A.11})$$

Now, the time derivative of the storage function (A.10) along the trajectories of (A.11) is

$$\dot{V}(\tilde{x}) = \tilde{x}^\top P \left[\left(A + \sum_{i=1}^m u_i B_i \right) \tilde{x} + \sum_{i=1}^m \tilde{u}_i B_i x_* \right] \quad (\text{A.12})$$

$$= -\tilde{x}^\top Q \tilde{x} + \sum_{i=1}^m \tilde{u}_i \tilde{x}^\top P B_i x_* \quad (\text{A.13})$$

$$\leq \sum_{i=1}^m \tilde{u}_i \tilde{x}^\top P B_i x_* \quad (\text{A.14})$$

$$= \sum_{i=1}^m \tilde{u}_i x_*^\top P B_i x_* \quad (\text{A.15})$$

$$= y^\top \tilde{u}, \quad (\text{A.16})$$

where we have used (A.7) of Assumption 1 to get the second identity, (A.6) for the first inequality, (A.7) again for the third equation and (A.9) for the last identity.

A.4 A PI global tracking controller

From Lemma 1 the next corollary follows immediately.

Corollary 1 Consider the system (A.1) verifying the LMI of Assumption 1 and an admissible trajectory x_* in closed loop with the PI controller

$$\begin{aligned}\dot{z} &= -y \\ u &= -K_p y + K_i z + u_*\end{aligned}\tag{A.17}$$

with output (A.9) and $K_p = K_p^\top > 0$, $K_i = K_i^\top > 0$. For all initial conditions $(x(0), z(0)) \in \mathbb{R}^n \times \mathbb{R}^m$ the trajectories of the closed-loop system are bounded and

$$\lim_{t \rightarrow \infty} y_a(t) = 0,\tag{A.18}$$

where the augmented output $y_a : \mathbb{R}_+ \rightarrow \mathbb{R}^{m+n}$ is defined as

$$y_a := \begin{bmatrix} \mathcal{C} \\ Q \end{bmatrix} \tilde{x}.$$

Moreover if

$$\text{rank} \begin{bmatrix} \mathcal{C} \\ Q \end{bmatrix} \geq n,\tag{A.19}$$

then global tracking is achieved, i.e., (A.5) holds.

Proof 2 Notice that the PI controller (A.17) is equivalent to

$$\begin{aligned}\tilde{u} &= -K_p y + K_i z \\ \dot{z} &= -y.\end{aligned}\tag{A.20}$$

Propose the following radially unbounded Lyapunov function candidate

$$W(\tilde{x}, z) := V(\tilde{x}) + \frac{1}{2} z^\top K_i z,$$

whose time derivative is

$$\begin{aligned}\dot{W} &= -\tilde{x}^\top Q \tilde{x} + y^\top \tilde{u} - z^\top K_i y \\ &= -\tilde{x}^\top Q \tilde{x} - y^\top K_p y\end{aligned}$$

which proves, via La Salle's invariance, principle [89] that (A.18) holds. The proof is completed noting that the latter convergence property ensures (A.5) if the rank condition (A.19) holds.

Remark 1 Notice that the matrix \mathcal{C} depends on the reference trajectory. Therefore, the rank condition (A.19) identifies a class of trajectories for which global tracking is ensured.

Remark 2 Condition (A.19) is sufficient, but not necessary for state convergence. Indeed, as shown in [101], global tracking is guaranteed if y_a is a detectable output for the closed-loop system. That is, if the following implication holds

$$y_a(t) \equiv 0 \implies \lim_{t \rightarrow \infty} [x(t) - x_*(t)] = 0.$$

A.5 Conclusions

Global asymptotic stability is ensured with a simple PI regulating the MMC passive outputs to zero. The obtained stability results are global and hold for all positive definite gains of the PI.

B

Lyapunov's Global Asymptotic Stability Proof

In this appendix, the global asymptotic stability proof for Modular Multilevel Converters is reviewed and extended to the case where a three phase configuration of the MMC provides support for the DC voltage regulation, and considering the grid currents as state variables.

B.1 Introduction

IN chapters 3, 4 and 5 of this Thesis manuscript, a strategy to calculate the Modular Multilevel Converter circulating current reference was derived considering both, phase independent energy regulation and the relationship between phases for constant power at the DC terminals. By means of two current control loops, such references were imposed and the MMC appeared to work in a stable way for the operating conditions selected. This means that the voltage sum of the upper and lower capacitors were successfully regulated to converge asymptotically to their desired equilibrium values, as well as the circulating and grid currents. Nonetheless, there is a clear interest for the MMC to work in a stable way for *any operating point*, within its physical limits. In order to guaranty such *global asymptotic stability*, and given the strong non-linear nature of the converter, linear techniques based on eigenvalues will not suffice. Thus Lyapunov global asymptotic stability proof, suitable for non-linear systems, is used instead.

Such issue has already been addressed by Antonopoulos *et al.* in [31] where global asymptotic stability for the single-phase MMC internal variables under open loop control was proven using this methodology. Later on, Harnefors *et al.* extrapolated those results in [88], where they proved that when closed loop current control was implemented, and under the presence of measurement delays, the MMC remained globally asymptotically stable. Even though their results are remarkable and of high impact in the field, the MMC system under study was not a three-phase voltage source converter; i.e., the relationship among phases was not considered, the voltage between the DC terminals of the MMC was taken as a constant, and the grid current was considered as a perturbation. In the present appendix, that missing gap was fulfilled: the proof was extrapolated

to the 3-phase VSC-MMC, since for the promising HVdc multiterminal application, the MMC will have to be capable of contributing to the DC link voltage regulation of the entire DC-grid, while regulating its stored energy, by means of the control of both the grid and circulating currents. A new Lyapunov candidate function is therefore required since the dynamical system has changed from the one studied in [31, 88]. Two new state variables have been added (v_{dc} and i_{vk}) and the relationship between phases has now to be considered.

This present appendix is organized as follows: In section B.2, the internal dynamics of the MMC converter are briefly revisited, as well as its control equations. In section B.3, the global asymptotic stability proof made by Antonopoulos *et al.* in [31] is detailed, in order to set the base for the rest of the sections. Such proof is valid for the internal MMC variables i_{ck} , u_{cuk}^Σ and u_{clk}^Σ for each phase of the converter considered independently. In section B.4, the results of Antonopoulos *et al.* are extrapolated to fit the MMC acting as a voltage source. Finally, some conclusions highlighting the drawbacks of this methodology and the need for a modular and robust approach for *SuperGrid* applications is given in B.5.

B.2 Revisiting the MMC equations

This section recalls both, the MMC internal state equations and the equations of the MMC internal voltages that drive the circulating and grid currents as they were presented in [3, 7].

B.2.1 State equations

The first three equations represent the dynamics of the converter internal variables, such as the circulating current i_{ck} , and sum of the capacitor voltages of the upper u_{cuk}^Σ and lower u_{clk}^Σ group of sub-modules or multi-valves. In addition, (B.4) represents the dynamics of the grid current.

$$\frac{di_{ck}}{dt} = -\frac{R}{L}i_{ck} - \frac{1}{2L}(n_{uk}u_{cuk}^\Sigma + n_{lk}u_{cl}^\Sigma) + \frac{v_{dc}}{2L} \quad (\text{B.1})$$

$$\frac{du_{cuk}^\Sigma}{dt} = \frac{Nn_{uk}\left(i_{ck} + \frac{i_{vk}}{2}\right)}{C} \quad (\text{B.2})$$

$$\frac{du_{clk}^\Sigma}{dt} = \frac{Nn_{lk}\left(i_{ck} - \frac{i_{vk}}{2}\right)}{C} \quad (\text{B.3})$$

$$\frac{di_{vk}}{dt} = \frac{n_{lk}u_{clk}^\Sigma - n_{uk}u_{cuk}^\Sigma}{2L'} - \frac{R'}{L'}i_{vk} - V_{pck} \quad (\text{B.4})$$

B.2.2 Control equations

Let u_{ck}^* be the reference voltage that drives the circulating current i_{ck} to i_{ck}^* , as follows:

$$u_{ck}^* = L\frac{di_{ck}^*}{dt} + Ri_{ck}^* = \frac{v_{dc}}{2} - \frac{n_{uk}u_{cuk}^{\Sigma*} + n_{lk}u_{clk}^{\Sigma*}}{2} \quad (\text{B.5})$$

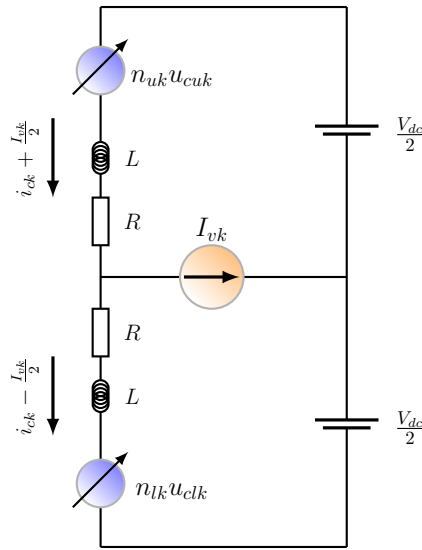


Figure B.1: Single phase MMC with I_{vk} and V_{dc} considered as perturbations

In a similar fashion, e_{vk}^* is the reference voltage that drives the load current i_{vk} to i_{vk}^* :

$$e_{vk}^* = \left(\frac{L}{2} + L_f \right) \frac{di_{vk}^*}{dt} + \left(\frac{R}{2} + R \right) i_{vk}^* + V_{pcck} = \frac{n_{lk}u_{clk}^{\Sigma^*} - n_{uk}u_{cuk}^{\Sigma^*}}{2} \quad (\text{B.6})$$

Finally, the insertion indexes for the upper and lower arms are calculated as follows:

$$n_{uk} = \frac{\frac{V_{dc}}{2} - e_{vk}^* - u_{ck}^*}{u_{cuk}^{\Sigma^*}} \quad (\text{B.7})$$

$$n_{lk} = \frac{\frac{V_{dc}}{2} - e_{vk}^* - u_{ck}^*}{u_{clk}^{\Sigma^*}} \quad (\text{B.8})$$

B.3 Single-phase MMC stability proof

In this section the demonstration of the global asymptotic stability of the internal variables of a single-phase MMC is revisited. As was mentioned in the introduction, such theoretical result was presented by Antonopoulos *et al.* in [31]. Nonetheless, knowledge of such procedure is required for the rest of the appendix. The system under study is a single-phase MMC, assuming a perfect balancing strategy among the arm capacitors. Furthermore, a constant voltage source is assumed to be between the DC terminals of the MMC, while a sinusoidal current source is imposing the grid current. This means, that both the DC voltage v_{dc} and the grid current i_{vk} are not considered as state variables in this section yet as perturbations. In Fig. (B.1) is depicted the equivalent MMC circuit under study. Another important consideration is that even if only open-loop control was considered in [31], the same proof is valid for a closed-loop current control; i.e., controllers that use the measured circulating current, as long as it is assumed that there is no lag due to the measurement ($i_c^{measured} = i_{ck}$). Refer to the article by Harnefors *et al.* [88] for the proof including the measurement lag.

B.3.1 Deviation variables equation system

Since the DC voltage and the grid current are considered as perturbations in this analysis, the only three state variables needed for the stability proof are those of i_{ck} , u_{cuk} and u_{clk} . However, it is necessary to work with their respective deviation quantities, so that the equilibrium point will be the origin, instead of the reference values of i_{ck}^* , $u_{cuk}^{\Sigma^*}$ and $u_{clk}^{\Sigma^*}$. Therefore, the deviation quantities are defined as

$$\tilde{i}_{ck} = i_{ck} - i_{ck}^* \quad (\text{B.9})$$

$$\tilde{u}_{cuk}^{\Sigma} = u_{cuk}^{\Sigma} - u_{cuk}^{\Sigma^*} \quad (\text{B.10})$$

$$\tilde{u}_{clk}^{\Sigma} = u_{clk}^{\Sigma} - u_{clk}^{\Sigma^*} \quad (\text{B.11})$$

Introducing the deviation quantities in (B.1),(B.2) and (B.3) gives

$$\frac{d\tilde{u}_{cuk}^{\Sigma}}{dt} = \frac{dv_{cuk}^{\Sigma}}{dt} - \frac{d\tilde{u}_{cuk}^{\Sigma^*}}{dt} = \frac{N}{C}n_{uk} \left(\frac{i_{vk}}{2} + i_{ck} \right) - \frac{C}{N}n_{uk} \left(\frac{i_{vk}}{2} + i_{ck}^* \right) = \frac{N}{C}n_{uk}\tilde{i}_{ck} \quad (\text{B.12})$$

$$\frac{d\tilde{u}_{clk}^{\Sigma}}{dt} = \frac{dv_{clk}^{\Sigma}}{dt} - \frac{d\tilde{u}_{clk}^{\Sigma^*}}{dt} = \frac{N}{C}n_{lk} \left(\frac{-i_{vk}}{2} + i_{ck} \right) - \frac{C}{N}n_{lk} \left(\frac{-i_{vk}}{2} + i_{ck}^* \right) = \frac{N}{C}n_{lk}\tilde{i}_{ck} \quad (\text{B.13})$$

$$\frac{d\tilde{i}_{ck}}{dt} = \frac{-1}{2L} (n_{uk}u_{cuk}^{\Sigma} + n_{lk}u_{clk}^{\Sigma}) + \frac{v_{dc}}{2L} - \frac{R}{L}i_{ck} - \frac{di_{ck}^*}{dt} \quad (\text{B.14})$$

Replacing $\frac{di_{ck}^*}{dt}$ by $\frac{u_{ck}^*}{L} - \frac{R}{L}i_{ck}^*$ in (B.14), and re-writing the variables using the deviation quantities gives:

$$\begin{aligned} \frac{d\tilde{i}_{ck}}{dt} &= \frac{-1}{2L} [n_{uk}(\tilde{u}_{cuk}^{\Sigma} + u_{cuk}^{\Sigma^*}) + n_{lk}(\tilde{u}_{clk}^{\Sigma} + u_{clk}^{\Sigma^*})] + \frac{v_{dc}}{2L} - \frac{R}{L}i_{ck} - \frac{di_{ck}^*}{dt} \\ &= \frac{-1}{2L} (n_{uk}\tilde{u}_{cuk}^{\Sigma} + n_{lk}\tilde{u}_{clk}^{\Sigma}) + \frac{u_{ck}^*}{L} - \frac{R}{L}i_{ck} - \left(\frac{u_{ck}^*}{L} - \frac{R}{L}i_{ck}^* \right) \\ &= \frac{-1}{2L} (n_{uk}\tilde{u}_{cuk}^{\Sigma} + n_{lk}\tilde{u}_{clk}^{\Sigma}) + \frac{R}{L}(i_{ck}^* - i_{ck}) \\ &= \frac{-1}{2L} (n_{uk}\tilde{u}_{cuk}^{\Sigma} + n_{lk}\tilde{u}_{clk}^{\Sigma}) - \frac{R}{L}(\tilde{i}_{ck}) \end{aligned} \quad (\text{B.15})$$

It is possible to see that u_{ck}^* is removed from (B.15), and does not appear neither in (B.12) nor in (B.13). Hence, the proof is valid independently of the open or closed loop nature of the controller, as long as no measurement delay is considered.

The dynamic system of the deviation quantities can be rewritten in state-space as ([31]):

$$\dot{\tilde{x}} = \frac{d}{dt} \begin{bmatrix} \tilde{i}_{ck} \\ \tilde{u}_{cuk}^{\Sigma} \\ \tilde{u}_{cl}^{\Sigma} \end{bmatrix} = \begin{bmatrix} -\frac{R}{L} & -\frac{n_{uk}}{2L} & \frac{-n_{lk}}{2L} \\ \frac{Nn_{uk}}{C} & 0 & 0 \\ \frac{Nn_{lk}}{C} & 0 & 0 \end{bmatrix} \begin{bmatrix} \tilde{i}_{ck} \\ \tilde{u}_{cuk}^{\Sigma} \\ \tilde{u}_{cl}^{\Sigma} \end{bmatrix} \quad (\text{B.16})$$

B.3.2 Global asymptotic stability

The origin point of \tilde{x} is clearly the equilibrium point, which would imply that $i_{ck} \rightarrow i_{ck}^*$, $u_{cuk}^{\Sigma} \rightarrow u_{cuk}^{\Sigma^*}$ and $u_{clk}^{\Sigma} \rightarrow u_{clk}^{\Sigma^*}$.

Theorem

The MMC deviation system expressed in B.16 is globally asymptotically stable about the origin if $R > 0$.

Proof

A candidate Lyapunov function is defined as follows:

$$V = L (\tilde{i}_{ck})^2 + \frac{1}{2} \frac{C}{N} (\tilde{u}_{cuk}^\Sigma)^2 + \frac{1}{2} \frac{C}{N} (\tilde{u}_{clk}^\Sigma)^2 \quad (\text{B.17})$$

It can be seen from (B.17) that V is a continuously differentiable positive definite function. It is defined as $V : \mathfrak{R}^3 \rightarrow \mathfrak{R}$, it is radially unbounded, and it is equal to zero only at the equilibrium point [31]. Differentiating (B.17) yields

$$\dot{V} = 2L\tilde{i}_{ck} \frac{d\tilde{i}_{ck}}{dt} + \frac{C}{N} \tilde{u}_{cuk}^\Sigma \frac{d\tilde{u}_{cuk}^\Sigma}{dt} + \frac{C}{N} \tilde{u}_{clk}^\Sigma \frac{d\tilde{u}_{clk}^\Sigma}{dt} \quad (\text{B.18})$$

Multiplying (B.15) by $L\tilde{i}_{ck}$ results in

$$L\tilde{i}_{ck} \frac{d\tilde{i}_{ck}}{dt} = -\frac{1}{2L} (n_{uk}\tilde{i}_{ck}\tilde{u}_{cuk}^\Sigma + n_{lk}\tilde{i}_{ck}\tilde{u}_{clk}^\Sigma) - \frac{R}{L} (\tilde{i}_{ck})^2 \quad (\text{B.19})$$

Replacing (B.12) and (B.13) in (B.19) yields

$$L\tilde{i}_{ck} \frac{d\tilde{i}_{ck}}{dt} = -\frac{C}{2NL} \left(\tilde{u}_{cuk}^\Sigma \frac{d\tilde{u}_{cuk}^\Sigma}{dt} + \tilde{u}_{clk}^\Sigma \frac{d\tilde{u}_{clk}^\Sigma}{dt} \right) - \frac{R}{L} (\tilde{i}_{ck})^2 \quad (\text{B.20})$$

Finally, by replacing (B.20) in (B.18) results in

$$\dot{V} = -2R (\tilde{i}_{ck})^2 \quad (\text{B.21})$$

Since $\dot{V} \leq 0$ if $R > 0$, V is a Lyapunov function implying that the deviation system (B.16) is globally stable [31]. Nonetheless, \dot{V} is only negative semidefinite, implying that V is not a strict Lyapunov function, which means that asymptotic stability is not yet proven. For completing the proof, LaSalle's invariance principle is applied.

- $\dot{V} = -R (\tilde{i}_{ck})^2$ implies that \tilde{i}_{ck} converges asymptotically to zero.
- $\tilde{i}_{ck} \equiv 0$ is replaced in (B.12), (B.13) and (B.15), in order to verify if \tilde{u}_{cuk}^Σ and \tilde{u}_{clk}^Σ converge to 0. This results in

$$\frac{d\tilde{u}_{cuk}^\Sigma}{dt} \equiv 0 \quad (\text{B.22})$$

$$\frac{d\tilde{u}_{clk}^\Sigma}{dt} \equiv 0 \quad (\text{B.23})$$

$$n_{uk}\tilde{u}_{cuk}^\Sigma + n_{lk}\tilde{u}_{clk}^\Sigma \equiv 0 \quad (\text{B.24})$$

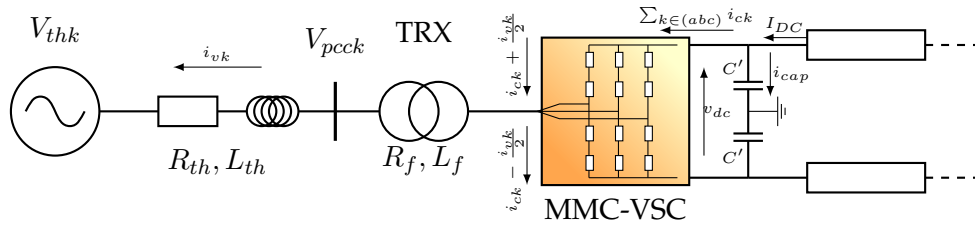


Figure B.2: Three-phase MMC acting as a voltage source

- The first two equations imply that both u_{cuk}^{Σ} and u_{clk}^{Σ} are constant.
- n_{uk} and n_{lk} are time varying and not linearly related. Therefore the only constant that satisfies (B.24) is $\tilde{u}_{cuk}^{\Sigma} = \tilde{u}_{clk}^{\Sigma} = 0$.

Therefore, it is possible to conclude that the origin is globally asymptotically stable for the deviation system (B.16) if $R > 0$.

B.4 Three-phase voltage source MMC stability proof

This section represents one of the scientific contributions of this Thesis. It stems from the need of verifying if the proof of global asymptotic stability regarding the MMC internal dynamics (made by [31] and revisited in the previous section) can be extrapolated to the case where the MMC is acting as a three-phase voltage source controller as depicted in Fig. B.2, aiming for multi-terminal hvdc (MTDC) application. In future MTDC systems, several 3-phased MMCs' will have to share the task of regulating the DC voltage of the MTDC network, therefore they will have to be able to perform as voltage source converters, whilst being able to regulate the distribution of their internal energy.

This implies that the voltage between the DC terminals of the MMC v_{dc} will be a state variable, and it should be controlled to reach its desired equilibrium point v_{dc}^* , provided by the secondary control loop. In addition, the new state variable v_{dc} depends on the relationship between the MMC phases, instead of considering them independently like in the previous section. Finally, the grid current i_{vk} is now considered as a state variable as well, for an expected task of the VSC is to regulate the AC grid active and reactive power.

B.4.1 Deviation equations

For the voltage source MMC, the deviation equations of the previous section are no longer valid, since two new variables have been added (v_{dc} and i_{vk}) and the relationship between the three-phases must now be considered. The derivation of such new equations is given below.

The DC voltage equation

Applying Kirchoff's node equation at the DC terminals of the voltage source MMC depicted in Fig. B.2 yields

$$I_{DC} = \frac{C'}{2} \frac{dv_{dc}}{dt} + \sum_{k \in (abc)} (i_{ck} + i_{vk}) \quad (\text{B.25})$$

If we assume no return wire for the grid currents, then $\sum_{k \in (abc)} i_{vk} = 0$. Rewriting v_{dc} and i_{ck} of (B.25) as a function of its deviation quantities yields in

$$\frac{C'}{2} \frac{d\tilde{u}_{dc}}{dt} = I_{DC} - \sum_{k \in (abc)} \tilde{i}_{ck} - \sum_{k \in (abc)} i_{ck}^* - \frac{dv_{dc}^*}{dt} \quad (\text{B.26})$$

Since the desired equilibrium point of the DC voltage v_{dc}^* is constant, $\frac{dv_{dc}^*}{dt} = 0$ and by consequence $I_{DC} = \sum_{k \in (abc)} i_{ck}^*$. Therefore, (B.26) may be expressed as

$$\frac{C'}{2} \frac{d\tilde{u}_{dc}}{dt} = - \sum_{k \in (abc)} \tilde{i}_{ck} \quad (\text{B.27})$$

The capacitor voltage equations

Not only the internal dynamics of the MMC are being considered, yet the dynamics of the whole three phased MMC acting as a Voltage Source Converter, implying that the equations (B.12) and (B.13) must be modified to take into account the grid currents as a variable and not as a perturbation as was done in the previous section.

$$\begin{aligned} \frac{d\tilde{u}_{cuk}^{\Sigma}}{dt} &= \frac{d(v_{cuk} - \tilde{u}_{cuk}^{\Sigma*})}{dt} = \frac{N}{C} n_{uk} \left(i_{ck} + \frac{i_{vk}}{2} \right) - \frac{C}{N} n_{uk} \left(i_{ck}^* + \frac{i_{vk}^*}{2} \right) \\ &= \frac{N}{C} n_{uk} \left(\tilde{i}_{ck} + \frac{\tilde{i}_{vk}}{2} \right) \end{aligned} \quad (\text{B.28})$$

$$\begin{aligned} \frac{d\tilde{u}_{cll}^{\Sigma}}{dt} &= \frac{d(v_{cll} - \tilde{u}_{cll}^{\Sigma*})}{dt} = \frac{N}{C} n_{lk} \left(i_{ck} - \frac{i_{vk}}{2} \right) - \frac{C}{N} n_{lk} \left(i_{ck}^* - \frac{i_{vk}^*}{2} \right) \\ &= \frac{N}{C} n_{lk} \left(\tilde{i}_{ck} - \frac{\tilde{i}_{vk}}{2} \right) \end{aligned} \quad (\text{B.29})$$

The circulating current equation

The circulating current deviation equation will slightly change from (B.15) since now the voltage on the DC terminals of the MMC is considered as a state variable instead of a perturbation.

$$\begin{aligned}
 \frac{d\tilde{i}_{ck}}{dt} &= \frac{-1}{2L} [n_{uk} (\tilde{u}_{cuk}^\Sigma + u_{cuk}^{\Sigma*}) + n_{lk} (\tilde{u}_{clk}^\Sigma + u_{clk}^{\Sigma*})] + \frac{(\tilde{u}_{dc} + v_{dc}^*)}{2} - \frac{R}{L} i_{ck} - \frac{di_{ck}^*}{dt} \\
 &= \frac{-1}{2L} (n_{uk} \tilde{u}_{cuk}^\Sigma + n_{lk} \tilde{u}_{clk}^\Sigma) + \frac{\tilde{u}_{dc}}{2} + \frac{u_{ck}^*}{L} - \frac{R}{L} i_{ck} - \left(\frac{u_{ck}^*}{L} - \frac{R}{L} i_{ck}^* \right) \\
 &= \frac{-1}{2L} (n_{uk} \tilde{u}_{cuk}^\Sigma + n_{lk} \tilde{u}_{clk}^\Sigma) + \frac{\tilde{u}_{dc}}{2} + \frac{R}{L} (i_{ck}^* - i_{ck}) \\
 &= \frac{-1}{2L} (n_{uk} \tilde{u}_{cuk}^\Sigma + n_{lk} \tilde{u}_{clk}^\Sigma) + \frac{\tilde{u}_{dc}}{2} - \frac{R}{L} (\tilde{i}_{ck})
 \end{aligned} \tag{B.30}$$

The grid current equation

Unlike the the previous section, the grid current is now a state variable. Therefore it is necessary to obtain its corresponding deviation equation. The grid current dynamics are represented by (B.4). By expressing the state variables as a function of their deviation quantities and equilibrium points, (B.4) may be rewritten as

$$\begin{aligned}
 \frac{L' d\tilde{i}_{vk}}{dt} &= \frac{n_{lk} (\tilde{u}_{clk}^\Sigma + u_{clk}^{\Sigma*}) - n_{uk} (\tilde{u}_{cuk}^\Sigma + u_{cuk}^{\Sigma*})}{2} - R' \tilde{i}_{vk} - R' i_{vk}^* - V_{pcck} - \frac{L' di_{vk}^*}{dt} \\
 &= \frac{n_{lk} \tilde{u}_{clk}^\Sigma - n_{uk} \tilde{u}_{cuk}^\Sigma}{2} - R' \tilde{i}_{vk} + \frac{n_{lk} u_{clk}^{\Sigma*} - n_{uk} u_{cuk}^{\Sigma*}}{2} - R' i_{vk}^* - V_{pcck} - \frac{L' di_{vk}^*}{dt}
 \end{aligned} \tag{B.31}$$

Since e_{vk}^* can be written as both: as (B.6) or as $\frac{n_{lk} u_{clk}^{\Sigma*} - n_{uk} u_{cuk}^{\Sigma*}}{2}$, (B.31) is expressed as

$$\frac{L' d\tilde{i}_{vk}}{dt} = \frac{n_{lk} \tilde{u}_{clk}^\Sigma - n_{uk} \tilde{u}_{cuk}^\Sigma}{2} - R' \tilde{i}_{vk} \tag{B.32}$$

Deviation equation system

The dynamic system of the deviation quantities representing a MMC in a Voltage Source Converter configuration is written in state-space as follows:

$$\frac{d\tilde{i}_{ck}}{dt} = \frac{-1}{2L} (n_{uk} \tilde{u}_{cuk}^\Sigma + n_{lk} \tilde{u}_{clk}^\Sigma) + \frac{\tilde{u}_{dc}}{2} - \frac{R}{L} (\tilde{i}_{ck}) \tag{B.33}$$

$$\frac{d\tilde{i}_{vk}}{dt} = \frac{n_{lk} \tilde{u}_{clk}^\Sigma - n_{uk} \tilde{u}_{cuk}^\Sigma}{2L'} - \frac{R'}{L'} \tilde{i}_{vk} \tag{B.34}$$

$$\frac{d\tilde{u}_{cuk}^\Sigma}{dt} = \frac{N}{C} n_{uk} \left(\tilde{i}_{ck} + \frac{\tilde{i}_{vk}}{2} \right) \tag{B.35}$$

$$\frac{d\tilde{u}_{clk}^\Sigma}{dt} = \frac{N}{C} n_{lk} \left(\tilde{i}_{ck} - \frac{\tilde{i}_{vk}}{2} \right) \tag{B.36}$$

$$\frac{d\tilde{u}_{dc}}{dt} = -\frac{2}{C'} \sum_{k \in (abc)} \tilde{i}_{ck} \tag{B.37}$$

B.4.2 Global asymptotic stability

Having the new deviation equation system of the voltage source MMC, it is possible to prove global asymptotic stability.

Theorem

The three phase voltage source modular multilevel converter deviation system expressed above is globally asymptotically stable about the origin if $R > 0$ and $R' > 0$.

Proof

A candidate Lyapunov function is defined as follows:

$$V = \sum_{k \in (abc)} \left[L (\tilde{i}_{ck})^2 + \frac{1}{2} L' (\tilde{i}_{vk})^2 + \frac{1}{2} \frac{C}{N} (\tilde{u}_{cuk}^\Sigma)^2 + \frac{1}{2} \frac{C}{N} (\tilde{u}_{clk}^\Sigma)^2 \right] + \frac{C'}{4} (\tilde{u}_{dc})^2 \quad (\text{B.38})$$

It can be seen from (B.38) that V is a continuously differentiable positive definite function. It is defined as $V : \mathfrak{R}^{13} \rightarrow \mathfrak{R}$, it is radially unbounded, and it is equal to zero only at the equilibrium point. Differentiating (B.38) yields

$$\dot{V} = \sum_{k \in (abc)} \left[2L \tilde{i}_{ck} \frac{d\tilde{i}_{ck}}{dt} + L' \tilde{i}_{vk} \frac{d\tilde{i}_{vk}}{dt} + \frac{C}{N} \tilde{u}_{cuk}^\Sigma \frac{d\tilde{u}_{cuk}^\Sigma}{dt} + \frac{C}{N} \tilde{u}_{clk}^\Sigma \frac{d\tilde{u}_{clk}^\Sigma}{dt} \right] + \frac{C'}{2} \tilde{u}_{dc} \frac{d\tilde{u}_{dc}}{dt} \quad (\text{B.39})$$

Multiplying (B.33) by \tilde{i}_{ck} results in

$$L \tilde{i}_{ck} \frac{d\tilde{i}_{ck}}{dt} + R (\tilde{i}_{ck})^2 = -\frac{n_{uk} \tilde{i}_{ck} u_{cuk}^\Sigma}{2} - \frac{n_{lk} \tilde{i}_{ck} u_{clk}^\Sigma}{2} + \frac{\tilde{u}_{dc}}{2} \tilde{i}_{ck} \quad (\text{B.40})$$

Multiplying (B.34) by $\frac{\tilde{i}_{vk}}{2}$ yields

$$L' \tilde{i}_{vk} \frac{d\tilde{i}_{vk}}{dt} + \frac{R'}{2} (\tilde{i}_{vk})^2 = \frac{n_{lk} \tilde{i}_{vk} \tilde{u}_{clk}^\Sigma}{4} - \frac{n_{uk} \tilde{i}_{vk} \tilde{u}_{cuk}^\Sigma}{4} \quad (\text{B.41})$$

Adding (B.40) with (B.41) gives

$$\begin{aligned} L \tilde{i}_{ck} \frac{d\tilde{i}_{ck}}{dt} + L' \tilde{i}_{vk} \frac{d\tilde{i}_{vk}}{dt} &= -\frac{n_{uk}}{2} \left(\tilde{i}_{ck} + \frac{\tilde{i}_{vk}}{2} \right) \tilde{u}_{cuk}^\Sigma - \frac{n_{lk}}{2} \left(\tilde{i}_{ck} - \frac{\tilde{i}_{vk}}{2} \right) \tilde{u}_{clk}^\Sigma \\ &\quad - R (\tilde{i}_{ck})^2 - \frac{R'}{2} (\tilde{i}_{vk})^2 + \tilde{u}_{dc} \tilde{i}_{ck} \end{aligned} \quad (\text{B.42})$$

Replacing (B.35) and (B.36) in (B.42) produces

$$\begin{aligned} L\tilde{i}_{ck} \frac{d\tilde{i}_{ck}}{dt} + L' \frac{\tilde{i}_{vk}}{2} \frac{d\tilde{i}_{vk}}{dt} = & -\frac{C}{2N} \tilde{u}_{cuk} \frac{d\tilde{u}_{cuk}^\Sigma}{dt} - \frac{C}{2N} \tilde{u}_{clk} \frac{d\tilde{u}_{clk}^\Sigma}{dt} - R(\tilde{i}_{ck})^2 \\ & - \frac{R'}{2} (\tilde{i}_{vk})^2 + \tilde{u}_{dc} \tilde{i}_{ck} \end{aligned} \quad (\text{B.43})$$

Adding up (B.43) for all three phases gives rise to

$$\begin{aligned} \frac{\tilde{u}_{dc}}{2} \sum_{k \in (abc)} \tilde{i}_{ck} = & \sum_{k \in (abc)} \left[L\tilde{i}_{ck} \frac{d\tilde{i}_{ck}}{dt} + L' \frac{\tilde{i}_{vk}}{2} \frac{d\tilde{i}_{vk}}{dt} + R(\tilde{i}_{ck})^2 + \frac{R'}{2} (\tilde{i}_{vk})^2 \right. \\ & \left. + \frac{C}{2N} \tilde{u}_{cuk} \frac{d\tilde{u}_{cuk}^\Sigma}{dt} + \frac{C}{2N} \tilde{u}_{clk} \frac{d\tilde{u}_{clk}^\Sigma}{dt} \right] \end{aligned} \quad (\text{B.44})$$

Replacing (B.37) in (B.44) results in

$$\begin{aligned} -\frac{C'}{4} \tilde{u}_{dc} \frac{d\tilde{u}_{dc}}{dt} = & \sum_{k \in (abc)} \left[L\tilde{i}_{ck} \frac{d\tilde{i}_{ck}}{dt} + L' \frac{\tilde{i}_{vk}}{2} \frac{d\tilde{i}_{vk}}{dt} + R(\tilde{i}_{ck})^2 + \frac{R'}{2} (\tilde{i}_{vk})^2 \right. \\ & \left. + \frac{C}{2N} \tilde{u}_{cuk} \frac{d\tilde{u}_{cuk}^\Sigma}{dt} + \frac{C}{2N} \tilde{u}_{clk} \frac{d\tilde{u}_{clk}^\Sigma}{dt} \right] \end{aligned} \quad (\text{B.45})$$

Finally substituting (B.45) in the derivative of the Lyapunov candidate function (B.39) yields

$$\dot{V} = -2 \sum_{k \in (abc)} \left[R(\tilde{i}_{ck})^2 + \frac{R'}{2} (\tilde{i}_{vk})^2 \right] \quad (\text{B.46})$$

Since $\dot{V} \leq 0$ if $R > 0$ and $R' > 0$, V is a Lyapunov function implying that the deviation system of the VS-MMC is globally stable. Nonetheless, \dot{V} is only negative semidefinite, implying that V is not a strict Lyapunov function, which means that asymptotic stability is not yet proven. For completing the proof, LaSalle's invariance principle is applied once more.

- $\dot{V} = -2 \sum_{k \in (abc)} \left[R(\tilde{i}_{ck})^2 + \frac{R'}{2} (\tilde{i}_{vk})^2 \right]$ implies that both \tilde{i}_{ck} and \tilde{i}_{vk} converge asymptotically to zero.
- $\tilde{i}_{ck} \equiv 0$ and $\tilde{i}_{vk} \equiv 0$ are replaced in (B.35), (B.36) and (B.34), in order to verify if \tilde{u}_{cuk}^Σ and \tilde{u}_{clk}^Σ converge to 0. This results in

$$\frac{d\tilde{u}_{cuk}^\Sigma}{dt} \equiv 0 \quad (\text{B.47})$$

$$\frac{d\tilde{u}_{clk}^\Sigma}{dt} \equiv 0 \quad (\text{B.48})$$

$$n_{lk} \tilde{u}_{clk}^\Sigma - n_{uk} \tilde{u}_{cuk}^\Sigma \equiv 0 \quad (\text{B.49})$$

- The first two equations imply that both u_{cuk}^Σ and u_{clk}^Σ are constant.

- n_{uk} and n_{lk} are time varying and not linearly related. Therefore the only constant that satisfies (B.49) is $\tilde{u}_{cuk}^\Sigma = \tilde{u}_{clk}^\Sigma = 0$.
- Replacing $\tilde{i}_c \equiv 0$ in (B.37) implies that \tilde{u}_{dc} is a constant.
- Finally, substituting $\tilde{i}_{ck} \equiv 0$, $\tilde{u}_{cuk}^\Sigma \equiv 0$ and $\tilde{u}_{clk}^\Sigma \equiv 0$ in (B.33) yields $\tilde{u}_{dc} = 0$.

Therefore, it is possible to conclude that the origin is globally asymptotically stable for the deviation system of a voltage source MMC if $R > 0$ and $R' > 0$.

B.5 Conclusion

The main contribution of this appendix is the extrapolation of the global asymptotic stability proof previously introduced in [31] to a three phase “DC voltage-regulating” modular multilevel converter or in other words, when acting as a voltage source converter. The proof is based on the Lyapunov theory and is valid for any operating point within the converter physical limits.

However, this methodology fails to include the discrete switching effect or the power converter, which is a potential cause for instabilities. A complementary linear-based stability study based on impedance representation is applied to the MMC in [C8] using Generalized Nyquist criteria. Even though the results are valid for only one point of operation (unlike the Lyapunov theory results), the results complement themselves quite well. Furthermore, the Lyapunov theory is valid for the case under study as a whole, which implies very complicated analytical demonstrations for larger interconnected systems, of different nature (power electronics, electrical machines, etc.) for which this technology is aimed for. A way of ensuring global asymptotic stability using a modular approach instead of analyzing the more complex “big-picture” as the one presented in chapter 6, might be more suitable for such task.

References

- [1] N. Ahmed, A. Haider, D. Van Hertem, L. Zhang, and H.-P. Nee, "Prospects and challenges of future hvdc supergrids with modular multilevel converters," in *Power Electronics and Applications (EPE 2011), Proceedings of the 2011-14th European Conference on*, 30 2011-sept. 1 2011, pp. 1 –10.
- [2] A. Lesnicar and R. Marquardt, "An innovative modular multilevel converter topology suitable for a wide power range," in *Power Tech Conference Proceedings, 2003 IEEE Bologna*, vol. 3, june 2003, p. 6 pp. Vol.3.
- [3] A. Antonopoulos, L. Angquist, and H.-P. Nee, "On dynamics and voltage control of the modular multilevel converter," in *Power Electronics and Applications, 2009. EPE '09. 13th European Conference on*, sept. 2009, pp. 1 –10.
- [4] E. Bompard, G. Fulli, M. Ardelean, and M. Masera, "It's a bird, it's a plane, it's a...supergrid!: Evolution, opportunities, and critical issues for pan-european transmission," *Power and Energy Magazine, IEEE*, vol. 12, no. 2, pp. 40–50, March 2014.
- [5] S. Rohner, S. Bernet, M. Hiller, and R. Sommer, "Modulation, losses, and semiconductor requirements of modular multilevel converters," *Industrial Electronics, IEEE Transactions on*, vol. 57, no. 8, pp. 2633 –2642, aug. 2010.
- [6] M. Glinka and R. Marquardt, "A new ac/ac-multilevel converter family applied to a single-phase converter," in *Power Electronics and Drive Systems, 2003. PEDS 2003. The Fifth International Conference on*, vol. 1, nov. 2003, pp. 16 – 23 Vol.1.
- [7] L. Harnefors, A. Antonopoulos, S. Norrga, L. Angquist, and H. Nee, "Dynamic analysis of modular multilevel converters," *Industrial Electronics, IEEE Transactions on*, vol. PP, no. 99, p. 1, 2012.
- [8] M. Saeedifard and R. Iravani, "Dynamic performance of a modular multilevel back-to-back hvdc system," *Power Delivery, IEEE Transactions on*, vol. 25, no. 4, pp. 2903 –2912, oct. 2010.
- [9] J. Xu, C. Zhao, W. Liu, and C. Guo, "Accelerated model of modular multilevel converters in pscad/emtdc," *Power Delivery, IEEE Transactions on*, vol. PP, no. 99, p. 1, 2012.
- [10] J. Peralta, H. Saad, S. Denetiere, J. Mahseredjian, and S. Nguéfeu, "Detailed and averaged models for a 401-level mmc hvdc system," *Power Delivery, IEEE Transactions on*, vol. 27, no. 3, pp. 1501 –1508, july 2012.
- [11] U. Gnanarathna, A. Gole, and R. Jayasinghe, "Efficient modeling of modular multilevel hvdc converters (mmc) on electromagnetic transient simulation programs," *Power Delivery, IEEE Transactions on*, vol. 26, no. 1, pp. 316 –324, jan. 2011.
- [12] S. Cole and R. Belmans, "Transmission of bulk power," *Industrial Electronics Magazine, IEEE*, vol. 3, no. 3, pp. 19–24, Sept 2009.

REFERENCES

- [13] R. Adapa, "High-wire act: HvdC technology: The state of the art," *Power and Energy Magazine, IEEE*, vol. 10, no. 6, pp. 18–29, Nov 2012.
- [14] M. Barnes and A. Beddard, "Voltage source converter {HVDC} links the state of the art and issues going forward," *Energy Procedia*, vol. 24, no. 0, pp. 108 – 122, 2012, selected papers from Deep Sea Offshore Wind;D Conference, Trondheim, Norway, 19-20 January 2012. [Online]. Available: <http://www.sciencedirect.com/science/article/pii/S1876610212011320>
- [15] P. Jones and C. Davidson, "Calculation of power losses for mmc-based vsc hvdc stations," in *Power Electronics and Applications (EPE), 2013 15th European Conference on*, Sept 2013, pp. 1–10.
- [16] G. Adam, K. Ahmed, and B. Williams, "Mixed cells modular multilevel converter," in *Industrial Electronics (ISIE), 2014 IEEE 23rd International Symposium on*, June 2014, pp. 1390–1395.
- [17] Q. Tu, Z. Xu, and L. Xu, "Reduced switching-frequency modulation and circulating current suppression for modular multilevel converters," *Power Delivery, IEEE Transactions on*, vol. 26, no. 3, pp. 2009–2017, July 2011.
- [18] M. Hiller and R. Marquardt, "A new converter concept for switched reluctance drives with multiple energy sources," in *Power Electronics and Drive Systems, 2003. PEDS 2003. The Fifth International Conference on*, vol. 2, Nov 2003, pp. 1235–1240 Vol.2.
- [19] H. Saad, S. Denetiere, J. Mahseredjian, P. Delarue, X. Guillaud, J. Peralta, and S. Nguefeu, "Modular multilevel converter models for electromagnetic transients," *Power Delivery, IEEE Transactions on*, vol. 29, no. 3, pp. 1481–1489, June 2014.
- [20] K. Strunz and E. Carlson, "Nested fast and simultaneous solution for time-domain simulation of integrative power-electric and electronic systems," *Power Delivery, IEEE Transactions on*, vol. 22, no. 1, pp. 277–287, Jan 2007.
- [21] M. Matar and R. Iravani, "Fpga implementation of the power electronic converter model for real-time simulation of electromagnetic transients," *Power Delivery, IEEE Transactions on*, vol. 25, no. 2, pp. 852–860, April 2010.
- [22] L. Grégoire, J. Bélanger, and W. Li, "Fpga-based real-time simulation of multilevel modular converter hvdc systems," *ELECTRIMACS 2011*, 2011.
- [23] H. Saad, T. Ould-Bachir, J. Mahseredjian, C. Dufour, S. Denetiere, and S. Nguefeu, "Real-time simulation of mmcs using cpu and fpga," *Power Electronics, IEEE Transactions on*, vol. PP, no. 99, pp. 1–1, 2013.
- [24] H. Saad, J. Peralta, S. Denetiere, J. Mahseredjian, J. Jatskevich, J. Martinez, A. Davoudi, M. Saeedifard, V. Sood, X. Wang, J. Cano, and A. Mehrizi-Sani, "Dynamic averaged and simplified models for mmc-based hvdc transmission systems," *Power Delivery, IEEE Transactions on*, vol. 28, no. 3, pp. 1723–1730, July 2013.
- [25] J. Peralta, H. Saad, S. Denetiere, and J. Mahseredjian, "Dynamic performance of average-value models for multi-terminal vsc-hvdc systems," in *Power and Energy Society General Meeting, 2012 IEEE*, July 2012, pp. 1–8.

- [26] J. Leon, S. Vazquez, J. Sanchez, R. Portillo, L. Franquelo, J. Carrasco, and E. Dominguez, "Conventional space-vector modulation techniques versus the single-phase modulator for multilevel converters," *Industrial Electronics, IEEE Transactions on*, vol. 57, no. 7, pp. 2473–2482, July 2010.
- [27] N. Ahmed, L. Angquist, S. Norrga, and H.-P. Nee, "Validation of the continuous model of the modular multilevel converter with blocking/deblocking capability," in *AC and DC Power Transmission (ACDC 2012), 10th IET International Conference on*, Dec 2012, pp. 1–6.
- [28] K. Ilves, A. Antonopoulos, S. Norrga, and H.-P. Nee, "Steady-state analysis of interaction between harmonic components of arm and line quantities of modular multilevel converters," *Power Electronics, IEEE Transactions on*, vol. 27, no. 1, pp. 57–68, Jan 2012.
- [29] L. Angquist, A. Antonopoulos, D. Siemaszko, K. Ilves, M. Vasiladiotis, and H.-P. Nee, "Open-loop control of modular multilevel converters using estimation of stored energy," *Industry Applications, IEEE Transactions on*, vol. 47, no. 6, pp. 2516–2524, nov.-dec. 2011.
- [30] G. Bergna, A. Garces, E. Berne, P. Egrot, A. Arzande, J.-C. Vannier, and M. Molinas, "A generalized power control approach in abc frame for modular multilevel converter hvdc links based on mathematical optimization," *Power Delivery, IEEE Transactions on*, vol. PP, no. 99, pp. 1–9, 2013.
- [31] A. Antonopoulos, L. Angquist, L. Harnefors, K. Ilves, and H.-P. Nee, "Global asymptotic stability of modular multilevel converters," *Industrial Electronics, IEEE Transactions on*, vol. 61, no. 2, pp. 603–612, 2014.
- [32] G. Bergna, J. Suul, E. Berne, P. Egrot, P. Lefranc, J.-C. Vannier, and M. Molinas, "Mitigating dc-side power oscillations and negative sequence load currents in modular multilevel converters - first approach using resonant pi," in *IECON Conference Proceedings, IEEE Montreal*, October 2012.
- [33] Q. Tu, Z. Xu, Y. Chang, and L. Guan, "Suppressing dc voltage ripples of mmc-hvdc under unbalanced grid conditions," *Power Delivery, IEEE Transactions on*, vol. 27, no. 3, pp. 1332–1338, July 2012.
- [34] J.-W. Moon, C.-S. Kim, J.-W. Park, D.-W. Kang, and J.-M. Kim, "Circulating current control in mmc under the unbalanced voltage," *Power Delivery, IEEE Transactions on*, vol. 28, no. 3, pp. 1952–1959, 2013.
- [35] M. Guan and Z. Xu, "Modeling and control of a modular multilevel converter-based hvdc system under unbalanced grid conditions," *Power Electronics, IEEE Transactions on*, vol. 27, no. 12, pp. 4858–4867, 2012.
- [36] Z. Yuebin, J. Daozhuo, G. Jie, H. Pengfei, and L. Zhiyong, "Control of modular multilevel converter based on stationary frame under unbalanced ac system," in *Digital Manufacturing and Automation (ICDMA), 2012 Third International Conference on*, 2012, pp. 293–296.
- [37] P. Rodriguez, J. Pou, J. Bergas, J. Candela, R. Burgos, and D. Boroyevich, "Decoupled double synchronous reference frame pll for power converters control," *Power Electronics, IEEE Transactions on*, vol. 22, no. 2, pp. 584–592, March 2007.
- [38] R. Teodorescu, M. Liserre, and P. Rodriguez, *Grid Converters for Photovoltaic and Wind Power Systems*. Wiley-IEEE Press, 2011.

REFERENCES

- [39] G. Bergna, E. Berne, P. Egrot, P. Lefranc, A. Amir, J. Vannier, and M. Molinas, "An energy-based controller for hvdc modular multilevel converter in decoupled double synchronous reference frame for voltage oscillations reduction," *Industrial Electronics, IEEE Transactions on*, vol. PP, no. 99, p. 1, 2012.
- [40] K. Ilves, S. Norrga, L. Harnefors, and H.-P. Nee, "On energy storage requirements in modular multilevel converters," *Power Electronics, IEEE Transactions on*, vol. 29, no. 1, pp. 77–88, Jan 2014.
- [41] M. Hagiwara and H. Akagi, "Control and experiment of pulsewidth-modulated modular multilevel converters," *Power Electronics, IEEE Transactions on*, vol. 24, no. 7, pp. 1737–1746, July 2009.
- [42] L. Angquist, A. Antonopoulos, D. Siemaszko, K. Ilves, M. Vasiladiotis, and H.-P. Nee, "Inner control of modular multilevel converters - an approach using open-loop estimation of stored energy," in *Power Electronics Conference (IPEC), 2010 International*, June 2010, pp. 1579–1585.
- [43] K. Ilves, A. Antonopoulos, S. Norrga, and H.-P. Nee, "A new modulation method for the modular multilevel converter allowing fundamental switching frequency," in *Power Electronics and ECCE Asia (ICPE ECCE), 2011 IEEE 8th International Conference on*, 30 2011–June 3 2011, pp. 991–998.
- [44] D. Siemaszko, A. Antonopoulos, K. Ilves, M. Vasiladiotis, L. Angquist, and H.-P. Nee, "Evaluation of control and modulation methods for modular multilevel converters," in *Power Electronics Conference (IPEC), 2010 International*, June 2010, pp. 746–753.
- [45] G. Bergna, M. Boyra, and J. Vivas, "Evaluation and proposal of mmc-hvdc control strategies under transient and steady state conditions," in *Power Electronics and Applications (EPE 2011), Proceedings of the 2011-14th European Conference on*, 30 2011–Sept. 1 2011, pp. 1–10.
- [46] G. T. Son, H.-J. Lee, T. S. Nam, Y.-H. Chung, U.-H. Lee, S.-T. Baek, K. Hur, and J.-W. Park, "Design and control of a modular multilevel hvdc converter with redundant power modules for noninterruptible energy transfer," *Power Delivery, IEEE Transactions on*, vol. 27, no. 3, pp. 1611–1619, July 2012.
- [47] M. Perez, J. Rodriguez, E. Fuentes, and F. Kammerer, "Predictive control of ac-ac modular multilevel converters," *Industrial Electronics, IEEE Transactions on*, vol. 59, no. 7, pp. 2832–2839, July 2012.
- [48] J. Qin and M. Saeedifard, "Predictive control of a modular multilevel converter for a back-to-back hvdc system," *Power Delivery, IEEE Transactions on*, vol. 27, no. 3, pp. 1538–1547, July 2012.
- [49] J.-W. Moon, J.-S. Gwon, J.-W. Park, D.-W. Kang, and J.-M. Kim, "Model predictive control with a reduced number of considered states in a modular multilevel converter for hvdc system," pp. 1–1, 2014.
- [50] R. Fard, H. Nademi, and L. Norum, "Analysis of a modular multilevel inverter under the predicted current control based on finite-control-set strategy," in *Electric Power and Energy Conversion Systems (EPECS), 2013 3rd International Conference on*, Oct 2013, pp. 1–6.

- [51] J. Bocker, B. Freudenberg, A. The, and S. Dieckerhoff, "Experimental comparison of model predictive control and cascaded control of the modular multilevel converter," *Power Electronics, IEEE Transactions on*, vol. 30, no. 1, pp. 422–430, Jan 2015.
- [52] K. Ilves, L. Harnefors, S. Norrnga, and H.-P. Nee, "Predictive sorting algorithm for modular multilevel converters minimizing the spread in the submodule capacitor voltages," *Power Electronics, IEEE Transactions on*, vol. 30, no. 1, pp. 440–449, Jan 2015.
- [53] K. Wang, Y. Li, Z. Zheng, and L. Xu, "Voltage balancing and fluctuation suppression method of floating capacitors in a new modular multilevel converter," *Industrial Electronics, IEEE Transactions on*, vol. PP, no. 99, p. 1, 2012.
- [54] H. Akagi, M. Aredes, and E. Watanabe, *Instantaneous Power Theory and Applications to Power Conditioning*. Wiley-IEEE Press, 2007.
- [55] P. Tenti, H. Paredes, and P. Mattavelli, "Conservative power theory, a framework to approach control and accountability issues in smart microgrids," *Power Electronics, IEEE Transactions on*, vol. 26, no. 3, pp. 664–673, march 2011.
- [56] L. Czarnecki, "Instantaneous reactive power p-q theory and power properties of three-phase systems," *Power Delivery, IEEE Transactions on*, vol. 21, no. 1, pp. 362–367, jan. 2006.
- [57] —, "Physical components (cpc) concept: A fundamental of power theory," in *Nonsinusoidal Currents and Compensation, 2008. ISNCC 2008. International School on*, june 2008, pp. 1–11.
- [58] V. Staudt, "Fryze - buchholz - depenbrock: A time-domain power theory," in *Nonsinusoidal Currents and Compensation, 2008. ISNCC 2008. International School on*, june 2008, pp. 1–12.
- [59] A. Garces, M. Molinas, and P. Rodriguez, "A generalized compensation theory for active filters based on mathematical optimization in {ABC} frame," *Electric Power Systems Research*, vol. 90, no. 0, pp. 1–10, September 2012. [Online]. Available: <http://www.sciencedirect.com/science/article/pii/S0378779612000806>
- [60] F. Z. Peng, J. Ott, G.W., and D. Adams, "Harmonic and reactive power compensation based on the generalized instantaneous reactive power theory for three-phase four-wire systems," *Power Electronics, IEEE Transactions on*, vol. 13, no. 6, pp. 1174–1181, nov 1998.
- [61] R. Herrera and P. Salmeron, "Instantaneous reactive power theory: A reference in the non-linear loads compensation," *Industrial Electronics, IEEE Transactions on*, vol. 56, no. 6, pp. 2015–2022, June 2009.
- [62] P. Rodriguez, "Aportaciones a los acondicionadores activos de corriente en derivacion para redes trifasicas de cuatro hilos," Ph.D. dissertation, Universitat Politecnica de Catalunya, 2005.
- [63] J. Willems, J. Ghijselen, and A. Emanuel, "The apparent power concept and the ieee standard 1459-2000," *Power Delivery, IEEE Transactions on*, vol. 20, no. 2, pp. 876–884, April 2005.
- [64] T. Furuhashi, S. Okuma, and Y. Uchikawa, "A study on the theory of instantaneous reactive power," *Industrial Electronics, IEEE Transactions on*, vol. 37, no. 1, pp. 86–90, Feb 1990.
- [65] G. Chang, S. Chen, Y. Chin, and W. Chen, "An a-b-c reference frame-based compensation strategy for series active power filter control," in *Industrial Electronics and Applications, 2006 1ST IEEE Conference on*, May 2006, pp. 1–4.

REFERENCES

- [66] M. Kazmierkowski and L. Malesani, "Current control techniques for three-phase voltage-source pwm converters: a survey," *Industrial Electronics, IEEE Transactions on*, vol. 45, no. 5, pp. 691–703, Oct 1998.
- [67] R. Teodorescu, F. Blaabjerg, M. Liserre, and P. Loh, "Proportional-resonant controllers and filters for grid-connected voltage-source converters," *Electric Power Applications, IEE Proceedings*, vol. 153, no. 5, pp. 750–762, September 2006.
- [68] P. Mattavelli, "A closed-loop selective harmonic compensation for active filters," *Industry Applications, IEEE Transactions on*, vol. 37, no. 1, pp. 81–89, Jan 2001.
- [69] A. de Heredia, H. Gaztanaga, I. Etxeberria-Otadui, S. Bacha, and X. Guillaud, "Analysis of multi-resonant current control structures and tuning methods," in *IEEE Industrial Electronics, IECON 2006 - 32nd Annual Conference on*, Nov 2006, pp. 2156–2161.
- [70] X. Yuan, W. Merk, H. Stemmler, and J. Allmeling, "Stationary-frame generalized integrators for current control of active power filters with zero steady-state error for current harmonics of concern under unbalanced and distorted operating conditions," *Industry Applications, IEEE Transactions on*, vol. 38, no. 2, pp. 523–532, Mar 2002.
- [71] P. Rodriguez, R. Teodorescu, I. Candela, A. Timbus, M. Liserre, and F. Blaabjerg, "New positive-sequence voltage detector for grid synchronization of power converters under faulty grid conditions," in *Power Electronics Specialists Conference, 2006. PESC '06. 37th IEEE*, June 2006, pp. 1 – 7.
- [72] P. Rodriguez, A. Luna, M. Ciobotaru, R. Teodorescu, and F. Blaabjerg, "Advanced grid synchronization system for power converters under unbalanced and distorted operating conditions," in *IEEE Industrial Electronics, IECON 2006 - 32nd Annual Conference on*, Nov. 2006, pp. 5173 –5178.
- [73] J.-A. Suul, "Control of grid integrated voltage source converters under unbalanced conditions - development of an on-line frequency-adaptive virtual flux-based approach," Ph.D. dissertation, Norwegian University of Science and Technology, 2012.
- [74] R. Teodorescu, F. Blaabjerg, M. Liserre, and P. Loh, "Proportional-resonant controllers and filters for grid-connected voltage-source converters," *Electric Power Applications, IEE Proceedings -*, vol. 153, no. 5, pp. 750 –762, September 2006.
- [75] M. Ciobotaru, R. Teodorescu, and F. Blaabjerg, "A new single-phase pll structure based on second order generalized integrator," in *Power Electronics Specialists Conference, 2006. PESC '06. 37th IEEE*, June 2006, pp. 1 – 6.
- [76] P. Rodriguez, A. Luna, I. Candela, R. Teodorescu, and F. Blaabjerg, "Grid synchronization of power converters using multiple second order generalized integrators," in *Industrial Electronics, 2008. IECON 2008. 34th Annual Conference of IEEE*, Nov. 2008, pp. 755 –760.
- [77] P. Rodriguez, A. Timbus, R. Teodorescu, M. Liserre, and F. Blaabjerg, "Flexible active power control of distributed power generation systems during grid faults," *Industrial Electronics, IEEE Transactions on*, vol. 54, no. 5, pp. 2583–2592, 2007.
- [78] F. Wang, J. Duarte, and M. Hendrix, "Pliant active and reactive power control for grid-interactive converters under unbalanced voltage dips," *Power Electronics, IEEE Transactions on*, vol. 26, no. 5, pp. 1511 –1521, May 2011.

- [79] L. Xu, B. Andersen, and P. Cartwright, "Vsc transmission operating under unbalanced ac conditions - analysis and control design," *Power Delivery, IEEE Transactions on*, vol. 20, no. 1, pp. 427–434, 2005.
- [80] X. Shi, G. Zhou, J. Wang, and C. Fu, "Control strategy for vsc-hvdc under unbalanced input voltages," in *Electrical Machines and Systems, 2008. ICEMS 2008. International Conference on*, 2008, pp. 1107–1110.
- [81] J. Zhang, H. Chen, W. Pan, and C. Wang, "Vsc-hvdc control under unbalanced supply conditions," in *Power Engineering Society General Meeting, 2007. IEEE, 2007*, pp. 1–6.
- [82] J. Suul, A. Luna, and P. Rodriguez, "Power control of vsc hvdc converters for limiting the influence of ac unbalanced faults on multi-terminal dc grids," in *AC and DC Power Transmission (ACDC 2012), 10th IET International Conference on*, 2012, pp. 1–7.
- [83] J. Qin and M. Saedifard, "Reduced switching-frequency voltage-balancing strategies for modular multilevel hvdc converters," in *PES General Meeting — Conference Exposition, 2014 IEEE*, July 2014, pp. 1–1.
- [84] X. Yuan, W. Merk, H. Stemmler, and J. Allmeling, "Stationary-frame generalized integrators for current control of active power filters with zero steady-state error for current harmonics of concern under unbalanced and distorted operating conditions," *Industry Applications, IEEE Transactions on*, vol. 38, no. 2, pp. 523–532, 2002.
- [85] P. Rodriguez, A. Luna, R. Muñoz-Aguilar, I. Etxeberria-Otadui, R. Teodorescu, and F. Blaabjerg, "A stationary reference frame grid synchronization system for three-phase grid-connected power converters under adverse grid conditions," *Power Electronics, IEEE Transactions on*, vol. 27, no. 1, pp. 99–112, 2012.
- [86] G. Bergna, J.-A. Suul, E. Berne, P. Egrot, J.-C. Vannier, and M. Molinas, "Generalized abc frame differential current control ensuring constant dc power for modular multilevel converters under unbalanced operation," in *Power Electronics and Applications (EPE), 2013 15th European Conference on*, 2013, pp. 1–10.
- [87] G. Bergna, E. Berne, A. Garces, P. Egrot, J.-C. Vannier, and M. Molinas, "A generalized power control approach in abc frame for modular multilevel converters based on lagrange multipliers," in *Power Electronics and Applications (EPE), 2013 15th European Conference on*, 2013, pp. 1–8.
- [88] L. Harnefors, A. Antonopoulos, and H.-P. Nee, "Global asymptotic stability of modular multilevel converters with measurement lag and circulating-current control," in *Power Electronics and Applications (EPE), 2013 15th European Conference on*, 2013, pp. 1–10.
- [89] H. Khalil, *Nonlinear Systems*. Prentice-Hall, Upper Saddle River, NJ, 2002.
- [90] B. Jayawardhana, R. Ortega, E. Garcia-Canseco, and F. Castanos, "Passivity of nonlinear incremental systems: Application to pi stabilization of nonlinear rlc circuits," in *Decision and Control, 2006 45th IEEE Conference on*, 2006, pp. 3808–3812.
- [91] S. R. Sanders and G. C. Verghese, "Lyapunov-based control for switched power converters," *Power Electronics, IEEE Transactions on*, vol. 7, no. 1, pp. 17–24, 1992.
- [92] F. Castaños, B. Jayawardhana, R. Ortega, and E. Garca-Canseco, "Proportional plus integral control for set-point regulation of a class of nonlinear RLC circuits," *Circuits, Systems and Signal Processing*, vol. 28, no. 4, pp. 609–623, 2009.

REFERENCES

- [93] M. Hernandez-Gomez, R. Ortega, F. Lamnabhi-Lagarrigue, and G. Escobar, "Adaptive pi stabilization of switched power converters," *Control Systems Technology, IEEE Transactions on*, vol. 18, no. 3, pp. 688–698, 2010.
- [94] M. Saeedifard and R. Iravani, "Dynamic performance of a modular multilevel back-to-back hvdc system," *Power Delivery, IEEE Transactions on*, vol. 25, no. 4, pp. 2903–2912, 2010.
- [95] J. M. Olm, X. Ros-Oton, and Y. B. Shtessel, "Stable inversion of abel equations: Application to tracking control in DC-DC nonminimum phase boost converters," *Automatica*, vol. 47, no. 1, pp. 221–226, 2011.
- [96] E. Fossas and J. M. Olm, "A functional iterative approach to the tracking control of non-minimum phase switched power converters," *Mathematics of Control, Signals, and Systems*, vol. 21, no. 3, 2009.
- [97] ———, "Generation of signals in a buck converter with sliding mode control," in *Circuits and Systems, 1994. ISCAS '94., 1994 IEEE International Symposium on*, vol. 6, 1994, pp. 157–160.
- [98] H. Sira-Ramirez and R. Silva-Ortigoza, *Control Design Techniques in Power Electronics Devices*, ser. Power systems. Springer, 2006.
- [99] D. Biel, F. Guinjoan, E. Fossas, and J. Chavarria, "Sliding-mode control design of a boost-buck switching converter for ac signal generation," *Circuits and Systems I: Regular Papers, IEEE Transactions on*, vol. 51, no. 8, pp. 1539–1551, 2004.
- [100] C. Meza, D. Jeltsema, J. M. Scherpen, and D. Biel, "Passive p-control of a grid-connected photovoltaic inverter," in *17th World Congress, Preceedings of the*, vol. 21, 2008, pp. 3808–3812.
- [101] A. Van der Schaft, *L₂-Gain and passivity techniques in nonlinear control*, ser. Communications and Control Engineering Series. Springer-Verlag, 2000.